Towards Designing Composite membranes for CO_2 Separation: The Inclusion of Hybrid TiO_2-PEG structures and the Study of their Interfaces

Vers la conception de membranes composites pour la séparation du CO_2: Inclusion de structures hybrides TiO_2-PEG et étude de leurs interfaces

by

Edgar Cao

A thesis
presented to the University of Waterloo
and the Université de Bordeaux
in fulfilment of the
thesis requirement for the degree of
Doctor of Philosophy
in
Chemical Engineering

Waterloo, Ontario, Canada / Bordeaux, France, 2015

Authors Declaration

I hereby declare that I am the sole author of this thesis. This is a true copy of the thesis, including any required final revisions, as accepted by my examiners. I understand that my thesis may be made electronically available to the public.

Abstract (English)

The continual release and increase of atmospheric pollutants continue to plague our world, with many governments and organizations aiming to mitigate these problems. However, even if there is to be a reached agreement between countries on reducing pollution (ex: COP21: UN Climate Change Conference in Paris 2015), the effects of climate change may still be difficult to stop. As many of these gases released into the atmosphere disrupt the delicate balance and have led to global warming (i.e. CO_2 as a greenhouse gas (GHG)), methods of eliminating the release of this combustion by-product on the large scale have been examined.

As fossil fuel power plants are one of the largest emitters of such pollutants, the analysis of different methods to counteract their release are assessed. While options for separation of the exhaust gas, also known as flue gas, exist (i.e. amine-based scrubbers from sorption based methods, cyrodistillation, membranes etc...), perhaps the least energy intensive process targetted at large volumes are membranes. With membranes, there are a plethora of different designs and structures that can be incorporated. Ranging from polymeric dense membranes (such as PEBAX® or Matrimid®), inorganic porous membranes (i.e. MCM-48) to mixed-matrix membranes, they provide a role in a variety of different applications. While membranes have been extensively used in liquid purification and specialty gas applications alongside catalysis, their adoption towards large scale gas separation in power plants have been limited. Due to the severity of the long-term stability of polymeric based membranes and the lower selectivity from inorganic membranes, their role in separating gases such as CO_2 has been limited. While research and patents exist on the formation of membranes for flue gas separation, the general trend has been towards mixed-matrix membranes. While a promising route, mixed-matrix membranes can sometimes suffer from material integration. An alternative route towards an integrated hybrid membrane would be to reverse the role of forming these hybrid membranes; using the inorganic particles as the "seeds" to grow the polymeric matrix to ensure good integration. **Thus the objective of**

this thesis is to explore a new route towards synthesizing a method of hybrid membrane coating on existing inorganic titania supports.

In order to accomplish this objective, the first step required the study of different surface anchoring groups for various inorganic titania surfaces. Many such groups exist, including (but not limited to) thiols, catechols, silanes and phosphonates/phosphonic acids. While each method has their merits, silanes and phosphonates were determined to be the best solution due to their commercial availablity and ease of application. From Specific Polymers, Propyl phosphonic acid -2-Bromo-2-methyl propanoate (or C3-Initiator) was obtained for use as the target grafting molecule studied for the phosphonate anchoring group. In the case of the silane grafting group, (3-aminopropyl)triethoxysilane (APTES) was used as the study case. These groups were then explored for their grafting potential onto varying shapes, such as curved (particles), flat (substrates) and porous (supports) of titania. However, grafting on each of these surfaces illustrated curved particles provided the highest grafting yield. It was determined (with destructive testing) that the grafting density on spherical particles between silanes and phosphonates differed; a yield of roughly 8-16 silane groups/nm^2 vs. the ~2.5 phosphonate groups/nm^2. Thus, phosphonates and silanes can be applied to form hybrid polymeric-titania materials.

With the C3-Initiator (or TiO_2-g-C3-Initiator), the bromine group behaves as an Atom-Transfer Radical Polymerization (ATRP) initiating group. This allowed the formation of a highly PEG-ylated structure (or polyethylene glycol/oxide) using PEGMEMA to polymerize into a core-shell structure by surface-initiated ATRP (si-ATRP). XPS, DLS and TGA show it is possible to form growing hybrid particles that have a degree of polymerization (DP) of roughly 1200.

While the APTES group does not hold a polymerizable group, the amine terminus can be used to react to a carboxylic acid to form an amide bond. With this in mind, a pre-synthesized PEG macromonomer with an α-carboxylic acid and an ω-norbornenyl group (NB-PEO-COOH) allowed the previously functionalized titania-APTES group (or TiO_2-g-APTES) to form norbornenyl coated titania particles (TiO_2-g-APTES-PEO-NB).

These exposed norbornenyl groups allow for ring-opening metathesis polymerization (or ROMP) from the functionalized surface (si-ROMP). The particles were further characterized to find a total grafting density of norbornenyl groups at 2.5 groups/nm^2. These particles were then activated with the Grubbs 1st generation initiator (Grubbs), and allowed for norbornene (NB) to be polymerized to yield a DP of 12,500.

Transfering the knowledge from studying these hybrid particles resulted in two methods of porous tubular ceramic modification; either a "Coating Onto" method or "Grafting From" method. The "Coating Onto" method involved well-dispersed hybrid particles to form the hybrid membrane direction on the surface of the porous ceramic tube. This was studied and achieved with the phosphonate based C3-Initiator hybrid particles. The "Grafting From" method involved post-functionalized titania particles (i.e. TiO_2-g-C3-Initiator or TiO_2-g-APTES-PEO-NB) to be coated on the porous ceramic tube prior to polymerization via si-ATRP or si-ROMP. These routes that were deemed promising were scaled up to longer ceramic tubes and were sent to study their gas permeation. It was discovered that the first set of scaled membranes were difficult to yield gas separation properties, but hypothesized to be due to sparsly separated pinholes and insufficient polymer content. However, this study still provides great promise for an eventual hybrid membrane that can effectively separate gas, as can be achieved from the recommended courses of action.

Résumé (Français)

Malgré les efforts de nombreux gouvernements et organisations pour réduire la pollution[1], le nombre et la concentration des polluants atmosphériques ne cessent de croître. En particulier, avec le maintien ou la réactivation des centrales thermiques à combustibles fossiles c'est plus de 20 milliards de tonnes de CO_2 qui sont libérés par an dans l'atmosphère, contribuant au réchauffement climatique.

Diverses options pour la capture et la séparation des gaz de combustion existent telles que : la « capture chimique » à l'aide de composés aminés, les méthodes de sorption, la cryodistillation, les membranes, etc .... Le procédé le moins énergivore est probablement celui des procédés membranaires. Il existe une pléthore de membranes modèles de compositions et de structures différentes allant des membranes denses polymères, *e.g*. PEBAX®, Matrimid®, aux membranes poreuses, *e.g.* MCM-48, en passant par les membranes à matrice mixte, *e.g.* MMM. Très largement employées au laboratoire dans le domaine de la purification en phase liquide et gazeuse et pour la catalyse, leurs utilisations dans les centrales électriques restent limitées. En particulier, le manque de stabilité à long terme des membranes polymères ou la plus faible sélectivité des membranes inorganiques, permet difficilement leur emploi si l'on veut fournir une réponse industrielle pertinente aux traitements de grands volumes de gaz, *e.g.* 240 000 m^3/h de CO_2 pour une centrale à charbon de 900 MW. Afin de préserver la sélectivité des membranes organiques et d'augmenter leur résistance, des membranes à matrice mixte associant un composant inorganique à un polymère ont été synthétisées. Dans ces membranes, la phase inorganique est toujours dispersée au sein du polymère. Bien que prometteuses, les membranes à matrice-mixte peuvent parfois manquées de cohésion. Une voie alternative vers une membrane hybride intégrée serait de changer la méthodologie de synthèse de ces membranes hybrides en utilisant les particules inorganiques comme les «germes» à partir desquels la matrice polymère pourrait

---

[1] COP21: Conférence ONU sur le changement climatique à Paris 2015 (Nov)

croître. Ceci permettrait d'assurer une meilleure intégration des composants. **L'objectif de cette thèse est d'explorer les différentes voies de synthèse permettant un meilleur contrôle et une plus forte interaction entre la phase inorganique présente sous différentes formes (nanoparticules, surfaces dense ou poreuse) et la phase organique. L'objectif ultime est de préparer ces structures élaborées à partir de supports de membrane commerciaux poreux d'oxyde de titane (TiO_2) et de les tester dans un traitement de séparation du CO_2.**

Dans le **premier chapitre**, nous présentons brièvement les différentes méthodes de séparation des gaz qui existent et expliquons pourquoi les membranes apparaissent comme les meilleurs candidats dans une optique de procédé à faible coût énergétique. Ensuite, nous présentons les différentes formes de matériaux membranaires et leurs propriétés, et expliquons pourquoi la croissance du polymère directement à partir de la composante inorganique nous semble la méthode la meilleure pour la formation de membranes robustes.

Le **chapitre deux** expose les principaux résultats de la littérature concernant les différentes formes de modification de surface. Afin d'atteindre cet objectif, la première étape nécessite d'identifier les différents groupes d'ancrage permettant le greffage sur des surfaces de TiO_2. Quatre groupes ont été identifiés, les thiols, les catéchols, les silanes et les phosphonates ou acides phosphoniques. Bien que chaque méthode ait ses avantages, les silanes et les phosphonates apparaissent comme les meilleures solutions en raison de leur disponibilité commerciale et la facilité de leur mise en œuvre. La société Specific Polymers (France) a conçu et commercialise le propyl phosphonique acide 2-bromo-2-méthyl propanoate (nommé C3-initiator dans notre document). Cette molécule a été étudiée en tant que molécule modèle pour le greffage par le groupe d'ancrage acide phosphonique. Dans le cas du greffage par le silane, le 3-aminopropyl triéthoxysilane (APTES) a été utilisé pour les besoins de l'étude. Les substrats utilisés dans cette étude sont, soit des particules de TiO_2 (particules Evonik™ et particules Sigma™), soit des surfaces de TiO_2 planes et denses ou tubulaires et poreuses (supports membranaires fournis par la Sté CTI (France)). Les surfaces de TiO_2 modifiées sont caractérisées par différentes techniques telles que les spectroscopies XPS et RMN et l'analyse thermique gravimétrique (ATG). L'analyse des résultats montre que les rendements de greffage les plus élevés sont obtenus sur les supports particulaires. Il a également été déterminé (avec contrôle destructif) que la densité de greffage sur des particules sphériques diffère suivant l'utilisation de silane ou d'acide phosphonique; un rendement d'environ 8 à 16 molécules de silane/nm^2 contre approximativement 2,5 molécules de phosphonate/nm^2 est observé. Il est déduit que les acides phosphoniques et les silanes peuvent être indifféremment utilisés pour former la base de matériaux hybrides polymère-oxyde de titane.

Le **chapitre trois** décrit la synthèse et la caractérisation de particules hybrides cœur /écorce obtenues par polymérisation radicalaire par transfert d'atome (si-ATRP) de poly(éthylène glycol) méthyl éther méthacrylate. La polymérisation est amorcée à la surface des particules de TiO_2 *via* l'atome de brome porté par C3-Initiator. Des particules de TiO_2 encapsulées dans une enveloppe de poly(oxyde d'éthylène) ramifié ont ainsi pu être isolées.

Dans le **chapitre quatre** c'est cette fois la polymérisation par métathèse (si-ROMP) qui est utilisée pour greffer sur des substrats poreux et particulaires de TiO_2 des chaînes de polynorbornène *via* les ponts silanes pré-fonctionnalisés par un macromonomère de poly(oxyde d'éthylène). Les densités de greffage obtenues sont de 2,5 macromolécules par nm^2 et les greffons de polynorbornène ont des DPs de 12 500.

Le **chapitre cinq** met en application les connaissances acquises dans les chapitres précédents pour développer une membrane polymère sur un tube céramique. Deux stratégies sont explorées : le «Grafting From», et le «Coating Onto». La méthode «Grafing From» passe par l'engobage directement sur la surface tubulaire poreuse (membrane CTI) de TiO_2 des particules de TiO_2 précédemment fonctionnalisées suivi de la formation de la couche de polymère par si-ATRP ou si-ROMP. La méthode «Coating Onto» utilise les nanoparticules hybrides préparées selon la méthode si-ATRP, déposées par engobage sur la surface intérieure de la surface du tube en céramique, pour former la membrane. Ces deux voies ont permis d'obtenir avec succès des tubes en céramique de 15 cm dont le comportement en perméation de gaz a pu être étudié dans le chapitre 6.

Le dernier chapitre, le **chapitre six,** présente brièvement les résultats préliminaires obtenus en séparation membranaire avec les deux méthodes. Les comparaisons des valeurs de perméance, avec ou sans film polymère, confirment la présence de ce film. Cependant, il a été découvert que le premier (et seul dans le cadre de ce travail) jeu de membranes testées ne donnait aucune sélectivité (mesure de sélectivité idéale CO_2/N_2). Bien que négatif, ce résultat n'est cependant pas surprenant car les membranes de perméation gazeuse requièrent une excellente qualité de surface et la présence de quelques défauts ponctuels (piqûres) suffit à détruire toute sélectivité. Un moyen simple de remédier à ce problème serait d'augmenter l'épaisseur du film polymère afin d'améliorer la qualité du revêtement.

Pour conclure, ce travail a permis de vérifier la pertinence de notre approche et la faisabilité de notre projet. Un certain nombre de questionnements demeurent néanmoins et nécessitent des essais complémentaires:

1) Pour le procédé «Coating Onto» : Réalisation d'essais de perméation sur des tubes céramique de ZrO_2 d'au moins 15 cm de long et présentant des pores de 10 à 15 nm.
2) Pour le procédé «Grafting From» : Réalisation de nouvelles membranes par copolymérisation d'un mélange norbornène/macromonomère de poly(oxyde d'éthylène).
3) Comme mise à l'échelle du procédé s'est révélée délicate, l'augmentation du nombre de couches de revêtement va engendrer l'augmentation de l'épaisseur de la membrane. Il n'est même pas certain que la correction des défauts sera observée car ceux-ci peuvent se « perpétrer ». C'est pourquoi d'autres paramètres comme l'augmentation de la viscosité du mélange ou l'addition d'autres matières de charge de polymère organique peuvent être étudiés afin d'améliorer la formation de la membrane.

4) Une température de recuit du polymère un peu plus élevée pourrait permettre d’améliorer l'uniformité de la membrane.

5) Une étude des paramètres rhéologiques des solutions de revêtement pourrait permettre d’augmenter le rendement de revêtement sur les tubes en céramique.

Bien que non exhaustive cette liste devrait mettre en évidence dans quelle direction ce projet doit être poursuivi. Jusqu’ici, nous avons défini la chimie à mettre en œuvre. Il va maintenant être nécessaire de développer la physico-chimie des procédés et leur mise en œuvre. En effet, la difficulté de la tâche a été plus importante que prévue, en particulier pour ce qui relève de la compréhension de la chimie du greffage et du contrôle de la polymérisation à partir d’une surface. Le temps passé à cette tâche n’a pu être alloué à la chimie des matériaux et aux procédés membranaires. Nous pensons toutefois qu’il était indispensable pour dégager le champ de prospection de ce domaine et aboutir à de nouvelles membranes nanocomposites offrant à la fois haute sélectivité et bonne perméabilité, avec une mise en œuvre adaptée à un procédé de fabrication industrielle, car partant de composants commerciaux.

Acknowledgement

I have had the pleasure in the last 3-4 years meeting all kinds of wonderful people from around the world, partaking in the IDS-FunMat PhD program (project funded by the Conseil de region d'Aquitaine). I have been privileged to be able to work between two different institutions: at the University of Waterloo (in Canada) and at the Université de Bordeaux (in France). While there have been many hardships along the path, there have been many colleagues, friends, administrators and family members that have helped me through this period.

I first want to thank Dr. Henri Cramail for allowing me to work at LCPO. I am truly grateful for this wonderful opportunity to be able to hone my knowledge in polymers. This experience not only educated me on how to design polymers, but to meet passionate individuals stretching the limits of what polymers can be used for.

In terms of the direction of my thesis, I must thank both my advisors: Dr. Eric Prouzet and the lovely Dr. Valérie Héroguez.

Eric, your endless wisdom, views and help in guiding this project have been invaluable. While we've encountered many bumps along the road, you have been encouraging whenever we discuss. While my time in Waterloo was shorter than expected, I will always be grateful for the labs I have been able to work in (both in ESC and QNC), all whilst granting me time to be sure I could complete all parts of the administrative process at Waterloo (from the long list of courses, to the intensive comprehensive exam). So I must thank you for all your help and support!

Valérie, your support, guidance, motivation, planning, thought process and wisdom is the fundamental reason why I was able to complete this thesis today. Your unwavering help and guidance taught me not just how to work more efficiently, but also how to think carefully. You accepted me as your student without hesitation, welcomed me like a second mother and have always stood by my decisions (even if you disagreed with them!). Alors, je suis tellement content quand je pense à mes aventures au LCPO. Nos longues discussions (entre anglais et "français" … donc.. anglais!), et nos reunions étaient très agréables! I will miss having your support close by! Un grand merci à vous!!! Merci beaucoup!

To past professors and guidance I have received from committee/jury members – Thank you! Thank you Dr. Xianshe Feng for your persistence with teaching membranes to our class, and for all the helpful advice you have provided us! Thank you Dr. Linda Nazar for providing inspiration during a difficult time in my project; to change my mindset in a vital period at Waterloo. Thank you Dr. Eric Croiset for your promptness and well wishes at the start (and finish) of my thesis. For the "rapporteurs" of my thesis, thank you for your thoroughness and valuable discussions on my project, Dr. Anne-Jonquières and Dr. Frédéric Vidal. I also enjoyed our pleasant exchanges and short discussions, Dr. Daniel Grande and Mr. Bertrand Pavageau. To my former advisor, Dr. Mustafa Yavuz, thank you for your wisdom and teaching your course with great enthusiasm! (Which almost made me switch topics into electronics).

To the administrators at both universities, a big thanks for helping to deal with the many hurdles along the way. At the University of Waterloo, thank you Judy Caron (especially with those fuzzy rules, last minute changes, talks in person and by phone), and Amanda Guderian (for constantly checking up on my case, and answering my emails so quickly!). At the Université de Bordeaux, specifically at the LCPO, there are many administrators that have to be thanked. None of this would have been possible without: Catherine Roulinat (your promptness, your kindness, your unwavering support, and your unmatched organization!), Corinne Gonçalves de Carvalho (merci à vous pour votre aide et votre patience), Bernadette Guillabert (pour votre aide avec des petits mots en français), Nicole Gabriel (désolé pour mon accent “canadien” – pas québecois!), Claude Le Pierres (thank you for always helping me when I pass by with any questions I had!) and of course, Dominique Richard (while our time at LCPO was short, thank you for making time to help me with all the small details when you were just starting in the lab!).

From the IDS-FunMat program, the endless help from the administration was invaluable and without: Marianne Delmas, Audrey Sidobre, Stéphane Carlotti, Marie-Christine Durrieu, Bernhard Zeimetz, Laurent Servant and Thierry Tassaing, the program would not have evolved to accommodate the many issues and hurdles that were experienced.

For my labmates, colleagues and other IDS-FunMat-ers, I thank you all! Thanks to: Dan B. (your never ending charm and positive attitude!), Natacha K. (the first French girl I met, I am proud to have met you!), Camille L. (for not just a great time in Canada, but making sure my adjustment in LCPO was awesome!), Yannick M. (from all those arguments/discussions, to wonderful “soirées”!), Rosine P. (for the wonderful days at CAES, then evenings for dinner!), Marie A. (the best of times, the worst of times – but we got through!), Floraine C. (teaching me all I know about polymers, then French!), Loïc P. (the “PEO” master!!), Hélène C. (“kitty Kandy” lady), Maud C. (your sincerity and wisdom), Vincent N. (your kindness and always positive attitude), Gauvin H. (listening, but also being a “like-able” guy), Benjamin D. (your cheerful attitude and sweets!), Silvia M. (your smile, your cheerfulness, your tiramisu!), Julie T. (for always bringing a good attitude to the office), Maréva F. (the first “soutenance” I attended – where I was blown away…), Mehdi N. (“Whaaaaa”!), Margot S. (your awesomeness), Uyxing V. (your never-relenting bursts of energy! Always refreshing and encouraging for me), Mylène L. (your “go-with-the-flow” attitude that help ground me), An T. (for listening to me when I needed it the most), Mathilde W-M (our coffees in the “mornings”), Erin B. (from undergrad to grad… we made it!) and Olivia C. (our conversations that also help me reflect on myself!).

Thank you again, Zoé, Zoiesha, Cony, Charlotte, Lise, Annhelen, Ariane, Dounia, Louis, Jani-Markus, Colin, Kévin, Vusala, Tuyen, Lucas/Haohao, Shusheng, Anne H., Ségolène, Jérémie B., Jérémie G., Mathilde C., Kévin R., Blandine, Estelle, Elise, Déborah, Julie, Ana, Arthur W., Manu I., Gilles P., Jean-Michael, Noël, Christine L., Guillaume, Geoffrey, Alex, Johanne, Laura, Anne-Laure, Loïc P., Océane, Pauline, Ioannis, and many many more wonderful people at LCPO and Bordeaux! To those in Waterloo, thanks: Andrew, Zach, Aiat, Manal and Haleema! For the IDS-FunMat-ers, thanks to: Hanbin, Victor, Yi-Shiang, Sven, Mathilde (#1, #2, and #3), Margot, Gregor, Deniz, Daniel, Can, Begüm, Carole, Ara, Aline, Alina, Annie, and all past and present program-mates.

Finally, I need to thank all my friends and family members for being there and supporting me outside the academic world.

For my dear friends Carmen T., Matt E., Bryan I., Wesley W., Alex I., Alexandre I., Imran, Adam and David (that time in Spain!), Jeremy S., Alan W., Jason L., Felicia H., Mayinza (what would I have done without you in Bordeaux?!), Jonathan B., Nicolas, Keith P., Uzair C., Steven C., Claire L., Kwan, Simon T., Neelmoy, and many more, thank you for spending all that time with me the last 4 years; checking up on me, or letting me crash at your place (even if you were 9,000 km away)!

To my parents, Jing-Kun He and Zhen Hua Cao, I thank you both for raising me and supporting me no matter what decision I have made; from giving me the freedom in my undergrad to move around, to spending most of my graduate studies abroad, thank you! To my wonderful sister, Fanny Cao, your endless support no matter how ridiculous it was is a very big reason why I am here today. You were always making sure I was fine, mentally and physically, and would make time for me no matter how busy your hectic schedule got! Finally, to my dear partner Tadhg Mahon, thank you for being so supportive in my final PhD year. From all the trips, evenings out and in, to making sure I had company while I was working into the late night/early mornings, thank you for always being there for me!

Table of Contents

List of Tables

List of Figures

Abbreviations and Nomenclature

“Coating Onto” – Method developed to coat hybrid particles directly to a porous surface

“Grafting From” – Living polymer grown from the surface (Buchmeiser)

“Grafting To” – Living polymer attached to the surface (Buchmeiser)

ACN – Acetonitrile

AFM – Atomic Force Microscopy

APDEMS – (3-aminopropyl)-diethoxy-methylsilane

APTES – (3-Aminopropyl)triethoxysilane

ATRP – Atom-Transfer Radical Polymerization

C1-initiator – Bromo Methylpropanoate C1 Phosphonic acid (or Methyl phosphonic acid -2-Bromo-2-methyl propanoate)

C3-initiator – Bromo Methylpropanoate C3 Phosphonic acid (or Propyl phosphonic acid -2-Bromo-2-methyl propanoate)

CMS – Carbon Molecular Sieves

CO_2 – Carbon Dioxide

CTA – Cellulose Triacetate

CTI – Céramiques Techniques Industrielles

CTI porous tubes – Ceramic porous tube obtained from CTI

CTI-g-APTES – CTI porous tube grafted with APTES

CTI-g-APTES-PEO-NB – CTI porous tube grafted with APTES and functionalized with NB-PEO-COOH

CTI-g-APTES-PEO-NB* – CTI porous tube grafted with APTES and functionalized with NB-PEO-COOH activated with G1

Cu – Copper

DCS – Destablization of Colloidal Solutions

DEA – 2-(diethylamino)ethyl methacrylate

DEA – Diethanolamine

DLS – Dynamic Light Scattering

DMF – Dimethylformamide

DMSO – Dimethyl sulfoxide

DOPA – 3,4-dihydroxyphenylalanine

DP – Degree of Polymerization

Evonik particles – AERODISP® W740 X water based dispersion of fumed TiO_2 by Evonik Industries

FS – Fumed Silica

G1 – Grubbs First Generation Initiator

G2 – Grubbs Second Generation Initiator

G3 – Grubbs Third Generation Initiator

GHG – Green House Gas

Grubbs – another term used to defined G1 – Grubbs First Generation Initiator

HFBAA – 4,4'-(hexafluoroisopropylidene) diphenyl azide

HSC^+ - NASA used solid amine beads (mixture of liquid amine on solid polymer supports)

IPA – isopropanol alcohol

K_{ATRP} – apparent kinetic rate of ATRP

L or L_n – Ligand

M41S – Designation for family of mesoporous materials (includes MCM-41/MCM50, MCM48)

MCM-41 – Hexagonal phase of M41S mesoporous structure

MCM-48 - Cubic phase of M41S mesoporous structure

MCM-50 - Lamellar phase of M41S mesoporous structure

MEA – Monoethanolamine

MEK – Methylethylketone

MES Co – Mitsui & Engineering Shipbuilding Co.

MFI – a code name for ZSM-5 membrane

MMM – Mixed-matrix membranes

MSU-X – Michigan State University – X (material)

N_2 – Nitrogen

NaA zeolite – Zeolite structure with 4 Å diameter pores (modified to 3Å or 5Å pores by ion exchange with aqueous soltion of Ca or K salts)

NB-PEO-COCH$_2$CH$_3$ - α-norbornenyl-ω-ester poly(ethylene oxide)

NB-PEO-COOH - α-norbornenyl-ω-carboxylic acid poly(ethylene oxide)

NB-PEO-OH - α-norbornenyl-ω-hydroxyl acid poly(ethylene oxide)

NMP – Nitroxide Mediated Polymerization

NMR – Nuclear Magnetic Resonance

NO_X – Nitrogen oxide

p(PEGMEMA) – poly((polyethylene glycol) methyl ether methacrylate)

PDMS – polydimethylsiloxane

PEGMEMA – Poly(ethylene Glycol) Methyl Ether Methacrylate

PEO/PEG – Poly(ethylene Oxide)/Poly(ethylene Glycol)

PIM – Polymer of Intrinsic Microporosity

PMP – Poly (4-methyl-2-pentyne)

pNB – polynorbornene

PSA – Pressure Swing Adsorption

RAFT – Reversible Addition-Fragmentation chain-Transfer

ROMP – Ring-Opening Metathesis Polymerization

Ru – Ruthenium

S.S – Stock Solution (of hybrid particles in aqueous solution)

SEM – Scanning Electron Microscopy

si-ATRP – surface-initiated Atom-Transfer Radical Polymerization

si-NMP – surface-initiated Nitroxide Mediated Polymerization

si-ROMP – surface-initiated Ring-Opening Metathesis Polymerization

Sigma particles – Titania particles obtained from Sigma Aldrich (21 nm)

Silicalite-1 – zeolite structure of ZSM-5 made with no aluminum content (Al/Si ratio of 0)

SIP – Surface-Initiated Polymerization

SO_2 – Sulfur oxide

Sol-Gel – solvent-gelation method

TiO_2-g-APTES-PEO-NB – Titania grafted with APTES which was functionalized with NB-PEO-OH

TiO_2-g-APTES-PEO-NB* - Grubbs/G1 activated TiO_2-g-APTES-PEO-NB

TiO_2-g-ATPES – Titania grafted with APTES

TiO_2-g-C3-initiator – Titania grafted with C3-Initiator

TSA – Temperature Swing Adsorption

TWEEN – Corda’s brand name for polyethoxylated sorbitan esters

XPS – X-ray Photospectroscopy

Zeolite-A - a synthetic zeolite with very small pores – a LTA membrane, or Linde Type A (by Linde Division, Union Carbide)

ZSM-5 – Zeolite Socony Mobil: part of the pentasil family of zeolites (patent by Mobil)

List of Equations

Chapter 1

Equation 1-1: Fick's First Law

$$J = \frac{P\Delta p}{l}$$

where J is the flux, P is the permeability, Δp is the difference in pressure, and l is the membrane thickness

Equation 1-2: Permeability

$$P = D * S$$

where D is the diffusion coefficient, and S is the solubility coefficient

Equation 1-3: Ideal Selectivity

$$\alpha_{i/_j} = \frac{P_i}{P_j}$$

where 'i' and 'j' are the different gas components, P_i is the permeability for gas "i", and $\alpha_{i/j}$ is the ideal selectivity

Chapter 2

Calculations made for determining grafting density of C3-Initiator

1) **Determining the total number of C3-Initiator molecules:**

$$Total\ Molecules_{C3-Initiator} = \left[\frac{Mass\ Loss_{TiO_2-g-C3-Initiator} - Mass\ Loss_{TiO_2}}{Molar\ Mass_{degraded\ C3-Initiator\ group}}\right] x\ N_A$$

where:

- $Molecules_{C3-Initiator}$ is in the units "molecules"
- $Mass\ Loss_{TiO2-g-C3-Initiator}$ is in the units "g"
- $Mass\ Loss_{TiO2}$ is in the units "g"
- $Molar\ Mass_{degraded\ C3-Initiator\ group}$ is in the units "g/mol" (or 208g/mol)
- N_A is Avogadro's Number, which is $6.022x10^{23}$ molecules/mol

2) Determining the volume of Evonik particles:

$$Total\ Volume_{TiO_2} = \left[\frac{Mass_{TiO_2\ Initial} - Mass\ Loss_{TiO_2}}{\rho_{TiO_2}}\right]$$

where:

- $Mass_{TiO_2\ Initial}$ and $Mass\ Loss_{TiO_2}$ are in units of "g"
- ρ_{TiO_2} is the density of TiO_2, which is 4.23g/cm^3
- $Total\ Volume_{TiO_2}$ is in units of "cm^3"

3) Determining the volume of each Evonik particle:

$$Volume_{each\ TiO_2} = \left[\frac{4\pi r^3}{3}\right]$$

where:

- r is the radius of the TiO_2 particle, in units of "cm"
- $Volume_{each\ TiO_2}$ is the volume of each TiO_2 particle, in units of "cm^3"

4) Determining the total surface area of each Evonik particle:

$$Surface\ Area_{\ each\ TiO_2} = 4\pi r^2$$

where:

- r is the radius of the TiO_2 particle, in units of "cm"
- $Surface\ Area_{\ each\ TiO_2}$ is the surface area of each TiO_2 particle, in units of "cm^2"

5) Number of TiO_2 particles:

$$Number\ of\ TiO_2\ Particles = \frac{Total\ Volume_{TiO_2}}{Volume_{each\ TiO_2}}$$

where:

- $Number\ of\ TiO_2\ Particles$ is in units of "particles"

6) Dividing the Molecules of C3-Initiator by the Number of TiO_2 Particles:

$$\frac{Molecules_{C3-Initiator}}{TiO_2\ Particle} = \frac{Total\ Molecules_{C3-Initiator}}{Number\ of\ TiO_2\ Particles}$$

where:

- $\frac{Molecules_{C3-Initiator}}{TiO_2\ Particle}$ is in units of "molecules/particle"

7) To determine grafting density

$$Grafting\ Density_{C3-Initiator} = \frac{Total\ Molecules_{C3-Initiator}}{(Surface\ Area_{\ each\ TiO_2}\ x\ Number\ of\ TiO_2\ Particles)x\ 10^{14}}$$

where:

- $\frac{Molecules_{C3-Initiator}}{TiO_2\ Particle}$ is in units of "molecules/particle"
- $Grafting\ Density_{C3-Initiator}$ is in units of "molecules/nm^2"
- 10^{14} is used to convert cm^2 into nm^2

Chapter 3

In order to calculate the amount of DI Water to add to the system (to mix with PEGMEMA), the following calculation is performed (note: Units are matched with each variable):

$$Mass_{PEGMEMA}(g) = Molarity\ (M)x\ Volume_{Final}\ (L)x\ Molar\ Mass_{PEGMEMA}\ \left({}^{g}/_{mol}\right)$$

Which eventually becomes (if we assume the volume is 25 mL):

$$Mass_{PEGMEMA}(g) = Molarity\ (M)x\ 0.025\ (L)x\ 475\left({}^{g}/_{mol}\right)$$

$$\boldsymbol{Mass_{PEGMEMA}(g) = 11.875\ \left({}^{g\cdot L}/_{mol}\right) Molarity\ (M)}$$

With the total volume of DI water to add as:

$$Volume_{DI\ Water}(mL) = Volume_{Total}(mL) - \left(\frac{Mass_{PEGMEMA}(g)}{Density_{PEGMEMA}\left({}^{g}/_{mL}\right)}\right)$$

As the density is 1.08 g/mL and assuming the total volume remains as 25 mL, then:

$$\boldsymbol{Volume_{DI\ Water}(mL) = 25\ mL - \left(\frac{Mass_{PEGMEMA}(g)}{1.08\left({}^{g}/_{mL}\right)}\right)}$$

Equation 3-1: Kamlet-Taft Expression

$$\boldsymbol{XYZ = XYZ_0 + a\alpha + b\beta + s\pi^* + h(\delta_H)^2}$$

where XYZ is the redox potential, α is the solvent hydrogen bond donor ability, β is the hydrogen bond acceptor ability, π^* is the polarizability parameter and δ_H is the Hildebrand solubility parameter, which measures the solvent-solvent interactions interrupted when the solute forces a cavity formation. NOTE: XYZ_0, a, b, and h are solvent independent coefficients characteristic of the process and use of linear-regression (from the work of Braunecker *et al.* (2009) – reference 214) determined the following equation, Equation 3-2.

Equation 3-2: Modified Kamlet-Taft Expression

$$\boldsymbol{XYZ = -11.54 - 0.80\alpha + 1.83\beta + 1.72\pi^* + 0.011(\delta_H)^2}$$

where XYZ is the redox potential, α is the solvent hydrogen bond donor ability, β is the hydrogen bond acceptor ability, π^* is the polarizability parameter and δ_H is the Hildebrand solubility parameter, which measures the solvent-solvent interactions interrupted when the solute forces a cavity formation.

Calculation of Degree of Polymerization in si-ATRP:

A). Total Surface Area Calculation:

$$Total\ Surface\ Area = \left(\frac{3.14x10^{-10}\left(\frac{Mass\ Remaining_{TiO_2}}{\rho_{TiO_2}}\right)}{5.24x10^{-16}} \right) x10^{14}$$

Where the total surface area is in units of nm^2

B). Total Moles of Initiators Calculation:

$$Total\ Moles\ of\ Initiators = \frac{Total\ Surface\ Area\ x\ 2.55}{6.022x10^{23}}$$

C). Moles of Monomers:

$$Moles\ of\ Monomers = \frac{Mass\ loss\ of\ Polymer}{500}$$

D). Degree of Polymerization:

$$Degree\ of\ Polymerization = \frac{Moles\ of\ Monomer}{Total\ Moles\ of\ Initiators}$$

Calculation of the Conversion (%) in si-ATRP

1). Calculation of the Initiator used (in moles):

$$Moles_{C3-Initiator} = \frac{0.0122 x Mass_{Total\ TiO2_2-g-C3-Initiator\ Used}}{208\ g/mol}$$

- The 208 g/mol is the molecular mass of the C3-Initiator group that is degraded
- $Mass_{Total\ TiO2_2-g-C3-Initiator\ Used}$ is in units of “g”

2). Ideal Degree of Polymerization (if all monomers are consumed):

$$DP_{Ideal} = \frac{\frac{Mass\ of\ Macromonomer\ Used}{500\ g/mol}}{Moles_{C3-Initiator}}$$

- Mass of the Macromonomer is in units of “g”
- Degree of Polymerization (DP) is unitless

3). Conversion (ratio of ideal vs calculated DP):

$$Conversion = \frac{DP_{calculated}}{DP_{Ideal}}$$

Chapter 4

Grafting density calculation of Norbornenyl group (from NB-PEO-COOH)

1) Determining the total number NB-PEO-COOH

$$Total\ Molecules_{NB-PEO-COOH} = \left[\frac{Mass\ Loss_{TiO_2-g-APTES-PEO-NB} - Mass\ Loss_{TiO_2-g-APTES}}{Molar\ Mass_{NB-PEO-CO*}}\right] x\ N_A$$

where:

- $Molecules_{NB-PEO-COOH}$ is in the units “molecules”
- $Mass\ Loss_{TiO_2-g-APTES-PEO-NB}$ is in the units “g”
- $Mass\ Loss_{TiO_2-g-APTES}$ is in the units “g”
- $Molar\ Mass_{NB-PEO-CO*}$ is in the units “g/mol” (or 3723 g/mol)
- N_A is Avogadro’s Number, which is $6.022 x 10^{23}$ molecules/mol

2) Determining the number of NB-PEO-COOH per Evonik Particle

$$Molecules\ Per\ Particle_{TiO_2} = \left[\frac{Total\ Molecules_{NB-PEO-COOH}}{Number\ of\ TiO_2\ Particles}\right]$$

where:

- $Total\ Molecules_{NB-PEO-COOH}$ is in units "molecules"
- $Number\ of\ TiO_2\ Particles$ is in units of "Particles"
- $Molecules\ Per\ Particle_{TiO_2}$ is in units of "molecules/particle"

3) To determine the NB-PEO-COOH grafting density

$$Grafting\ Density_{NB-PEO-COOH} = \frac{Total\ Molecules_{NB-PEO-COOH}}{(Surface\ Area_{\,each\ TiO_2}\ x\ Number\ of\ TiO_2\ Particles) x\ 10^{14}}$$

where:

- $Surface\ Area_{\,each\ TiO_2}$ is in units "cm^2" (is $3.14x10^{-10}$ cm^2)
- $Grafting\ Density_{NB-PEO-COOH}$ is in units of "molecules/nm^2"
- 10^{14} is used to convert cm^2 into nm^2

Calculation the Degree of Polymerization of polynorbornene from si-ROMP:

1). Total Surface Area Calculation:

$$Total\ Surface\ Area = \left(\frac{3.14x10^{-10}\left(\frac{Mass\ Remaining_{TiO_2}}{\rho_{TiO_2}}\right)}{5.24x10^{-16}}\right) x10^{14}$$

- Where the total surface area is in units of nm^2

2). Total Moles of Initiators Calculation:

$$Total\ Moles\ of\ Initiators = \frac{Total\ Surface\ Area\ x\ 2.73}{6.022x10^{23}}$$

3). Moles of Monomers:

$$Moles\ of\ Monomers = \frac{Mass\ loss\ of\ Polymer}{94.15}$$

4). Degree of Polymerization:

$$Degree\ of\ Polymerization = \frac{Moles\ of\ Monomer}{Total\ Moles\ of\ Initiators}$$

"The light at the end of the tunnel is the headlamp of an oncoming train"
– Murphy's Law

Live for today
Ponder about tomorrow
but never dwell on the past!

General Introduction

There are currently an estimated 7 billion people on this planet, with that number projected to balloon to 9 billion people by 2050.[1] If this trend holds true, provided that no catastrophic events occur, then there will be a serious need for higher power production due to higher demand for energy within cities. A good example of this can be noted from Figure Intro-1 below:

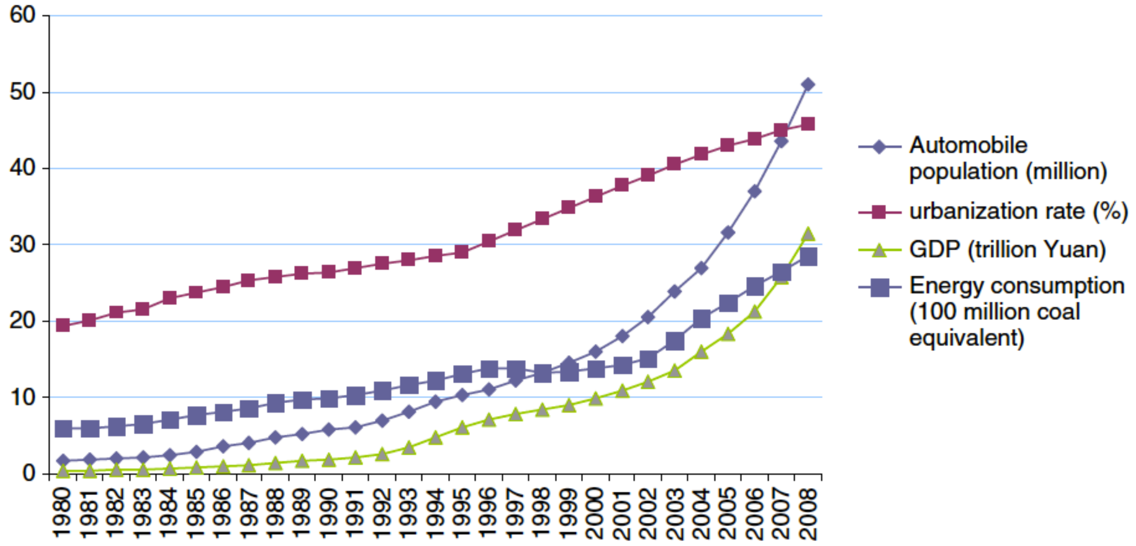

Figure Intro-1: Data on Automotive, Urbanization Rate, GDP (Gross Domestic Product), and Energy Consumption in China.[2]

Note the data indicates that with increasing population shift in China to more urban areas, the more drastic increases to the amount of energy is consumed. In most developing nations, this trend is true. Of particular interest for this correlation is the steady increase in energy consumption by the world, as seen in Figure Intro-2.

It is evident that the total energy consumption worldwide has been increasing for the past few decades. However, this increase in production has been primarily met by use of natural gas, oil, and coal type power plants. As a result of the ever-growing energy demands, there is need to find more sustainable forms of energy production compared to the current domination of power generated by non-renewable sources (ex: Fossil Fuels and Gas).

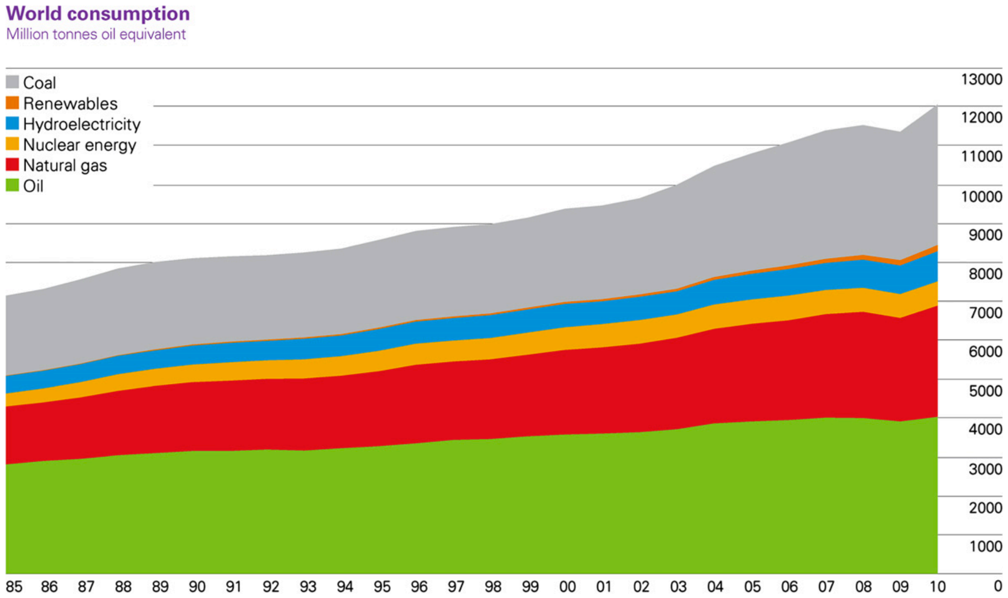
World consumption
Million tonnes oil equivalent

World primary energy consumption grew by 5.6% in 2010, the strongest growth since 1973. Growth was above average for oil, natural gas, coal, nuclear, hydroelectricity, as well as for renewables in power generation. Oil remains the dominant fuel (33.6% of the global total) but has lost share for 11 consecutive years. The share of coal in total energy consumption continues to rise, and the share of natural gas was the highest on record.

Figure Intro-2: Energy usage based on type of electric generation over time[3]

These older, dirty technologies are unfortunately the simplest to implement, and for developing countries that are experiencing economic boom (such as China and India), the use of fossil fuels may not be dropping anytime soon.

This fact leads to the point that as renewable energies are unable to completely replace the current use of fossil fuels, work still needs to be done to convert fossil fuel power plants into cleaner alternatives. With many more power plants polluting the atmosphere with higher concentrations of CO_2, NO_x and SO_2, there is a clear need to help prevent the release of these gases as to help prevent global warming.[4] As such, there is a need to make fossil fuels into a cleaner energy source.

The main objective of this thesis will be to provide the readers a look into the study of membrane materials; that one re-evaluate the use of membranes from just a purely inorganic perspective or organic/polymeric perspective, and imagine them in terms of hybrid materials. In this, we want to present a relatively regenerative method to quickly replace the polymeric portion of a selective membrane and thus form a regenerative (and scalable) system that can be easily (re-)applied.

In the **first chapter**, we will briefly go through the different methods of gas separation that exist, and evaluate why membranes are the best choice. Then, upon a brief literature search and background, we will evaluate the different forms of membrane materials and discover that functionalization directly from the inorganic component to form the organic (polymer) layer was the most ideal method of membrane formation.

Chapter two will dive into literature regarding the different forms of surface modification, focused on work that used anchoring groups, such as phosphonic acids and silane-based anchors. The substrates that will be first used in this study range from titania particles (Evonik particles and Sigma particles), flat titania surfaces, and CTI porous tubes. The modified titania surfaces will then be characterize using techniques such as XPS, TGA and NMR. The grafting density of each moiety will be determined and discussed.

Chapter three focused on the work of surface-initiated Atom-Transfer Radical Polymerization, or si-ATRP. Using the phosphonic acid functionalized titania surfaces (i.e. particles and flat substrates), si-ATRP was applied to form hybrid structures, and will be studied with the help of XPS, TGA and DLS.

Similarly, **chapter four** applied surface-initiated Ring-Opening Metathesis Polymerization (si-ROMP) on the silane functionalized titania porous supports and titania particles. Work for further functionalization of the silane-based titania was required; specifically the addition of a norbornenyl terminated group that could become the initiator in si-ROMP. XPS and TGA were also applied to study this polymerization technique.

Chapter five would apply the knowledge learned in the previous chapters to develop the two methods of ceramic tube modification – either through a "Grafting From" method, or a "Coating Onto" method. The "Grafting From" method would capitalize on the functionalized titania particles directly onto the CTI porous tubular surface. This would enable a polymeric film to be formed directly on the surface, utilizing either si-ROMP or si-ATRP techniques to accomplish this. The “Coating Onto” method utilized si-ATRP hybrid particles to directly coat and modify the interior ceramic tube surface to form the membrane.

In the final chapter, **chapter six** will briefly introduces the preliminary results with the two methods. The results are analyzed and recommendations are provided for improving the ceramic tube modification.

Chapter 1

State-of-the-art of polymeric and inorganic membranes for gas separation

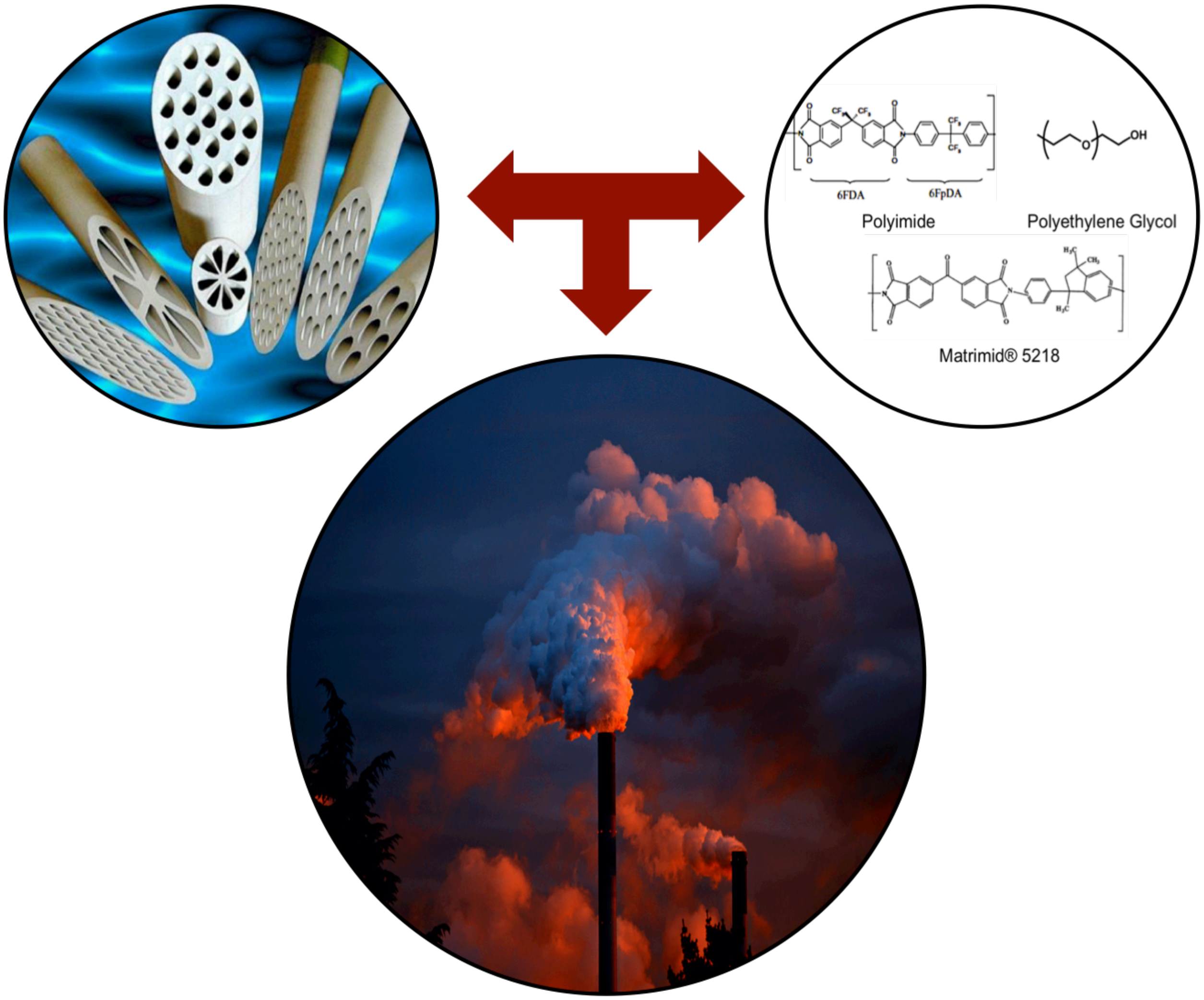

Figure displays the membrane types that can be used for CO_2 separation in flue gas. The arrows represent a combination and effect result

1.0 Target Problem

As we previously presented, the growing concern with the releasing of CO_2 into the atmosphere is an area of grave concern with respect to the environment. Notably, current estimated figures of between 20-30 billion tons of CO_2 are annually released into the atmosphere from power generation and industrial activities.[5,6] It is clear that the CO_2 emissions due to human activity have drastically changed over the years. Aaron *et al*. reported that 7 Gt of CO_2 was released annually in 2005,[7] while Favre in 2007 reported 20 Gt.[6] More recently, Du *et al.* reported 30 Gt estimate in 2010.[5] What seems clear is that the estimated figure of released CO_2 into our atmosphere is only increasing; a serious issue as the release of CO_2, a Greenhouse Gas (GHG) with a very long atmospheric lifetime of 100 years, is expected to contribute to the global increase in temperature in the long term (also known as "global warming").[4]

With this information in mind, it is vital that we reduce/mitigate the amount of this greenhouse gas released into the atmosphere. As previously shown, one of the most vital places of emissions are from coal and gas power plants. Since the world will not switch abruptly from fossil to non-fossil fuels, the next best alternative is to help reduce/eliminate the release of CO_2 into the atmosphere before it is released, and possibly inject this gas back into a recycling/production process. Taking this fact into consideration, we must consider the post-combusted exhaust gas, also known as flue gas, to be where we are to extract the target gas. However, it is also vitally important to understand what gases are present within this flue gas mixture.

Du *et al.* (2012) reported the typical composition of flue gas mixtures, as summarized in Table 1-1:

Table 1-1: Representative coal-fired flue gas composition versus normal atmospheric composition[5,8]

Gas	Concentration	Ambient Concentration
Carbon-Dioxide	12.5 %-12.8 %	0.03 %
Water (gas)	6.2 %	0-3 %
Oxygen	4.4 %	21 %
Carbon-Monoxide	50 ppm	1 ppm
Nitroxides	420 ppm	-
Sulphur-Dioxide	420 ppm	-
Nitrogen	76-77 %	78 %
Argon	-	0.9 %

Continuing from the report, there is typically a low-pressure difference (reported to be around 1.5 atm in the post-combustion gas) along with a somewhat high temperature (approximately 80 °C) found within the stream.[5]

1.1 Existing Solutions

There have been various methods of separation that have been explored and utilized over the years to help combat the issue of releasing this greenhouse gas into the atmosphere. While the list of methodologies can be extensive, one can narrow down the different removal techniques to: absorption, adsorption, cryogenic distillation and use of membranes.[6,7]

1.1.1 Absorption

CO_2 absorption can be achieved by two methods, either within a solvent/liquid route, or through a solid matrix route. In either case, the process requires CO_2 to be absorbed into the new medium at a higher rate than any other component present in the flue gas (such as nitrogen and oxygen).[7] The absorption method is a two-step process with successive absorption/desorption cycles, which means that the quantity of absorbing material usually has to be doubled to accommodate these cycles in a continuous absorption process.

1.1.1.1 Liquid Absorption

Perhaps the most commonly known system for absorption are amine-based scrubbers. As amine groups have a high affinity for CO_2, liquid absorption functions by using liquid amine to capture and transport CO_2. In this case, the liquid amine reversibly reacts with CO_2 to create an intermediate compound, ammonium carbamate.[9] Figure 1-1 below shows the general reaction of MEA (or monoethanolamine) with CO_2, provided the correct conditions are present for the absorption of CO_2:

$$\mathbf{CO_2 + R_2NH \rightarrow R_2NCOOH} \qquad \mathbf{(1)}$$

$$\mathbf{R_2NCOOH + R_2NH \rightarrow R_2NCOO^- + R_2NH_2^+} \qquad \mathbf{(2)}$$

Figure 1-1: Reaction of CO_2 with MEA to form Ammonium Carbamate.[10]

Once the reacted liquid is collected, it is then transferred to another chamber in which the reverse reaction is thermally induced. This thermal change results in the release of CO_2, which can be collected and stored as a high purity product.[7] Figure 1-2 below shows a typical system for chemical absorption systems (including amine scrubbers):

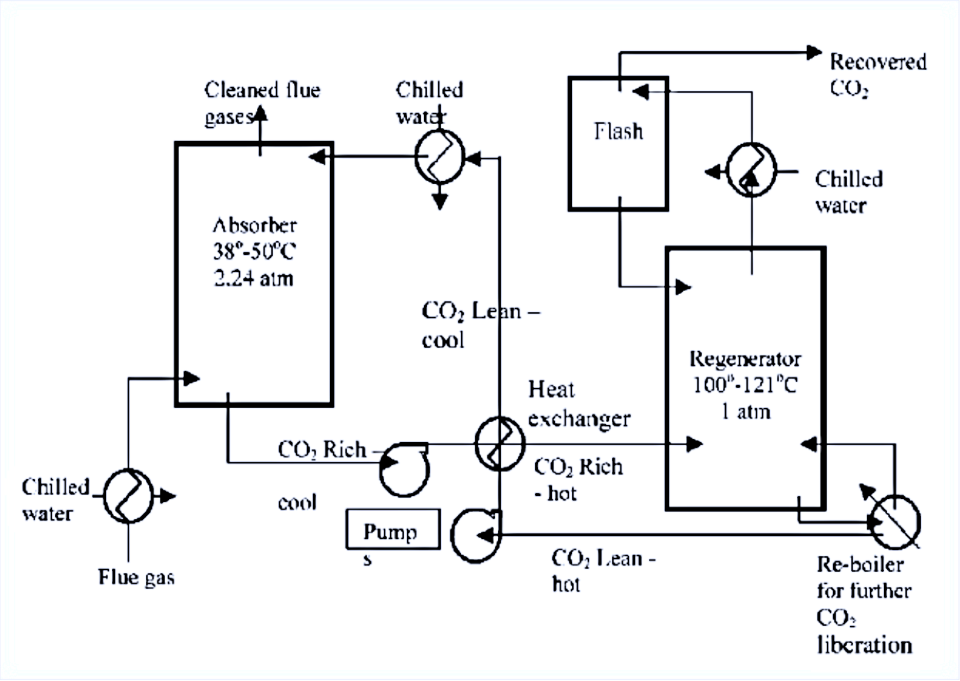

Figure 1-2: Typical chemical absorption system.[7]

From Figure 1-2, we see that the chemical absorption system represents a methodology of absorbing CO_2 into a liquid phase, and further transferred into another chamber for separation/solvent regeneration. Figure 1-2 is also noted for the case of MEA solvent, with an absorption temperature around 40-50°C and a higher stripping temperature for CO_2 (around 120°C).[6]

1.1.1.2 Solid Absorption

With solid absorption, the basic principle of removing CO_2 from the flue gas is the same as with liquid absorption, where compounds such as calcium hydroxide,[7] lithium hydroxide,[7,11] or solid amine (such as the HSC^+ solid amine beads, developed for space exploration use and used by NASA)[12] absorb the target gas, and is processed later to be released. However, some of these materials require higher temperatures with absorption and desorption, typically found to be 800°C and 1000°C respectively, which reserve these methods for some specific industrial processes where the flue gas is already at a rather high temperature. This usually results in much higher costs for implementation, but with the advantage of faster absorption and desorption of the solid absorbent.[7]

1.1.2 Adsorption

Unlike absorption, adsorption is a surface phenomenon with CO_2 being physisorbed onto the surface. Adsorption is restricted by the limiting factor of the specific surface area and diffusion within the porosity of a system, as opposed to the diffusion into the bulk of the system with absorption. In this case, the CO_2 from the flue gas system is adsorbed onto the surface of the system to be removed at a later stage. Materials such as zeolites, solid sorbents or mesoporous materials become essential due to their high surface area to volume ratio.[7,13]

There exist different methods of CO_2 adsorption, with Pressure Swing Adsorption (PSA) and Temperature Swing Adsorption (TSA) being two examples of this process that will be discussed.

1.1.2.1 Pressure Swing Adsorption (PSA)

PSA is a very simple process. The incoming flue gas is cooled and flows through filters, where CO_2 is adsorbed at a pressure of about 1 atm. The resulting exit gas should be very low in terms of CO_2 concentration. In the desorption part of this process, the material used for adsorption is then transferred to another chamber, where it is exposed to lower pressures (or vacuumed), and to a slightly higher temperature.[14] In an industrial process, there are two parallel chambers working alternatively in adsorption or desorption. Figure 1-3 shows some of the conditions that can be expected with PSA.

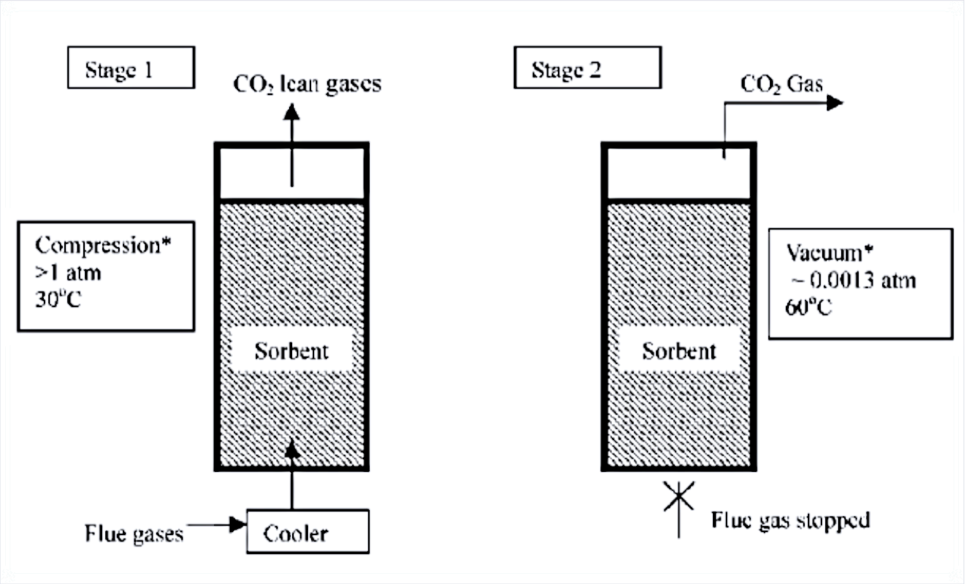

Figure 1-3: Two-step PSA system for adsorption and desorption of gas.[7]

The resulting released gas stream of rich CO_2 is then transported to a storage area.

1.1.2.2 Temperature Swing Adsorption (TSA)

Similar to PSA, TSA is primarily focused on loading of the target gas (such as CO_2) through alternating the temperature for the adsorption and desorption processes. In this case, the setup can be similar with the PSA system, but the release of the immobilized gas would require higher temperatures and the absence of pressure variations.[14]

1.1.3 Distillation

With cryogenic distillation, the input system is assumed to be free of contaminates and is preferably composed of only two gases with significantly different liquefaction temperatures. In the case of filtering out CO_2 from flue gas, the mixture of gases from the flue gas should be primarily N_2 and CO_2. Indeed, CO_2 deposits directly as a solid below 195 K, whereas N_2 liquefies at 77 K, unless the pressure increases. Subsequently, the mixture N_2 and CO_2 gas temperature is reduced until the CO_2 is liquefied (under pressure) and the resulting N_2 (which as a lower liquefaction temperature) is removed from the system. As reported, the point of interest for CO_2 is the triple point -56.6 °C,[7,15,16] and with a pressure of ~7 bars.[16] Figure 1-4 shows the phase diagram for CO_2 while Figure 1-5 shows the general assembly of the system for separation.

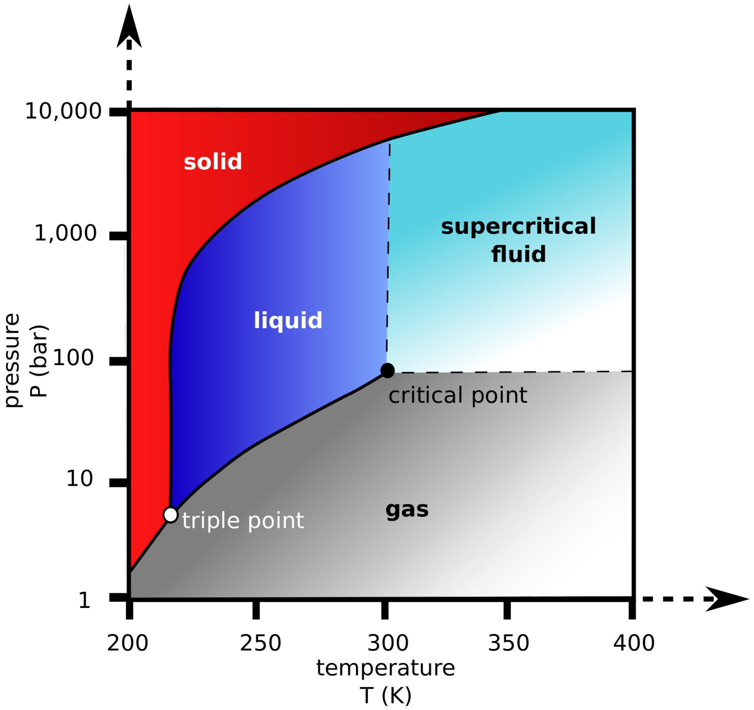

Figure 1-4: Phase diagram for CO_2. We can see the triple point of interest to be about ~210K (-57°C) and with a pressure 7 bar.[17]

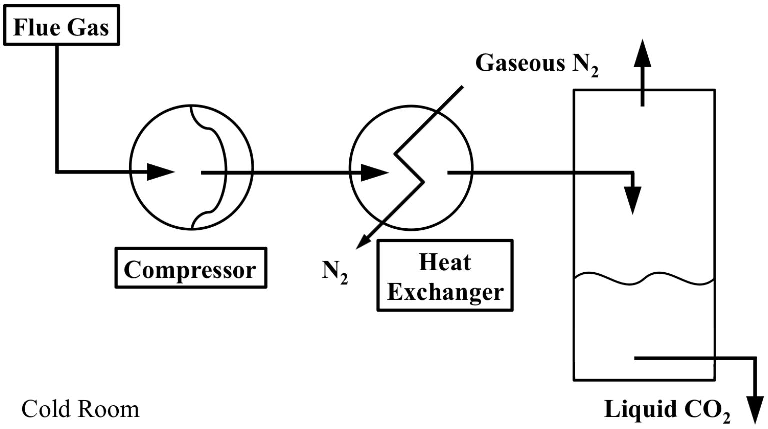

Figure 1-5: Cryogenic Distillation Process.[7]

It is important to highlight that while this process is quite energy intensive and somewhat harder to scale up/work with in high concentrations, there does exist the benefit of extracting extremely pure CO_2 (>99.9% purity), which is a clear asset for storage or reuse.

1.1.4 Membranes

Membranes are probably the most versatile systems available for gas separation. While there can be many different types of membranes, such as zeolites/mesoporous structures[18,19] or polymeric membranes,[5-7,19-22] they all still achieve the same process, based on selective permeability, of allowing certain gases to pass through the membrane, while retaining or preventing other gases to pass. A driving force always induces this separation mechanism, which is usually a pressure difference upstream and downstream of the membrane seen as a semipermeable medium. Selectivity toward one component can be increased if some chemical groups within the membrane (i.e. dense membrane), or on its surface (in the case of porous membranes) have specific interactions with one component of the gaseous mixture. Different geometries can exist, which we will described in section 1.3 Forms of Membranes.

The geometry selected for our study is a porous tube, with the flow (or feed gas) entering within the tube window. The upstream side of the membrane is where the feed gas first enters, and later becomes the retentate (or unfiltered portion of gas). As this feed gas gets filtered through the membrane walls to become the retentate, the gas composition recovered downstream (or outside the membrane walls) is called the permeate. For CO_2 separation, the membranes are preferentially designed to enrich the permeate in CO_2, as illustrated in Figure 1-6 showing the resulting case of gas flow.

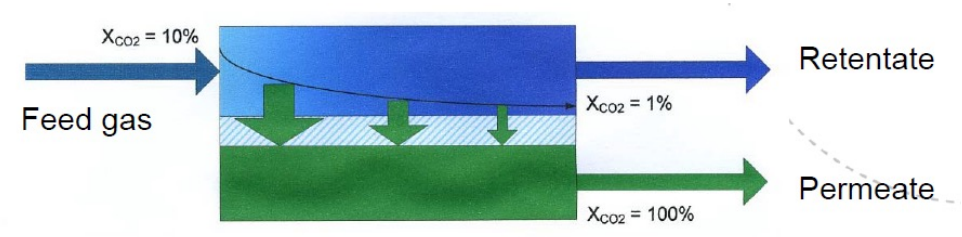

Figure 1-6: Representation of gas separation using membranes. The feed gas (flue gas) is passed through a tubular membrane (represented only one cross section), and the gas is separated through the membrane. Whatever is kept from diffusing through the membrane is now called the retentate, while the permeated gas is now the permeate.[23]

Most of the membranes for gas separation are dense membranes, named affinity membranes because one chemical group in the membrane displays a positive affinity toward one gas, which favours its diffusion, hence the membrane selectivity. To provide a significant flow per surface unit, the gas flow rate across the membrane, which depends on the pressure difference applied, is an important characteristic to be determined. In general, the method of characterizing this parameter is through considering the flux across the membrane as a function of the pressure difference and the permeability of the membrane. This property is described by the equation:

$$J = \frac{P\Delta p}{l}$$

Equation 1-1: Fick's First Law

where J is the flux, P is the permeability, Δp is the difference in pressure, and l is the membrane thickness. As seen in Equation 1-1, a reduction of the flux can be a result of (i) thick membranes, which is an manufacturing parameter, (ii) a reduction in permeability, which is a material parameter, or (iii) a reduction in the pressure difference, which is a process parameter. In this equation, the permeability is a value normalized to the membrane thickness. If not, which exists if the membrane thickness is unknown, one uses the “permeance” term. Since the permeability is highly relevant to the membrane material structure or composition, it is the one part that cannot be easily controlled in the physical design of the setup (considering pressure can be adjusted/controlled, as well as the membrane thickness during manufacturing); we note the permeability drop is the factor that will change. Permeability is taken into consideration through the equation:

$$P = D * S$$ **Equation 1-2: Permeability**

where D is the diffusion coefficient, and S is the solubility coefficient.[24-26] This relation is important as the coefficients take into account the nature of the gas, and its interaction with the membrane material. Specifically, "D" is determined by the type of diffusion across the membrane (i.e. either by Knudsen diffusion or the solution-diffusion method as discussed in the next section). This parameter is related to the gas interaction with the membrane surface while the "S" parameter is due to ability of the gas to solubilize and pass through the membrane.

This relation further gives rise to the concept of "ideal selectivity" when we compare the permeability of a membrane for different gases. Ideal selectivity has been defined as:

$$\alpha_{i/j} = \frac{P_i}{P_j}$$ **Equation 1-3: Ideal Selectivity**

where 'i' and 'j' are the different gas components, and $\alpha_{i/j}$ is the ideal selectivity. Equation 1-3 does not describe the actual or optimal selectivity of a membrane, but instead the ability of the membrane to separate two different gases. It is usually used as a membrane performance descriptor, when it should be better used as a material parameter.

From this equation 1-3, we can quantify the selectivity of the membrane material toward one gas from another, which is an important parameter to further assess the membrane selectivity. For instance, if the permeability of CO_2 is 100 times greater than the permeability of N_2, then the ideal selectivity of the membrane is 100, and we can state that the material has an affinity for CO_2 100 times higher than for N_2. Therefore, the ideal selectivity is a key parameter when considering materials for gas separation, and a key reason to characterize the permeability (factors affected by sample thickness, diffusivity and flux).

Looking into literature regarding this ideal selectivity factor (α), the work by Robeson[27,28] shows perhaps the most fundamentally important graph for any researcher in the membrane field. Dubbed the "Robeson Curve", this "theoretical empirically determined upper bound" for a membrane's physical properties for gas separation exists when comparing various gases. As mentioned by Robeson, the first data collected regarding CO_2/N_2 separation did not yield enough points to establish a good fit however, the updated data points were able to establish a relation,[28] as illustrated in Figure 1-7.

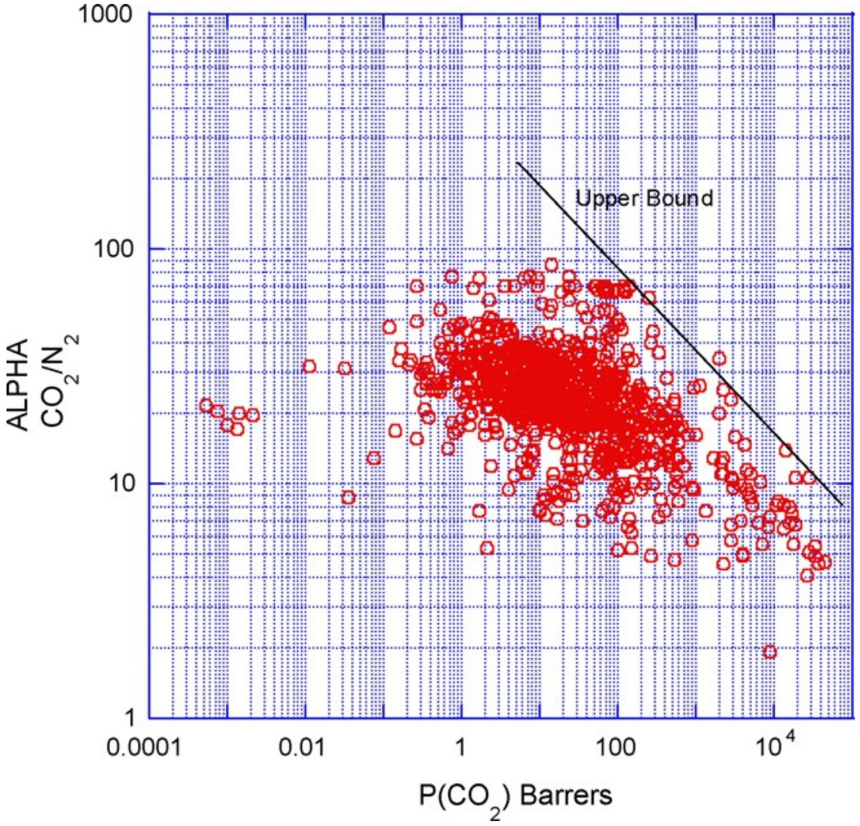

Figure 1-7: Robeson updated upper bound curve for CO_2/N_2 (Selectivity vs. Permeability of CO_2).[28]

Perhaps more notable are the polymeric membranes of the polymer of intrinsic microporosity (PIM) that were mentioned by Budd *et al.* with a selectivity for CO_2/N_2 around 25-26,[29] to the work by Orme *et al*. on phosphazene membranes that led to a separation factor around 62.[30]

It is important to note that there are several methods of gas separation based on the way the membrane is structured. For the purpose of this report, the 'simple' sorption diffusion membranes will be reported. This is also known as polymeric solution-diffusion, molecular sieving, and selective surface flow[23,31]. Table 1-2 summarizes each type of separation presented.

Table 1-2: Types of separation in membranes (simple sorption-diffusion membranes).[31]

Type	Typical Features of Current Primary Membrane Types
A. Asymmetric polymeric solution-diffusion	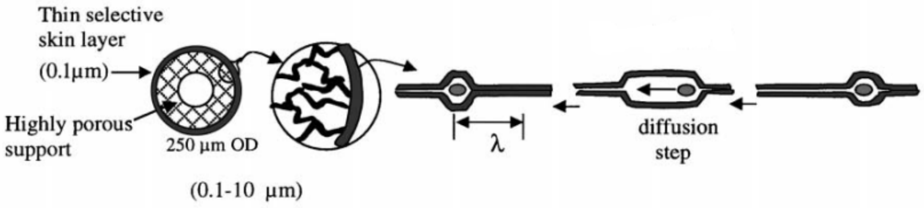
B. Molecular sieving (zeolite or carbon)	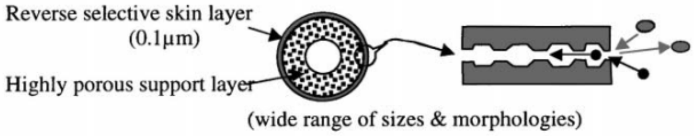
C. "Reverse selective" surface diffusion	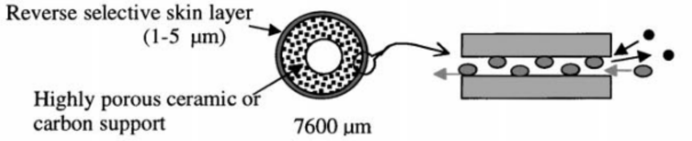

1.1.4.1 Polymeric Solution-Diffusion model

In this model, the membrane is primarily polymer based, where the diffusing solute (or gas particle in this case) travels through a dense polymer layer in a two-step process. The solute/gas molecule first is absorbed by the membrane material, and is thus able to solubilize within the polymeric matrix. Upon an applied force (in this case, pressure gradient), the gas molecule is pushed to the opposite end of the membrane (or lower pressure side) to be desorbed. This can be a somewhat complex scenario as the polymer layer can be in crystalline or amorphous form. In the case of crystalline form, as the polymer is extremely dense and highly organized, the flux through the membrane is reduced,[24] hence the permeability of the membrane.[24,25] With amorphous or semi-crystalline polymer chains, a higher permeability is observed as a result of the lower density chain packing. Thus, crystallinity can effectively lower permeability and potentially affecting the selectivity. The chemical properties, besides the polymer backbone organization, can also affect the permeability of the target molecule for separation, if certain chemical/functional groups have an affinity toward one gaseous molecule. This will be discussed in section 1.3.1 Polymer Based Membranes.

1.1.4.2 Molecular Sieving

With molecular sieving, the sample passes through a microporous structure. The actual molecular sieving mechanism requires the porosity to be well calibrated, thus zeolite structures, which are crystalline microporous architectures, are the best candidates. Zeolites or similar molecular sieves (aluminosphates, gallophosphates) are obtained by the crystallization of an inorganic framework around a given molecule. It is worth mentioning that some zeolites are also natural minerals.[32] In this respect, we note that from Table 1-2, the separation of the gas molecules are completely based on size, and that the ability for one particle to pass is due to the pore size (which can restrict the passage of the molecule through the framework).[7,18,31] Thus, provided that there is simple diffusion of the gas (or there is a higher driving force created by a pressure differential), the molecular sieving system can separate based on size, leaving larger molecules within the retentate.

1.1.4.3 "Reverse Selective" surface diffusion

From this method, a microporous structure is used to separate gas molecules.[23] The idea of separation is reversed in the sense that the larger particles are able to pass through the pores as there is higher selectivity for the larger particle. At the same time, the smaller particles tend to remain within the retentate, as they're unable to transport along with the larger particles across the pore. As mentioned by Merkel *et al.*, the selectivity equation is a ratio between two gases solubility and diffusivity.[33] In general, as the particle size increases, the solubility increases.[34] However, the diffusivity decreases in parallel, as was illustrated by the permeability equation (Equation 1-2).

From this relationship, we can see that it is possible to cater a polymer that has a higher solubility for a large molecule when compared to a smaller molecule, thus effectively creating a separation based on size.[33]

1.2 Analysis of Separation Technologies

By comparing the presented four methods of CO_2 gas separation, we can assess the possible solutions to be implemented for our project. Table 1-3 below summarizes some of the advantages and disadvantages of the methods.

Table 1-3: Advantage and Disadvantage for various gas separation methods[7]

Method	Advantage	Disadvantage
Absorption	-Versatility (both liquid and solid together cover a wide range of concentrations)	-Cost of maintenance -High Energy input due to heating
Adsorption	- Use of more resistant materials for adsorbing gases	-Low throughput and deals with lower concentrations (0.04-1.5%)
Cryogenic Distillation	-High purity of CO_2 extracted (>99.9%)	-Energy intensive -Low throughput in continuous large scale applications
Membranes	-Simplest system to implement without specialized equipment (compared to other options) -Variety of polymers to select from to improve selectivity	-If selectivity increases, permeability decreases (due to denser membranes) -Resistance to corrosion and high temperatures (if polymer) -Developing large surfaces of defect-free membranes is technically challenging

Expanding on the description for Table 1-3, problems exist for each method of implementation. With absorption, while there is a high versatility with the different solvents and even solid absorbers, there is a large capital and maintenance costs as, impurities formed by the amine-based reactions can occur (ex: sulphites and nitrites), resulting in precipitate formation and loss of amine-based solvents. There is also the case of corrosion caused by the build-up of CO_2 in the liquid phase, to produce a more concentrated and acidic solution.

In the case of adsorption, the most effective method would probably be pressure swing adsorption (PSA).[15] However, this method is suited in handling up to 1.5% of CO_2, and cannot handle the flue gas CO_2 concentration, which is equal to about 13%.

Cryogenic distillation is a well-mastered industrial process, and it can yield extremely high purity of CO_2 extracted. However, it greatly suffers from being the most energy intensive method due to the pressure and temperature shifts that are required for the process, and still barely compatible with large flue gas volumes.

Membranes appear to be the simplest technology to implement as the main components consists of a compressor, the membrane and some fans.[7] However, the membranes themselves suffer from a trade-off between selectivity and permeability that must be optimized, along with issues in material manufacturing. We can also note that there is still place for material -or combination of- developments able to meet requirements in both selectivity and permeability.

Considering the work and assessment that Aaron (2005), Favre (2007) and José (2008) have stated and made, it is clear that while there are many advantages to the current realm of liquid scrubbers utilizing amine solvents, membranes are an attractive option for gas separation. Membranes are extremely versatile when utilizing different polymers for selectivity, and fewer requirements for specialized equipment.[5,7] Their success will be demonstrated if high performance materials can be used for large surface membranes at a competitive manufacturing cost, along with a suitable lifetime against corrosive flue gas, or the insertion of a pretreatment stage before the membrane.

1.3 Forms of Membranes

From our literature search, a series of membranes were found to target post-combustion scale separation. Such membrane functions can be categorized into several areas, which range from passive to facilitated/active transport. As we are aiming towards membranes of the passive nature in this work, we will briefly touch upon the different membranes that are composed of polymeric materials, inorganic based membranes, and the mixed-matrix membranes.

1.3.1 Polymer Based Membranes

When considering the different types of polymers that are possible for use, a good resource would be to refer to the paper by Du *et al.* (2012),[5] which provides a very good summary of the different polymer options available for use in membranes for CO_2 separation. However, as there is a plethora of polymers used for CO_2 separation, we will focus only on several types of polymers including: polyimide, amine exposed polymers, poly(ethylene glycol)/poly(ethylene oxide), polysulfones, and cellulose acetate.

1.3.1.1 Polyimide

Polyimides are polymer structures formed by the reaction of a carboxylic anhydride with an amine to form one repeating monomer unit (note that each molecule must posses either two carboxylic anhydride groups or two amine groups for the molecules to create a repeating polymer chain). Figure 1-8 below shows the general form of the polyimide:

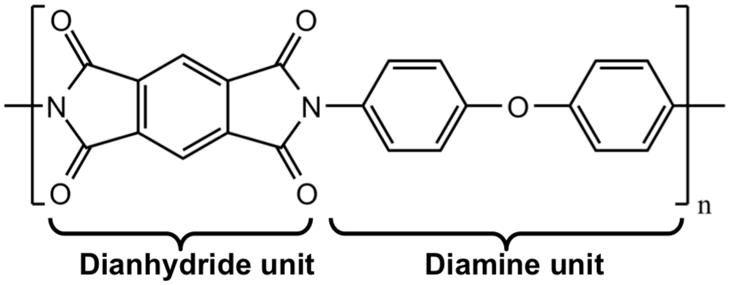

Figure 1-8: Polyimide structure formed from a dianhydride unit reacted with a diamine unit.

The material has been reported to be attractive in the sense of its high robust mechanical properties,[35] including thermal stability and chemical tolerance.[5] While this material is very strong, it has been shown that interaction with CO_2 can cause the membrane to swell and plasticize, which increases the permeability for all gases over time.[5] However, side groups have been crosslinked to help maintain the formed polymeric channel across the membrane, and subsequently help increase the selectivity of CO_2.[35]

Probably the most well known membrane within the polyimide realm are the Matrimid® membranes, with a significant selectivity for CO_2/CH_4 and CO_2/N_2, equal to 36 and 31, respectively.[36] The typical structure of this commercially available (albeit expensive) membrane is given in Figure 1-9.

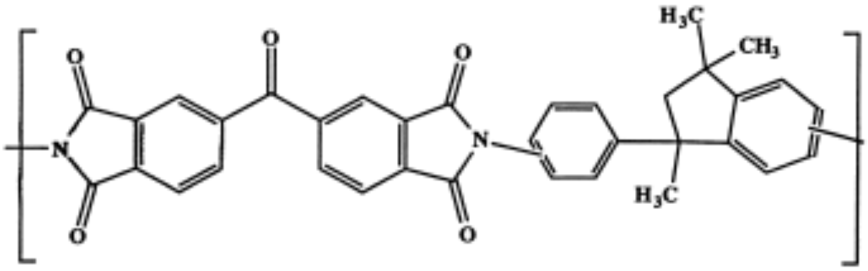

Figure 1-9: Chemical structure of Matrimid® 5218.[37]

1.3.1.2 Amine exposed Polymers

Amine exposed polymers come in a variety of shapes and sizes. In this case, these polymers exist with functionalized or exposed amine groups that can interact with the target case (i.e. CO_2). Considering that with the method of transport found in absorption using solvents like MEA and DEA (diethanolamine), the expectation is that such exposed groups can also interact similarily with the target gas. In this case, such groups have the ability to attract and convert CO_2 into a carbamate complex. The subsequent addition of water will produce a bicarbonate group that can be removed, or reversibly regenerate CO_2 if water is removed from the system. This reversible reaction enables the release of CO_2 for storage elsewhere. This means that these membranes can only work in presence of water vapor, and that laboratory tests with dry gases do not give a good representation of their intrinsic performances. Figure 1-10 below shows the schematic:

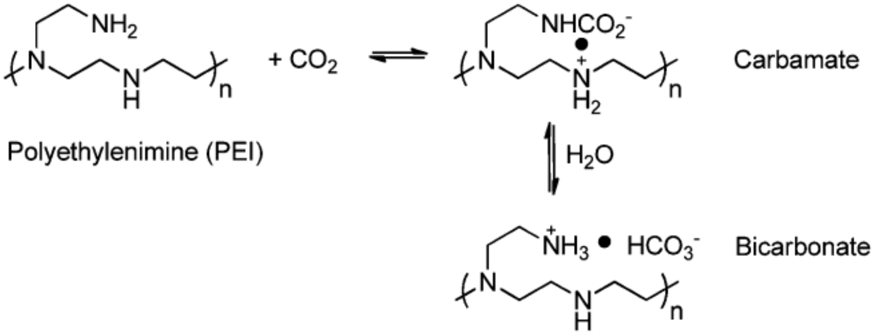

Figure 1-10: Schematic of polyethyelenimine reaction with CO_2.[38] Note that the exposed amine group is the portion involved with interacting with the CO_2. Reprinted (adapted) with permission from reference 38. Copyright 2011 American Chemical Society.

In another case, polyvinylamine can under a similar process. Figure 1-11 shows the reaction of polyvinylamine with CO_2.

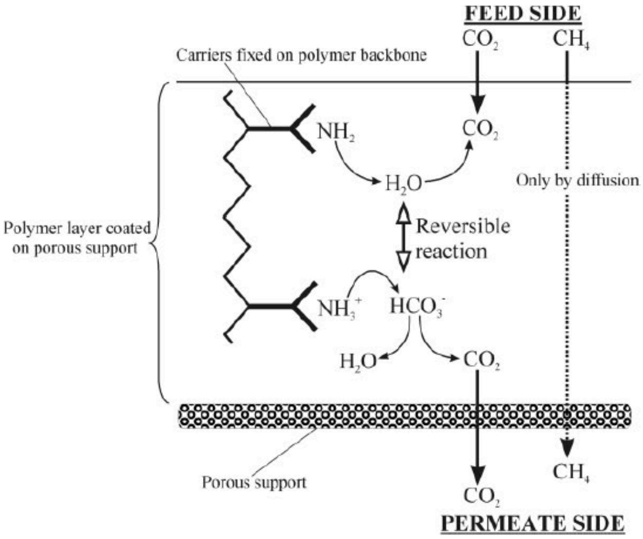

Figure 1-11: Method of transport of CO_2 across a polyvinylamine containing membrane.[39]

The immobilized amine group helps to convert CO_2 from the feed side into a bicarbonate molecule and eventually regenerates the CO_2 on the permeate side.

1.3.1.3 Polyethylene Oxide/Polyethylene Glycol

These polymers represent a carbon backbone chain with embedded oxygen molecules that alternate within the polymer backbone. The structure of poly(ethylene glycol) can be seen from Figure 1-12.

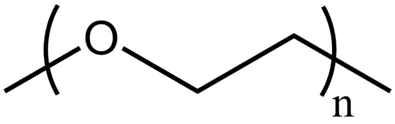

Figure 1-12: Poly(ethylene glycol) polymer chain structure

While the oxygen molecules do not chemically alter the form of CO_2 in the same way as the amine groups to help facilitate diffusion, the high performance of these membranes are attributed to the high affinity of CO_2 with the polar oxygen molecule.[5,24] This enables the CO_2 to be attracted to the membrane and subsequently diffuse through the membrane to permeate.

One of the first commercially available products for this type of polymer, Pebax® membranes were invented/sold by Atochem[40], currently part of Arkema. In this product, the structure is comprised of a block copolymer of one portion polyamide and another portion of poly(ethylene glycol),[41-46] which can yield an expected separation factor of CO_2/N_2 from 40 – 55.[42,44] This structure can be seen in Figure 1-13.

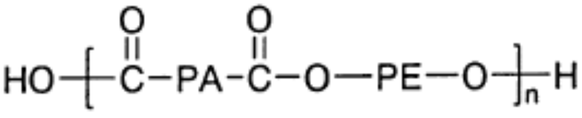

$$\mathrm{HO}\left[\overset{\overset{\displaystyle O}{\|}}{C}-\mathrm{PA}-\overset{\overset{\displaystyle O}{\|}}{C}-O-\mathrm{PE}-O\right]_n\mathrm{H}$$

Figure 1-13: Chemical structure of Pebax - PA = Polyamide, PE = Polyether/Polyethylene Oxide.[46 45]

1.3.1.4 Polysulfone

Polysulfones are perhaps one of the most chemically stable membrane material one can achieve.[47] Thanks to its ridged backbone structure, as noted from the many phenyl groups present in Figure 1-14, the structure provides limited mobility. This gives polysulfone membranes their high stability, strength and rigidity.[48]

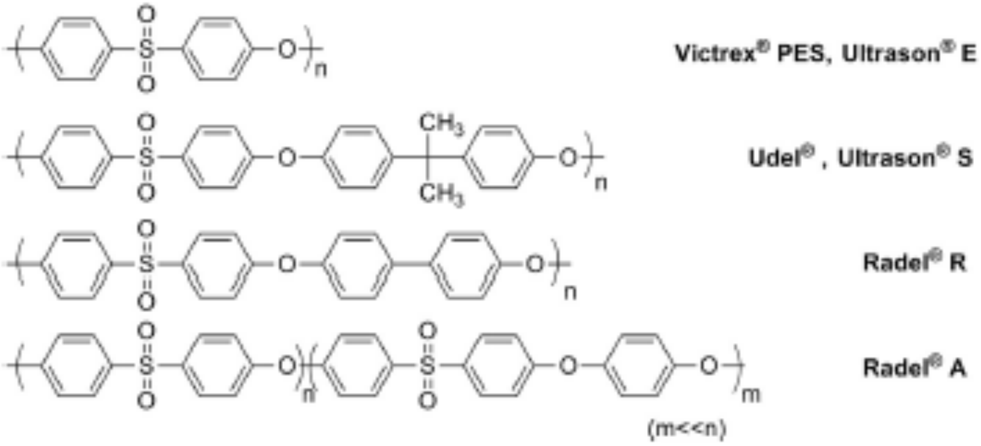

Figure 1-14: Polysulfone based membranes on the market.[47]

Found readily in industry with the aforementioned product names,[49] Figure 1-14 shows polysulfones membranes currently available. However, it was Monsanto in the 1980's that were able to produce the first large-scale polysulfone membrane system, which utilized an asymmetric hollow fiber structure with a silicone coating. This process helped to seal the membrane in case of cracks or pores formed.[50]

Due to the high packing factor and subsequently low free volume within the polymer structure,[51] polysulfones are known for their higher separation factors for H_2 when compared to CO_2. This makes them less ideal for CO_2/H_2 separation, but has the potential to be adapted for used in syngas.

1.3.1.5 Cellulose Acetate

Cellulose Acetate films were first commercially manufactured on a large scale thanks to Loeb and Sourirajan.[52] These films can be considered the birth of modern day membrane technologies.[25] Their composition is displayed in Figure 1-15.

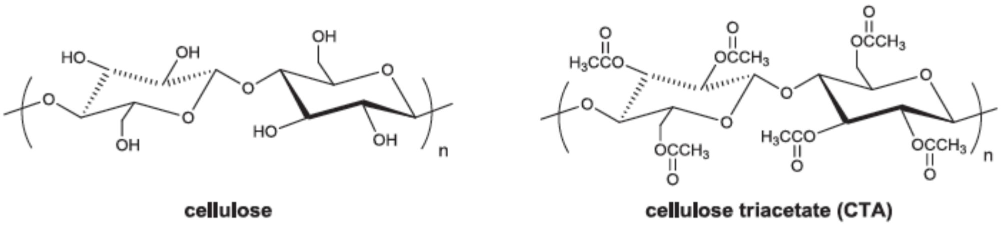

Figure 1-15: Structure of cellulose and cellulose triacetate (CTA) [47]

One route to achieve cellulose acetate is to functionalize cellulose via acetic anhydride mixed with sulfuric acid.[53] Their original use were first made as desalination membranes, as shown by the early work of Loeb and Sourirajan.[52,54] However, they slowly trickled into use for other separation of gases, primarily due to their low cost and abundance for synthesis compared to other commercial membranes.[55]

1.3.1.6 Processing of Membranes

Independently from their chemical nature, as described above, polymeric membranes are often prepared by the process of phase-inversion.[52] Indeed, what is often named as the “loeb-sourirajan” membranes, have been the best scalable method to form the asymmetric membranes that yield higher selectivity factors/values. Therefore, this principle has been adapted towards the formation of membranes.

1.3.1.6.1 Film formation – Phase Inversion

The principles of phase inversion film formation are summarized in this section. With the information known from the first patent filed on large scale production of cellulose acetate membranes,[52] this process has been easily transferred to other polymeric materials with ease of film formation.[47] The basic principles follow as shown in Figure 1-16 and Figure 1-17.

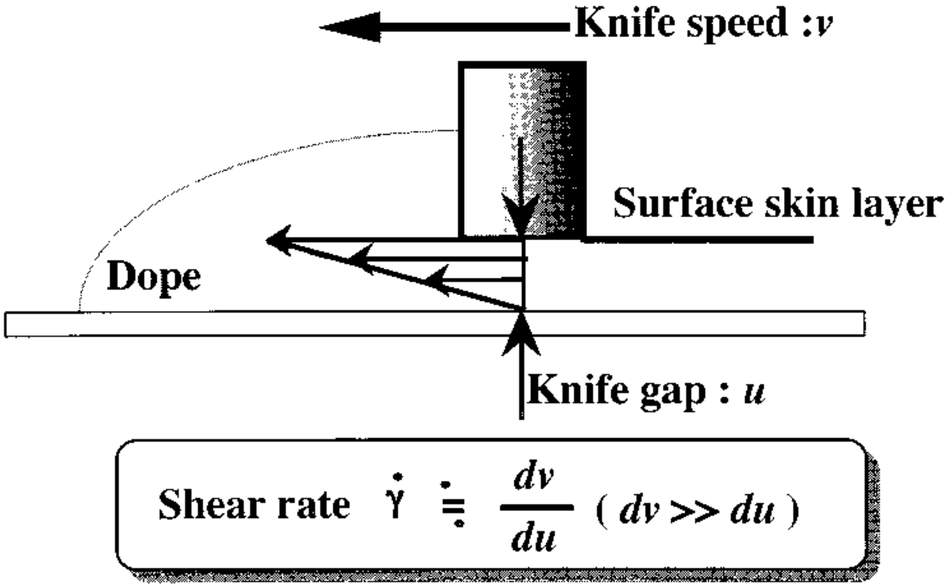

Figure 1-16: Doctor-blade method to form thin film membranes.[56] Reprinted (adapted) with permission from reference 56. Copyright 2001 American Chemical Society.

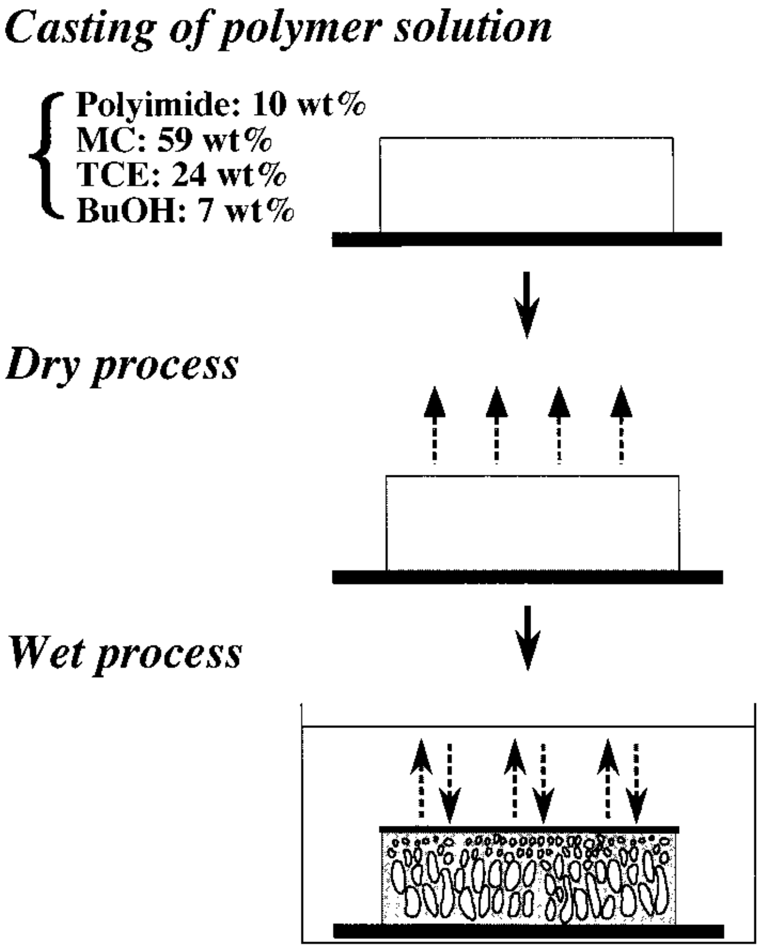

Figure 1-17: Dry-Wet Phase Inversion process as outlined by Niwa *et al.*[56] Reprinted (adapted) with permission from reference 56. Copyright 2001 American Chemical Society.

From these figures, we note that the formation of film is controlled first by the thickness made through the doctor-blade method. Subsequently, the film is dried in air (or oven) until the first solvent is removed, and then placed into a bath of another solvent that reduces the rate of evaporation in the membrane, forming the asymmetric membrane structure.[56]

1.3.1.6.2 Hollow Fibers via Extrusion

The formation of hollow fibers was first commercially developed by DuPont,[57] and has sevolved into a much more stream-lined system. More current day systems are similar to the setup found in Figure 1-18.

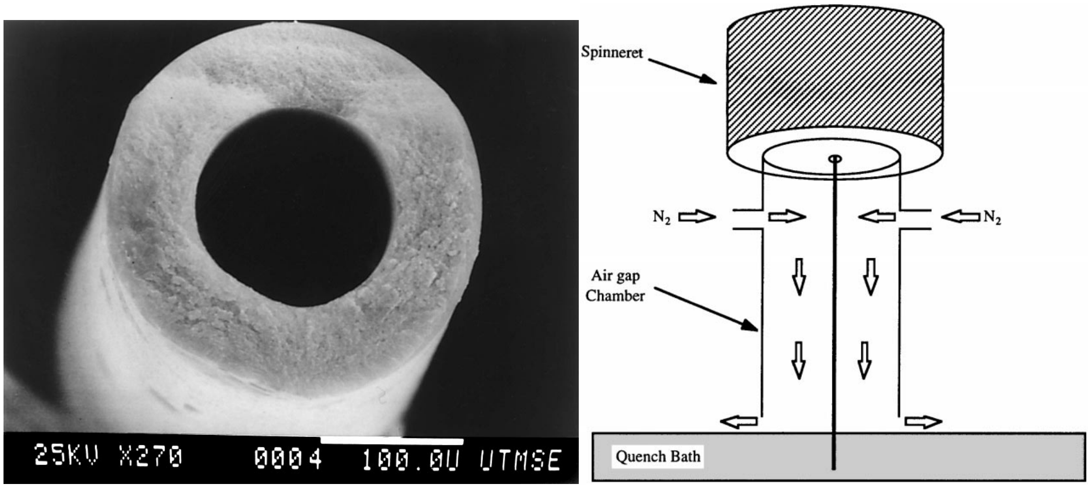

Figure 1-18: Left: Hollow fiber formed from extruding unit (on Right). The extruder found at the top can push out the polymer mixture and subsequently dry during droping to quench and form the asymmetric membrane structure found with the phase-inversion membranes.[37]

The setup entails that a precursor of polymer melt is mixed with a solvent (not the same as the quenching bath), and extruded through the nozzle to produce a continuous and controlled hollow fiber. Inert gas is blown to help the hollow fiber dry before entering the quenching bath (or the wet-phase noted in the phase inversion method).

One can easily draw similarities between both processes, as they involve the same mechanism of dry-wet phase inversion, making the contribution Leob and Sourirajan vital in the realm of large-scale polymer membrane production.

1.3.2 Inorganic Membranes – Metal Oxide Supports

Metal oxide based inorganic membranes have been extensively researched, particularly by Larbot and his group at Montpellier (France). Larbot and his colleagues have shown that there are three pathways in which one can synthesize or modify inorganic membranes, as illustrated in Figure 1-19.

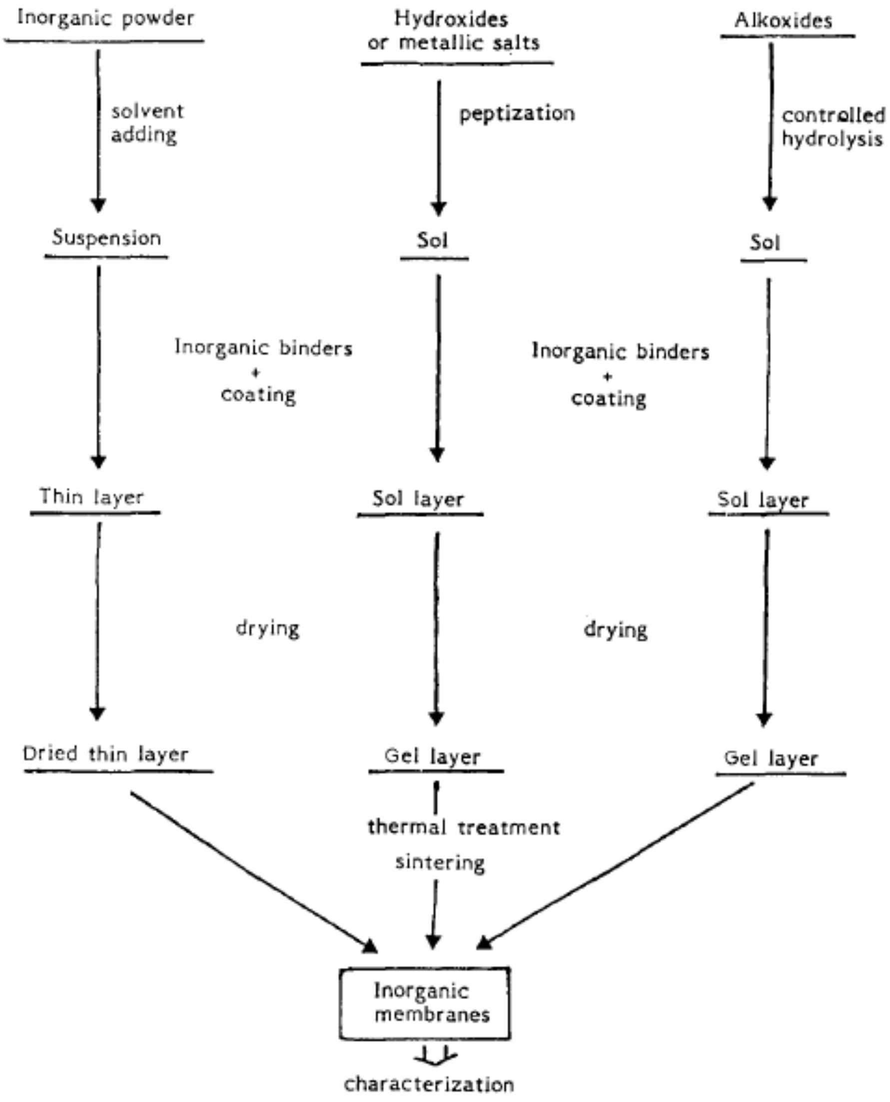

Figure 1-19: Three synthesis pathways to obtaining inorganic membranes: using inorganic powder, use of metal salts or hydroxides, or use of alkoxides.[58]

As Figure 1-19 suggests, there are three options for making inorganic membranes. The first column shows that existing inorganic powder can be suspended and ultimately be coated to form the bulk of a membrane (albeit use of a mold is required). The remaining two methods are sol-gel based methods; metallic salts or alkoxides can undergo the sol-gel (or solution-gelation) process to form the inorganic membrane. These methods, while capable of making full membranes themselves, are usually applied to existing porous tubular or flat substrates made by usual ceramic processes. Their applications towards surface modification are achieved by layer-by-layer coating from a slurry using to the engobe (or slip-cast) technique. The membranes substrates are synthesized through methods such as dry-pressing, paste processing, or agglomeration of colloidal particles (Table 1-4).[59]

Table 1-4: Influence of homogeneity on the properties of inorganic membranes[59]

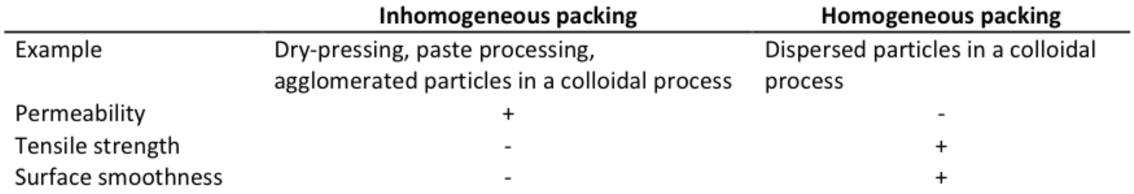

	Inhomogeneous packing	Homogeneous packing
Example	Dry-pressing, paste processing, agglomerated particles in a colloidal process	Dispersed particles in a colloidal process
Permeability	+	-
Tensile strength	-	+
Surface smoothness	-	+

We see that with this larger scale processing of membrane substrates, rougher surfaces are formed. Fortunately, these defects are usually repaired/eliminated by the sol-gel coating that can complement these properties by being more resistant to cracks and providing a smooth surface to work with (note the column “homogenous packing”).

Unlike polymer membranes, ceramic membranes are more resistant to chemical attack and particle attrition, which makes them suitable for treatment of industrial effluents. They can also withstand the counter-flushing process for decontamination and unclogging due to surface solute build-up. In other applications like water treatment or possibly gas separation, they can compete with polymer membranes if their longer lifetime balances their higher manufacturing cost. It is important to note that when using such inorganic membranes, the application must always be the first question to ask. As the structure of the different types of membranes yield different pore sizes, knowing the final use is vital. For instance, the first method of using inorganic particles to form the membrane yields pores from 100 nm to 1 µm (thus forms a microfiltration membrane). The two sol-gel methods yield pore sizes from 1-100 nm, thus are used for ultrafiltration applications.

1.3.2.1 Examples of Metallic Salt Sol-Gel Route

As noted in Figure 1-19, there are generally three pathways to prepare ceramic membranes. In this example, we will describe the metallic salt route as the synthesis pathway involving inorganic powders are relatively straightforward, and those involving alkoxides (while interesting) are beyond the scope of this current study. In the metallic salt route, also known as DCS (destabilization of colloidal solutions), a metal salt is dissolved in a liquid media with an electrolyte that can stabilize the precipitate into a colloidal suspension (also known as peptization). The control of this step is vital, because metal salts can hydrolyze rapidly upon uncontrolled pH change, and precipitate out of solution. Once particles form, it is important to prevent them from aggregating by combining their surface charge with an electrolyte that can create a repulsive shield between particles (forming a electric double layer) to keep the particle suspension dispersed. If the solvent (in this case is water) is progressively removed by evaporation, proximity between particles decreases and the repulsive double layer cannot prevent these particles from coming into contact thus creates a gel made of aggregated particles. However, it is important to highlight that this gel is a physical gel. Unlike chemical gels that form covalently linked networks, physical gels that are redistributed into a solvent will partially redisperse and “break” the gel. As the forces keeping the gel together are physical interactions, thermal treatment (i.e. sintering) will help form grain boundaries between the particles, and form a more solid structure.

When colloidal suspensions are used for the preparation of porous coatings, the dehydration process leading to DCS results from water diffusing through the porous ceramic substrate. This process leaves behind a “cake” of aggregated particles coated onto the substrate surface to form the final coating. In the work presented by Larbot (Figure 1-20) we visualize this process.

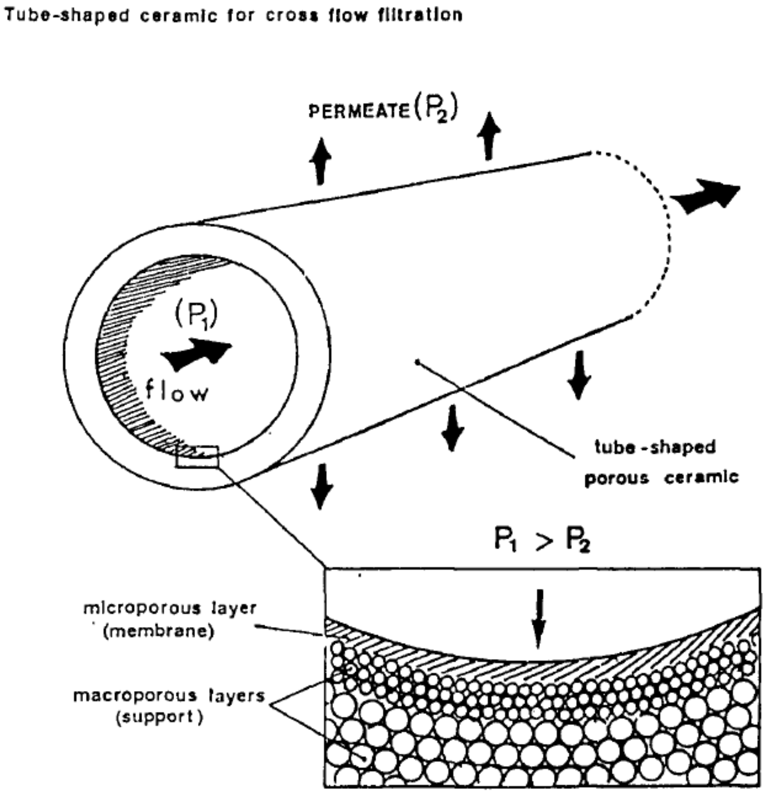

Figure 1-20: Porous tubular support after DCS process coating. The tube (standing upright) will be filled with the gel and left to diffuse through the membrane wall. What remains will be dried and sintered to form the final membrane structure seen.[58]

The thickness of this coating depends on the initial concentration of the colloidal suspension and the time left for this “engobe” operation. The interparticle pore size (textural porosity) depends on the initial particle size and the degree of sintering applied to the membrane. In the later work from Larbot *et al.*[60], they synthesized both titania and zirconia sol-gels to be applied to membranes using the DCS method. The control parameters of electrolyte concentration (which could range from nitric acid or hydrochloric acid), along with effect of sintering temperature are displayed in Figure 1-21.

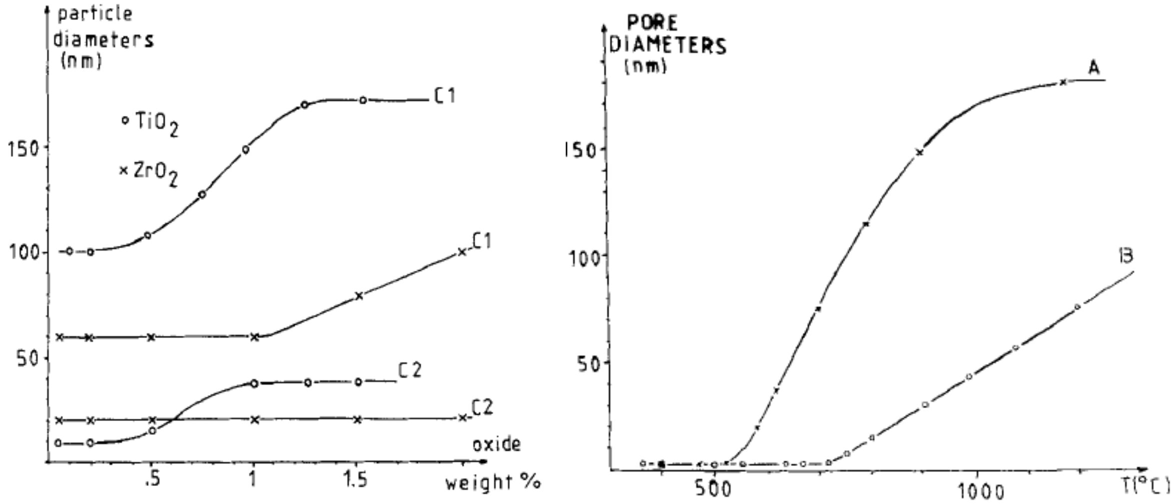

Figure 1-21: Left: Colloidal particle sizes for two different values of electrolyte concentration (C1 = 100C2) Right: Pore diameter as a function of sintering temperatures: - A: TiO_2 membranes and B: ZrO_2 membranes.[60]

In another example, Benito *et al.* were able to synthesize aluminum oxide membranes using both a slipcast coating method in addition to a sol-gel method to form the final thin membrane.[61] The slipcasting method was performed at room temperature with another colloidal suspension of α-Al_2O_3 and carboxymethylcellulose as a stabilizer. The coating was dried and sintered at 1100˚C. The final top layer was made with aluminum secbutoxide, hydrolyzed at 90˚C and with a water to alkoxide molar ratio of 21:1. Nitric acid (0.07 mol) was used as the peptizer and was left to react for 16 hours. Figure 1-22 shows the resulting cross-section of the formed alumina membrane.

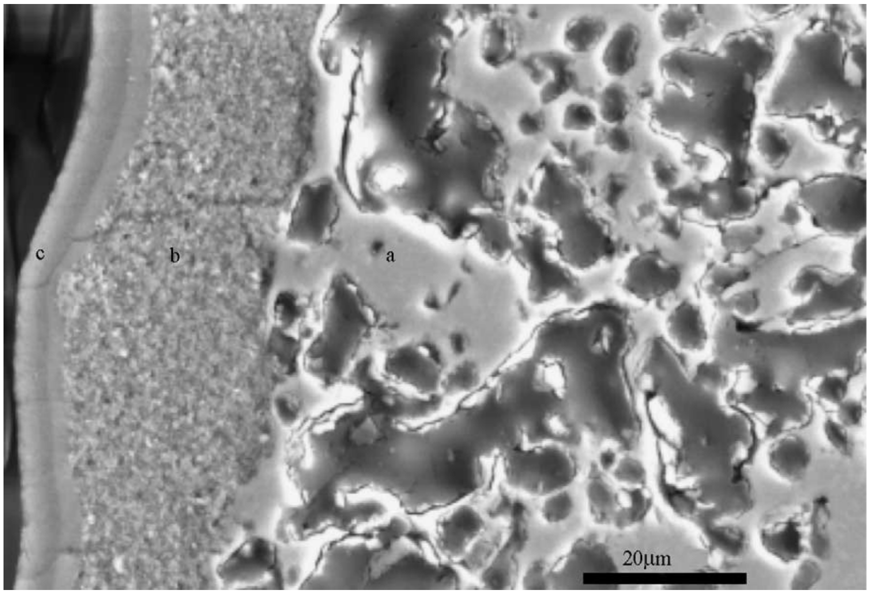

Figure 1-22: Micrograph of a multilayer system formed by macroporous support of: a) cordierite, b) intermediate alumina formed by slipcasting and c) alumina membrane formed via sol-gel route (alkoxide method).[61]

1.3.2.2 Mesoporous and Zeolite Membranes

Mesoporous and zeolite-based membranes have had a profound impact on our ability to control and design different compounds and products. They have influenced areas including microelectronics, optical laser equipment, to photochromic materials.[62,63] However, these materials continue to make its largest impact in the areas of catalysis, being able to efficiently and effectively increase reaction yields. Designing these materials for membrane applications requires sufficient transmembrane flux, easy manufacturing and stable, consistent structures. Indeed, both mesoporous materials and zeolites possess an internal (structural) porosity, which can only be used in the separation process if there is no interparticle (textural) porosity. As a result, the formation of membranes requires one to achieve defect-free monolithic layers. It is from this point that such materials essentially behave as membranes. These inorganic membranes separate fairly well based on size, and enable us to purify a solution (or mixture). Additionally, the small pore size also allows for nanofiltration based on surface charge repulsion instead of steric exclusion. Figure 1-23 shows the influence that pore size has on the ability of a membrane to select molecules based on several factors.

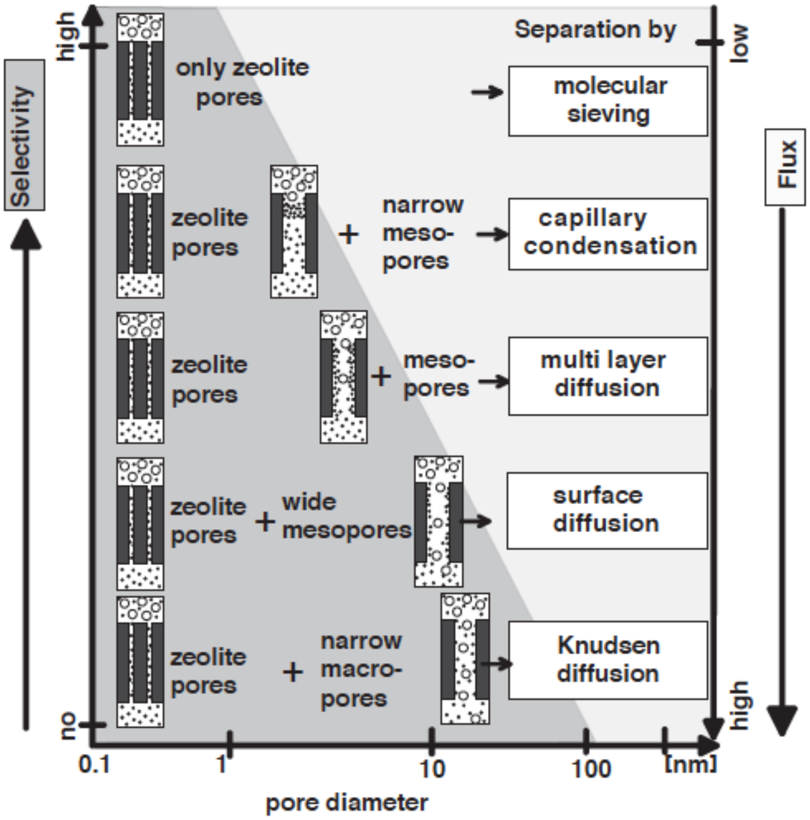

Figure 1-23: Influence of pore size on molecular diffusion/flux for a membrane.[64]

It is important to remember that this separation on size works for both liquid and gaseous mediums, which is important as gas separation membranes remains a large area of research.[65] In this section, we will explore the different synthesis and results obtained using mesoporous and zeolite membranes.

1.3.2.2.1 Mesoporous Membranes

Mesoporous membranes have the advantage of being on a scale/size larger than their zeolite counterparts. With the larger pore volume and systems that exists within the framework, these membranes become more valuable in separation of larger and more complex materials. Surfactant choice is definitely of great importance, as it determines the final structure of the membrane.[66] These mesoporous materials result from material developments from a material that has been designated M41S, which was reported in 1992.[67,68] This resulted in several different mesoporous structures, including MCM-41 (hexagonal), MCM-50 (lamellar), and MCM-48 (cubic).[62,69] We will also discuss how we obtain a very unique type of mesoporous material, developed initially at Michigan State (MSU-X), before being refined at Montpellier (France).

1.3.2.2.1.1 General Synthesis

Mesoporous materials are generally synthesized in a fairly similar process to the sol-gel process, under moderate conditions.[70] These moderate conditions usually include a hydrothermal treatment between 100-130˚C after the template structure is formed by the micelles (which form fairly quickly). The versatility of the system allows for the synthesis in both acidic and basic conditions. There exist different synthesis pathways that mostly lie between two extremes: a liquid crystal templating system (Figure 1-24) and a cooperative assembly method (Figure 1-25).

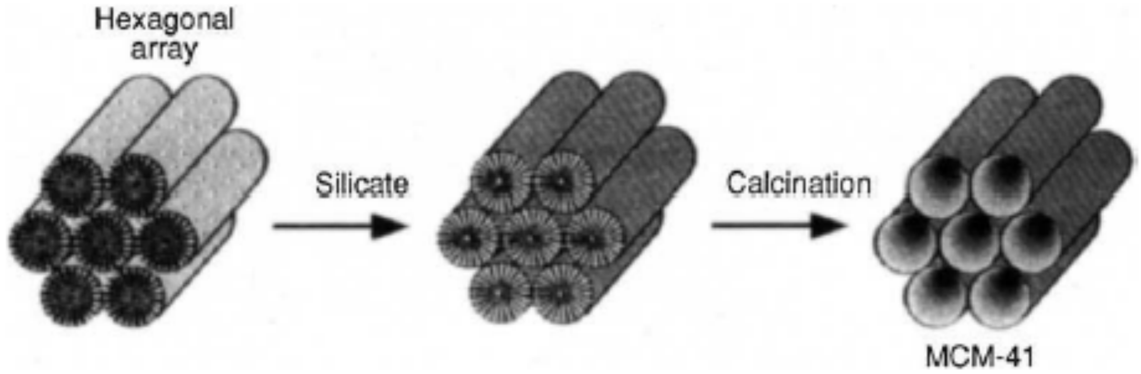

Figure 1-24: Liquid crystal templating method for the synthesis of MCM-41.[67]

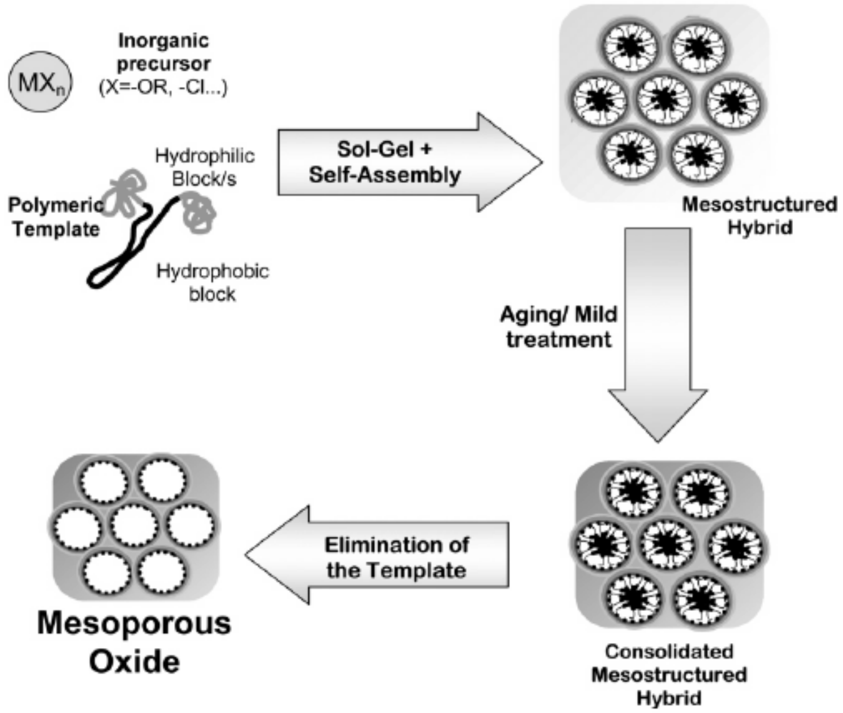

Figure 1-25: Cooperative assembly for the formation of mesoporous materials.[71]

The resulting figures show us that one can either create a micelle (or rod-like) structure within a liquid medium, and subsequently "polymerize" the silica around, or allow all the components to self-assemble during an hydrothermal treatment from the initial components mixed together. Note that for the reaction to proceed, we would need: surfactant (or block-copolymer), salt, water, and a silicon containing group (i.e. TEOS).[63] Of course, depending on the properties of each component, the concentration of each may change in order to reach each macrostructure.

1.3.2.2.1.2 Results

We can identify two main classes of components used for the synthesis of mesoporous materials. The first class corresponds to structure-directing agents, which act as molds or templates. Usually, surfactants or copolymers are used. Depending on their nature, structure, and concentration, both pore size and geometry can be controlled. For instance, Higgins *et al.* used Pluronic P123 (non charged) polymer, and was able to obtain pore diameters between 15-40 nm with an hexagonal “honeycomb” geometry.[72] Alternatively, Liu *et al.* (2007) used CTAB (cetyltrimethylammonium bromide), and yielded an average pore size of 2.74 nm for the MCM-48 structure with a cubic porous framework.[73] Table 1-5 shows the resulting formulation ratios in synthesizing specific mesoporous products using M41S powders.

The second class corresponds to the inorganic precursors, which create the stable inorganic framework by hydrolysis and condensation reactions. This inorganic framework must be very flexible to adapt the structural evolutions during reactions, and solid enough to resist to the template extraction without collapsing. Therefore, most of mesoporous materials are silica based because of the versatility of the tetrahedral silica configuration. Achieving non-silica mesoporous structures is still a challenge, and barely fully successful, except for thin films[74], where mechanical constraints are reduced.

Table 1-5: Composition of synthetic mixtures for the formation of various M41S powders.[69] (Sur = Surfactant)

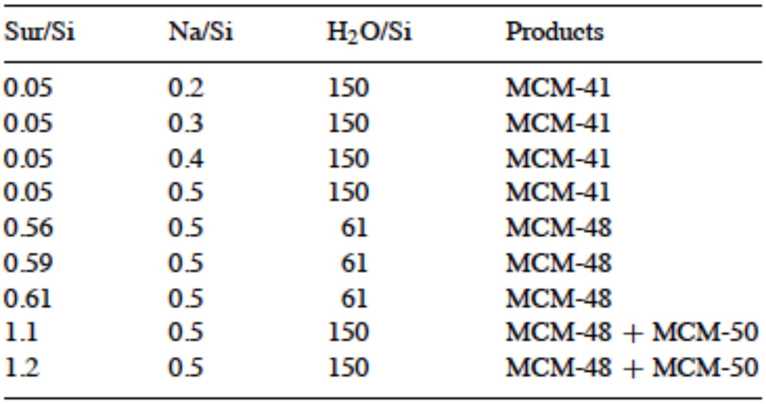

Sur/Si	Na/Si	H_2O/Si	Products
0.05	0.2	150	MCM-41
0.05	0.3	150	MCM-41
0.05	0.4	150	MCM-41
0.05	0.5	150	MCM-41
0.56	0.5	61	MCM-48
0.59	0.5	61	MCM-48
0.61	0.5	61	MCM-48
1.1	0.5	150	MCM-48 + MCM-50
1.2	0.5	150	MCM-48 + MCM-50

Most of the gas selectivity of mesoporous membranes is the result of Knudsen diffusion mechanism, a surface diffusion governed by the molecular mass of the gas molecules. Nishiyama *et al.* (2001) determined that the porous network/structure is fairly small due the Knudsen like behavior as seen in Figure 1-26. The graph indicates that as we increase temperature, we decrease the associated gas permeance, because permeance is inversely related to the temperature in Knudsen diffusion. We previously mentioned that it can be very difficult to obtain a fully defect free ceramic membrane, and interfacing layers can prove to be a challenge (particularly with mismatch lattices).[75]

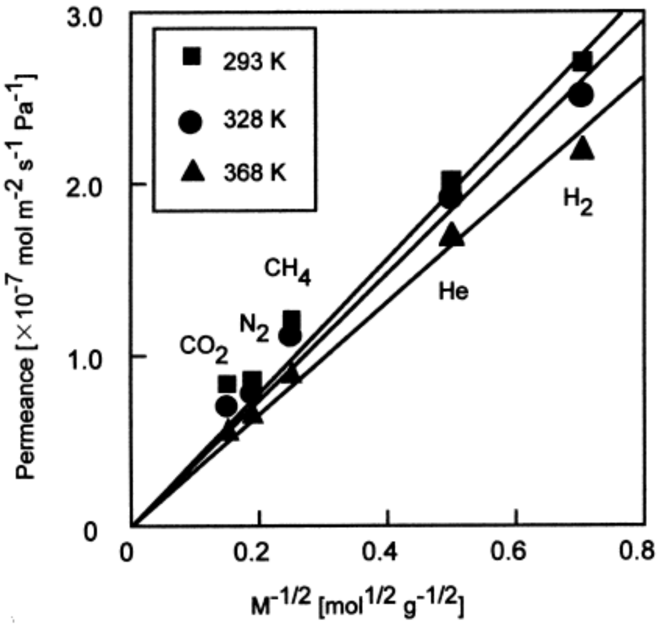

Figure 1-26: MCM-48 membrane as a function of reciprocal molecular weight vs. permeance (at pressure difference of 270kPa).[69]

Another example of mesoporous membranes was made with MSU-X silica. MSU-X (MSU-Michigan State University) was developed using surfactants which are nonionic in nature (such as alkyl-PEO, alkylaryl-PEO, polypropylene oxide-PEO block copolymers, or TWEEN).[76-78] Due to a specific preparation process that resulted in parallel, continuous mesopores spanning the entire length of the membrane thickness, a particular filtration behavior was observed as a function of the pH and charge created on the silica surface. It was observed that despite a small pore diameter ranging between 2-3 nm, it was possible to enable larger (slightly charged) molecules to pass through if the silica surface charge was creating an additional interaction force. As a result of these unique, non-connected straight pores, the water flow was sufficient to push these polymers through the membrane. On the contrary, if the surface charge was incompatible, the steric exclusion was sufficient enough for the polymers to remain on the retentate side. This was particularly true with PEO 10,000, as it has a mean hydrodynamic diameter of ~6.8 nm (Figure 1-27).[78] For pH below 2, the silica displays a positive surface charge, the oxygen groups found in PEO will interact and pass through the membrane. For a pH above 2, this interaction disappears, and the membrane recovers its size selective behavior.

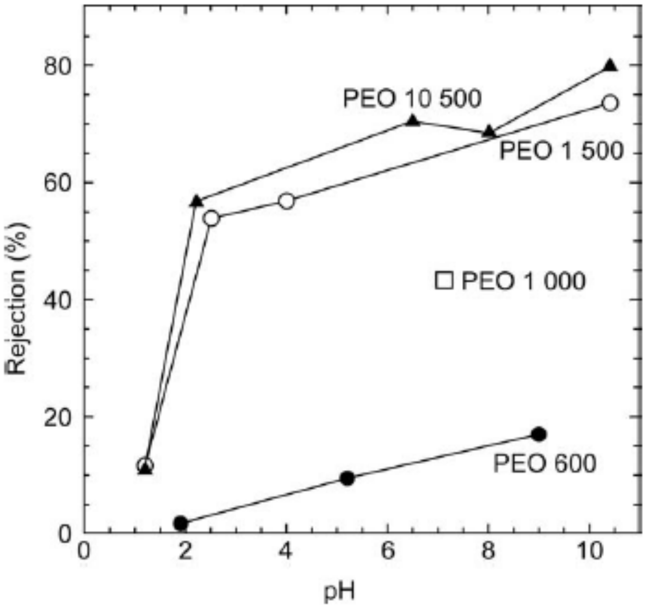

Figure 1-27: The rejection rate of silica mesoporous membranes as a function of pH, for PEO of varying molecular weight. Note that the test was performed in water, with a filtration pressure differential of 4 bars.[78] Reprinted with permission from reference 76. Copyright 2003 American Chemical Society.

1.3.2.2.2 Zeolite Membranes

1.3.2.2.2.1 General Synthesis

Aluminosilicates known as zeolites, or other molecular sieves like aluminophosphates or gallophosphates, are typically crystaline microporous materials with pores usually smaller than 1 nm in diameter.[79-81] Because of their crystalline structures (unlike mesoporous materials that are amorphous)[70], they can endure higher temperatures and especially hydrothermal conditions without structure collapsing. There have been a tremendous amount of research in fabrication and use of zeolite-based membranes.[79,80] However, the only known industrially manufactured membrane is the Zeolite A-based membranes by Mitsui & Engineering Shipbuilding Co (MES Co) used for dehydration or pervaporation, specifically in water/ethanol separation.[82] It is actually very challenging to synthesize a zeolite membrane with a reduced thickness to favour permeability, with no defects or interparticle porosity, and to extend this synthesis up to industrial manufacturing. Regarding the potential of zeolite membranes, we can also note the work by Lai *et al*. (Science, 2003) on the use of zeolite crystal growth control to separate isomers by pervaporation with a zeolite membrane.[83]

The synthesis of zeolite membranes follows a different path, as illustrated from Figure 1-28 and Figure 1-29:

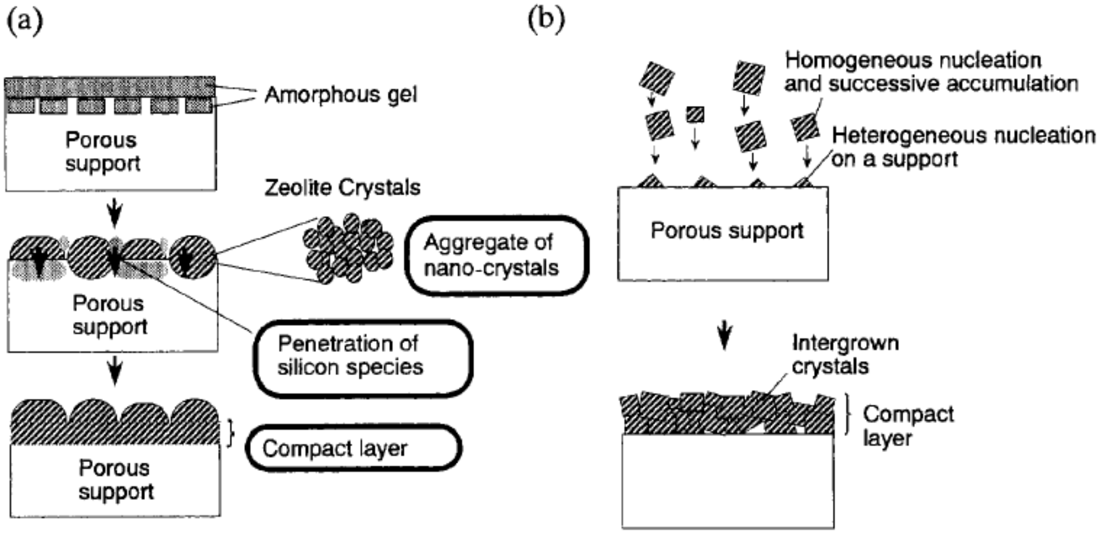

Figure 1-28: Different zeolite membrane synthesis methods: a) Vapour-Phase Transport (VPT) method vs. b) hydrothermal synthesis.[84] VPT has vapour forms of the precursors interact and grow with the porous support while the regular hydrothermal synthesis enables more surface deposition.

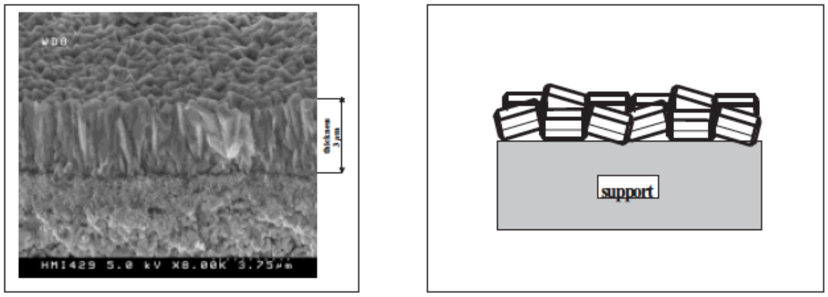

a)

preparation → two-step-crystallization with seeds
layer thickness → 1- 5 μm, ordered crystals
separation → due to molecular size

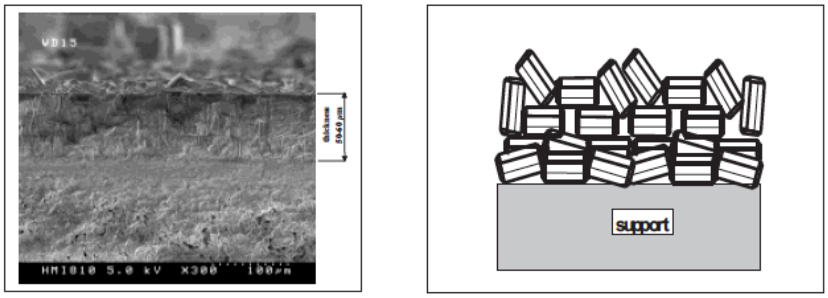

b)

preparation → one-step in situ-crystallization
layer thickness → 5-50 μm, unordered crystals
separation → by adsorption and / or diffusion

Figure 1-29: Different MFI membranes: a) Mono layer of crystals and b) Poly layer of crystals.[64]

As we can see, there are two methods of synthesis that basically requires us to deposit a growing seed layer, and subsequently control and grow the crystals on the surface (or inside the pores). The synthesis process can require significant time to allow for a defect free layer growth, with temperatures ranging from 80-300˚C, requiring several days or months to form, basic pH conditions, and be restricted in the final shape due to the crystalline network.[13,83,85,86] These processes are also not limited to only one form of crystals per membrane, as demonstrated by the work of Zhang *et al.* (2005). Zhang *et al.* were able to successfully deposit a layer of NaA zeolite on a porous alumina disk, with a top silicalite-1 layer.[87] However, beyond the interesting synthesis demonstration, potential development for large scale applications are almost impossible due to the nature and cost of porous alumina disks.

1.3.2.2.2.2 Results

Table 1-6 below compares the different properties of zeolite membranes as a function of their nature.

Table 1-6: Zeolite membranes and their separation properties

Type of Membrane	Type of Separation	Separation Material	Separation Factor (alpha)	Substrate	Thickness	Ref
MFI	Gas Separation	Alcohol/Alcohol:Oxygen (Ethanol+Oxygen/Methanol)	7000+ (25˚C)	alpha-alumina	~20 µm	88
MFI	Gas Separation	n-butane/isobutane (50 kPa/50 kPa)	- 9 (25˚C)	alpha-alumina	500 nm	89
MFI	Gas Separation	n-pentane/i-pentane (1:1)	- 14.7 (125˚C, Si/Al = 270) - 119 (125˚C, Si/Al = 1000)	alpha-alumina	-	90
Silicalite-1	Gas Separation	n-hexane/2,2-dimethyl-butane	- ~45 (100˚C) - 85 (350˚C)	alpha-alumina	500 nm	91
ZSM-5	Gas Separation	n-hexane/2,2-dimethyl-butane	- 75-80 (100˚C - 400˚C)	alpha-alumina	500 nm	91
ZSM-5	Gas Separation	n-butane/isobutane	- 45 (185˚C) - 32 (30˚C)	- alpha alumina disks	~10 µm zeolite + 50 µm barrier	92
ZSM-5 (Ge)	Pervaporation	Organic/Water (5%:95%)	- Acetone/Water yielded max 330 (at 50˚C)	- Stainless Steel Tubes	~20-35 µm	93
ZSM-5	Pervaporation	Xylene Isomers (p-Xylene/o-Xylene)	- up to ~500	- alpha-alumina substrate	~1-3µm	83
NaA (hollow fiber)	Gas Separation	He/N2 and He/Ar	range of 2 - 4	- hollow fiber (ceramic)	~5 µm	94

Type of Membrane	Type of Separation	Separation Material	Separation Factor (alpha)	Substrate	Thickness	Ref
Mistui Zeolite (NaA)	Pervaporation	Water/Ethanol (5%:95%)	5000 (95˚C) - 2.35 kg/(m2 h)	- mullite - alpha-alumina - cristobalite	~10 µm	95,96
Mistui Zeolite (NaA)	Pervaporation	Water/Ethanol (10%:90%)	- 46000 (50˚C) - 0.772 kg/(m2 h) - 42000 (75˚C) - 2.08 kg/(m2 h) - 47000 (120˚C) - 8.37 kg/(m2 h)	- mullite - alpha-alumina - cristobalite	~10 µm	95,96
Ferriete	pervaporation	benzene/p-xylene (58%:42%)	- 100 (30˚C)	- support made via dip-coating aluminosilicate gel on porous alpha-alumina	- 30nm-50nm nanoparticles inside aluminosilicate pores	84
Ferriete	pervaporation	benzene/p-xylene (0.5%:99.5%)	- 600 (30˚C)	- support made via dip-coating aluminosilicate gel on porous alpha-alumina	- 30nm-50nm nanoparticles inside aluminosilicate pores	84

The table reaffirms there exist a vast number of zeolite membranes developed and studied at the laboratory scale, with many more variations as researchers continue to work with. For instance, the work of Yan *et al.* (1997) showed us that the addition of a carbon barrier layer helped improve the permeability of the membrane (ZSM-5 zeolite) when compared to a membrane made without the barrier.[92] The authors were able to achieve an increase of 1.6 times the flux and 4 times the selectivity for the membranes with barrier.

The ratio between Si/Al within the growing zeolite layer is also important in the control of the permeability when dealing with pervaporation with water, because it controls the zeolite acidity, hence its hydrophilic properties. It has been found that as the aluminum content increased, a more hydrophilic structure is obtained, allowing water (or other more polar molecules) to interact favorably with the structure and pass through the membrane.[64,90] For instance, Noack *et al.* (2005) showed that the effect of increasing the Si/Al value in an MFI zeolite from 270 to 1000 resulted in a 10-fold increase in selectivity for n-pentane/i-pentane.[90]

1.3.2.2.2.3 Example: Mitsui Membranes

From our knowledge, the Mitsui (MES) membrane (or NaA zeolite) is the only known/documented commercially available membrane.[82,94,97] If we consider the results on the performance of the NaA (Mitsui) membrane, we can see extremely high selectivities, particularly when compared to other polymer based or ion membranes, as seen in Table 1-6 and Table 1-7.

Table 1-7: Pervaporation performances of the NaA zeolite (Mitsui Membrane).[96]

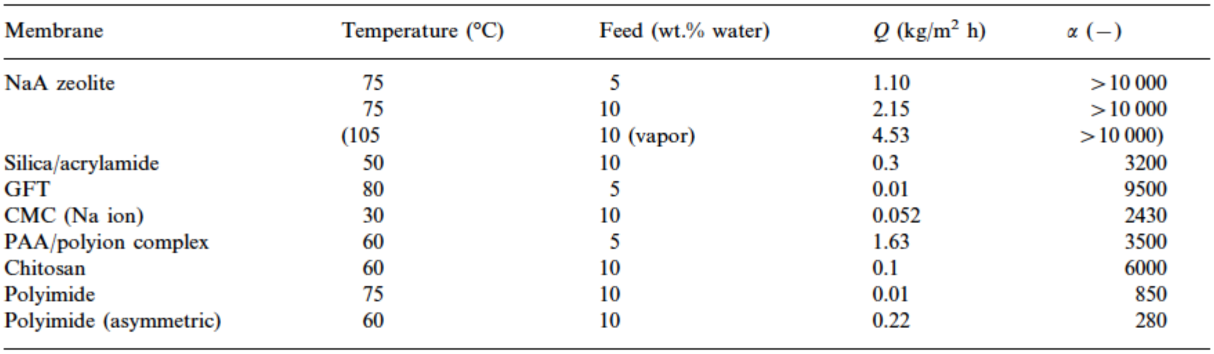

Membrane	Temperature (°C)	Feed (wt.% water)	Q (kg/m^2 h)	α (−)
NaA zeolite	75	5	1.10	>10 000
	75	10	2.15	>10 000
	(105	10 (vapor)	4.53	>10 000)
Silica/acrylamide	50	10	0.3	3200
GFT	80	5	0.01	9500
CMC (Na ion)	30	10	0.052	2430
PAA/polyion complex	60	5	1.63	3500
Chitosan	60	10	0.1	6000
Polyimide	75	10	0.01	850
Polyimide (asymmetric)	60	10	0.22	280

These membranes use the well-defined crystallized porous framework to apply size exclusion, especially in ethanol/water separation. Indeed, the zeolite NaA has a pore size that lies between water and ethanol molecular sizes. This results in water diffusing across the membrane into the permeate, leaving ethanol to remain in the retentate. With such high affinity for water compared to other solvents, this gave way for Mitsui Engineering and Shipbuilding Co. Ltd. to design and create the first large-scale plant using tubular modules for separation of 0.2 wt% water from other solvents.[82,94] Figure 1-30 shows the resulting water separation when working with low concentrations of water mixed with solvents (IPA: isopropanol alcohol, MEK: methylethylketone, ACN: acetonitrile).

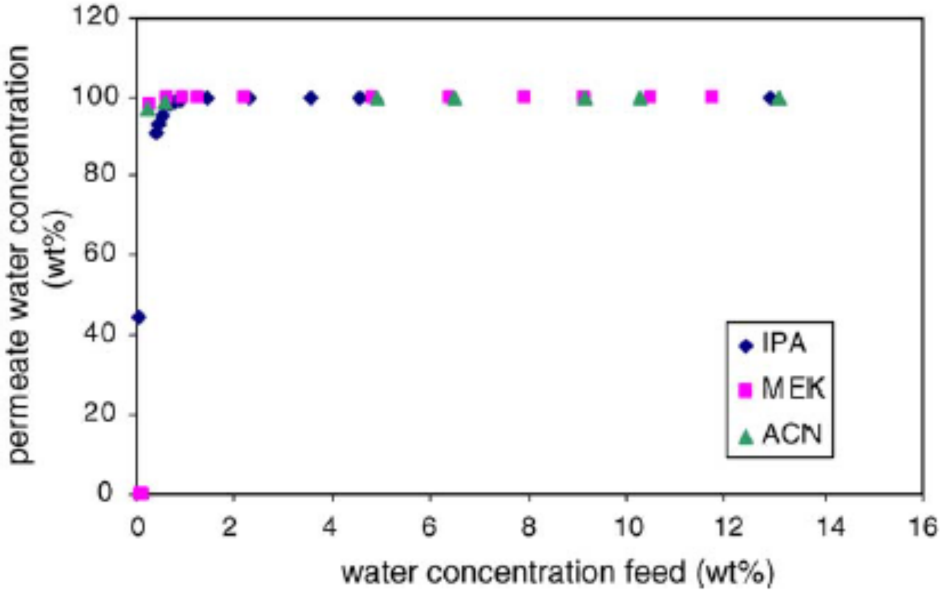

Figure 1-30: Water concentration in permeate vs. water in feed for dehydration with Mitsui Membrane (70˚C).[97]

While the plant was composed of 16 modules, totaling 125 pieces of NaA zeolite membrane, the resulting packing density (or area/module) is low compared to polymeric membranes.

1.3.3 Mixed-Matrix Membranes

The basic premise of mixed-matrix membranes has been an unavoidable direction in the realm of membrane development. In the prior sections, we have highlighted that there has been a series of work on polymeric membranes and inorganic/ceramic based membranes for different applications,[98] all of which range from water purification to gas separation in the pre/post combustion gas process.

It should be conceivable that researchers would begin to look at membrane mixtures of both organic and inorganic membranes to merge their advantages. This is illustrated by the early work by Paul and Kemp showing that adding 5A aluminosilicate zeolite into a polymeric matrix of PDMS showed a time lag effect between the adsorption of CO_2 and CH_4.[99] However, this effect did not last or make a big difference during the steady-state gas separation for the composite membrane. Still, the actual influence of adding discrete inorganic fillers, even porous, within a continuous polymer films, are not clearly defined, beyond the creation of local interfaces that can help to increase gas flux. A later patent by Kulprathipanja and coworkers showed that it was possible to incorporate silicalite into a cellulose acetate membrane, resulting in an increase selectivity of O_2 vs N_2.[100] Duval *et al.* showed that different zeolites such as the silicate-1 or KY forms were fairly good for CO_2 sorption selectivity, while the zeolite 5A performed poorly/less than expected.[101] Thus the following section will serve to explain how such mixed-matrix membranes, or MMM, are formed, along with a brief introduction to the fillers that can be used.

1.3.3.1 Formation

The formation of the MMM are fairly straightforward. As described in various texts,[102-104] the formation of mixed-matrix films involve a process similar to the formation of membranes *via* the phase-inversion method. However, the precursor is formed with a mixture of the inorganic component (whether they be zeolites or other materials such as carbon molecular sieves, also known as the dope solution) directly with the polymeric system first, as shown in Figure 1-31.

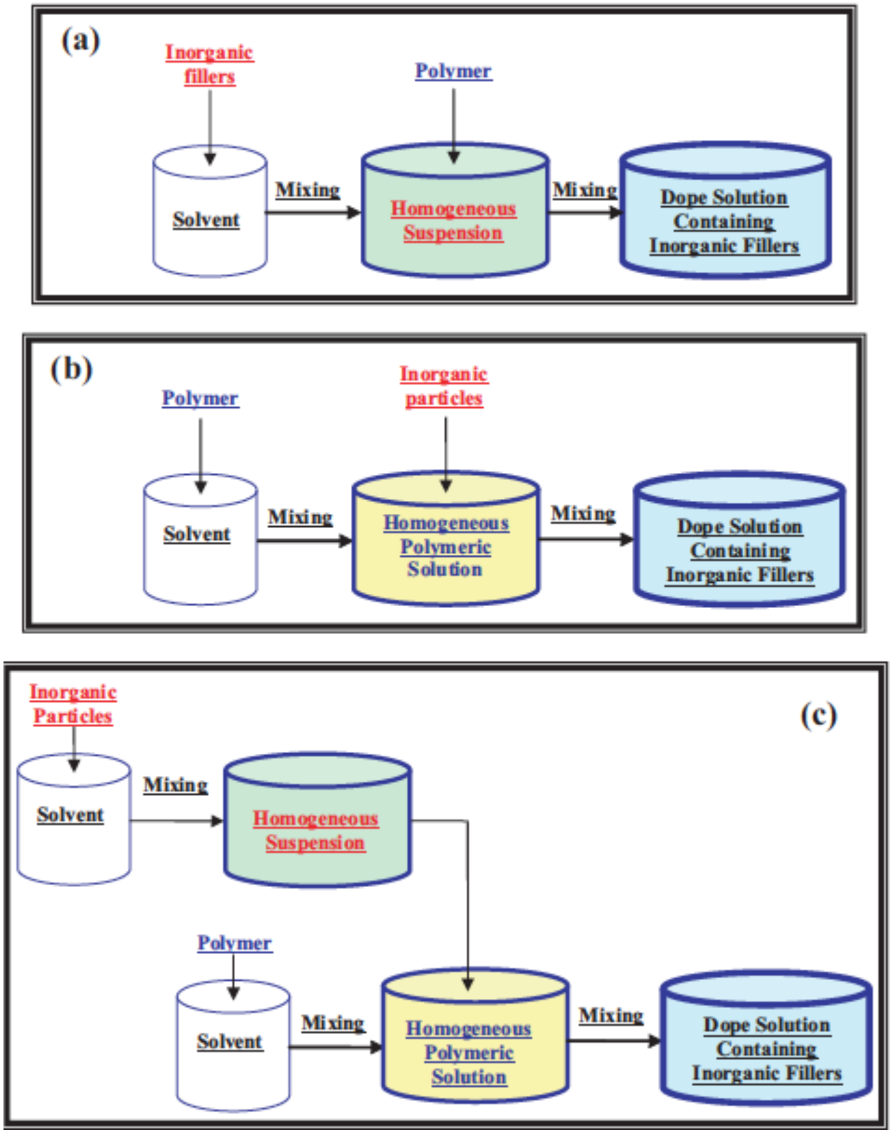

Figure 1-31: Three different methods of mixing inorganic phase with the polymeric phase before the formation of the dope solution for mixed matrix membrane formation. A) shows first step of inorganic dispersion and subsequent addition of polymer to form dope solution. B) shows the reverse, with the polymeric solution made first, and then the inorganic fillers are added to form the dope solution. C) shows how both inorganic particles and polymers are each dispersed in a solvent separately before mixture to form the dope solution.).[102]

This composite solution can then be used in one of two different methods to form the membrane. Either the membranes undergo a similar phase inversion method to form flat membranes (as illustrated previously with other polymeric membranes), or with the formation of hollow fibers, as shown in Figure 1-32. In either methods, the inorganic additive is only a filler that does not significantly disturb the polymer membrane formation process.

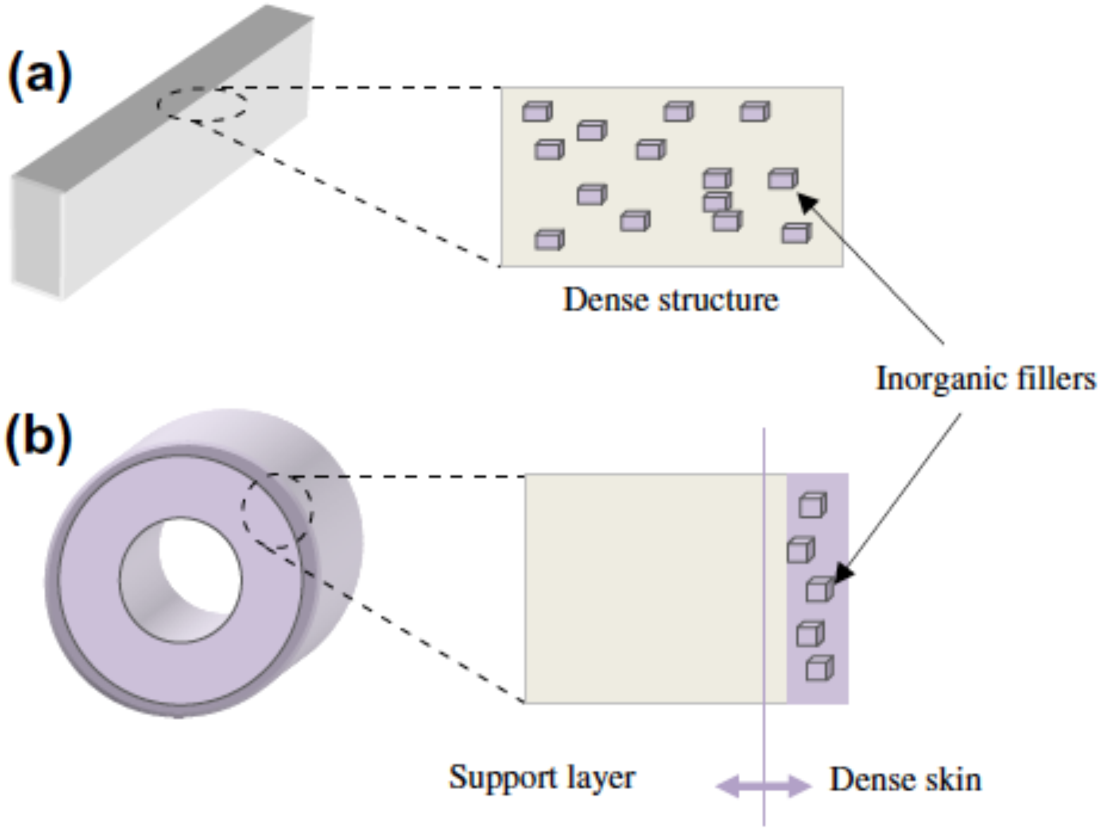

Figure 1-32: Two main structures that mixed-matrix membranes can form. A) shows a flat membrane with a coating of the inorganic fillers, while B) shows a hollow fiber with an exterior layer of the inorganic fillers to help with gas separation, as illustrated by Goh *et al.*[103]

The synthesis method becomes more challenging if true composite structures are manufactured. Figure 1-33 illustrates the many different components required for the formation of a hollow fiber mixed-matrix membrane. In this setup, the three different solvent mixtures (bore fluid, core and MMX sheath, or the dope solution) are all extruded at different rates in order to form the subsequent layers. Optimizing these parameters is essential, as working with different interfaces here has the possibility to cause delamination between the phases.

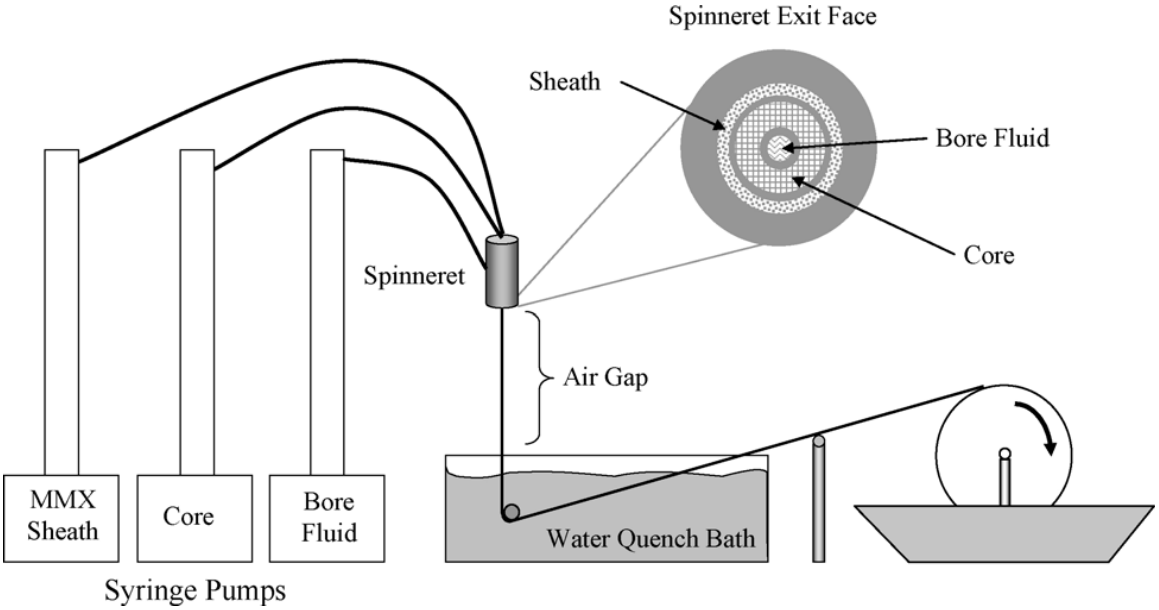

Figure 1-33: Hollow fiber formation setup for membranes with mixed-matrix composite (asymmetric system).[104]

Subsequent systems with this multicomponent system are able to form a nice hollow fiber systems where the majority of the inorganic fillers/components are found in the outer surface region of the hollow fiber. However, it has been shown that integration of these fillers is vital to the stability and formation of the hollow fibers, thus being sure that the surface of the inorganic component must interact well with the organic portion.[104]

1.3.3.2 Unfunctionalized Fillers

In this first section on fillers, or inorganic component of the dope solution, we will briefly look at some of the unfunctionalized fillers one can use to form a MMM membrane. In this case, these inorganic components are directly mixed in without modification to interface with the polymeric matrix.

1.3.3.2.1 Carbon Molecular Sieves (CMS)

Carbon molecular sieves, or CMS, are essentially porous carbon structures that are able to separate gaseous molecules based on their molecular size (or by what is known as a sieving effect). CMS are formed from polymer pyrolysis,[103,105] and the subsequent integration with other polymeric matrices have been exploited. For example, Vu and Koros presented work done on laboratory synthesized CMS that were successfully integrated into Matrimid® 5218 and Ultem® 1000 (glassy polymers) that yielded superior permeation properties.[36]

1.3.3.2.2 Zeolites

When discussing zeolites, we must be clear that this includes most common structures of zeolites, such as silicate-1, which were previously presented for gas separation. Without going into too much depth, such materials have shown to aid the gas separation process when used for MMM. For instance, the work by Mahajan and Koros in 2000 showed that the use of zeolite 4A enabled an increase (and consequently, "breaking" the Robeson curve/barrier (1991)), as illustrated in Figure 1-34.

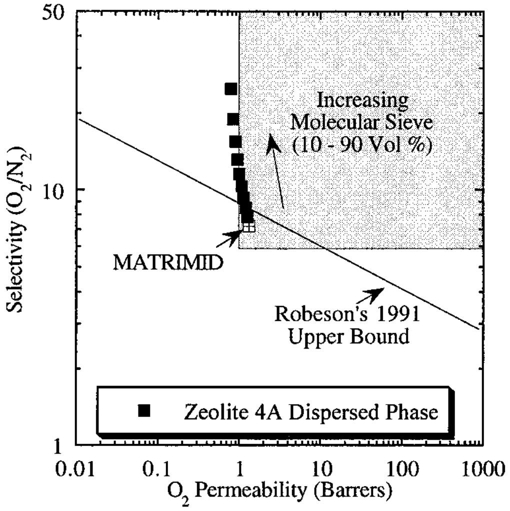

Figure 1-34: Zeolite 4A dispersed into Matrimid matrix and subsequent analysis of the gas selectivity (O_2/N_2) as a function of oxygen permeability (taken from the work by Mahajan and Koros).[106] Reprinted with permission from Reference 106. Copyright 2000 American Chemical Society.

However, the integration of such zeolites has remained a challenge. As the inorganic interfaces do not always mix/interact well with the polymeric interface, there exists the ability to create better interaction, as explained in section 1.3.3.3 Functionalized Fillers.

1.3.3.2.3 Metal-Oxides

Metal oxides themselves come in a variety of different elements, including (but not limited to) zirconium, iron, or titanium oxides. For each metal oxide, it has been shown that their addition led to some improved property in one form or another. While we acknowledge that there are a variety of properties that can be improved (such as permeability, selectivity, strength and hydrophobicity),[107] we will only focus on a couple of examples and their integration into gas separation membranes. Those interested in more information can examine the review that was published by Ng *et al.*[107]

Shao *et al.* showed that the addition of some TiO_2 to a polymer of PMP (or Poly (4-methyl-2-pentyne)) (Figure 1-35), did not drastically change the gas selectivity (Table 1-8).

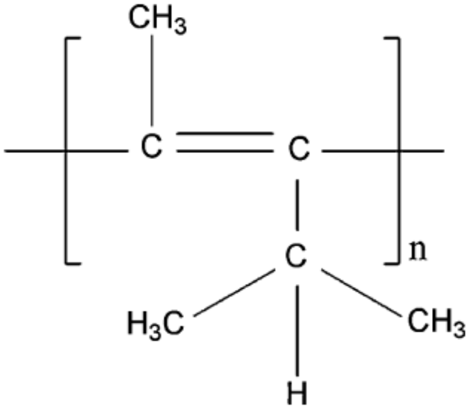

Figure 1-35: Chemical structure of PMP (as illustrated by Shao *et al.*)[108]

Table 1-8: Gas permeabilities (in barrer) and selectivities of pure PMP and PMP/TiO_2 membranes operated at 35˚C and at 2 bars pressure.[108]

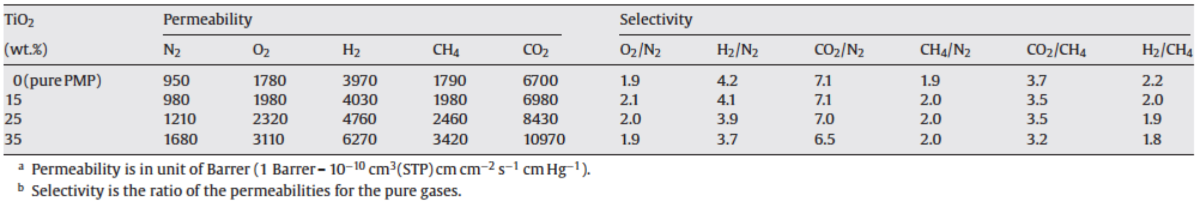

TiO_2	Permeability					Selectivity					
(wt.%)	N_2	O_2	H_2	CH_4	CO_2	O_2/N_2	H_2/N_2	CO_2/N_2	CH_4/N_2	CO_2/CH_4	H_2/CH_4
0 (pure PMP)	950	1780	3970	1790	6700	1.9	4.2	7.1	1.9	3.7	2.2
15	980	1980	4030	1980	6980	2.1	4.1	7.1	2.0	3.5	2.0
25	1210	2320	4760	2460	8430	2.0	3.9	7.0	2.0	3.5	1.9
35	1680	3110	6270	3420	10970	1.9	3.7	6.5	2.0	3.2	1.8

[a] Permeability is in unit of Barrer (1 Barrer = 10^{-10} cm^3(STP) cm cm^{-2} s^{-1} cm Hg^{-1}).

[b] Selectivity is the ratio of the permeabilities for the pure gases.

However, upon the addition of a cross-linking agent of 4,4'-(hexafluoroisopropylidene) diphenyl azide (HFBAA), the subsequent improvement on the selectivity of different gases were achieved (compared to regular PMP), and shown in Figure 1-36. Note that the graphs also have an addition data comparison, with FS (or fumed silica).

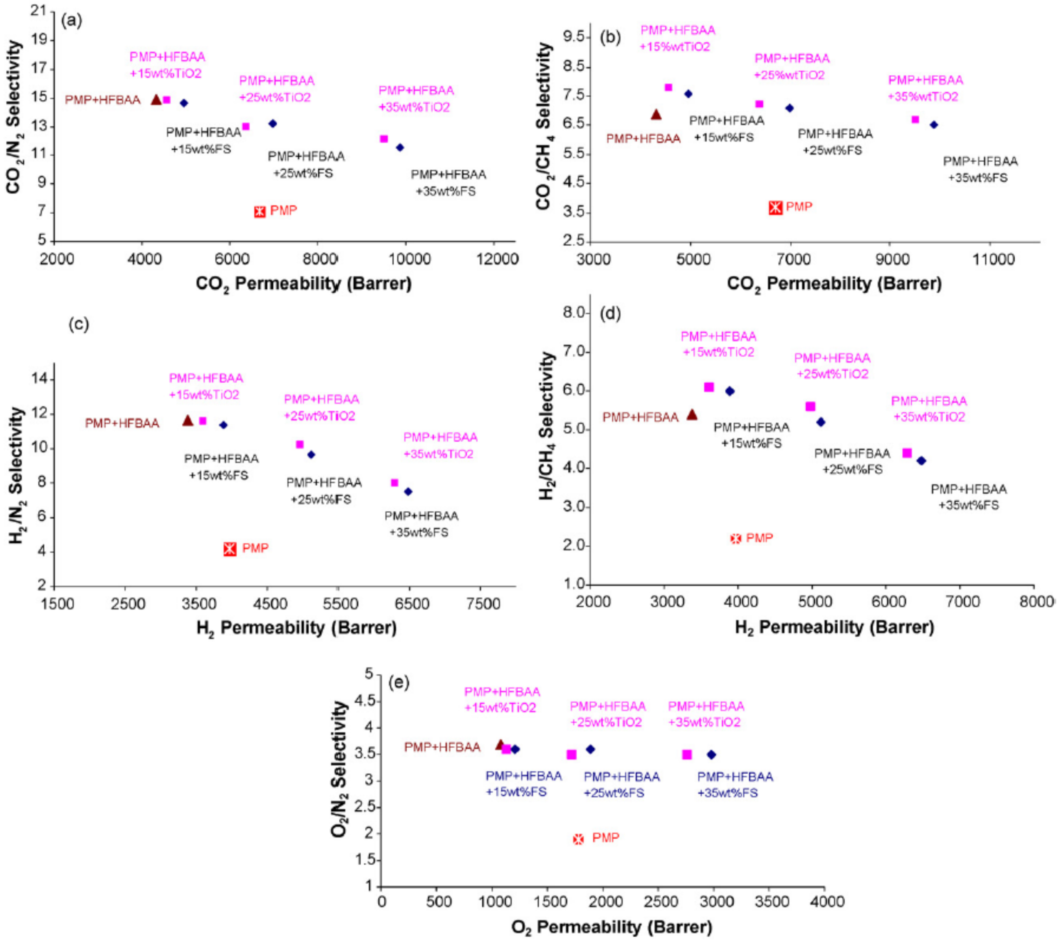

Figure 1-36: Effect of nanoparticles (FS/fumed silica and TiO_2) on gas permeabilities and selectivities of PMP membranes containing 2% wt HFBAA crosslinked and measured at 35˚C at 2 bar.[108]

This study perfectly illustrates that the simple addition of an inorganic filler like TiO_2 cannot be effective without optimizing the organic/inorganic interface. This was also illustrated in work by Merkel, where a slight manipulation of the polymeric matrix, allowed them to achieve higher CO_2/N_2 selectivity upon addition of fumed silica.[33,109]

Magnesium oxide (MgO) nanoparticles can also be incorporated into membranes for gas separation, as MgO has an affinity for CO_2.[110] In their work, Hosseini *et al*. compared a commercially available Matrimid® membrane with a series of composite Matrimid® membranes with different MgO loading weights.[111] They observed an increase in the permeability of each gas as the quantity of MgO increased (see Figure 1-37), but with a reduction in selectivity, which the researchers hypothesized was due to the larger porosity of the MgO than the gas molecules.[111]

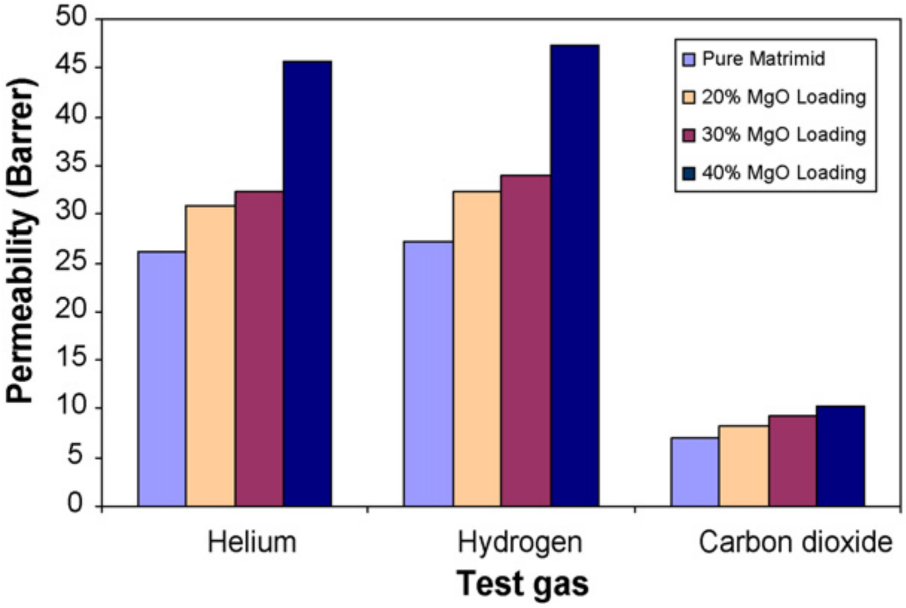

Figure 1-37: comparison of Matrimid® with composite mixtures with MgO on the permeability of different gases.[111]

Matteucci *et al*. showed that it was possible to incorporate MgO into the matrix of poly (1-trimethysilyl-1-propyne), or PTMSP.[112,113] In their work, the increase in volume of MgO results in a logarithmic increase in permeability for each gas that is studied. However, the subsequent effect of this is that there is also a linear decrease in the selectivity ratios for different gases (of which, particular interest can be found in the decrease of CO_2/N_2) (Figure 1-38). They later reported another study with 1,2-

polybutadiene polymer membranes,[112] without reaching significantly different conclusions.

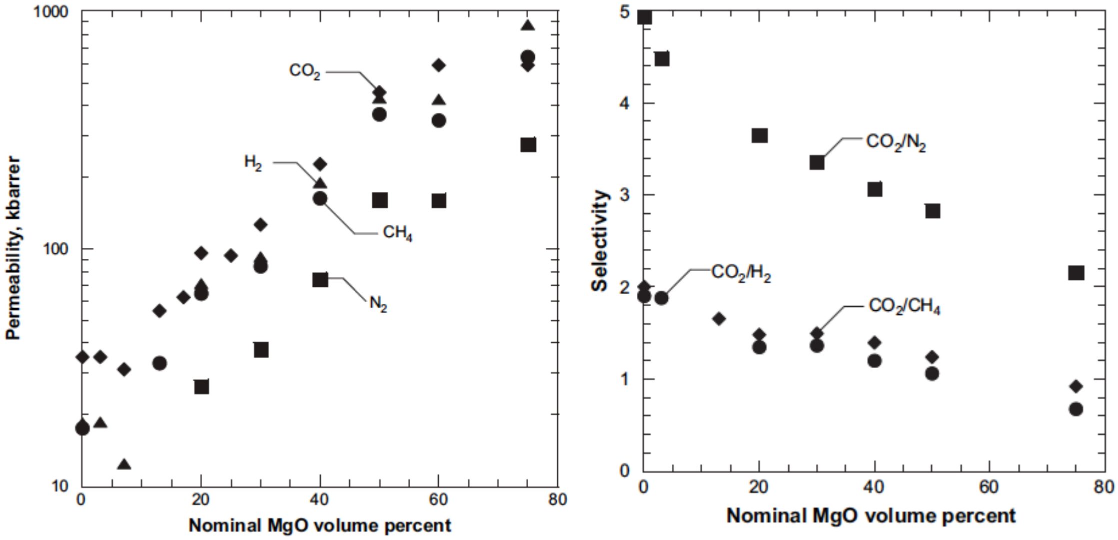

Figure 1-38: Left - permeabilities of 4 different gases (CO_2, H_2, CH_4, N_2). Right - Selectivities of different gas combintions. Note that the increase in MgO volume percent results in higher permeability, but decreasing selectivities.[113] The measurements were made with a pressure difference of 3.4 atm at 35˚C.

1.3.3.3 Functionalized Fillers

As this section implies, there exists functionalized fillers, or functionalized inorganic additives. In this case, the inorganic components that were mentioned in the previous section are functionalized with organic ligands that enable easier integration into their respective polymeric matrix. For instance, Pechar *et al.* showed in 2002 that it was possible to modify zeolites (ZSM-2) with APTES in order to better integrate the inorganic component into a polyimide matrix (Figure 1-39).[114]

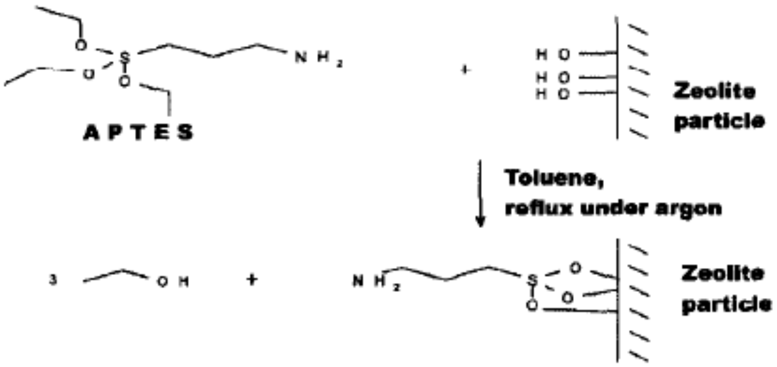

Figure 1-39: APTES functionalization of zeolite surface, as illustrated by Pechar *et al.*[114]

This modification resulted in an increase in permeation of various gases, and subsequently changed the selectivity of the membrane for several gases: increase in N_2/CH_4, but decrease in CO_2/CH_4 selectivity.[114] Li *et al.* in 2006 showed that it was possible to functionalize different zeolites (3A, 4A and 5A) with APDEMS ((3-aminopropyl)-diethoxy-methylsilane) to protect and subsequently form a better interface for integration with the matrix (in this case, was polyethersulfone) (Figure 1-40).[115]

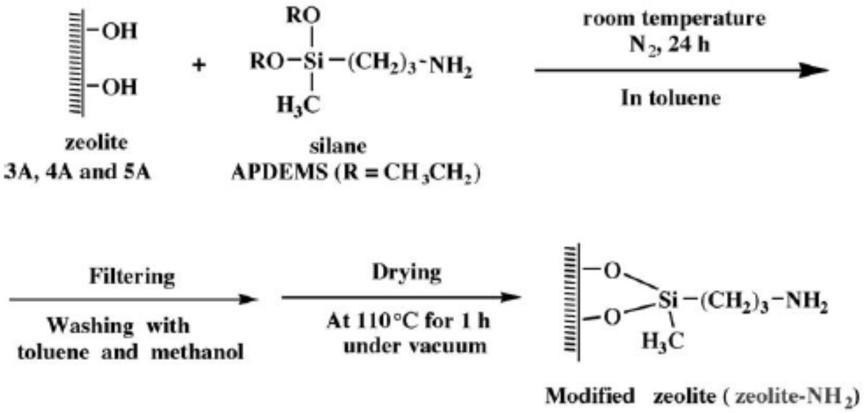

Figure 1-40: APDEMS functionalization of zeolite surface, as illustrated by Li *et al.*[115]

More recently, a patent by Koros and coworkers in 2015 showed the use of mesoporous silica in the formation of hollow fiber mixed-matrix membranes. Here, surfactants were also used to help stabilize the integration and formation of the mesoporous silica structure.[116]

1.3.3.4 Expectations of MMM

The expectations with MMM remain high with this field of research. While there is the potential for many researchers to thrive in this environment of mixing both organic and inorganic components, there remains a major issue with the processing of these materials. One should be aware that no matter how perfect a membrane is made in the lab, scaling up remains to be a huge challenge; that the process-ability of such membranes is not perfect and will pose challenges during technology transfer to large scale production. The main lag with such a process is ensuring the defect formed are those purposely put in, and does not propagate uncontrollably to reduce the selectivity of the polymeric portion of the membrane when making large batches. Subsequently, this point of inorganic component integration (or, without breaking the matrix) is extremely difficult.[104,117,118] Nonetheless, such challenges are expected to be alleviated in the near future.

1.4 Project Concept and Design

As previously presented in our introduction, our problem at hand is trying to reduce the amount of pollutants being released into our atmosphere. While membranes are an attractive alternative to the many options available, there still is an abundant amount of work in order to achieve an efficient system, including cost cutting and material design for increased gas selectivity. As noted in the previous section, mixed-matrix membranes yield superior systems for use yet their process ability and uniform membrane formation continues to present problems.[104,117,118] Some researchers have presented the concept of functionalizing the surface of the inorganic fillers to help with integration, but such options still have problems with ensuring even mixture/dispersion within the polymer matrix.

Assessing all the presented information thus far, the goal of this thesis will be to design a new setup for gas separation that can help the system resist the effects of flue gas, or prolong the life of the membrane.

If we consider the system/membrane design, there are several points we can take into consideration for the overall design:

1. The bulk of the material should be inorganic in nature (specifically ceramic membranes), as they resist the conditions of flue gas more readily than their organic/polymeric counterparts, and offer a long lifetime (roughly 5 times the lifetime of a polymer)[119] especially if the actual membrane can be regenerated on the same substrate.
2. Any polymeric layer introduced should be fairly thin (at least in comparison to the inorganic portion), to help increase flux through the membrane
3. The system should combine the advantages from both worlds; that is, long lifetime (+20 years) from the inorganic portion, and high selectivity from the organic portion. If the organic component (the denser membrane) is thin enough, cross-membrane diffusion could be enhanced.
4. The system must be easily regenerated upon polymeric degradation

From our knowledge, all MMMs introduced until now see the inorganic additive as a filler of the polymer membrane. None have tried to create a true composite structure with a high permeability/low selectivity ceramic support hosting on its surface a high selectivity/low permeability polymer (or composite) membrane. The aim of this design is to reduce as much as possible the thickness of the polymer membrane to increase its permeability. This design is challenging because it must prevent any polymer delamination, which would happen if the polymer layer were only coated onto the ceramic substrate. It must also be compatible with future large scale manufacturing techniques, if a realistic membrane concept is developed.

Taking these all into account, we propose a system that will involve inorganic ceramic tubes that are surface modified with the selective polymeric layer (i.e. a highly PEG-ylated monomer). The decision for polyethylene glycol was made due to the nature of the polymer – we previously mentioned that while amine based polymers were better at separation (especially as amines are thought to form complexes with the CO_2) however, if one is to expect degradation of the polymer layer, the release of amine by-products is undesired. In this case, PEG would degrade more into hydrocarbon derivatives, including components that the membrane is meant to separate. As a result, one should expect our target membrane with this design has a permeability of roughly 12 Barrers (for CO_2) and a selectivity of approximately 45 (as illustrated by the studies by Lin and Freeman).[120,121]

The inorganic component should be a titanium oxide based material (whether particles, flat surfaces or porous substrates), as they have been shown to be used in existing inorganic membranes, alongside their use in mixed-matrix membranes. Functionalization of these surfaces will be explored, and will be presented in Chapter 2.

From this point onwards, to form the polymer layer, we can either directly mix the polymeric layer together or grow the polymer from the surfaces of these titanium oxide surfaces. As the formation of the polymeric layer from the surfaces is more appealing (particularly ensuring direct integration/mixing with the inorganic phase), the approach of the project will follow in this manner.

1.5 Conclusion

As this chapter provided an overview of the work being performed in the domain of membranes, this work serves to bring the reader up to speed with the expected design and implementation of the project and understanding how we reached this objective.

In many respects, membranes and their developments have been an ongoing challenge; they are versatile systems with many different routes and materials available for application. However, engineering these membranes is not always easy, in addition to providing a method that is scalable and defect free. Learning from the drawbacks of conventional designs, we aim to change this by redesigning the synthesis route of these membranes and present a more scalable and easily regenerative design.

Chapter 2

Surface Modification of Titania

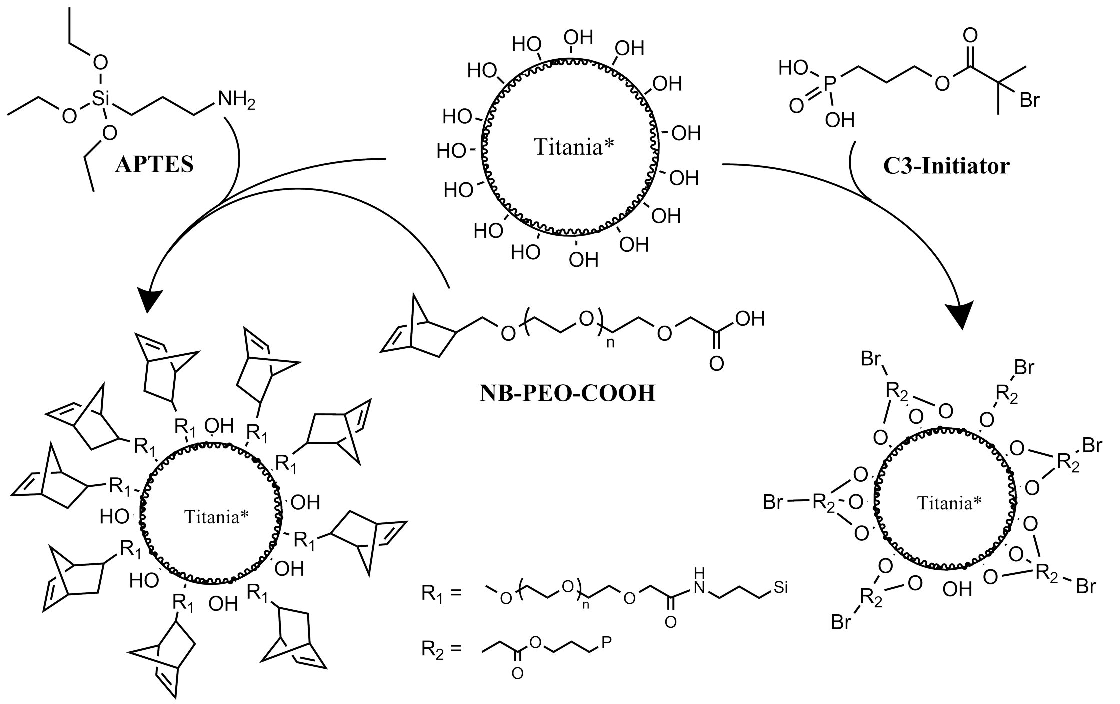

*** Titania can be represented by particles, flat planar surfaces, and porous support surface.**

2.1. Introduction

In any composite or hybrid structure, the nature and structure of the interfaces is very important, as it controls the cohesion and/or diffusion properties. Therefore a plethora of work exists on the topic of surface modification, ranging from interfacial development in the electronics industry,[122,123] to medical systems.[124,125] While the scope of surface modification is near endless, we will focus on areas that consequently limit this field towards materials that have influence on our intended final product; that is to say, hybrid organic-inorganic membranes.

There are several forms of hybrid organic-inorganic systems that can be formed, ranging from integration via direct mixing (i.e. addition of the inorganic phase directly into the organic phase),[122] functionalizing the inorganic phase with an organic stabilizer (whether physisorbed or covalently bonded),[126] or *via* growth/formation of the organic phase directly from the surface of the inorganic phase (such as Surface-Initiated Polymerization, or SIP).[127-131] These methods of incorporating inorganic phase into the organic phase have proved to be effective in creating composite materials. However, in the former two cases, the integration suffers from stability of the inorganic phase/fillers over time.[132] The use of many surface modification techniques is explored in order to help integrate one object with another through various means. In most cases, these particles or surfaces are modified to change their material properties or structure to integrate a new material into a system, and subsequently create a new composite/hybrid material. A lot of work has been placed into the development of such systems for the sole purpose of improved properties or structural characteristics for a vast spectrum of applications.[123,133,134]

Expanding on the various methods of creating hybrid organic-inorganic composites via growth/formation direction from the surface involve many interactions ranging from weak interactions, such as physical adsorption[135-137] to covalent bonds from anchoring groups such as, but not limited to, catechols,[138,139] silanes,[140] phosphonates'[141] or thiols,[142,143] as illustrated in Figure 2-1.

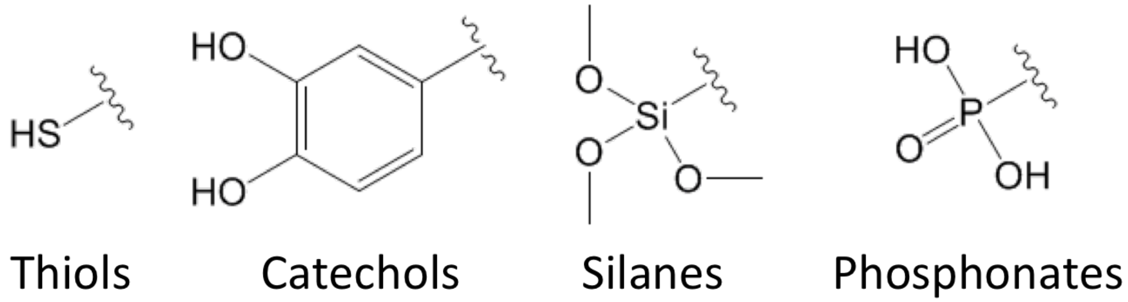

Figure 2-1: Examples of Functional anchoring groups available for surface modification/binding

Of course, it is very important to consider the nature of the substrate material when determining each type of functional group that can be used to bond to any specific surface. As we have mentioned several formats of surface modification, we will first discuss each of the functional anchoring groups presented and with what respective surfaces they can interact. The subsequent studies performed on two types of anchoring groups will be presented and their ultimate grafting densities used for later chapters will be shown.

2.2. Anchoring Groups

As shown in Figure 2-1, each of the anchoring groups presented serves a function for very specific surfaces. We will briefly present how each group behaves and their application towards hybrid material formation.

2.2.1. Thiols

Thiols represent an essential form of surface modification on gold surfaces. The nature of the bonds themselves have been disputed, as it has appeared the bond formation of sulfur on gold alternates between a coordination and covalent bond.[144] It has been repeatedly reported in literature that these sulfur-gold bonds form very good SAM (Self Assembled Monolayers) on the surface of gold plated substrates. Many research papers have reported the use of this technique for surface modification and attachment of ligands for biological or electronic applications.[145,146] For instance, alkylthiols can provide a simple method of attachment, as illustrated by Laibinis *et al. via* ethanol or isooctane solvents,[142] or Folkers *et al.* also using ethanol.[147] This method enabled other researchers to bind various functional groups on the surface, including, but not limited to, norbornenyl groups,[145] lactams,[148] or other atom-transfer radical polymerization (ATRP) initiators.[149,150,151] The last variation allowed them to perform a second polymerization to form a block copolymer structure on the sample surface. However, the limitation of this method is evident, as the surface must be gold in order for the thiol group to form such a strong bond. As a result, one is limited to specialty devices, such as sensors, because large surface scale-up production would be definitively too expensive for applications in membrane.

2.2.2. Catechols

Catechols are considered a very good surface-binding group, which have been intensively studied for its binding mechanism. Catechol structures have been noted in a variety of biological systems, specifically those found in the attachment mechanism of mussels. The study of their reversible binding to almost any surface substrate led to the discovery of components like DOPA (3,4-dihydroxyphenylalanine) or catecholamine structures governing their surface attachment.[152-155] Understanding this structural chemistry that has worked well for biological organisms, researchers, such as Messersmith *et al.,* showed how the structure of dopamine (also a known neurotransmitter) can be applied to surface coating and modification.[138,153,156-158] Figure 2-2 illustrates the subsequent structure of dopamine alongside how researchers collect the DOPA/Catacholamine based materials.

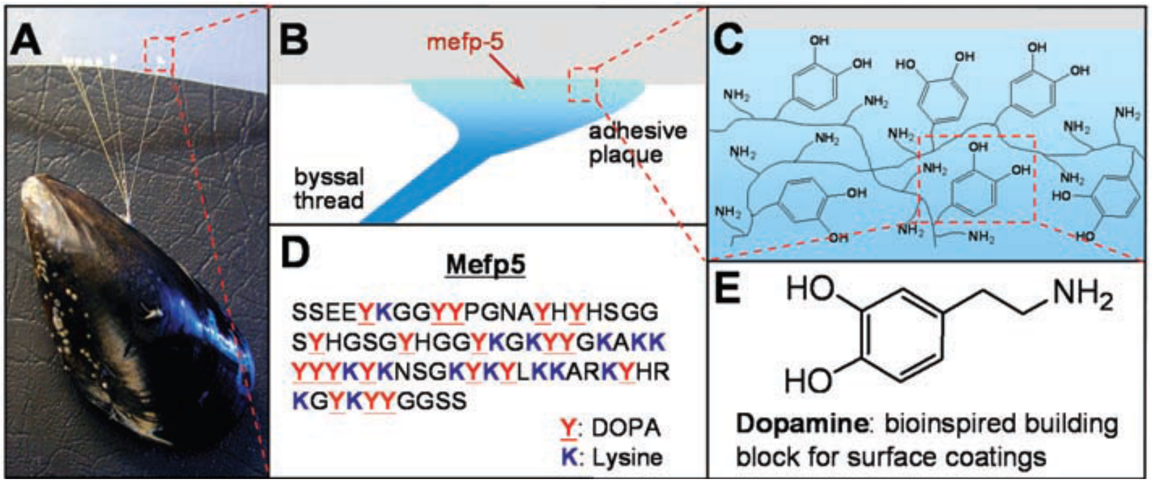

Figure 2-2: Adapted figure for A) Mussel bound to hydrophobic surface, B) The adhesive thread formed by the mussel for attachment, C) The zoomed in structural look of the binding proteins used to interact with almost any surface, D) the simplified protein structure for the byssal thread and E) The structure of dopamine – a simple catecholamine that can be used as a DOPA substitute.[157]

There have been continual advances from using catecholamine-based modification of surfaces, partially thanks to the simplicity of the reaction, which involves submerging the substrate into a basic (pH = 8.5) aqueous solution of catechol precursor.[155,157] There have been in parallel attempts to derive new pathways to find catechol based groups from other bio-sources (i.e. wine, tea and chocolate).[158]

Continued functionalization of these modified surfaces has also yielded other groups, which were later bonded by forming a peptide bond. In such cases, these "initiators" have been formed to yield norbornenyl groups,[139,159-161] to bromo initiators/ATRP,[154,156] or even RAFT based initiators.[154] Figure 2-3 shows the versatility of using catecholamine derivatives in various applications, including use as si-ATRP and si-RAFT anchors, which were illustrated by the review by Yang *et al*.[154] While catechols are very interesting systems, their application and use are still relatively young, making them a great area for research with space for improvement until commercial maturity is reached.

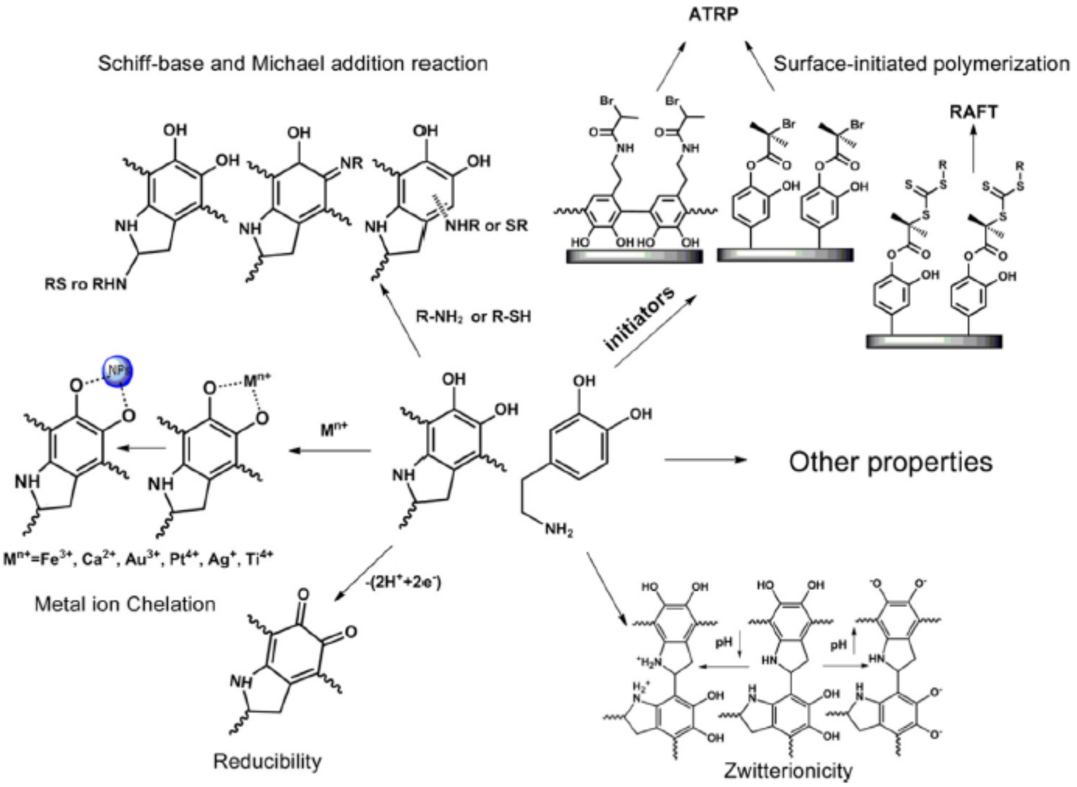

Figure 2-3: Catecholamine (also known as dopamine) modification route for use as si-ATRP or si-RAFT initiators. Adapted from work by Yang *et al.* [154]

2.2.3. Silanes

Silanes, or more commonly known as alkoxysilanes, are perhaps the most well known commercial anchoring group. [126,162] Unlike thiol groups, silane functions are very versatile toward surface binding, and they interact with a large range of metal oxides, such as titanium dioxide and zirconium dioxide to name a few.[163,164] However, alkoxysilane modification surfaces are mostly used on other siloxane based surfaces due to their ability to form strong, stable bonds and elemental similarities between the bulk and anchoring materials.[162,165]

While there are several ways that alkoxysilanes can be used, as highlighted by Judeinstein and Sanchez,[122] the method of silane anchorage is through a sequential synthesis pathway. It is a two-step process where the silane polycondenses on the surface and enables the opposite terminal end (or free alkyl end of the alkoxysilane molecule) to react and form the interface of the second layer, if a reactive group is present. The silane acts as an interface between the metal oxide surface and another material that can grow/extend from the reactive surface created by the reactive group. For example, silanes can also be functionalized to contain a polymer initiating function. This point was illustrated by Matyjaszewski *et al.*,[127,166] or by Kobayashi *et al.*,[167] *via* the si-ATRP route. Other routes have been explored, such as si-RAFT, have been reported by Li and Benicewicz,[168] or through the si-NMP (surface-initiated Nitroxide Mediated Polymerization), as shown by Husseman *et al.*[169]

While alkoxysilanes are also very eager to react with silicon oxide surfaces, this ability is a bit detrimental because homopolymerization of alkoxysilanes is also possible, leading to multilayer interfaces.

2.2.4. Phosphonates/Phosphonic Acid

While less commercially known, phosphonic acids (also known as phosphonates) are also very good anchoring groups. For instance, phosphonate groups are good grafting groups because, unlike silanes, they do not stand homopolymerization due to their lower sensitivity to nucleophilic substitution when compared to silanes.[162] However, it has been previously shown that the Si-O-P bond is very sensitive to hydrolysis. For instance, Mutin *et al.* showed that when the grafting reaction of phosphonic acids onto silica is performed in aqueous media, very few Si-O-P species could be detected.[162,165] On the contrary, this reaction can be observed in higher yields when using organic media. However, this trend does not follow when observed with the Ti-O-P bond. The binding and anchoring of the phosphonate group to the titania surface can be achieved with the use of aqueous media, yielding a more versatile method of controlled targeted coating on different surfaces. This leaves phosphonate-anchoring groups to effectively pattern non-siliceous metal oxides like titania when using an aqueous media, ensuring no other surfaces, such as glass, would be affected.

Noting this special ability of phosphonate groups enables not only greater control of the substrate, but also the ability to use phosphonates as one terminal end of a linker molecule that can function as a transition layer towards a new interface. For instance, we can modify the exposed terminal end (or opposite end to the phosphonate group) with a nitroxide mediated radical polymerization,[167,170,171] or with ATRP initiators.[167,172,173,53]

2.3. Inorganic Surface

While the previous section briefly touched upon the possible anchoring groups for surface modification of inorganic substrates, the nature of the material used as the anchoring substrate also needs to be assessed. As it was concluded in Chapter 1, the use of a metal oxide surface was the main target. Indeed, porous ceramic supports are available at the commercial scale, making them suitable for the development of nanocomposite membranes if they can be integrated with a polymeric layer. Unlike dense flat substrates such as gold used with thiol groups, porous ceramics offer a significantly rough surface, which becomes also an important parameter to consider. At a more local level, the microscopic roughness becomes a problem of surface shape and curvature, as molecules must graft and stack onto the particle surface. While there are studies that focus on the substrate format, such as the work by Bernardoni *et al.*,[174] we first need to determine the different surface morphology that will govern our work.

Diving further into the presented work by Bernardoni, one discovers that the surface shape along with the size of the grafting molecule determines the ability of the molecule to anchor. Figure 2-4 shows the results obtained for varying the anchoring molecules alkyl length along with the grafting density on titania.

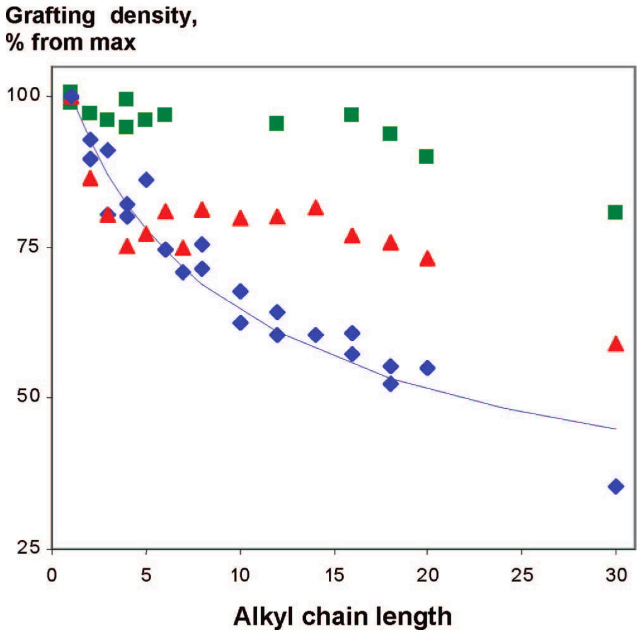

Figure 2-4: Data taken from the work by Bernardoni *et al.* regarding the ability to graph silane based linkers onto different curvature inorganic oxides. The plot compares the ability for different alkyl chain lengths to bind to different curvature surfaces. (green box: Curved nonporous surface/particles, Red Triangles: flat gels, Blue Diamonds: porous particles).[174] Reprinted with permission from Reference 174. Copyright 2008 American Chemical Society.

The graphical data shows a relationship between the surface curvature shape and the subsequent effect from the alkyl chain length. Spherical particle are shown to yield the highest anchoring density when compared to other surface morphologies. This factor, specifically in the case of increasing the length of the grafting moiety, illustrates that particles are the best surface for modification if one wishes to obtain the highest grafting density possible. As such, it appears that the transferring of these results between different surface morphologies is not straightforward. All parameters being constant, the same grafting process applied to a flat dense surface and spherical particles should lead to a higher grafting density on the spherical particles, according to Bernardoni's study.

2.4. Design Pathway

As we have briefly presented work on the anchoring groups possible alongside the type of surface that will be used, we need to determine what will the most optimum pathway for the project to proceed. Taking into account the work presented on the types of anchoring groups, we compared their advantages and disadvantages (Table 2-1).

Table 2-1: Comparative analysis of typical anchoring groups

Type	Advantages	Disadvantages
Thiols	- Well studied/characterized - Ease of attachment	- Surfaces need to be gold coated
Catechols	- Strong covalent bond formed with ease - Relatively young field/area of research	- Bind to almost all surfaces (hard to be sure of correct concentration) added but can be adapted - no known commercial product available on market
Silanes	- Well studied (products out in market) - Ease of use for applications	- Homopolymerize - detached from metal oxides in presence of water (bond is less stable)
Phosphonates	- Stable covalent bond when subjected to small amounts of water - Does not homopolymerize	- Harder to synthesize full functional molecule - commercial competitively might not be on par with silanes

While each system has its merits, one must remember that the target surface is a metal oxide. As thiols are not good at binding towards metal oxide surfaces, we are left with catechols, silanes and phosphonates. Assessing the commercial availability of the three products, silanes and phosphonates are much more common in the market than their catechol counterparts. Subsequently, we decided to explore the pathways of silanes and phosphonates for binding to surfaces.

As the target surface is a metal oxide, we chose titanium dioxide, also known as titania, to proceed forward as both phosphonates and silanes have plenty of prior work with this metal oxide,[162,164,165,175-179] and because titania is frequently used in ceramic membranes. In order to proceed with this, the decision was made to study various titania surfaces to be sure that the results from Bernardoni could also be applied. Thus, the different titania based substrates can be seen from Table 2-2

Table 2-2: Titania substrates used in this study

Substrate Name	Used Name in Report	Porous	Particle or Flat	Size
Evonik coating - AERODISP W740X	**Evonik particles**	No	Particle	~100 nm
Sigma Aldrich (CAS 13463-67-7)	**Sigma particles**	No	Particle	21 nm (dry)
In-house made Titania Disks	**Flat titania substrates**	Low	Flat (some roughness)	N/A
CTI Ceramics D10/6 (ID: 10.4 mm, OD: 6 mm)	**CTI porous tubes**	Yes	Curved/Flat	200 nm pores

The resulting substrates vary from the three different surface forms we can study for grafting: (i) nonporous particles (from Evonik and Sigma particles), (ii) flat dense surfaces (from the Flat titania substrates), and (iii) rough porous surfaces (using the CTI porous tubes with an OD (outer-diameter) of 10.4 mm, and an ID (inner-diameter) of 6 mm). The subsequent design pathway to be followed first can be noted from Figure 2-5.

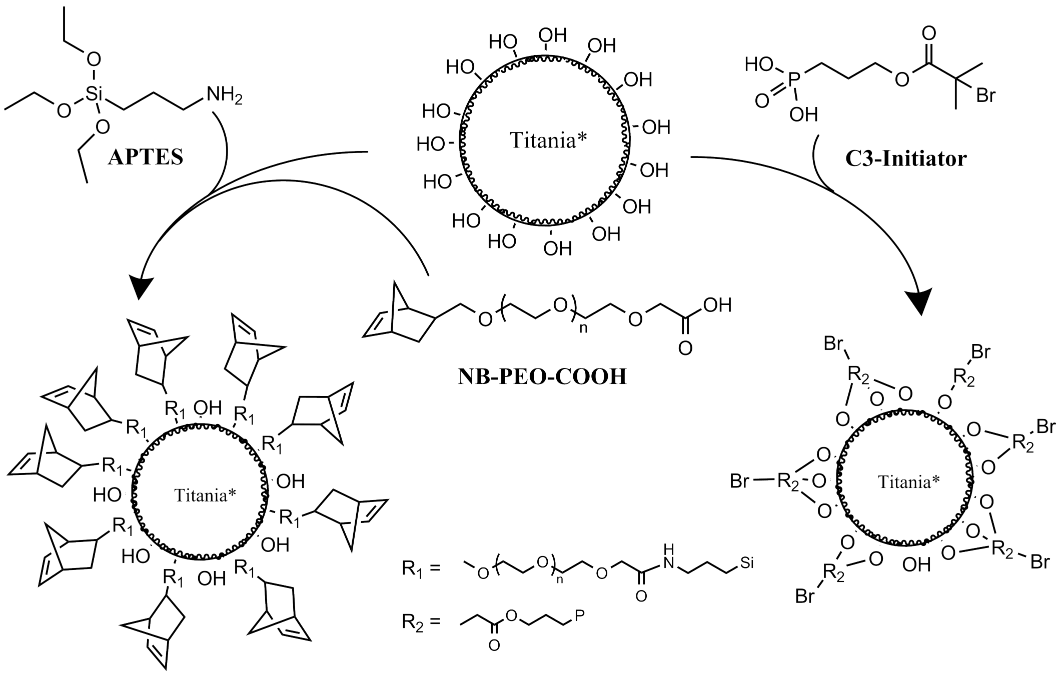

Figure 2-5: Pathway towards functionalization of titania surfaces *via* use of phosphonic acid group and silane group. C3-Initiator (purchased from Specific Polymers) is Propyl phosphonic acid -2-Bromo-2-methyl propanoate, APTES is (3-Aminopropyl)triethoxysilane, and NB-PEO-COOH is α-norbornenyl-ω-carboxylic acid-poly(ethylene oxide). *Note that while the image depicts particles, the system is not limited to just particles, but also includes flat surfaces and porous surfaces.

The inorganic surfaces were modified *via* two routes: (i) the phosphonic acid route, and (ii) the silane grafting route. This surface modification was only an intermediate step toward the formation of a continuous polymer membrane, using polymerization *via* (i) surface-initiated atom transfer radical polymerization (si-ATRP), or (ii) surface-initiated ring-opening metathesis polymerization (si-ROMP). These methods are discussed in Chapters 3 and Chapters 4, respectively.

2.5. Synthesis of Substrate

2.5.1. Materials

Two types of titanium oxide particles were used, including a nanopowder (average size 21 nm) from Sigma Aldrich (>99.7% anatase, CAS 1317-70-0), and an aqueous slurry of anatase (Aerodisp W740X) kindly provided by Evonik. Poly(ethylene Glycol) (PEG4000, Sigma Aldrich) was used for the synthesis of the flat titania substrates. Ceramic Tubular internal monochanel membranes (D10/6 – OD = 10.4 mm, ID = 6 mm) composed of either TiO_2 or ZrO_2 were purchased from Céramiques Techniques Industrielles (CTI, Salindres, France). Ethanol (96% purissimum grade pur; Xilab) was obtained and used after ultrafiltration using 0.45 µm cellulose filter.

2.5.2. Titania Particles

The titania particles, both Evonik particles and Sigma particles, were used as received. The Evonik particles were received dispersed in solution at a concentration of 0.55 g/mL used by syringing the dispersion into the target medium. The Sigma particles were powder in form (particle diameter roughly 21 nm), thus were dispersed in ethanol before use.

2.5.3. Flat Titania Substrates

These titania flat supports were made in-house. The titania flat substrates were prepared first via a mixture of 90% w/w Sigma particles and 10% w/w PEG4000 compressed at 200 psi for 10 minutes. The flat substrate (1 cm diameter) was then sintered at 800˚C in a temperature-controlled oven for 1 hour, with a ramp-up at 5˚C/minute from room temperature. The procedure was as follows:

1). 25˚C to 800˚C in 155 minutes (rate of 5˚C/min)
2). Temperature unchanged at 800˚C for 60 minutes
3). 800˚C to 25˚C for 60 minutes (*NOTE: this procedure was programed to be this, but in reality, could never be achieved thus was left to cool down for several hours)

The final sample substrate was then rinsed quickly with ethanol and left to dry before use.

2.5.4. CTI Titania Tublar Supports (TiO_2 and ZrO_2)

As mentioned, the samples were purchased from CTI. Each tubular membrane support was approximately 20 cm in length, and cut (using a diamond saw) to be cut into 5 cm length tubes for coating experiments. Note that after cutting, an ethanol rinse (shook several times inside a vial) was made and then left to dry in an oven at 80˚C.

2.6. Surface Binding Results

The first experiments were designed to provide good insight as to whether the silane or phosphonate based anchors were effective in binding on the different titania surfaces mentioned in Table 2-2.

2.6.1. Phosphonic Acid

Unlike silanes, phosphonic acids are beginning to appear more commonly in the marketplace. However, there is not the same level of knowledge on their stability during storage. A short study of the stability of the phosphonate-based molecule will be presented and subsequently used to evaluate this new product, which was provided by Specific Polymers. The compounds of the studied structures can be noted in Figure 2-6 below.

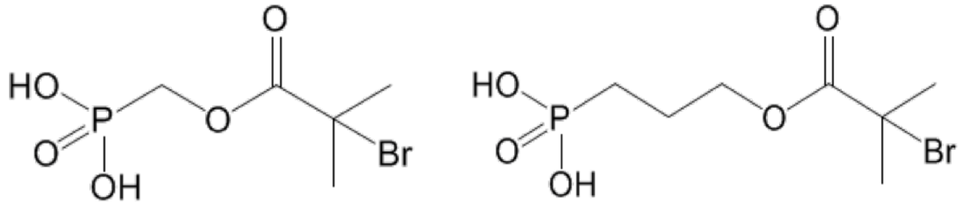

C1-Initiator

C3-Initiator

Figure 2-6: Structures of C1-Initiator (Methyl phosphonic acid -2-Bromo-2-methyl propanoate) and C3-Initiator (Propyl phosphonic acid -2-Bromo-2-methyl propanoate), provided by Specific Polymers. Reproduced from Ref. 223 with permission from the Centre National de la Recherche Scientifique (CNRS) and The Royal Society of Chemistry.

Note that from this point forward, we will define the Methyl phosphonic acid-2-bromo-2-methyl propanoate as **C1-Initiator** (due to the single carbon atom between the phosphorous and oxygen), and the Propyl phosphonic acid-2-bromo-2-methyl propanoate as **C3-Initiator**.

2.6.1.1. Grafting Procedure for Phosphonic Acid

2.6.1.1.1. Materials

Propyl phosphonic acid -2-Bromo-2-methyl propanoate ($Br-C(CH_3)_2(CO)O(C_3H_6)PO_3H_2$) from Specific Polymers (France) was used as a combined grafting molecule and polymerization initiator (also referred to as C3-Initiator). A slightly modified version of the initiator, Methyl phosphonic acid -2-Bromo-2-methyl propanoate (($Br-C(CH_3)_2(CO)O(CH_2)PO_3H_2$, which will be referred to as C1-Initiator) was also provided by Specific Polymers. Ethanol (96% purissimum grade pur; Xilab) was obtained and used after ultrafiltration using 0.45 µm cellulose filter. The particles and different substrates used were described in section 2.5 Synthesis of Substrate.

2.6.1.1.2. Grafting Procedure for Titania Particles

Both Sigma particles and Evonik particles were subjected to a similar process. In a typical reaction with Sigma particles, 0.1 g of the titania particles was dispersed with a Powergen 125 homogenizer (Fischer Scientific) into 15 mL of ethanol containing 0.245 g of the C3-Initiator grafting molecule and subsequently were dispersed in. The suspension was homogenized for 3 minutes, before being heated at 85˚C for 2 hours in a thermostated bath. The mixture was then centrifuged at 1,000 rpm for 5 minutes and the supernatant was removed. Final grafting was achieved by heating the collected powder in an oven for 4 hours at 155˚C. The particles were washed from ungrafted molecules by re-dispersing them with vortex stirring in 40 mL DI water. The mixture was left for several minutes, and then centrifuged at 5,000 rpm for 10 minutes. The supernatant was then removed and the remaining powder was dried overnight.

In the case of Evonik particles, larger quantities were made. 1 mL of the Evonik particle slurry (or about 1.55 g) was syringed into a mixture of the C3-Initiator (1.26 g) dissolved in ethanol (62.9 g). The mixture was homogenized for 3 minutes by shaking in a round-bottom flask and left to reflux for 2 hours at 85˚C in an oil bath. The mixture was then centrifuged (2,000 rpm for 10 minutes), decanted and then left to heat at 155˚C for 4 hours to mirror the final heating step. Washing was then performed using filtered ethanol and redispersion of the particles followed by re-centrifugation and recollection of the particles.

In the non-heated case, the Evonik particle dispersion in ethanol and the C3-Initiator remained the same (both quantity and method presented in the previous paragraph), but was left to stir at room temperature for 6 hours (unless it was a timed experiment of either 2 hours or 24 hours). The sample was then removed and centrifuged at 8,500 rpm for 10-15 minutes, decanted, and re-dispersed in ethanol to wash. The sample was then re-centrifuged (8,500 rpm for 15 minutes), decanted and left to dry overnight. In the case without exposure to UV-light, aluminium foil was used to cover all reagents and glassware during the reaction. Light exposure was also minimized (i.e. every container was covered with aluminium foil, and fumehood left under darkness).

2.6.1.1.3. Grafting of Flat Titania Surfaces

After the titania support (1 cm x 1 cm) were dried and cooled down, they were grafted in a similar manner to the titania particles. In a typical experiment, the C3-initiator (0.24 g) was mixed with ethanol (15 mL) and sonicated for 5 minutes, or until all the initiator particles were dispersed. The titania substrates were then heated with the C3-initiator/ethanol mixture at 85˚C for 2 hours. The titania substrate was then removed, rinsed with DI water quickly, and then heated at 155˚C for 4 hours before cooling down. A final rinse with water and ethanol was performed to remove any unbound initiators at this point.

2.6.1.1.4. Grafting of Porous Titania Surface (CTI porous substrates)

The rinsed/washed CTI porous tubes (TiO_2) were broken into smaller pieces (roughly 1 cm x 1 cm), and were re-washed with ethanol and dried. After the smaller pieces of the porous titania surfaces were dried, they were grafted in a similar manner to the titania particles. In a typical experiment, the C3-initiator (0.24 g) was mixed with ethanol (15 mL) and sonicated for 5 minutes or until all the initiator particles were dispersed. The porous titania substrates were then heated with the C3-initiator/ethanol mixture at 85˚C for 2 hours. The substrate was then removed, rinsed with DI water quickly, and then heated at 155˚C for 4 hours before cooling down. A final rinse with water and ethanol was performed to remove any unbound initiators at this point.

2.6.1.2. Stability of Organophosphorous Coupling Agent

Based on known literature, we initially assumed that the molecules were stable. However, we believe that the proximity between the phosphonic acid group and the ester-bond modify this stability. After a round of inconsistent results using the C1-initiator, we decided to examine the stability and to identify any potential problems that could affect our process. Thus, the decision was made to request our partner, Specific Polymers, to provide another candidate (C3-initiator) to compare. Therefore, upon receiving the provided products/reagents of the organophosphorous linkers (both C1-Initiator and C3-Initiator), we performed UV-Visible Spectroscopy to quickly determine the structure's stability with heat exposure, alongside ^{1}H NMR for comparison overtime.

2.6.1.2.1. UV-Visible Spectroscopy

When considering UV-Visible Spectroscopy, it was important to illustrate that the results obtained were accurate and without any impedance with this subsequent equipment/containers. As such, the first step was to verify that the spectrum was able to obtain all the necessary data. In order to be able to record the UV-visible spectra over the largest wavelength, we used a Quartz-based SUPRASIL® cuvette, which allow the largest spectrum range to be recorded (Figure 2-7).

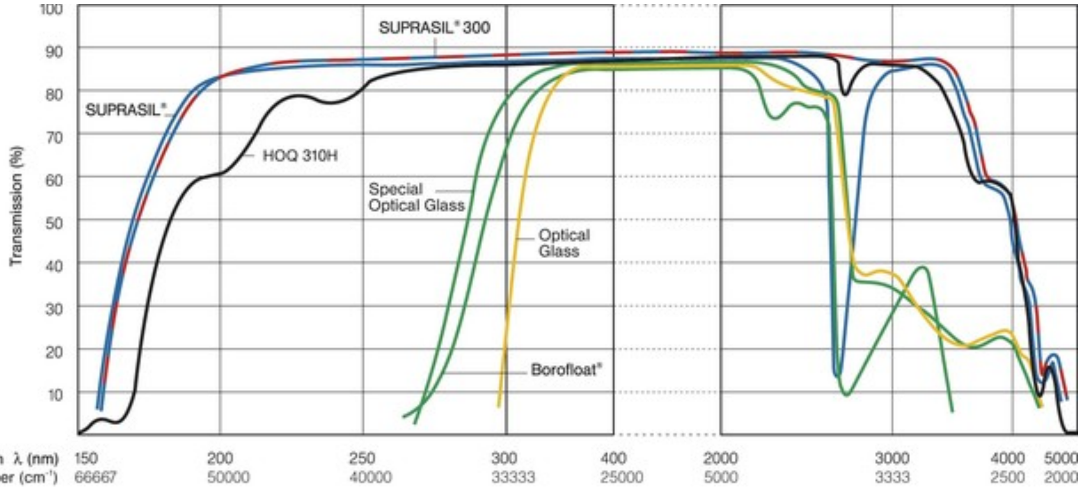

Figure 2-7: UV-Vis spectra for cuvette materials and range that is possible with each material.

The identification of the different components of the organophosphonic acid linkers (C1- and C3-initiators), was made by comparing their spectra with those of chemical groups belonging to these initiators, present in simple molecules. Figure 2-8 shows the chemicals used to compare the structure for their UV-Vis spectra and Figure 2-9 shows the resulting spectra.

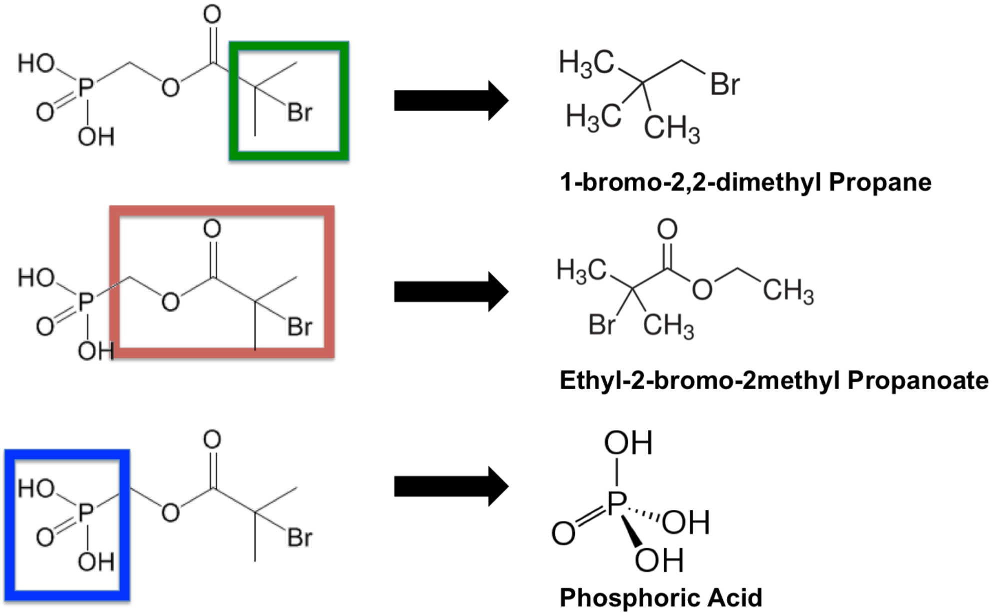

Figure 2-8: Component study of C1-Initiator for UV-Visible Spectroscopy.

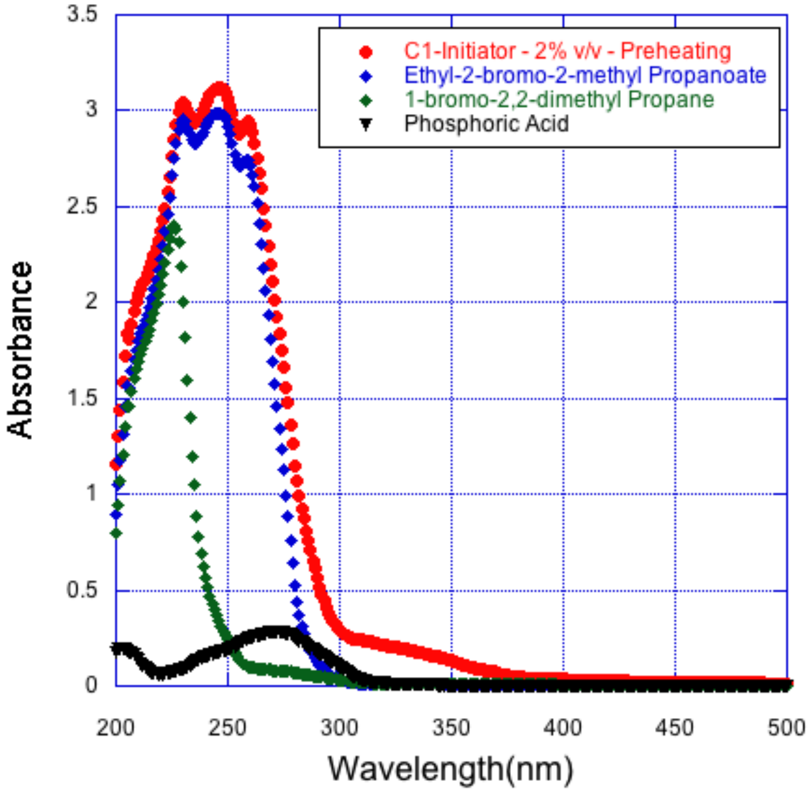

Figure 2-9: UV-Visible spectra for C1-Initiator preheating and subsequent spectra for components (as noted in Figure 2-8).

The resulting spectrum confirms the need for use of quartz cells, as the spectra peaks begin beyond the limits of other types of cells. More specifically, the entire UV-visible spectrum for both initiators can be explained by the contributions from each component, when compared with our reference compounds. This means that any additional feature in the future would result from a chemical modification of our molecules.

As observed in Figure 2-9, the molecules present a high absorbance beyond the value of 2 in addition to the unstable peaks at the apex of the absorbance curve. This is due to the absolute value of the absorbance being beyond the sensibility limit, which prevented us from quantitatively comparing these values with literature/expected excitation wavelength. However, qualitative observations can still serve as a good comparative method for probing the molecule stability.

Because heating is part of the grafting procedure normally used with phosphonic acid grafting, we studied if heating at 85˚C for a couple of hours would destabilize these molecules (Figure 2-10).

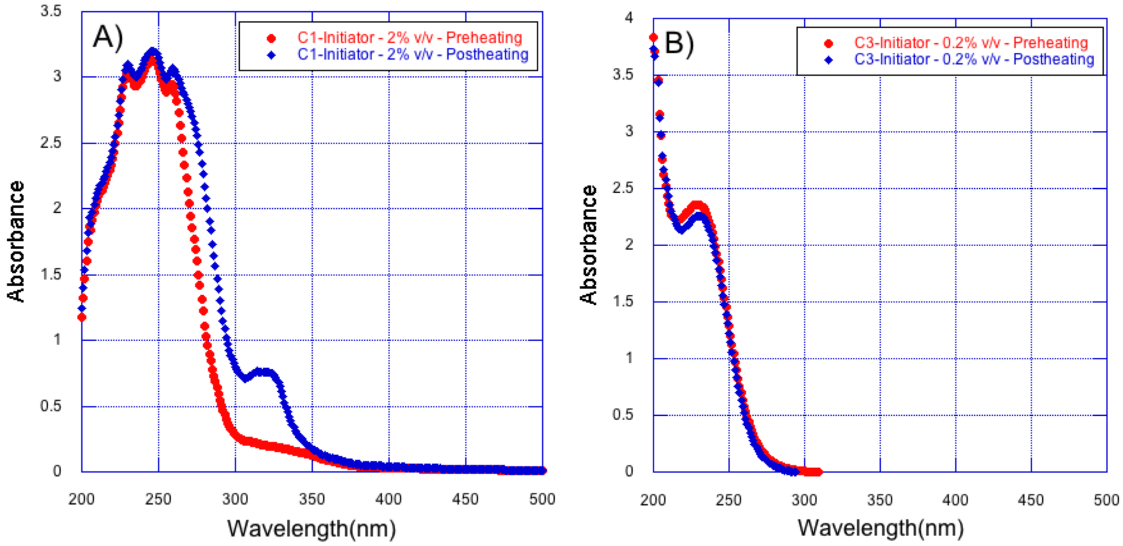

Figure 2-10: UV-Vis spectra obtained for A) C1-Initiator and B) C3-Initiator with preheating, and postheating (after 2 hours at 85˚C).

The UV-Vis spectra for the C1-initiatior reveal a modification after heating at 85°C, with an additional "hump", compared to the fresh, preheated sample. As for the C3-initiator, the shape of the spectra is different from what observed with the C1-initiatior, but it remains unchanged upon heating. We conclude from this first analysis that the C1-Initiator could present stability issues when heated. Therefore, we conducted additional analyses to find out the origin of this instability, and confirm the higher stability found with the C3-Initiator.

2.6.1.2.2. ^{1}H NMR

Liquid ^{1}H NMR was used to validate the structure and characterize the stability of the initiators. The ^{1}H NMR was monitored for the C1-initiator and C3-initiator over a 3-month period of time to check if the storage mode, as initially recommended by the provider (storage in air at 4°C), could prevent the destabilization of the C1-initiator. ^{1}H NMR spectra results reveal degradation over time, according to the degradation scheme shown in Figure 2-11. Table 2-3 displays the ^{1}H NMR integration values obtained with the C1-initiator, as received and after a three-month storage at room temperature. Note that the spectra can be found in Appendix A.

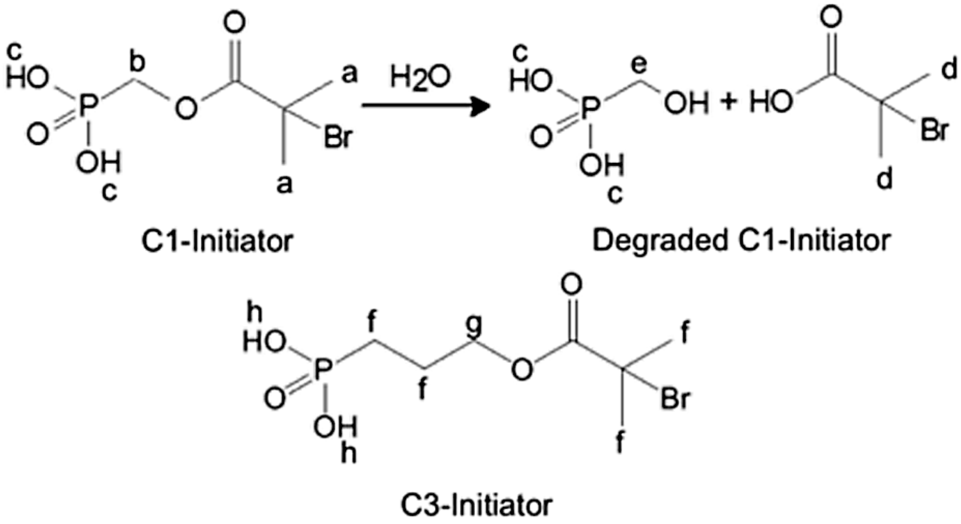

Figure 2-11: Organophosphorous initiator: C1-Initiator, degraded C1-Initiator and C3-Initiator with their associated 1H NMR labeling. Reproduced from Ref. 223 with permission from the Centre National de la Recherche Scientifique (CNRS) and The Royal Society of Chemistry.

Table 2-3: Integration values for C1-Initiator taken from ^{1}H NMR spectra provided from Specific Polymers and after 3 months storage. Reproduced from Ref. 223 with permission from the Centre National de la Recherche Scientifique (CNRS) and The Royal Society of Chemistry.

Peak	Integration Value (original)	Integration Value (3 months)
a (1.93 ppm)	6	4.8
d (1.95 ppm)	-	1.1
e (3.8 ppm)	-	0.3
b (4.5 ppm)	2	1.4
c (10-11 ppm)	2.3	2.2

These ^{1}H NMR spectra demonstrate that the stability of the C1-initiator is fairly poor (Figure 2-11 & Table 2-3), with its degradation resulting in the appearance of two new peaks formed by the hydrolysis of the ester group (note the peak formation 'd' and 'e'). It is hypothesized that the short length between the ester group and the phosphonic acid group results in an easily hydrolizable bond. Unlike the C1-initiator, the C3-Initiator was successfully tested in parallel without noticeable evolution after a three month storage (Table 2-4). We concluded that the C3-initiator should be used in this study, and that all preliminary tests conducted with C1-initiator should be discarded.

Table 2-4: Integration values for C3-Initiator taken from ^{1}H NMR spectra - measurements upon receiving C3-Initiator and post 3 months. Reproduced from Ref. 223 with permission from the Centre National de la Recherche Scientifique (CNRS) and The Royal Society of Chemistry.

Peak	Integration Value (original)	Integration Value (3 months)
f (1.93 ppm)	9.8	10.2
g (4.23 ppm)	2.0	2.0
h (8-10 ppm)	2.4	3.1

2.6.1.3. C3-Initiator anchoring onto Titania

The procedure for the binding of the C3-Initiator can be found in the previous section, 2.6.1.1 Grafting Procedure for Phosphonic Acid. We studied this binding with three different supports that were mentioned in Table 2-2: particles (Evonik or Sigma particles), flat titania supports, and porous tubes (from CTI SA.).

2.6.1.3.1. Solid-State NMR

Actual grafting of the C3-Initiator was followed by ^{31}P solid-state NMR made on the unbound C3-Initiator along with the C3-initiator bound to the titania based surface (with and without washing). The results are presented in Figure 2-12.

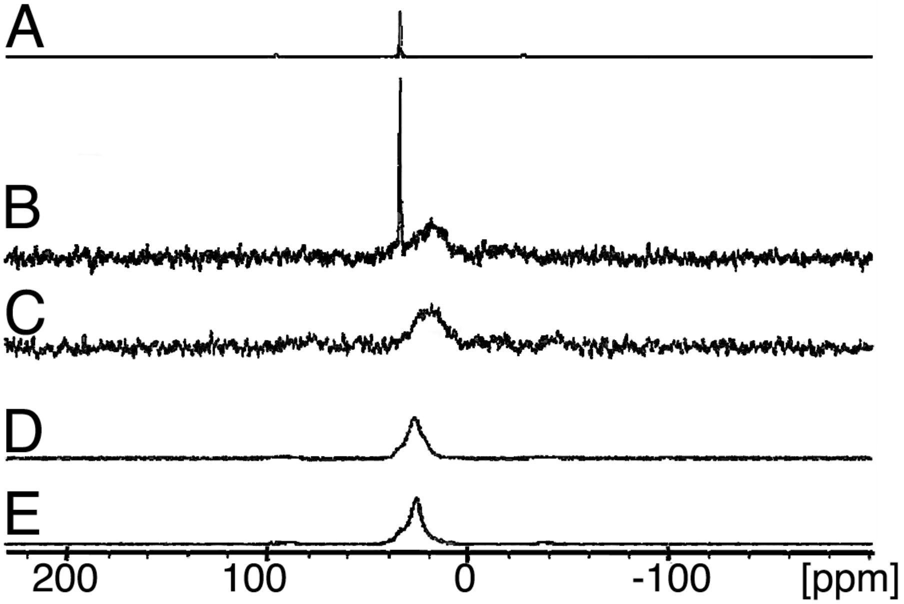

Figure 2-12: ^{31}P Solid State NMR spectra for A) C3-initiator, B) C3-initiator bound to the CTI porous tube (unwashed), C) the C3-initiator bound to the CTI porous tube (after washing), D) C3-initiator bound to Evonik particles after washing and E) C3-initiator bound to Sigma particles after washing. Reproduced from Ref. 223 with permission from the Centre National de la Recherche Scientifique (CNRS) and The Royal Society of Chemistry.

A narrow peak at around ~35 ppm is observed for the unbound initiator (Figure 2-12-A), which is assigned to the free phosphonic acid group. This peak remains after grafting but before washing (Figure 2-12-B) along with a broader peak at 18 ppm. This broadening and peak shift is consistent with previous results found with phosphonic acid group binding.[176,59] Upon washing (Figure 2-12-C), the narrow peak disappears and only the broad peak assigned to the phosphonic group bound to the titania surface remains. This is observed with flat porous titania substrates (Figure 2-12-C) and particles (Figure 2-12-D&E). Confirmation with use of both Evonik and Sigma particles yielded similar results, but with the exception that the binding ability of the phosphonic acid increased substantially with particles, as the signal intensity was much greater than that performed with the solid flat surface, in agreement with the silane-based route as seen from the work by Bernardoni (Figure 2-4).[174] ^{31}P NMR analyses also revealed that this grafting mechanism could take place at room temperature with the ability to form bonds with the titania, as shown from the broad peaks in Figure 2-13 and Figure 2-14. The spectra displayed in Figure 2-15 indicates that the signal collected from grafted porous tubes provided by CTI was extremely weak, but present. This low intensity is believed to be the result of sample preparation, where some powder is scratched from the tube top surface, whereas grafted molecules were distributed over the whole internal surface within the porous ceramic. Compared with grafting onto a flat dense surface with the same concentration in initiator, the grafted density is thus lower. Note that the number of scans required were over 10,000 while compared to the 1,000 scans needed for the Sigma and Evonik particle samples.

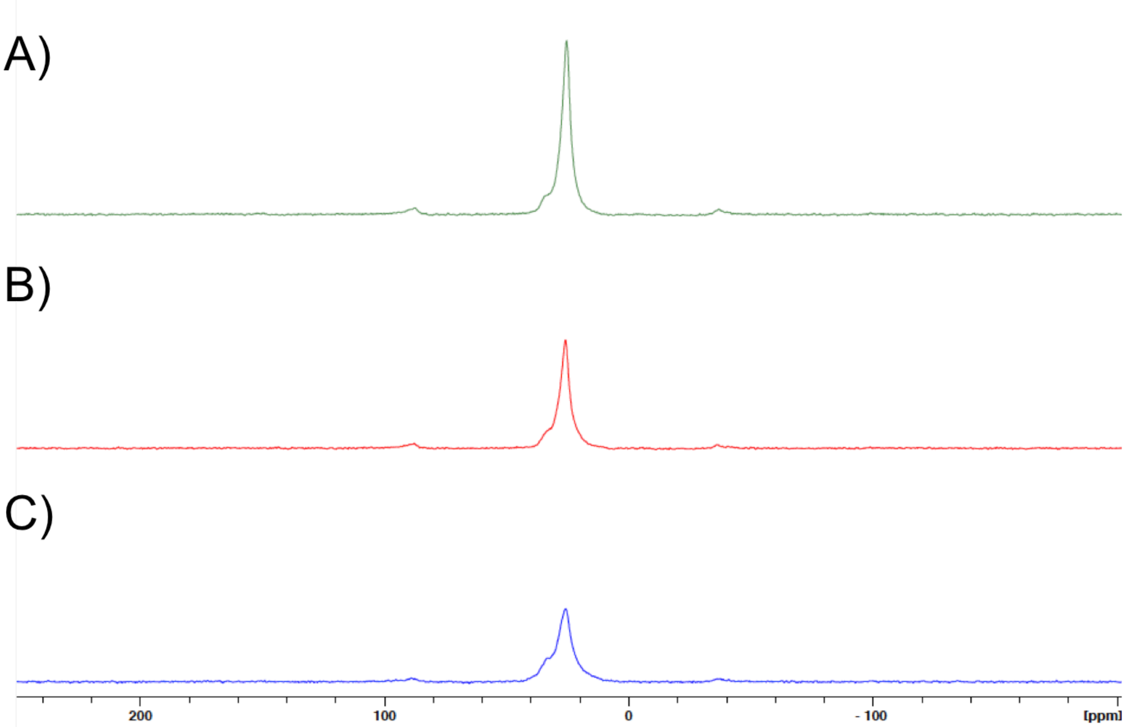

Figure 2-13: ^{31}P solid state NMR spectra for Sigma particles bound to C3-Initiator molecules – A) performed at room temperature (20˚C) for 2 hours, B) performed at 85˚C for 2 hours and C) performed at 85˚C for 2 hours, centrifuged and then heated at 155˚C for 4 hours.

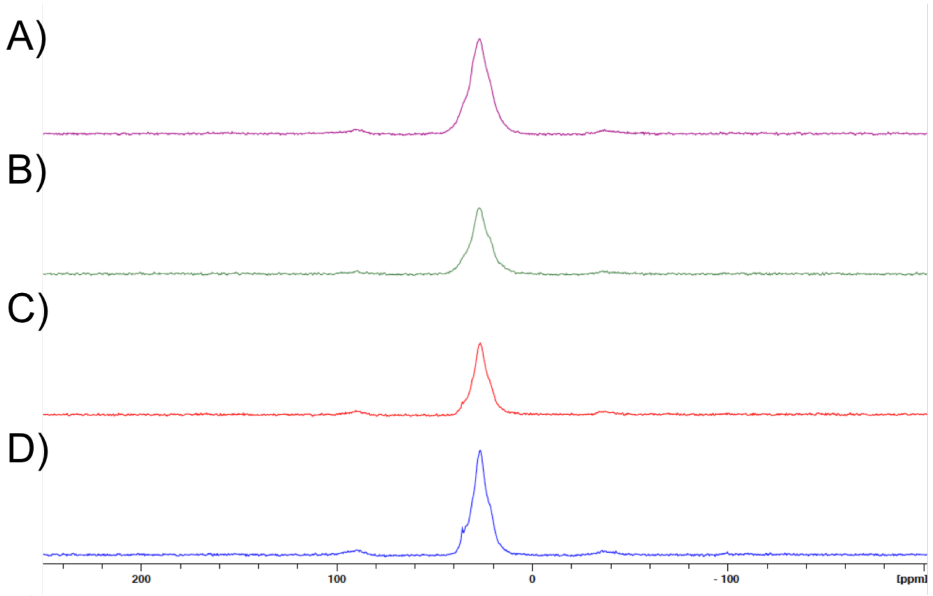

Figure 2-14: ^{31}P **solid state NMR for Evonik particles bound with C3-Initiator molecules – A) performed at room temperature (20˚C) for 2 hours, B) performed at 85˚C for 2 hours, C) performed at 85˚C for 2 hours then centrifuged and heated at 155˚C for 4 hours, and D) performed at 85˚C for 2 hours then centrifuged and heated at 155˚C for 4 hours then washed with DI water and dried.**

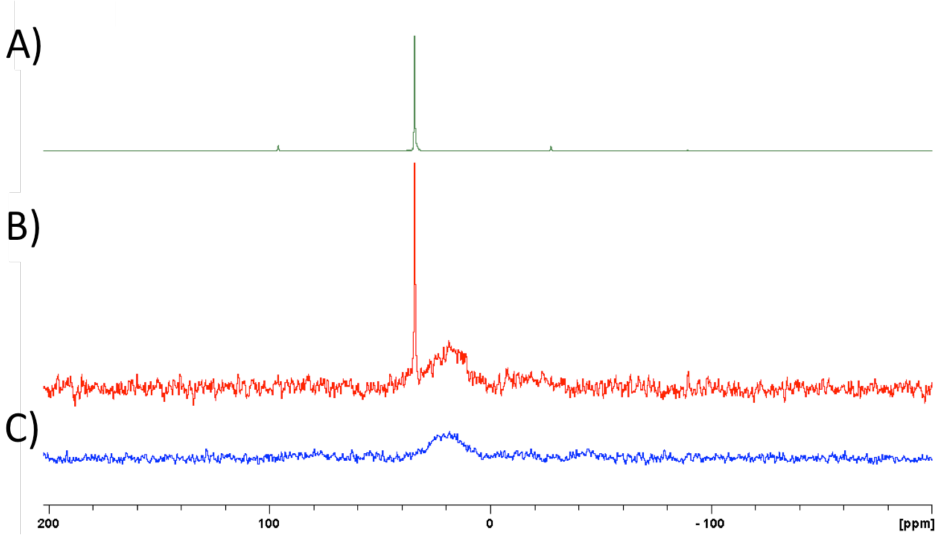

Figure 2-15: ^{31}P **solid state NMR spectra for porous CTI** TiO_2 **supports with C3-Initiator molecules – with A) unbound C3-Initiator, B) bound C3-Initiator with the titania support unwashed, and C) bound C3-Initiator with the titania support after washing.**

The usefulness of ^{31}P **solid state NMR cannot be dismissed. We have determined grafting onto particles is much simpler than on flat or porous surfaces from this route, and that the grafting procedure will occur even at room temperature with no heating. In addition, the quantity of grafted C3-Initiators is much higher in particles than in the CTI porous tubes, due to the signal intensity.**

2.6.1.3.2. X-Ray Photospectroscopy (XPS)

XPS allowed us to further characterize the nature of the surface on the powders, flat supports and porous supports with a special emphasis on the stability of the bromine group located at the exposed terminus of the initiator molecule. Both bromine and phosphorous atoms are clearly identified on the XPS spectra, shown in Figure 2-16, which confirms the actual grafting and the stability of the initiator function upon grafting. Table 2-5 and Table 2-6 show the subsequent XPS values obtained for each element of interest.

Table 2-5: XPS atomic percentages obtained for the Sigma particles, Evonik particles and Flat Titania Substrates. Reproduced from Ref. 223 with permission from the Centre National de la Recherche Scientifique (CNRS) and The Royal Society of Chemistry.

Element	Sigma particle	Sigma particles + C3-Initiator*	Evonik particles	Evonik particles + C3-Initiator*	Flat Titania Substrate	Flat Titania Substrate + C3-Initiator**
Br3p3	-	0.46%	-	0.41%	-	0.13%
P2p	-	3.73%	-	3.59%	0.22%	2.86%
C1s	30.44%	28.03%	21.39%	27.37%	17.6%	22.3%
N1s	0.38%	0.38%	1.04%	0.45%	0.19%	1.8%
Ti2p	19.34%	17.25%	21.64%	17.40%	23.3%	20.1%
O1s	47.38%	48.79%	53.40%	49.04%	53.8%	52.2%

*data was obtained via averaging of 4 different points on the surface of the particles

** data was obtained via one point measurement

Table 2-6: XPS atomic percentages obtained for CTI porous tubes provided by CTI

Element	CTI porous tube	CTI porous tube + C3-Initiator
Br3d	0.08%	0.15%
Al2p	6.62%	4.15%
Si2p	0.87%	1.26%
P2p	2.79%	3.6%
C1s	25.38%	31.65%
Ti2p	9.41%	9.7%
O1s	52.91%	47.67%

These resulting signals only exist for samples that were bound with the organophosphorous/C3-initiator, not with C1-initiator, which confirms *a posteriori* the lack of stability of C1-initiator. We quantified the proportion of each component as shown in Table 2-5 and Table 2-6. Assessing these values, the comparison can be made directly as these measurements are made quantitatively (calibrated to a reference) as these percentages are the atomic concentrations of the surface. Surprisingly, the actual phosphorus to bromine ratio is not the expected 1:1 ratio.

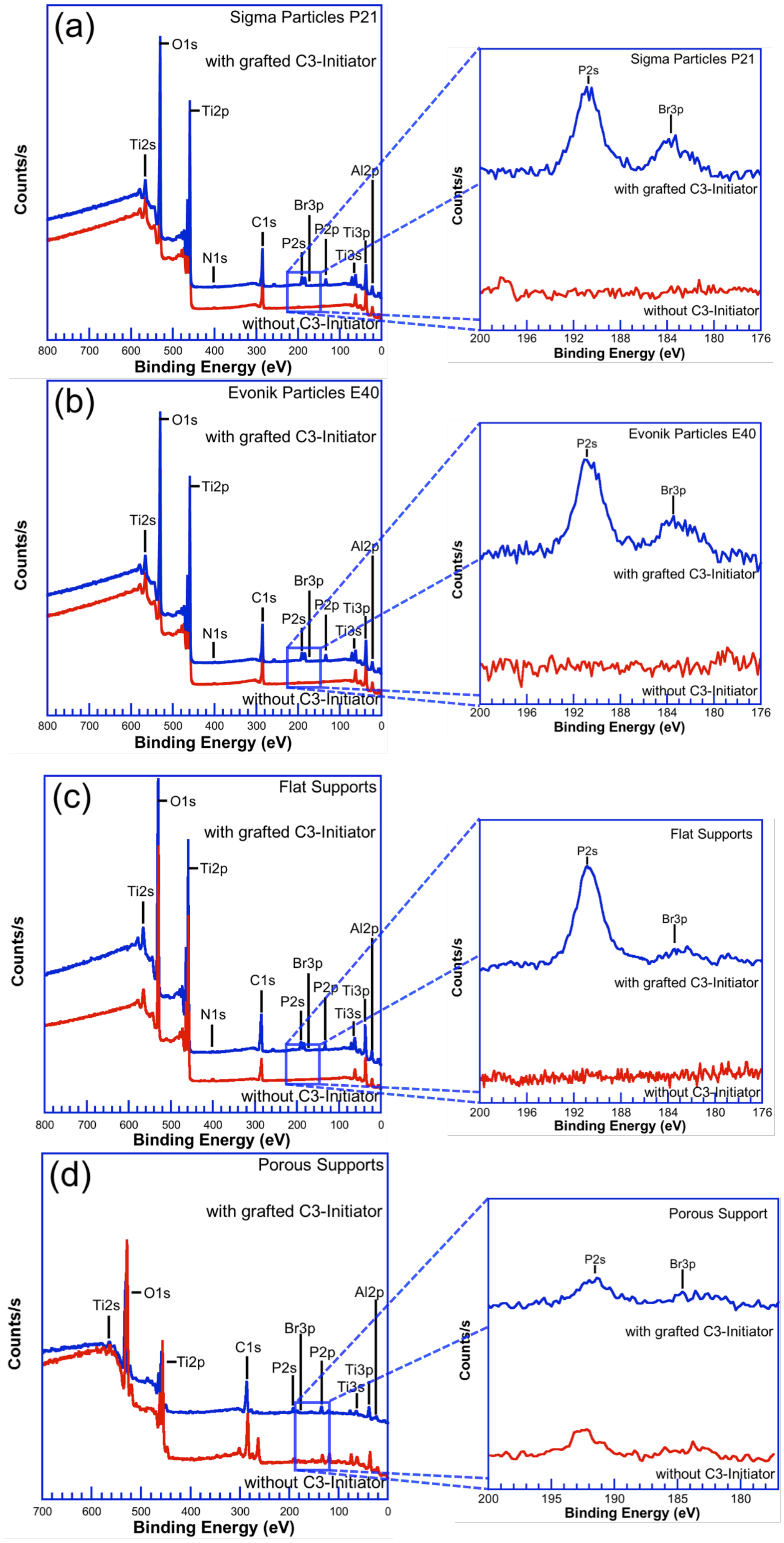

Figure 2-16: XPS results for Sigma Particles, Evonik Particles, Flat Titania Supports and CTI Porous Tubes. Adapted from Ref. 223 with permission from the Centre National de la Recherche Scientifique (CNRS) and The Royal Society of Chemistry.

We presume that is is due to potential exposure to sunlight during reaction, as literature has previously shown this can potentially break the P-C bond.[176] However, comparative tests with grafted samples exposed and hidden from UV light did not reveal any significant change, which appears to indicate this was not the main cause of bromine loss in our case, as noted in Table 2-7.

Table 2-7: XPS results for UV-free binding reaction

Element	Sigma particles + C3-Initiator	Evonik particles + C3-Initiator	Flat Titania Substrates + C3-Initiator
Al2p	1.2 %	1.46 %	1.56 %
Si2p	-	-	0.7 %
P2p	4.27 %	4.06 %	3.73 %
Br3p3	0.42 %	0.59 %	0.22 %
C1s	26.39 %	26.95 %	23.18 %
N1s	0.39 %	0.21 %	0.25 %
Ti2p	17.08 %	16.9 %	16.58 %
O1s	50.07 %	49.59 %	52.34 %

It could be hypothesized that the loss of bromine could have been due to the grafting reaction itself. Nonetheless, we determined that the best outcome was for us to continue using the Evonik particles, as candidates for the project. In this regard, the comparison between the different reaction times for the Evonik particles set at room temperature was also studied *via* XPS. The results are shown in Table 2-8 below.

Table 2-8: XPS results for UV-Free binding over time of C3-Initiator to Evonik particles

Element	2 hr	6 hr	24 hr
Al2p	0.73%	1.59%	0.78%
P2p	5.4%	4.64%	5.73%
Br3p3	0.49%	0.44%	0.57%
C1s	29.84%	28.52%	32.27%
N1s	0.13%	0.14%	0.12%
Ti2p	14.84%	15.63%	13.45%
O1s	48.39%	48.81%	46.98%

The evidence here tells us that even in the best-case scenario (without UV light), we obtain results that are fairly similar within the first several hours. While there is an observed slight increase in the phosphorous and bromine content after 24 hours compared to the 6 or 2 hour mark, this could also be due to localized area scanning (even being averaged over 3-4 different points of the powdered sample). This is very well within acceptable error, leaving us to believe that the sample binding was achieved early on during the reaction. As a result, the decision to leave the reaction time of the C3-Initiator with the Evonik particles was set at 6 hours at room temperature.

In continuing the study with binding the C3-Initiator to the surface of the Evonik particles, alterations from different solvents were also briefly studied. In most of our studies, ethanol was the first solvent of choice. However, other solvents were also attempted, including dichloromethane (DCM) and acetone, with reactions under nitrogen flow. However, evaporation was too quick for the DCM sample, and as such, the solvent was removed as a choice. Comparing both acetone and ethanol based solvents for their grafting is displayed in Table 2-9.

Table 2-9: XPS results for Evonik particles comparing blank to ethanol and acetone routes (for solvent)

Name	Evonik particle (unmodified)	Ethanol	Acetone
Br3d	-	0.44%	0.47%
P2p	-	1.67%	2.07%
C1s	21.39%	25.53%	24.32%
N1s	1.04%	0.56%	0.59%
Ti2p	21.64%	19.53%	19.33%
O1s	53.40%	52.29%	52.81%

The results show minimal effect from the change in solvent, with acetone being marginally higher in terms of bromine and phosphorous yield. This lower quantity left the conclusion that ethanol, while slightly lower, was much easier to use during processing as it did not evaporate as quickly as acetone during the grafting procedure. The final consensus from this result was ethanol still remained the best solvent for grafting.

The verification of the existence of the bromide group was effectively determined to exist *via* XPS. While NMR can determine the grafting occurs, XPS was able to help verify that bromine (or the ATRP initiator) remained on the surface.

2.6.1.3.3. Quantifiable Yield (TGA)

While XPS is an extremely powerful tool for nondestructive elemental analysis of a sample, it was difficult to determine the total amount of product that was grafted for a given batch of samples. In this respect, thermogravimetric analysis (TGA) was deployed to determine the quantity of product being grafted, in a similar method presented by Matsuno *et al.*[170,171] We first measured the thermal evolution of the unmodified Evonik particles, as a reference. We then measured the post-functionalized Evonik particles (TiO_2-g-C3-Initiator). Figure 2-17 compares the TGA curves between unmodified Evonik particles and C3-Initiator modified ones.

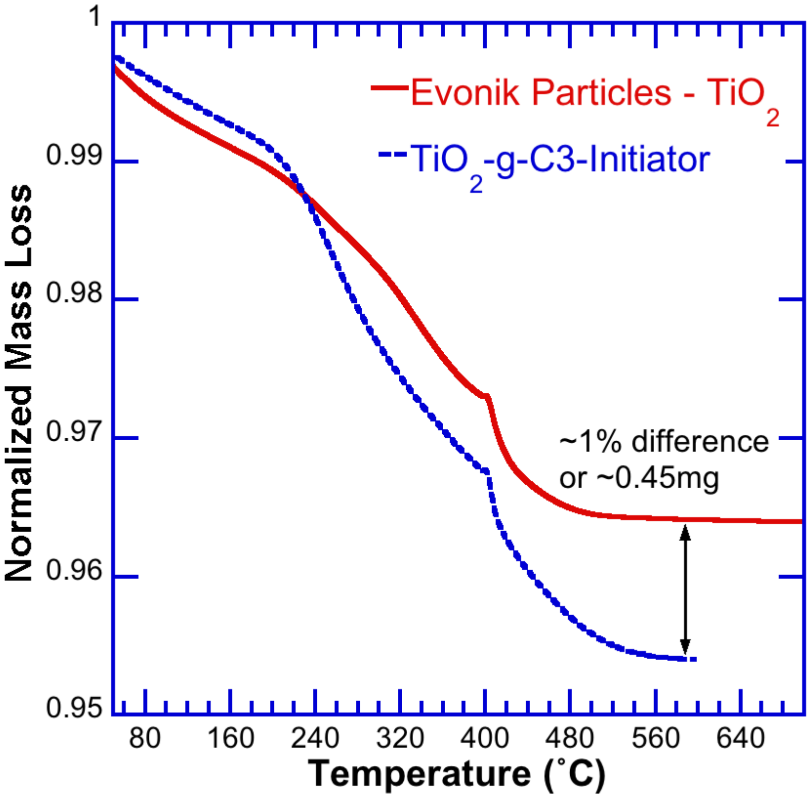

Figure 2-17: Comparison between Evonik particles compared to after grafting with the C3-Initiator.

Despite the very small differences between both curves, we could identify the difference in the total mass change due solely to the C3-Initiator. The results, determined *via* the final absolute difference in weight from the samples are shown in Table 2-10.

Table 2-10: Analysed sample weights and subsequent mass loss from TGA

Sample	Original Mass (mg)	Mass Loss (%)	Mass Loss (mg)
TiO_2(Evonik)	37.64mg	2.45%	0.92mg
TiO_2-g-C3-Initiator	37.62mg	3.67%	1.38mg

About 0.45mg of weight difference is assigned to the C3-Initiator. We used this value to evaluate the number of C3-Initiator molecules bound to the surface of the titania particles, according to some assumptions:

1) Every Evonik particle has a diameter of 100 nm
2) The phosphorous end/phosphonic acid group bound to the Evonik particle surface is not removed/vapourized during the TGA analysis, thus changing our molecular mass from 289 g/mol to 208 g/mol (Ramadan *et al.* showed that the bidentate phosphonic group persisted up to 800˚C).[180]
3) The particles are uniformly coated on the particle surface
4) The density of the Evonik particles is the same as regular titanium dioxide density (4.23g/cm^3)
5) Each Evonik particle is perfectly spherical

In this respect, we used the following equations to determine the subsequent grafting density.

1) Determining the total number of C3-Initiator molecules:

$$Total\ Molecules_{C3-Initiator} = \left[\frac{Mass\ Loss_{TiO_2-g-C3-Initiator} - Mass\ Loss_{TiO_2}}{Molar\ Mass_{degraded\ C3-Initiator\ group}}\right] x\ N_A$$

where:

- $Molecules_{C3-Initiator}$ is in the units “molecules”
- $Mass\ Loss_{TiO2-g-C3-Initiator}$ is in the units “g”
- $Mass\ Loss_{TiO2}$ is in the units “g”
- $Molar\ Mass_{degraded\ C3-Initiator\ group}$ is in the units “g/mol” (or 208g/mol)
- N_A is Avogadro’s Number, which is 6.022x10^{23} molecules/mol

2) Determining the volume of Evonik particles:

$$Total\ Volume_{TiO_2} = \left[\frac{Mass_{TiO_2\ Initial} - Mass\ Loss_{TiO_2}}{\rho_{TiO_2}}\right]$$

where:

- $Mass_{TiO_2\ Initial}$ and $Mass\ Loss_{TiO_2}$ are in units of "g"
- ρ_{TiO_2} is the density of TiO_2, which is 4.23g/cm^3
- $Total\ Volume_{TiO_2}$ is in units of "cm^3"

3) Determining the volume of each Evonik particle:

$$Volume_{each\ TiO_2} = \left[\frac{4\pi r^3}{3}\right]$$

where:

- r is the radius of the TiO_2 particle, in units of "cm"
- $Volume_{each\ TiO_2}$ is the volume of each TiO_2 particle, in units of "cm^3"

4) Determining the total surface area of each Evonik particle:

$$Surface\ Area_{\ each\ TiO_2} = 4\pi r^2$$

where:

- r is the radius of the TiO_2 particle, in units of "cm"
- $Surface\ Area_{\ each\ TiO_2}$ is the surface area of each TiO_2 particle, in units of "cm^2"

5) Number of TiO_2 particles:

$$Number\ of\ TiO_2\ Particles = \frac{Total\ Volume_{TiO_2}}{Volume_{each\ TiO_2}}$$

where:

- $Number\ of\ TiO_2\ Particles$ is in units of "particles"

6) Dividing the Molecules of C3-Initiator by the Number of TiO_2 Particles:

$$\frac{Molecules_{C3-Initiator}}{TiO_2\ Particle} = \frac{Total\ Molecules_{C3-Initiator}}{Number\ of\ TiO_2\ Particles}$$

where:

- $\frac{Molecules_{C3-Initiator}}{TiO_2\ Particle}$ is in units of "molecules/particle"

7) To determine grafting density

$$Grafting\ Density_{C3-Initiator} = \frac{Total\ Molecules_{C3-Initiator}}{(Surface\ Area_{each\ TiO_2}\ x\ Number\ of\ TiO_2\ Particles) x\ 10^{14}}$$

where:

- $\frac{Molecules_{C3-Initiator}}{TiO_2\ Particle}$ is in units of "molecules/particle"
- $Grafting\ Density_{C3-Initiator}$ is in units of "molecules/nm^2"
- 10^{14} is used to convert cm^2 into nm^2

The results for these seven steps of calculations are given in Table 2-11.

.

Table 2-11: Calculated grafting density of C3-Initiator per nm^2 of TiO_2 Evonik particles

Step	Values	Units
Total Molecules of C3-Initiator	$1.33x10^{18}$	molecules
Total Volume of TiO_2	$8.68x10^{-3}$	cm^3
Volume of each TiO_2	$5.24x10^{-16}$	cm^3/particle
Surface Area of each TiO_2	$3.14x10^{-10}$	cm^2
Number of TiO_2 Particles	$1.66x10^{13}$	particle
Molecules of C3-Initiator/Particle	$8.01x10^{4}$	molecules/particle
Grafting Density	2.55	molecules/nm^2

From the results, we conclude that we have obtained a grafting density of around 2.5 molecules of C3-Initiator per nm^2 of the Evonik particle surface. This does not represent the maximum packing, as other researchers have shown higher packing from alkyphosphonate derivatives.[164] However, this represents a significant amount that can be used for surface-initiated polymerization. Furthermore, we have shown that this method of determining the number of initiators appears to be accurate enough to give quantitative grafting density, which will be required with determination of the degree of polymerization (see Chapter 3).

TGA helped determine that the grafting density of the C3-Initiator on the Evonik particles is about 2.5 molecules/nm^2.

2.6.2. Silane Pathway

While the previous pathway of using the C3-Initiator was perhaps easier in approach, the use of silanes must also not be neglected. As we mentioned previously in section 2.2.3 Silanes, they are probably the most commercially available product. In this respect, we will first present the results obtained in functionalizing the Evonik particles with the silane molecule (3-Aminopropyl)triethoxysilane, also known more commonly as APTES (see Figure 2-18).

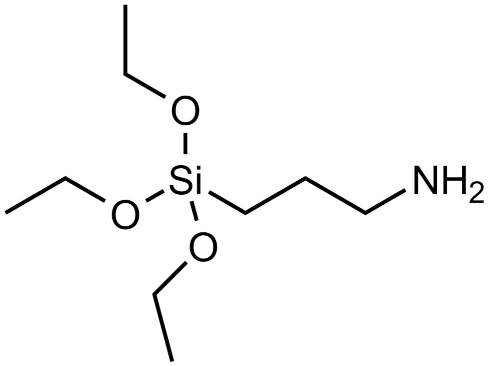

Figure 2-18: Molecular structure of (3-Aminopropyl)triethoxysilane(APTES)

It is evident from the structure of this molecule that the binding of the silicon atom to the surface of the titania particles will result in the release of ethanol. In addition, the presence of water can also help homopolymerize the APTES, resulting in a precipitate (highly undesired). Therefore, performing the reaction in an anhydrous environment is mandatory to counteract homopolymerization in this case.

The possibility to graft APTES molecule onto titania particles is important as the amine terminus of the molecule should be exposed around the particles. As mentioned previously by Song *et al.*, the slight charge from the amine has the ability for it interact and bond with the titania surface, also known as reverse attachment.[175] While this may seem trivial, it is important that the amine function faces outward, owing to the fact that it will be later reacted with a carboxylic acid terminated molecule, as illustrated in Figure 2-5 previously (and explained in more depth in Chapter 4).

This following section will investigate specifically the binding of the APTES molecules onto two different titania surfaces (for the Evonik particles and the CTI porous tubes), and our parallel attempts to quantify the number of molecules grafted after considering the effect of reverse attachment.

2.6.2.1. Grafting Procedure for Silane

2.6.2.1.1. Materials

(3-Aminopropyl)triethoxysilane – APTES (99%, Aldrich) and hexane (anhydrous 95%, Sigma-Aldrich) were used without further processing. DMF (anhydrous 99.8%, Sigma-Aldrich), Toluene (ACS reagent, 99.5%, Sigma-Aldrich) were kept anhydrous and stored with molecular sieves.

2.6.2.1.2. Grafting of Titania Porous Substrates (CTI) with APTES

Small pieces of the CTI porous substrates (1 cm x 1 cm x 0.5 cm) were cleaned with ethanol and dried in an oven (80˚C) overnight. The samples were then introduced into a glovebox with a vacuum-heating unit, and were left at 150˚C under vacuum (10^{-4} torr) for 19 hours to finish cleaning. Afterwards, each sample was submerged into a mixture of APTES in hexane (10^{-2} M, or about 4.7 µL APTES in 2 mL Hexane for each sample). The samples were left in the hexane solution for 2 hours, and then rinsed with heptane several times. The now functionalized CTI-g-APTES is then vacuumed dried under heat (150˚C) for 4 hours.

2.6.2.1.3. Grafting of Titania Particles with APTES

The Evonik particles taken from the slurry (AERODISP® W 740X; 5 mL) was mixed with Ethanol (96% Xilab; 10 mL). Afterwards, 10 mL of the mixture was added into a flamed 250 mL round bottom flask. Anhydrous toluene (stored under molecular sieves;

20 mL) was added to the round bottom flask, and a 3-cycle freeze-pump-thaw was performed to degas the liquid. The mixture was then entered into the argon glovebox in order to add APTES (0.75 mL). The round bottom flask was then subjected to a thermostat oil bath set at 70˚C for 4 hours. The mixture was then filtered and washed with ethanol several times before vacuum drying overnight. (This forms the TiO_2-g-APTES particles)

2.6.2.2. Grafting Method and Study – Particles vs. Surface

First, we quantified the amount of silanes grafted onto CTI titania porous tubes, and analyzed the resulting materials by XPS. In this first case, the grafting protocol was that first established by Pichavant *et al.* in 2012.[125] The results of the XPS analysis are given in Table 2-12.

Table 2-12: XPS results for porous titania support (CTI) bound with APTES

Element	CTI Porous Tubes	CTI Porous Tubes + APTES
Al2p	8.56%	8.78%
Si2p	1.49%	3.25%
P2p	3.47%	3.14%
C1s	24.85%	25.61%
N1s	0.71%	1.45%
Ti2p	11.86%	10.99%
O1s	45.81%	44.02%

The comparison of analyses between ungrafted and grafted APTES on the CTI porous tubes show fairly low changes in the Silicon (<2%) and Nitrogen (<1%) percentages. Noting this lower conversion, we decided to continue to use Evonik particles for our binding studies. A process adapted to flat titania surfaces was adapted from Song *et al.* to use the Evonik particles.[175] Results are shown in Table 2-13.

Table 2-13: XPS results for Evonik particles - pre and post modified with APTES

Name	Evonik particles	Evonik particles + APTES
Al2p	2.27%	0.72%
Si2p	-	6.13%
C1s	21.39%	29.98%
N1s	1.04%	4.29%
Ti2p	21.64%	14.51%
O1s	53.40%	44.17%

Compared to the previous study on the CTI porous tubes, the present analysis shows a significant increase in Silicon alongside the 3% increase of Nitrogen, indicating the presence of APTES on the surface our Evonik particles. As we have determined the best substrate choices are the Evonik particles, the following studies will be focused on attempting to quantify the APTES bound.

XPS determined that the CTI porous substrates could not graft as much APTES compared to the Evonik particles.

2.6.2.3. Quantification of APTES via TGA

As previously illustrated in section 2.6.1.3.3 Quantifiable Yield (TGA), TGA was used to calculate the grafting yield on the Evonik particles. Utilizing a similar methodology for the APTES molecule, we can also perform the same calculation and analysis. In this case, we will make the following similar assumptions:

1. As the particles are the same (Evonik), the particle diameter will be 100 nm for all particles
2. The silicon end of the APTES bound to the Evonik particle surface is not removed/vapourized during the TGA analysis, thus the change in our molecular mass (or the molecular weight of the "leaving" group) is 58 g/mol
3. The particles are uniformly coated on the particle surface
4. The density of the Evonik particles is the same as regular titanium dioxide density (4.23g/cm^3)
5. Each Evonik particle is perfectly spherical

The resulting thermograph and calculated results based off the five assumptions can be found in Figure 2-19 and Table 2-14, respectively.

Table 2-14: TGA calculations for TiO_2 vs TiO_2-g-APTES

Step	Values	Units
Total Molecules of APTES	$8.41x10^{18}$	molecules
Total Volume of TiO_2	$8.63x10^{-3}$	cm^3
Volume of each TiO_2	$5.24x10^{-16}$	cm^3/particle
Surface Area of each TiO_2	$3.14x10^{-10}$	cm^2
Number of TiO_2 Particles	$1.65x10^{13}$	particle
Molecules of APTES/Particle	$5.10x10^{5}$	molecules/particle
Grafting density	16.25	molecules/nm^2

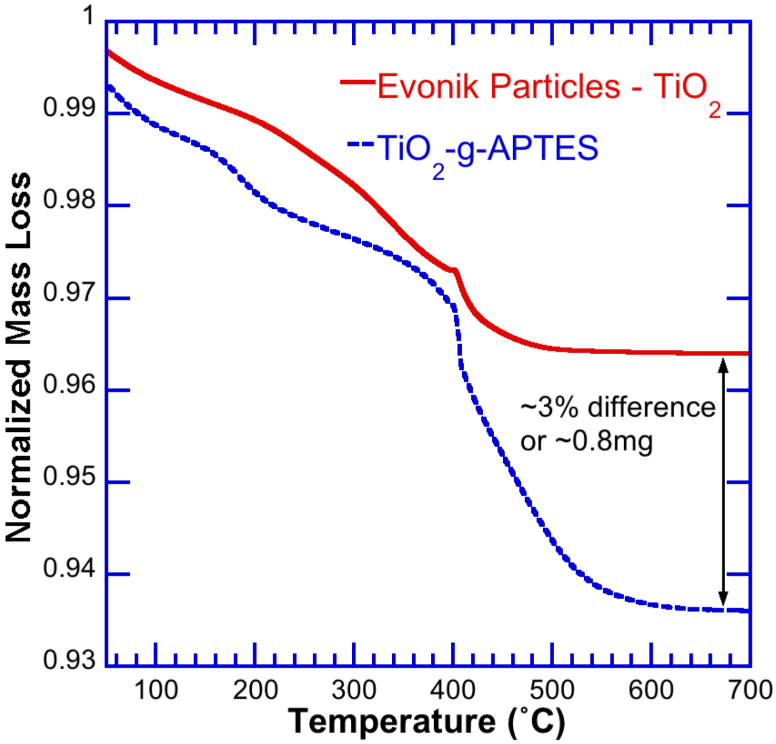

Figure 2-19: Thermogravametric Analysis graph of the unmodified Evonik particles (TiO_2) vs. the APTES modified Evonik particles (TiO_2-g-APTES)

From the collected data, there is evidence to conclude that a higher amount of APTES has bound onto the surface of the Evonik particles. While a value of roughly 16 APTES molecules per nm^2 is higher than the C3-Initiator grafting density, Song *et al.* points out that the chance of the amine function from APTES interacting with the titania surface instead of the silane one, is quite high (almost 50%).[175] In assuming this has occurred, we can estimate that there should be roughly 8 APTES molecules per nm^2, with a free amine function that can be used later.

In taking these results, the surface of the Evonik particles have effectively been modified, which are fairly reproducible. These calculated values would become influential in Chapter 4 for further calculations in forming the surface bound initiator groups.

TGA helped determine that we have an APTES grafting on Evonik particles of approximately 16 APTES/nm^2, but with the potential for the amine group to face the titania surface, we can lower this value to about 8 APTES/nm^2.

2.7. Conclusions with Key Results

This chapter served as the first chapter to present findings on the anchoring/surface modification of different titania surfaces. In this respect, the introduction of different anchoring groups alongside what other opportunities exist was showcased, followed by a possible pathway in which the modification of titania, specifically that of Evonik particles. The first conclusion resulted in reducing the study down to two pathways – use of an organophosphonic acid molecule as a first study, and a subsequent study using a silane-based molecule was explored.

In the first study with the commercial organophosphonic acid molecule, it was discovered that the anchoring of the phosphonic group functioned fairly similarly to the silane-based anchors in terms of ability to bind to surface morphology. The more porous the system, the lower the binding density. The next conclusion was that the stability of the organophosphonic acid (i.e. C1-Initiator and C3-Initiator) varied, based off the length of carbon units between the phosphonic acid group, and the ester group. This point of degradation was evident with the C1-initiator when analyzing the UV-Visible spectra and ^1H NMR spectra between both C1-Initiator and C3-Initiators over time. Continuing the study with the C3-Initiator, several assumptions were made to translate TGA graphs into information that could help us to calculate a grafting density of 2.5 C3-Initiator molecules per nm^2 on the Evonik particles.

In the second study with the silane based molecule known as APTES, it was determined that Evonik particles were much more effective being grafted by the APTES than the CTI porous tubes. XPS results showed fairly good binding of the APTES with a yield that was much higher than what was found with the C3-Initiator. In terms of the grafting density determined via TGA, the calculations showed a much higher binding of approximately 16 molecules per nm^2. However, literature has shown that the ability of APTES for reverse attachment from the amine group interacting with the titania was roughly 50%. This allowed us to reduce the grafting density to approximately 8 molecules per nm^2; still a much higher grafting density than with the C3-Initiator.

From this chapter's studies, the results clearly indicate that modification of titania surfaces with different chemical groups is achieved, and that further functionalization is possible. These tests conducted with bifunctional molecules demonstrate that the formation of a strong interface between inorganic and organic media is possible. Polymerization of the particles to form hybrid particles (shown in both chapter 3 and chapter 4) will also be achieved.

Chapter 3

Surface-Initiated Atom Transfer Radical Polymerization of PEGMEMA

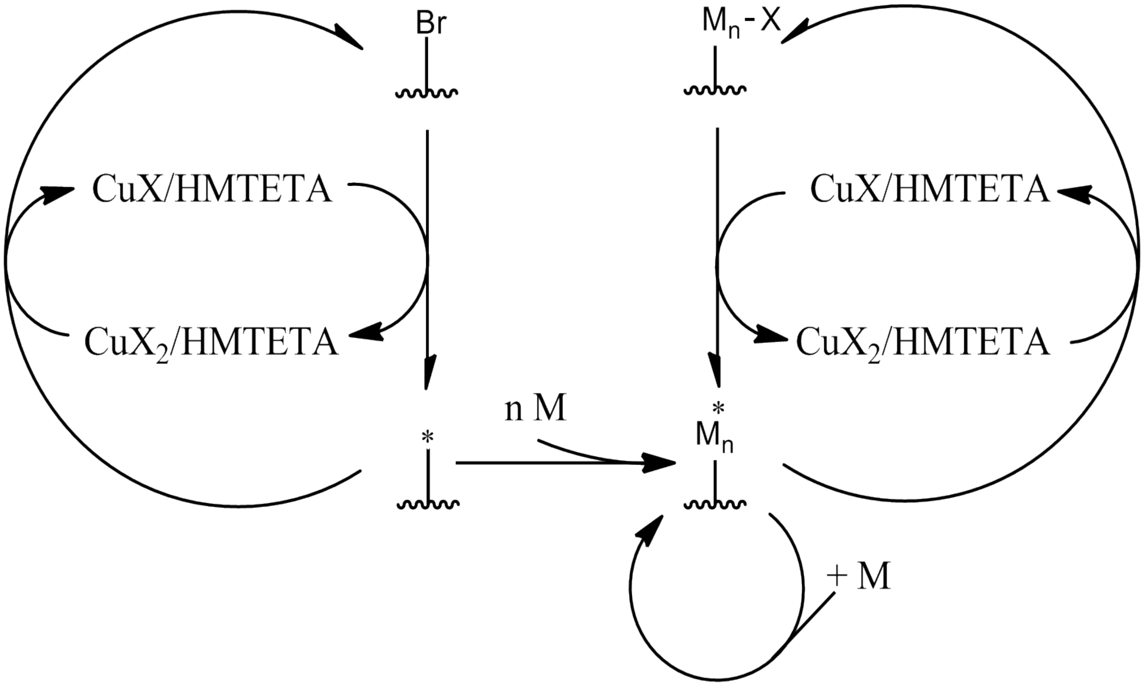

General mechanism of si-ATRP (surface-initiated atom-transfer radical polymerization) as performed in this work. This chapter intends to educate on the background, advances, and subsequent application of ATRP/si-ATRP techniques for the formation of hybrid particles.

3.1. Introduction

The previous chapter presented the background and experiments that have been carried out on surface modification of different titania surfaces in order to graft polymer initiators. In a second step, the creation of a hybrid/nanocomposite material must yield an organic component – namely a polymeric layer formed on the surfaces of the inorganic component. One suitable technique is atom-transfer radical polymerization, or ATRP.

ATRP is a CRP (controlled radical polymerization) technique, and it essentially enables researchers or users to control free radical polymerization in order to form polymers of the same/similar molecular weight, at the same time. In this method, the monomer (or macromonomer) unit must contain a double bond that is vital to the reaction, as required for any free radical polymerization. Some typical examples are shown in Figure 3-1.

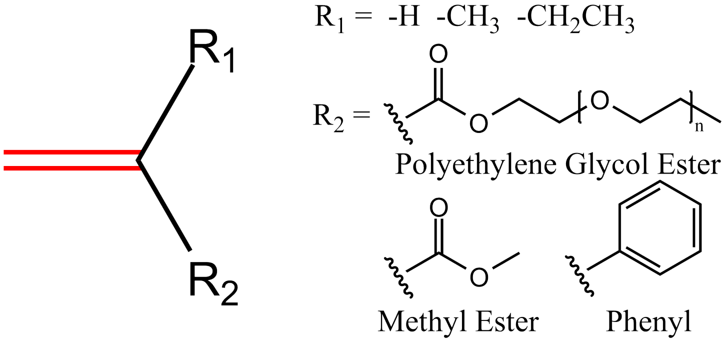

Figure 3-1: Image of a typical format of an ATRP monomer unit, were the red coloured double bond represents the region where the propagation stage of ATRP is sustained. Some examples of pendant groups (R1 and R2) can be seen illustrated, but are not limited to these.

The double bond will be broken by a free radical or electron, in order to create a new free radical from the newly bonded monomer unit. Although this method was heavily studied in the 1980's using control agents, there still exists much work to improve upon the control of polymer growth. It is important to note that although methods like cationic and anionic polymerizations came about during this period,[166] these techniques helped us to understand the concept of group transfer polymerization; a form of polymerization where the initiator (or molecule that kick-starts the reaction) transfers a side-group/functional group to the monomer for propagation of the reaction.[181] These concepts and experiments with catalytic chain transfer agents in the mid/late 1980's by the USSR and other Japanese groups led to the discovery of ATRP.[166]

Officially coined with the term of ATRP in 1995 by Wang and Matyjaszewski,[182] ATRP is a form of free radical polymerization, but utilizes a metallic transfer agent to slow down the polymerization for better control. This also enabled new, complex structures to be formed including: block copolymers, stars-shaped, comb-shaped, and brush-shaped like polymers with a very narrow dispersity, or Đ; formerly known as polydispersity index (PDI), or variation of polymer size.[166] This ability from ATRP is fairly relevant in an industrial setting, as the consistency of polymer size, depending on its application, has been a key issue with free radical polymerization techniques.

Understanding this brief history and the simplistic overview of how ATRP functions, this chapter will present a brief fundamental look at the ATRP mechanism, a literature background on what other researchers have done in the domain of surface-initiated ATRP (si-ATRP), along with the approach taken in this project of synthesizing hybrid materials with the Evonik particles and flat titania substrates previously functionalized with the ATRP C3-initiator.

3.2. Fundamentals of ATRP

In order to understand the theory of ATRP, it is important to note that the method is still a form of free radical polymerization. Hence, ATRP can be easily illustrated as an extension of this mechanism. In free radical polymerization, several steps must occur, as illustrated in Figure 3-2.

$$\begin{array}{ll}
\text{Initiator Decomposition} & I_2 \xrightarrow{k_d} 2\,I^* \\
\text{Chain Initiation} & I^* + M \xrightarrow{k_i} R_I^* \\
\text{Chain Propagation} & R_I^* + M \xrightarrow{k_p} R_{I+1}^* \\
\text{Chain Transfer} & R_i^* + S \xrightarrow{k_{tr}} R_I^* + P_i \\
\text{Chain Termination} & R_i^* + R_j^* \xrightarrow{k_{t,c,d}} P_{i+j} \text{ or } P_i + P_j
\end{array}$$

Where R_i^* is a radical of chain length i, I_2 is the initiator, M is the monomer, S is a transfer agent, and P is polymer

Figure 3-2: Process of free radical polymerization.[183]

The figure shows the multistep mechanism: (i) decomposition of the initiator, (ii) initiation of the chain, (iii) chain propagation, (iv) chain transfer, and (v) chain termination. The decomposition of the initiator is vital to start this reaction, as it creates the propagating free radicals. However, the propagation of the polymer chain is perhaps the most difficult step, being fairly spontaneous, susceptible to chain transfer (which leads to high dispersities) and extremely difficult to control.[183]

In order to control the polymer growth, ATRP requires the addition of a metallic-ligand complex, whilst the initiator to be of a halide nature instead of the dissociative nature from regular free radical polymerization. This complex must contain a metallic component with two oxidation states (ex: Cu^{+1} and Cu^{+2}) in order to allow the donation or withdrawal of the electron responsible for the propagating end of the free radical chain to reversibly terminate.[184] The initiator is required to be a halogen, as it acts as the agent that moves between the propagating chain and the metal-ligand complex (denoted as 'X' in the figures). This ability of the halogen atom ensures that the polymer chain remains 'living', or able to react slowly during the reaction.

The ligand (usually a large molecule) is used to stabilize the two-oxidation states of the metal ion, but the key with this is that it creates a balance between both oxidation states, as shown in Figure 3-3.

$$\text{R-X} + \text{Cu(I)X/L} \rightleftarrows \text{R*} + \text{X-Cu(II)X/L} \qquad (1)$$

$$\text{Cu(I)X/L} \rightleftarrows \text{Cu(II)X/L} + e^- \qquad (2)$$

$$\text{R-X} + e^- \rightleftarrows \text{R}^* + \text{X}^- \qquad (3)$$

$$\text{X}^- + \text{Cu(II)X/L} \rightleftarrows \text{X-Cu(II)X/L} \qquad (4)$$

Figure 3-3: Redox equations for the metal-ligand complex mixture. In this case, the metal is copper and the overall equation is noted from line 1.[184] Reprinted with permission from Reference 184. Copyright 2004 American Chemical Society.

The figure shows that the addition of the metal-ligand creates an additional mechanism, which must be added to the list displayed in Figure 3-2 to account for ATRP. In this case, the overall reaction can be summarized as shown in Figure 3-4.

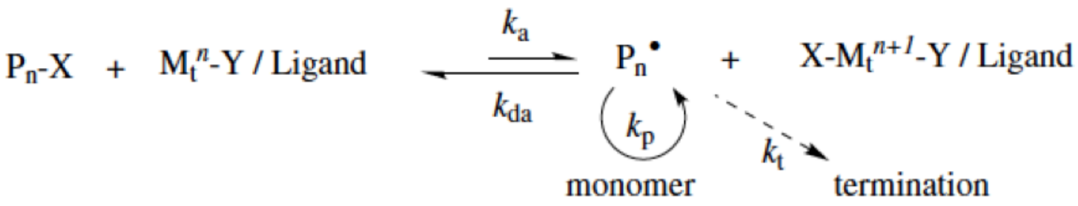

Figure 3-4: Schematic of the propagation and termination step for ATRP.[185] Reprinted with permission from Reference 185. Copyright 2001 American Chemical Society.

The image shows us that the additional metal-ligand complex helps to create an intermediate step that affects the growing polymer during the propagation stage. The propagation step will then slow down due to the de-activation of the free radical portion. As a result, the associated kinetics for propagation (K_p and K_a) is much lower than the deactivation (or K_{da}), and slows down the overall polymerization kinetics. This point is important as it is the fundamental reason for why one would use ATRP – for a very controlled living radical polymerization where all growing chains grow at the same pace due to the overall equilibrium of the system shifting to the left (Figure 3-4).

Since ATRP is a very controlled reaction, the reaction would yield very consistent sized polymer chains, which is experimentally confirmed, as illustrated in Figure 3-5.

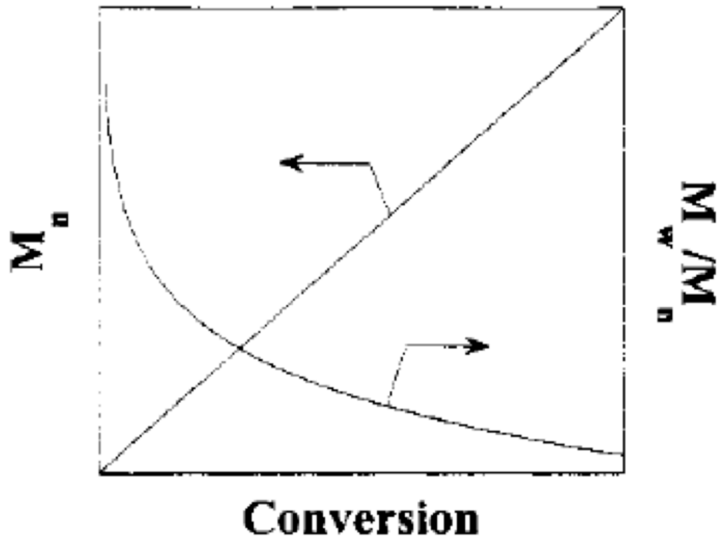

Figure 3-5: Molecular weight and dispersity (Đ) as a function of conversion in ATRP.[185] Reprinted with permission from Reference 185. Copyright 2001 American Chemical Society.

The Mw/Mn represents the dispersity (Đ), a factor that is effected by the conversion rate. Note that as the conversion increases, the resulting variance in polymer size is reduced to a value close to 1, meaning that all the chains have the same length/molecular weight. Figure 3-5 also indicates that the average weight of the growing chain increases at a steady rate as conversion increases. This reinforces the point that ATRP is a 'living' polymerization,[185] because the conversion rate does not appear to diminish. This means that the chains could theoretically continue polymerizing infinitely, provided that the supply of monomer is consistently replenished.

Considering the images shown in Figure 3-4, the modeling the reaction rate for the propagation step, has to be revised because of the addition of the metal-ligand complex to slow down the original propagation step. Figure 3-6 shows how the reaction rate equations for ATRP must be written.

$$K_{\mathrm{eq}} = \frac{k_{\mathrm{act}}}{k_{\mathrm{deact}}} = \frac{[\mathrm{P}_n^{\bullet}][\mathrm{Cu^{II}X}]}{[\mathrm{Cu^{I}}][\mathrm{P}_n\mathrm{X}]}$$

$$R_{\mathrm{p}} = k_{\mathrm{app}}[\mathrm{M}] = k_{\mathrm{p}}[\mathrm{P}_n^{\bullet}][\mathrm{M}] = k_{\mathrm{p}}K_{\mathrm{eq}}[\mathrm{In}]_0\frac{[\mathrm{Cu^{I}}]}{[\mathrm{Cu^{II}X}]}[\mathrm{M}]$$

Figure 3-6: ATRP rate equations for propagation with K_{eq} (or equilibirum constant) considered.[186] Note that K_{eq} is also known as K_{ATRP} as it represents the overall kinetic rate of ATRP. Reprinted with permission from Reference 186. Copyright 1998 American Chemical Society.

As Figure 3-4 shows an equilibrium equation, it is fair to state that the overall equilibrium kinetics (K_{eq} which is also known as K_{ATRP}) is related to the concentration of growing chains [P*] and the metal-ligand complex in the highest oxidation state [Cu(II)-X], and inversely related to the concentration of the reduced metal concentration [Cu(I)] and the reversibly terminated polymer chain [PX]. In addition, all free radical polymerization have a reaction rate in the form of Rate = K[M][P*], where K is the apparent reaction kinetics, [M] is the concentration of monomers and [P*] is the concentration of growing chains. Combining both equations leads us to the results displayed in Figure 3-6 (Note: the equilibrium kinetic equation is rearranged to isolate [P*] and applied to the rate equation). Also, we see [PX]=[I] as the initiator is what provides the halogen group (X) for this system. Therefore, we conclude that the rate of reaction is directly proportional to the initiator concentration, which makes sense as the number of initiators would (ideally) represents the number of possible growing chains.

3.3. Development in ATRP

It has been reported that although over 50% of polymers made today are from free radical polymerization, the use of ATRP in industrial processing is still not widely adopted.[187] However, more recent developments have resulted in the formation of startups dealing with ATRP for industrial applications,[188] and the formation of a consortium of companies formed by Dr. Krzysztof Matyjaszewski.[189,190] The biggest issue with industrial adoption lies in its products containing trace amounts of the copper catalyst, which drives up costs, causes environmental issues and issues adopting metal-ridden polymers in products.[191] As a result, the current target of ATRP development is not only characterizing other types of monomers for use in polymerization, but for researchers to work on reducing/eliminating the amount of metal catalyst in the final product. For this to occur, several methods have been developed to help achieve lower metal usage along with higher chemical stability. These methods include, but are not limited to, AGET ATRP,[192,193] ARGET ATRP,[194] ICAR ATRP,[193] SARA ATRP,[189,195,196] (or SET-LRP,[197,198] depending on the perspective of the researcher), eATRP,[199] and metal-free ATRP.[200-202] These techniques are all important in the realm of developing industrial scale applications of ATRP, but are beyond the scope of this present review.

3.4. Surface-Initiated ATRP (si-ATRP)

The most logical application of ATRP, being a form of control radical polymerization, is in surface modification. From the seminal paper by Wang and Matyjeszewski in 1995,[182] there has been a significant amount of work that expanded ATRP to surface modification (see Figure 3-7).

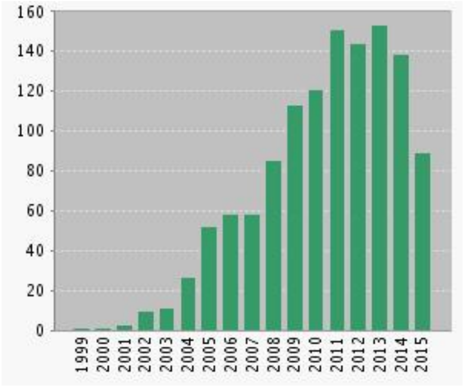

Figure 3-7: citation report generated by Web of Science with search terms si-ATRP or surface-initiated ATRP (Generated July 2015).

We see that the work focused in the area of surface modification *via* ATRP is a field that continues to grow and find applications in a variety of fields, ranging from biological screenings[203] to membrane surfaces.[24] In this following section, we will briefly go through the history and describe certain controls that can be used for ATRP and surface-initiated ATRP in general.

3.4.1. To use or not to use Sacrificial Initiators?

Perhaps one of the earliest indications that surface-initiated ATRP was possible was presented by the work Huang *et al.* in 1998, with the formation of a SAM using a chlorosilane based initiator for the formation of a layer of polyacrylamide.[204]. However, there was a slight problem with full control as it required the use of sacrificial initiators in order to control the reaction. Note that the mechanism of changing Cu^{+2} to Cu^{+1} caps the free radical end of the growing chain, but would not exist in sufficient quantities without a sacrificial initiator used to control/regenerate the Cu^{+2} complex. Matyjaszewski *et al.* had shown in 1999 that it was possible to develop surface-initiated ATRP without the need for an untethered initiator to control the polymer film formation.[127] This method was achieved *via* addition of Cu^{+2} atoms, as described in section 3.4.3 Oxidation Level of Metal Atoms.

Since then, many other researchers have generally used one of these methods to perform si-ATRP. The use of sacrificial initiators enable easier measurement of the degree of polymerization (DP) and characterization of the growing polymer if we can assume that the rate of polymer growth is the same for the free chain and the unbound chain. This enables one to control the reaction by adding the higher oxidation state of copper to quickly cap the free chain, and prevent what is known as the persistent free radical effect.[205-207] However, if there is insufficient free initiator in solution, the resulting control is lost.

3.4.2. Halide Effect

The effect of the halide group (i.e. use of bromine or chlorine atoms) is also a factor to be considered in the mechanism of ATRP. Matyjaszewski and coworkers in 1997 showed that the enthalpy of reaction between bromine and chlorine was different, with bromine displaying a lower apparent enthalpy activation than chlorine.[208] This point was derived from the apparent kinetic rate noted from Figure 3-8.

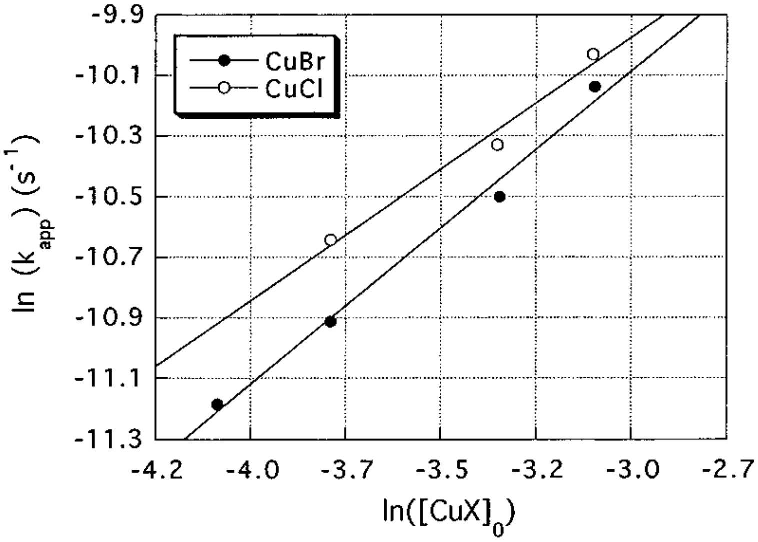

Figure 3-8: Reaction orders for CuBr (110 °C) and CuCl (130 °C) for the ATRP of styrene in diphenyl ether. Slope (Cl) = 0.87; Slope (Br) = 1.03.[208] Note that the higher the value of the slope, the higher the kinetic rate (or apparent rate of activation in ATRP – and is not the overall ATRP rate, or what is known as K_{ATRP}). Reprinted with permission from Reference 208. Copyright 1997 American Chemical Society.

As illustrated, the kinetic rate appears slightly higher with CuBr than CuCl, indicating that bromine leads to faster reaction rates. Additional work established that the bromine based halide was much easier at starting/initiating the start of the ATRP reaction, but chlorine provided a better controlled reaction, with a lower dispersity.[209] This was further proven later by Jousset *et al.* in 2001 with a water-borne system.[210]

Subsequently, Jewrajka *et al.* showed that the bond between the carbon and bromine is much weaker than the carbon-chlorine bond in the case of methyl methacrylate,[211] an explanation reinforced in an earlier review by Fischer in 2001.[205]

Additional studies showed that a surface initiated system in aqueous medium could yield thicker films with a mixed halide system than with a single bromine system (Figure 3-9).[212] The mixture of CuCl and $CuBr_2$ results in thicker films formed over time as opposed to a system with a single bromine system, which appears to plateau after about 200 minutes of reaction. This would indicate that the mixed halide system possesses a slightly superior live-ability, with a better control.

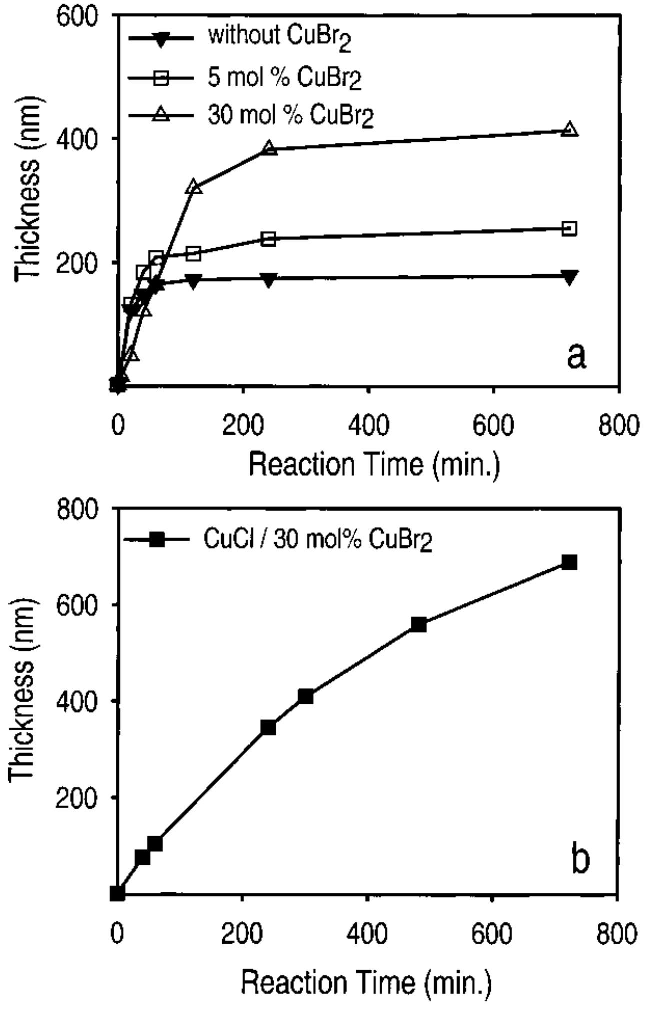

Figure 3-9: Thickness dependance on the polymerization time (of aqueous ATRP on PHEMA films) at room temperature, with a) varying concentrations of $CuBr_2$ with CuBr/bpy catalyst and b)using a mixed halide system of CuCl and $CuBr_2$ (NOTE: the mol% was in reference to the Cu^{+1} concentration)[212] Reprinted with permission from Reference 212. Copyright 2002 American Chemical Society.

The best design of an ATRP system, at least in reference for use of halides, is for the initiator to be bromine-based, and to use chloride (or a mixture of chloride and bromide based halides) for the copper based salts to form the catalyst. Particularly in the case of surface-initiated systems, one should consider the use of bromine-based initiators from the surface, as the reaction would be easier to proceed. Additionally, the use of some chlorine-based halide counter-ions would also be suggested, in order to help slow down any fast reactions, and thus provide greater control.

3.4.3. Oxidation Level of Metal Atoms

The metal oxidation level is an important parameter, because it controls the kinetics of propagation in ATRP (as seen by K_{eq} in Figure 3-6). However, with surface-initiated polymerization (SIP), it has been previously shown that without the use of sacrificial initiators, the reaction rate is uncontrolled.[127,169] Therefore, the addition of Cu^{+2} ions directly into the mixture of Cu^{+1} catalyst mixture is required to ensure the control of the reaction during the initiating step, thus helps to prevent the persistent radical effect, as illustrated from Figure 3-10.

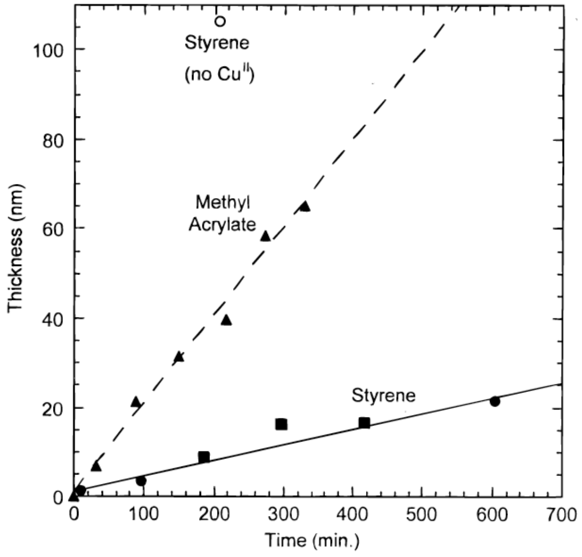

Figure 3-10: Thickness correlation to time for si-ATRP samples made on silicon substrates by Matyjaszewski and coworkers.[127] Filled triangles represents the thickness for Methyl Acrylate in the presence of both Cu^{+1} and Cu^{+2}, filled squares and circles represents the thickness for Styrene in the presence of both Cu^{+1} and Cu^{+2}, and the empty circle represents the polymerization of styrene in the absence of Cu^{+2}. Reprinted with permission from Reference 127. Copyright 1999 American Chemical Society.

The resulting plot shows how the addition of Cu^{+2} slows down the rate of polymerization. In the case of styrene, when comparing the sample with 0.05 mol% of $CuBr_2$ against the sample without, we clearly see a massive difference in the thickness observed (i.e. 110 nm *vs* 12 nm without Cu^{+2} and with Cu^{+2}, respectively). This point indicates that the addition of $CuBr_2$ resulted in a slower rate of polymer layer thickness formation, as noted from the lower slope found in Figure 3-10. The use of 1 mol% CuBr alone resulted in a very fast reaction rate in the polymerization and film formation of polystyrene, due to the persistent radical effect and subsequent lower control.[127]

In the work by Huang *et al.* in 2002 (see Figure 3-9a),[212] increasing the concentration in $CuBr_2$ gave a slightly better control over the reaction and could terminate the reaction much later. This result reinforces the point that the addition of a higher oxidation transition metal in si-ATRP can allow us to achieve more controlled reactions, hence enable users to precisely target their desired polymer film thickness.

3.4.4. Solvent Effect

In this section, we will briefly discuss the effect solvent has on ATRP. While there are many factors that influence the reaction, ranging from temperature to the ligand selected, solvent effects are of great importance as they directly interface with all components of the reaction. From papers that have studied solvent effect, we conclude that there is evidence that the more polar the solvent, the faster the reaction.[213,214] For example, the work published by Nanda and Matyjaszewski in 2003 clearly shows an the effect of solvent polarity on the reaction rate (Figure 3-11).[213]

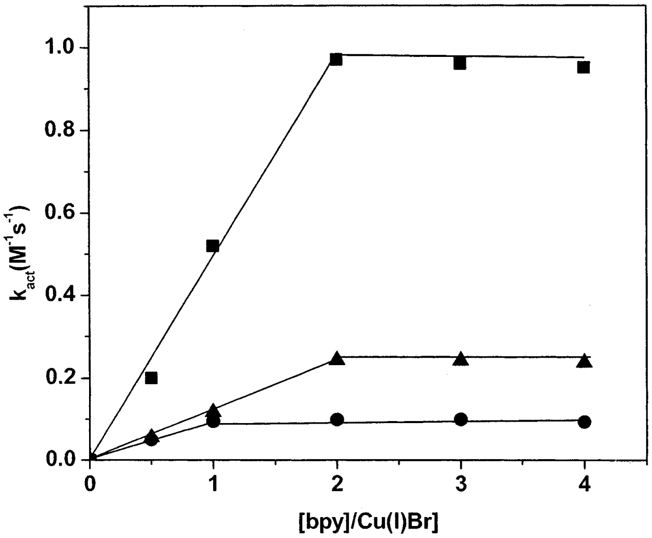

Figure 3-11: Plot of k_{act} with respect to the concentration of the ligand bpy/CuBr complex with (■) acetonitrile (44%) with water, (▲) pure acetonitrile, and (●) acetonitrile (41.5%) with chlorobenzene.[213] In this case, we see the trend that with increasing polarity (water+acetonitrile > acetonitrile > acetonitrile+chlorobenzene) come higher activation of the free radical species in ATRP.[213] Reprinted with permission from Reference 213. Copyright 2003 American Chemical Society.

The figure illustrates how the rate of activation for ATRP, specifically the formation of the free radical due to breaking the halide-carbon bond, is higher in polar solvents (up until the concentration ratio of 2 for the ligand:CuBr ratio). As the paper also confirms that two ligands are required to stabilize one CuBr molecule, this figure reinforces that any additional amount of ligand will not hinder the reaction.

Braunecker *et al.* in 2009[214] elaborated on the Kamlet-Taft Expression, which is shown in Equation 3-1:

$$\boldsymbol{XYZ = XYZ_0 + a\alpha + b\beta + s\pi^* + h(\delta_H)^2}$$

Equation 3-1: Kamlet-Taft Expression

where XYZ is the redox potential, α is the solvent hydrogen bond donor ability, β is the hydrogen bond acceptor ability, π^* is the polarizability parameter and δ_H is the Hildebrand solubility parameter, which measures the solvent-solvent interactions interrupted when the solute forces a cavity formation.

This equation was further simplified, via regression of the parameters of various expected log(K_{eq}) data collected to Equation 3-2.

$$\boldsymbol{XYZ = -11.54 - 0.80\alpha + 1.83\beta + 1.72\pi^* + 0.011(\delta_H)^2}$$

Equation 3-2: Modified Kamlet-Taft Expression

It is believed that this equation could adequately predict the solvent effect on the ATRP kinetic rate, or K_{eq}, with respect to these solvent parameters. The application of this model on several solvents is illustrated in Figure 3-12 for the HMTETA/CuBr catalyst system.[214]

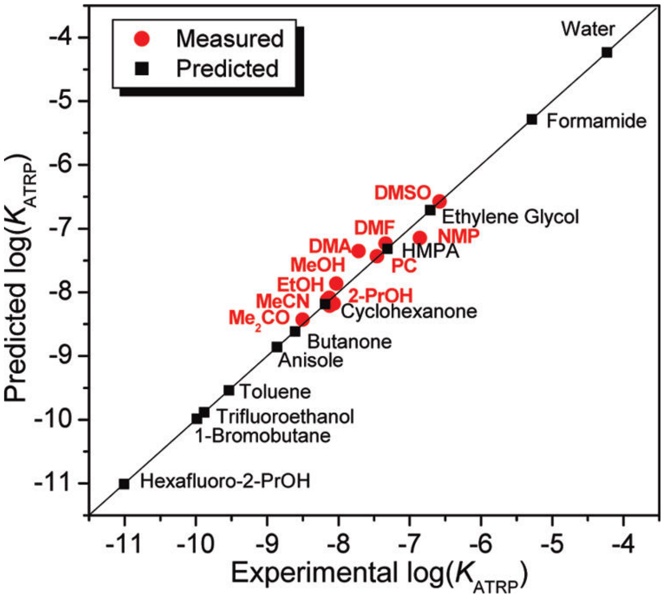

Figure 3-12: Log (K_{ATRP}) of predicted vs experimental values using the modified Kamlet-Taft relationship. The line is the subsequent expected trend from the plot with predicted values and subsequently measured values. Note that the measured values fall fairly well into the general trend from the Kamlet-Taft relationship, enabling one to predict the subsequent K_{ATRP} value possible.[214] Reprinted with permission from Reference 214. Copyright 2009 American Chemical Society.

Figure 3-12 shows a rather good agreement between the predicted values and the experimentally observed examples, reinforcing the fact that higher kinetic values are proportional to solvent polarity. For instance, as water is highly polar, it has a high-expected K_{ATRP} while hexafluoro-2-PrOH, being least polar, has a lower K_{ATRP}. However, certain values do not necessarily follow this trend. For example, ethanol and methanol are more polar than DMSO or DMF, yet they lay below the K_{ATRP} values such that DMSO and DMF.

It can be noted that while polarity can be an important factor in the determination of kinetic rate, and that higher activation occurs with more polar solvents, the apparent K_{ATRP} rate does not always follow this trend, and that some solvents might perform better than others overall.

Looking into specific examples found with si-ATRP, one can consider the work by Armes and his group. In a 2007 paper by Edmondson *et al.*, they presented work on the effect due to polarity of a solvent by varying the methanol:water ratio on a si-ATRP reaction of 2-(diethylamino)ethyl methacrylate (or DEA). They found that while water provided thick polymer films compared to methanol, the mixture of solvent provided even thicker films, as illustrated in Figure 3-13 and Figure 3-14. Such work provided the basis that the more polar the system, the thicker the film when dealing with single solvent systems. However, these results show that a simple relationship is not such straightforward. For example, a 1:1 MeOH/H_2O mixture yielded a thicker polymer layer than when using pure water (Figure 3-13). In another case, a 4:1 ratio resulted in thicker films when compared to a 2:1 ratio (Figure 3-14).[215]

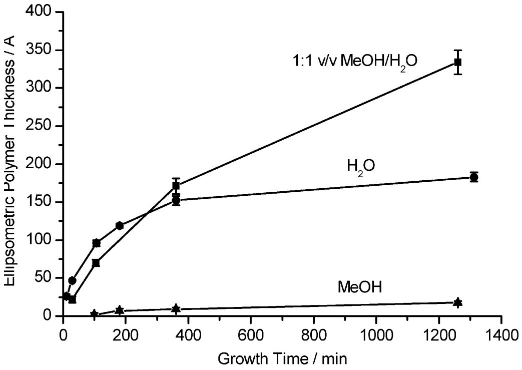

Figure 3-13: Ellipsometry measurements of thicknesses obtained from si-ATRP samples of DEA (2-(diethylamino)ethyl methacrylate for methanol (MeOH), water (H_2O) and 1:1 v/v mixture of MeOH/ H_2O.[215] Reprinted with permission from Reference 215. Copyright 2009 American Chemical Society.

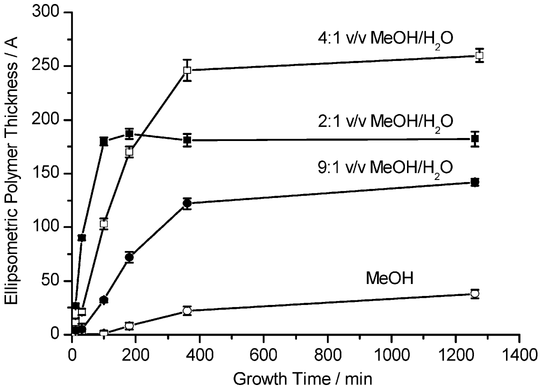

Figure 3-14: Ellipsometry measurements of thicknesses obtained from si-ATRP samples of DEA (2-(diethylamino)ethyl methacrylate) in varying volume ratios of methanol (MeOH) and Water (H_2O). Film thickness maximum ratio appears to be 4:1 v/v MeOH/H_2O is hypothesized due to the termination caused by higher water concentration in the 2:1 system.[215] Reprinted with permission from Reference 215. Copyright 2009 American Chemical Society.

3.4.5. Ligand Effect

In the previous section, it was shown how more polar solvents led to thicker polymer films. However, the ligand also has an effect on the final as well. Some typical ligands for ATRP are illustrated in Figure 3-15.

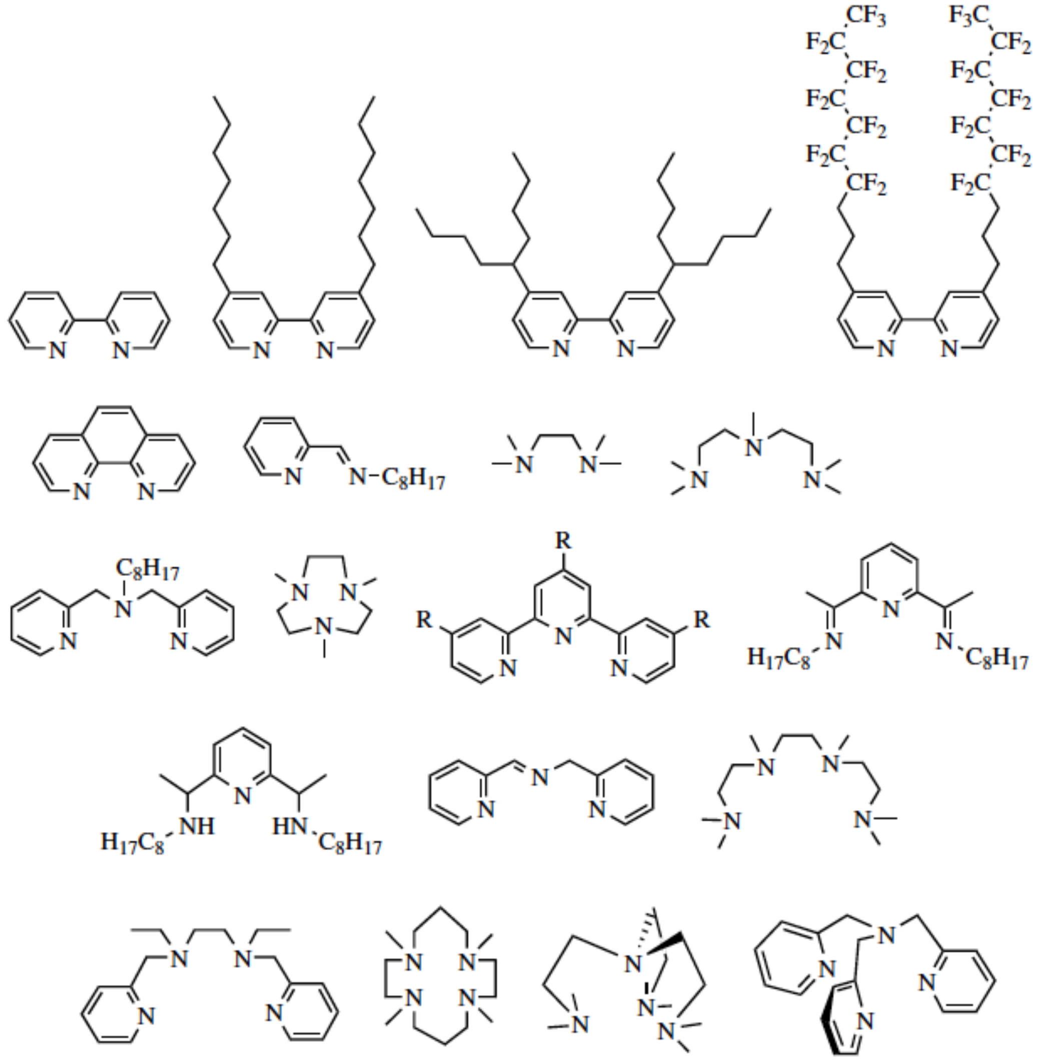

Figure 3-15: Typical nitrogen-containing ligands for ATRP.[185] Reprinted with permission from Reference 185. Copyright 2001 American Chemical Society.

While this is not an exhaustive list of structures, most of these behave fairly well with nonpolar solvents. They follow a general rule where the K_{ATRP} increases with more nitrogen atoms per molecule and the rate decreases the longer the alkyl groups that separate the nitrogen atoms.[185,216]

However, these rules slightly change in polar solvents. In the group of Matyjaszewski, Tsarevsky *et al.* published an excellent paper in 2007 on the electron transfer reactions found in ATRP.[217] This work mentioned that polar solvents (specifically aqueous systems) could cause disproportionation between the Cu^{+1} atoms to form Cu^{+2} and Cu^0. However, depending on the ligand stability constant of the Cu-L complex, represented by the value "β", one could deduce the stability of both the Cu^{+1}/Ligand and Cu^{+2}/Ligand complexes (i.e. $\beta^I = Cu^{+1}$ and $\beta^{II} = Cu^{+2}$). Subsequently, the overall activity of the catalyst complex in a polar solvent appears to be proportional to the β^{II}/β^I ratio, and the disproportionation was shown to be proportional to $\beta^{II}/(\beta^I)^2$. The resulting plotted log/log graph can be seen in Figure 3-16.

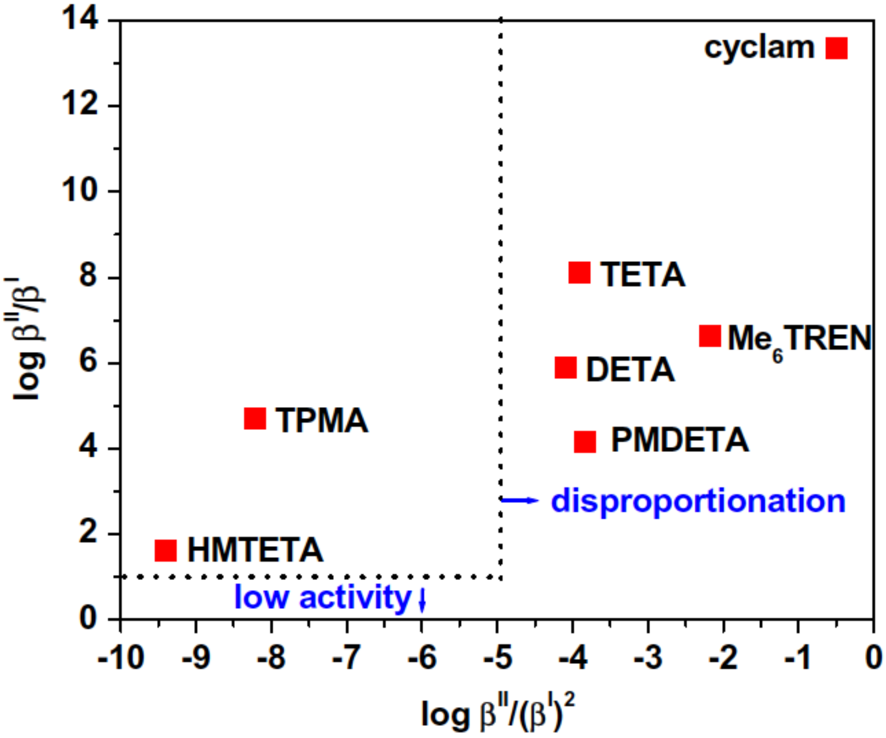

Figure 3-16: Correlation plot between the ATRP catalytic activity ($\log \beta^{II}/\beta^I$) and the disproportionation ($\log \beta^{II}/(\beta^I)^2$) for several typical Cu-Ligand complexes.[217]

As the graph implies, most of the ligands to the right of the dotted line result in disproportionation, leaving the ligands to the left (i.e. HMTETA, or 1,1,4,7,10,10-Hexamethyltriethylenetetramine and TPMA, or Tris(2-pyridylmethyl) amine) to be better at functioning in aqueous and polar solvents.

While considering the fact that si-ATRP is a special form of ATRP, the physics controlled by the catalyst should not vary too significantly. We could consider both HMTETA and TPMA ligands for their use in si-ATRP however, there exists more literature on HMTETA,[24,218,219] than TPMA.[220] For instance, Grajales *et al.* showed p(PEGMEMA) films formed on the surface of alumina could reach up to 250 nm within 2 hours.[24] Bozukova *et al.*, showed that the use of HMTETA on si-ATRP was much slower in an aqueous solvent, but provided a much better dispersity.[218] More recently, Liu *et al.* showed how HMTETA yielded a thicker polymer layer than PMDETA (N,N,N',N'',N'''-Pentamethyldiethylenetriamine) in an aqueous solution.[219] In the case of TPMA, Qian and He showed that it was possible to perform si-ATRP with TPMA, but the thickness remained very low (i.e. ~16 nm thickness after 90 minutes for a concentration 10x that found with the work by Grajales *et al.*).[220]

3.5. Design of si-ATRP route

As Chapter 2 investigated the modification of titania particles with the C3-Initiator, this part will focus on the study of the surface-initiated ATRP process for these modified particles. Recalling the information in Chapter 1, ideal gas separation for CO_2 over N_2 also favours polyethylene glycol/oxide, or PEG/PEO chains. As such, and understanding the method of how ATRP proceeds as a radical polymerization technique, the subsequent design of the reaction scheme can be seen in Figure 3-17.

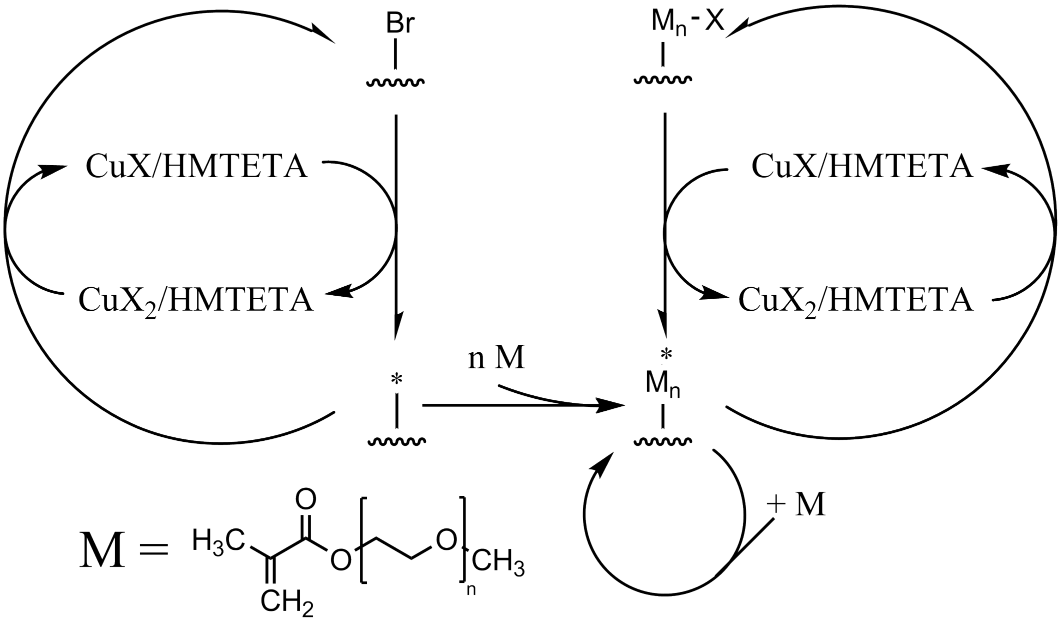

Figure 3-17: si-ATRP mechanism applied for this work. The left side of the image represents the initiation step, where the alkyl halide is activated with the catalyst, and the first free radical is formed. Subsequent addition of monomers (or PEGMEMA, polyethylene glycol methyl ether methacrylate, in this case) allows the reaction to proceed to the right side of the mechanism; where the addition of monomer continues, alongside control via the catalyst. Note that the dormant state of the grafted polymer chain is capped using "X", which represents a halide. In this case, the halide can be Cl or Br, as both halides are used in this reaction (thus X = Cl or Br).

As one clearly notes from the mechanism, the reaction proceeds primarily with the help of the catalyst, HMTETA complexing with the copper-halide, a system that has been demonstrated to work well with si-ATRP.[24] The use of Cu^{+2} and Cu^{+1} mixture is necessary to ensure the reaction is controlled. In addition, as the reaction can be quite slow to form polymeric layers, an aqueous mixture should be the ideal solvent of choice. As water is a polar solvent, it will speed up the reaction, which makes the use of a mixed halide system (i.e. X(halide) = Br + Cl) necessary to proceed with good reaction control. The macromonomer used is a highly PEG-ylated chain with a methacrylate endgroup; a system that works well with ATRP and si-ATRP. Having defined these parameters, we can thus proceed with the functionalized particles using the C3-initiator and study their polymerization.

3.6. Sample Preparation

3.6.1. Materials

CuCl (>90% purity, Sigma Aldrich), $CuBr_2$ (Sigma Aldrich), and N,N-dimethyl formamide (DMF, Sigma Aldrich) were used as received. 1,1,4,7,10,10-Hexamethyl tetraethyltriamine (HMTETA, Sigma Aldrich) was also obtained and used as received. Poly(ethylene glycol) methyl ether methacrylate (PEGMEMA-475) (Sigma) was chosen as macromonomer, and used as received and stored at 4˚C before use. 18 MΩ Ultra pure DI water was used. Ethanol (96% purissimum grade pur; Xilab) was obtained and used after ultrafiltration using 0.45 µm cellulose filter.

3.6.2. Preparation of the Macromonomer Solution

A 0.3 M aqueous solution of the macromonomer stock solution was prepared by gently dispersing 7.15 g PEGMEMA into 45 mL DI water. The resulting mixture was slowly rocked back and forth for one minute to mix, and the resulting mixture was then stored at 4°C until required for use, at which point was subjected to a 3-cycle freeze-pump-thaw degasing cycle before use.

Higher concentrations were also prepared in a similar manner, with the help of the following equation

$$Mass_{PEGMEMA}(g) = Molarity\ (M) x\ Volume_{Final}\ (L) x\ Molar\ Mass_{PEGMEMA} \left({}^{g}/_{mol} \right)$$

Which eventually becomes (if we assume the volume is 25 mL):

$$Mass_{PEGMEMA}(g) = Molarity\ (M) x\ 0.025\ (L) x\ 475 \left({}^{g}/_{mol} \right)$$

$$\boldsymbol{Mass_{PEGMEMA}(g) = 11.875 \left({}^{g \cdot L}/_{mol} \right) Molarity\ (M)}$$

With the total volume of DI water to add as:

$$Volume_{DI\ Water}(mL) = Volume_{Total}(mL) - \left(\frac{Mass_{PEGMEMA}(g)}{Density_{PEGMEMA}\left({}^{g}/_{mL} \right)} \right)$$

As the density is 1.08 g/mL and assuming the total volume remains as 25 mL, then:

$$\boldsymbol{Volume_{DI\,Water}(mL) = 25\,mL - \left(\frac{Mass_{PEGMEMA}(g)}{1.08\left(^{g}/_{mL}\right)}\right)}$$

Thus for a volume of 25 mL at 0.1 M, it required 1.19 g of PEGMEMA-475 (or about 1.1 mL) with 23.9 mL DI Water, while a 0.5M sample required 5.94 g of PEGMEMA-475 (or 5.5 mL) with 19.5 mL DI Water.

3.6.3. Preparation of Catalyst Solution

Following the work prepared by Grajales *et al.*,[24] 30 mL of N,N-dimethylformamide (DMF) was degassed using a three-cycle freeze-pump-thaw cycle. Copper I Chloride (0.06 g) was added into a vial inside a glovebox, along with Copper II Bromide (0.04 g) and the degassed DMF was added into the vial and stirred for 3 hours. The degased HMTETA ligand (490 µL) was then added to the vial and was left stirring for another 4 hours. The remaining mixture was then stored in the glove box until use.

3.6.4. Polymerization (si-ATRP)

The polymerization mixture was prepared by taking a 9:1 volume ratio between the degassed macromonomer solution to the oxygen free catalyst (normally with a final volume of 10 mL, with a macromonomer concentration of 0.27 M unless specified that the macromonomer concentration was higher or lower (i.e. 0.5 M -> 0.45 M, or 0.1 M -> 0.09 M)). This was achieved using a glass neck that was able to mix both volumes together without exposure to oxygen. The mixture was stirred for several minutes before use. In many cases, the target sample (either flat titania substrate or the CTI porous supports) were directly added into the polymerization mixture and left to react for 24 hours (unless specified for a shorter period, as was mentioned in Chapter 3). However, as the Evonik particles were more difficult to work with, re-dispersion was first required.

The re-dispersion of the functionalized Evonik particles (TiO_2-g-C3-Initiator) was achieved by mixing the particles (0.3 g) with 20 mL of DI Water (final concentration of 0.015 g/mL). This dispersion was then sonicated for 1 minute with an ultrasonic probe and used as a stock solution. Normally, 1 mL of the mixture was degassed in the typical 3-cycle freeze-pump-thaw process in a round bottom flask. Afterwards, a glass neck with a flow of nitrogen is attached to introduce the polymerization mixture to start the reaction (normally left to run for 24 hours, or more).

There were several cases that scaling up the quantity was used to produce a stock solution of hybrid particles. In this case, the macromonomer:catalyst mixture was left at 9:1, but totaled a volume of 100 mL. Using 10 mL of the Evonik particle dispersion, the same ratio of particles:polymerization mixture of 1:10 was added into the 100 mL mixture. In this larger volume, the 3-cycle freeze-pump-thaw process would be too time consuming, thus nitrogen bubbling (30 minutes) was used to de-oxygenate the macromonomer solution before the addition of the catalyst.

3.7. si-ATRP Reaction

The modified particles (Evonik particles) and surfaces (Flat Titania Substrates) obtained in Chapter 2, were immersed into a mixture of the ATRP catalyst and macromonomer mixture to produce the hybrid structures. The mixture of the macromonomer was set primarily at 0.27 M, with a concentration of 0.6 mM $CuBr_2$, 2.0 mM CuCl and 6.0 mM HMTETA (or excess ligand). Polymerization was set at room temperature for various amount of time. Our first objective was to ensure that the functionalized surfaces could be polymerized with ease. Various analyses allowed us to confirm the formation of hybrid materials *via* si-ATRP on the Evonik particles and Flat Titania surfaces.

3.7.1. Particle Study

In the first validation step, we studied the growth of the particles grafted with the initiator. Upon polymerization, the particle were checked *via* DLS (Dynamic Light Scattering). The presence of polymer was verified by XPS (X-Ray Photoelectron Spectroscopy) and we deduced the total amount of polymer by TGA (Thermogravimetric Analysis). All hybrid particles used in this study were carefully washed after polymerization by ultrafiltration in order to remove any unreacted reagents (including ligands, catalysts and unreacted macromonomers).

3.7.1.1. DLS – Dynamic Light Scattering

As a result of our previous studies on the initiator grafting, we explored the effectiveness of polymerization with the C3-Initiators grafted onto Evonik particles. Dynamic light scattering was used as a means to confirm that the grafted molecules could initiate polymer growth, as to determine the particle growth rate during the reaction. The functionalized Evonik Particles were polymerized in a solution of 0.27 M macromonomer (PEGMEMA) to form the polymeric hybrid core-shell structure. Samples were collected at varying polymerization time intervals from the same solution. The system converts fluctuations of intensity into an auto-correlation function, which changes over time. The collected data is reported in Figure 3-18a as a Y/Ln(X) representation. All parameters being equal, a shift of the curve slope to the right reveals a size increase (which is observed in these results) at least for the first minutes of reaction. The corresponding hydrodynamic diameters (Figure 3-18b) were calculated from these curves.

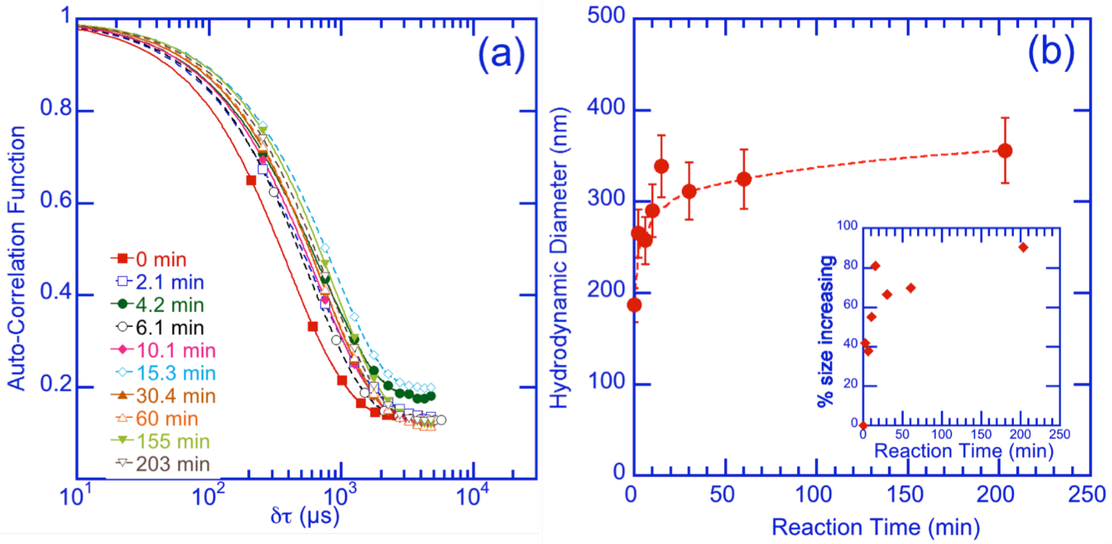

Figure 3-18: Dynamic light scattering of growing core-shell hybrid particles of titania taken at different reaction times. The samples shown are a) log-scale graph of Evonik particles, and b) subsequent size of the Evonik particles over time. Reproduced from Ref. 223 with permission from the Centre National de la Recherche Scientifique (CNRS) and The Royal Society of Chemistry.

All autocorrelation functions could be fitted with a single size cumulant fit, as a proof of a monodisperse suspension of particles all along the polymerization step. The decay of these autocorrelation functions, as a function of time, translates in a concomitant increasing hydrodynamic diameter, which is quantified in the size evolution as a function of time. The kinetics of reaction is very fast, in line with the fairly quick reaction rates reported in literature of under an hour.[221,222] Thus, there is clear evidence that the grafted initiator particles are able to initiate a homogeneous polymerization on a curved surface to create an integrated hybrid core-shell structure.

It should be noted that from the finalized stabilization of the particles, the Evonik particle series appear to stabilize around 300-400 nm, and do not appear to continue to aggregate into larger clusters (as noted by the DLS results). We carried out the same study with TiO_2 Sigma particles (mentioned briefly in Chapter 2), but the results, reported elsewhere, were not as conclusive.[223]

Most of the experiments were performed with a final concentration of 0.27 M macromonomer. We also studied if a change in concentration could yield a slight change in the particle size. This next study dived into the effect of macromonomer concentration on the measured particle sizes, with results displayed in Figure 3-19.

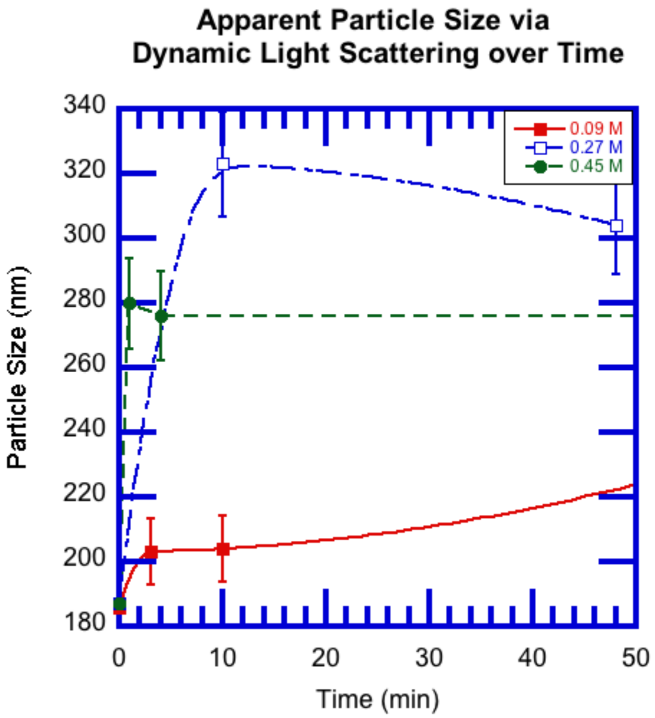

Figure 3-19: Resulting particle size over time for the Evonik particles grafted with C3-Initiator, and growing with addition of the PEGMEMA macromonomer mixture (with catalyst). Note that the change in concentration results in different stable particle sizes.

The change in PEGMEMA concentration results in a general plateau for each concentration at a different specific size. However, a slightly odd result found showed the sample with 0.27 M forming larger particle dispersions than its 0.45 M counterpart. While this appeared to be an odd result, it was observed during the polymerization that the solution/mixture became more and more viscous during the reaction (in the case of the 0.45 M sample). This continued increase of solvent viscosity led to increasing difficulty for the stir-bar to function, which could have hampered the homogeneity of the reaction and resulted in particle aggregates that could not be compared to other samples in the DLS study.

DLS helped to confirm polymeric growth stemming from the Evonik particles, while a short study macromonomer concentration helped illustrate that 0.27 M was a suitable concentration for aqueous si-ATRP for our system.

3.7.1.2. XPS

In Chapter 2, we demonstrated that XPS could confirm the actual grafting of C3-Initiator particles on various forms of surfaces (i.e. curved, flat and porous surfaces). In the post-polymerization and post-modification of the Evonik particles, we used XPS to verify the change in the particle composition which, when coupled with the information discovered in DLS, could validate the formation of a polymeric layer. Table 3-1 illustrates the additional XPS results obtained for "post-polymerized" Evonik particle sample.

Table 3-1: XPS results for Evonik particles evolution from functionalization with C3-Initiator to subsequent polymerization.

Element	Evonik-Blank	Evonik + C3-Initiator	Evonik + p(PEGMEMA)
Br3p3	-	0.41%	-
P2p	-	3.59%	-
C1s	21.39%	27.37%	71.07%
N1s	1.04%	0.45%	-
Ti2p	21.64%	17.40%	-
O1s	53.40%	49.04%	23.96%

The results here indicate that the surfaces of the Evonik particles are evenly coated with a polymeric layer, as phosphorous and titanium elements are no longer visible in this surface probing technique. Additionally, the bromine signal has disappeared, which can be explained by its loss in a side reaction, or termination by coupling on the surface. From this point, there is agreement with our initial expectations that the polymer layer should fully engulf the inorganic particle to form the core-shell structure.

3.7.1.3. TGA

We used TGA to obtain a rough estimate on the degree of polymerization *via* mass loss of the hybrid particles when compared to the pure/unmodified Evonik particles. From this method, and taking our previously reported result of 2.55 C3-Initiator molecules per nm^2, one could easily calculate the polymer contribution. The degradation curves are given in Figure 3-20.

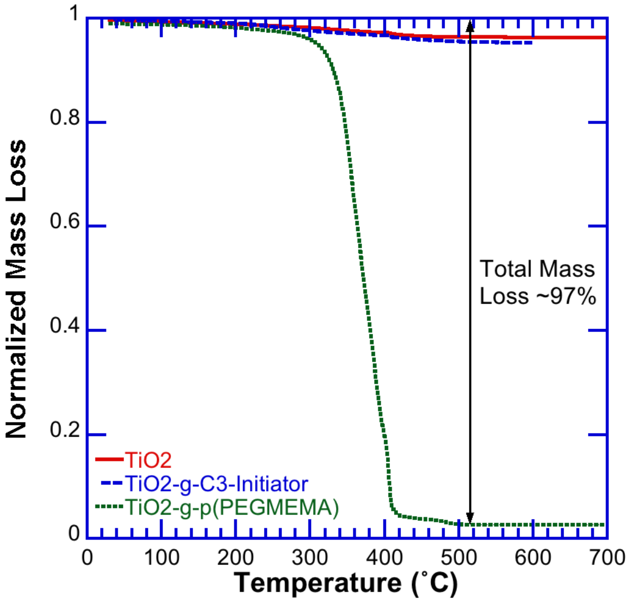

Figure 3-20: TGA mass loss of TiO_2-g-p(PEGMEMA) sample (post polymerization of Evonik particles modified with C3-Initiator). The subsequent mass loss was used to calculate the subsequent degree of polymerization of the particles.

Making similar assumptions to those found in Chapter 2 (2.6.1.3.3. Quantifiable Yield (TGA)), we assumed that:

1). The Evonik particles (core of the hybrid particles) remain 100 nm in size after polymerization
2). The remaining mass after the TGA cycle is solely due to the Evonik particles themselves.
3). Due to the lower mass of the initiator component, we can assume that the initiator contribution to the mass loss to be negligible, thus all the mass loss is due to the polymer layer only.
4). Each Evonik particle has a total volume of $5.24x10^{-16}$ cm^3/particle and a surface area of $3.14x10^{-10}$ cm^2/particle
5). The density of initiators on the surface is 2.55 initiators /nm^2
6). Each macromonomer unit remained at 500 g/mol

Making such assumptions, we can calculate the DP of the polymeric layer by following the calculations as follows:

A). Total Surface Area Calculation:

$$Total\ Surface\ Area = \left(\frac{3.14x10^{-10} \left(\frac{Mass\ Remaining_{TiO_2}}{\rho_{TiO_2}} \right)}{5.24x10^{-16}} \right) x10^{14}$$

- Where the total surface area is in units of nm^2

B). Total Moles of Initiators Calculation:

$$Total\ Moles\ of\ Initiators = \frac{Total\ Surface\ Area\ x\ 2.55}{6.022x10^{23}}$$

C). Moles of Monomers:

$$Moles\ of\ Monomers = \frac{Mass\ loss\ of\ Polymer}{500}$$

D). Degree of Polymerization:

$$Degree\ of\ Polymerization = \frac{Moles\ of\ Monomer}{Total\ Moles\ of\ Initiators}$$

From these calculations, we obtain the calculated results found in Table 3-2.

Table 3-2: Calculated degree of polymerization process for Evonik particles

Step	Values	Units
Total Surface Area	$1.43\text{x}10^{16}$	nm^2
Total Moles of Initiators	$6.06\text{x}10^{-8}$	mole
Moles of Macromonomer	$7.40\text{x}10^{-5}$	mole
Degree of Polymerization	1220	

With our assumptions in mind, these results led us to conclude that the degree of polymerization for the core-shell titania particles should be around 1,200 (if all the unreacted macromonomer were assumed to be removed). Taking this value, the hypothetical conversion can be calculated and used to determine how much of the macromonomer is used. To perform this, the same assumptions used in the TGA calculations should be applied. The value for the initiator weight due to loss of the C3-Initiator is roughly 1.22% of the total mass, as shown in Table 3-3.

Table 3-3: Analysed sample weights and subsequent mass loss from TGA. Difference in weight due to C3-Initiator.

Sample	Mass Loss (%)
TiO_2(Evonik)	2.45%
TiO_2-g-C3-Initiator	3.67%
Difference	**1.22%**

Taking this knowledge forward, we can calculate the conversion as follows:

1). **Calculation of the Initiator used (in moles):**

$$Moles_{C3-Initiator} = \frac{0.0122 x Mass_{Total\ TiO2_2-g-C3-Initiator\ Used}}{208\ g/mol}$$

- The 208 g/mol is the molecular mass of the C3-Initiator group that is degraded
- $Mass_{Total\ TiO2_2-g-C3-Initiator\ Used}$ is in units of "g"

2). **Ideal Degree of Polymerization (if all monomers are consumed):**

$$DP_{Ideal} = \frac{\frac{Mass\ of\ Macromonomer\ Used}{500\ g/mol}}{Moles_{C3-Initiator}}$$

- Mass of the Macromonomer is in units of "g"
- Degree of Polymerization (DP) is unitless

3). **Conversion (ratio of ideal vs calculated DP):**

$$Conversion = \frac{DP_{calculated}}{DP_{Ideal}}$$

From these equations, the calculation of the conversion can be performed and be found in Table 3-4.

Table 3-4: Calculated conversion of hybrid particles made from 0.27M PEGMEMA solution

Parameter	Value
Initiator Used	0.176 g
Macromonomer Used	12.315 g
Moles of Initiator	$1.03x10^{-5}$
DP (Ideal)	2386
DP (calculated)	1220
Conversion	51.1%

While these hybrid particles were characterized to determine their properties, their further application towards the formation of a membrane will be discussed later in Chapter 5.

TGA proved its versatility in determining the degree of polymerization (DP = 1220) for the hybrid particles in addition to helping determine the subsequent conversion of ~51%.

3.7.2. Flat Titania Supports

Flat titania supports provide a slightly different means to confirm that the hybrid structures can be formed using si-ATRP. Unlike titania nanoparticles used in the previous sections, the geometry of flat supports allows us to characterize the polymerization reaction when applied on a simple 2D geometry with a unidirectional growth (or growth perpendicular to the surface). In addition to other techniques already described, the reaction efficacy can be observed *via* direct visual inspection and SEM imaging, which serves as an excellent tool in the confirmation and local characterization of a polymer film.

3.7.2.1. XPS

In the first analysis after polymerizing the flat titania supports, verification that components of the polymer exists were measured through XPS. Table 3-5 illustrates the results obtained for post-polymerized samples.

Table 3-5: XPS results for Flat Titania surfaces from functionalization with C3-Initiator to subsequent polymerization

Element	Flat Titania- Blank	Flat Titania + C3-Initiator	Flat Titania + p(PEGMEMA)
Br3p3	-	0.13%	-
P2p	0.22%	2.86%	0.41%
C1s	17.60%	22.30%	71.27%
N1s	0.19%	1.80%	0.13%
Ti2p	23.30%	20.10%	0.34%
O1s	53.80%	52.20%	27.01%

These results show that the support after polymerization still reveals traces of titania, which means that the polymer coverage was not uniformly coated on the support. The same conclusion can be drawn from the remaining signature of phosphorus belonging to the C3-initiator after polymerization. While previous indication of tripling the quantity of carbon and halving the oxygen quantity is apparent, less than 1% for each subsequent element shows that there is uneven coating of the surface, and that the polymer uniformity may not be perfect. Additionally, a tiny fraction of bromine originally found after the C3-Initiator was bound to the surface is gone after polymerization, indicating that the surface potentially is terminated via coupling at this point.

XPS illustrated that the Flat Titania Supports have a polymeric layer formed on the surface but might not be fully uniformly distributed/formed.

3.7.2.2. SEM

SEM was further utilized to observe the film formation on the surface. In this study, the flat titania substrates were grafted with the C3-initiator and were left to polymerize in either 0 M (used as a reference), or 0.27 M macromonomer solution (with the catalyst). Comparison of the 0.27 M macromonomer sample with the reference (0 M macromonomer) yields striking differences after a 15 or 30 minute reaction time. We do observe the formation of a polymer veil coating the ceramic surface, with a concomitant reduction of the surface roughness. This helps to further confirm and solidify that these commercially available C3-initiator molecules are able to effectively bond and initiate an ATRP reaction from a metal oxide surface, regardless of the surface topology. The resulting images can be found in Figure 3-21.

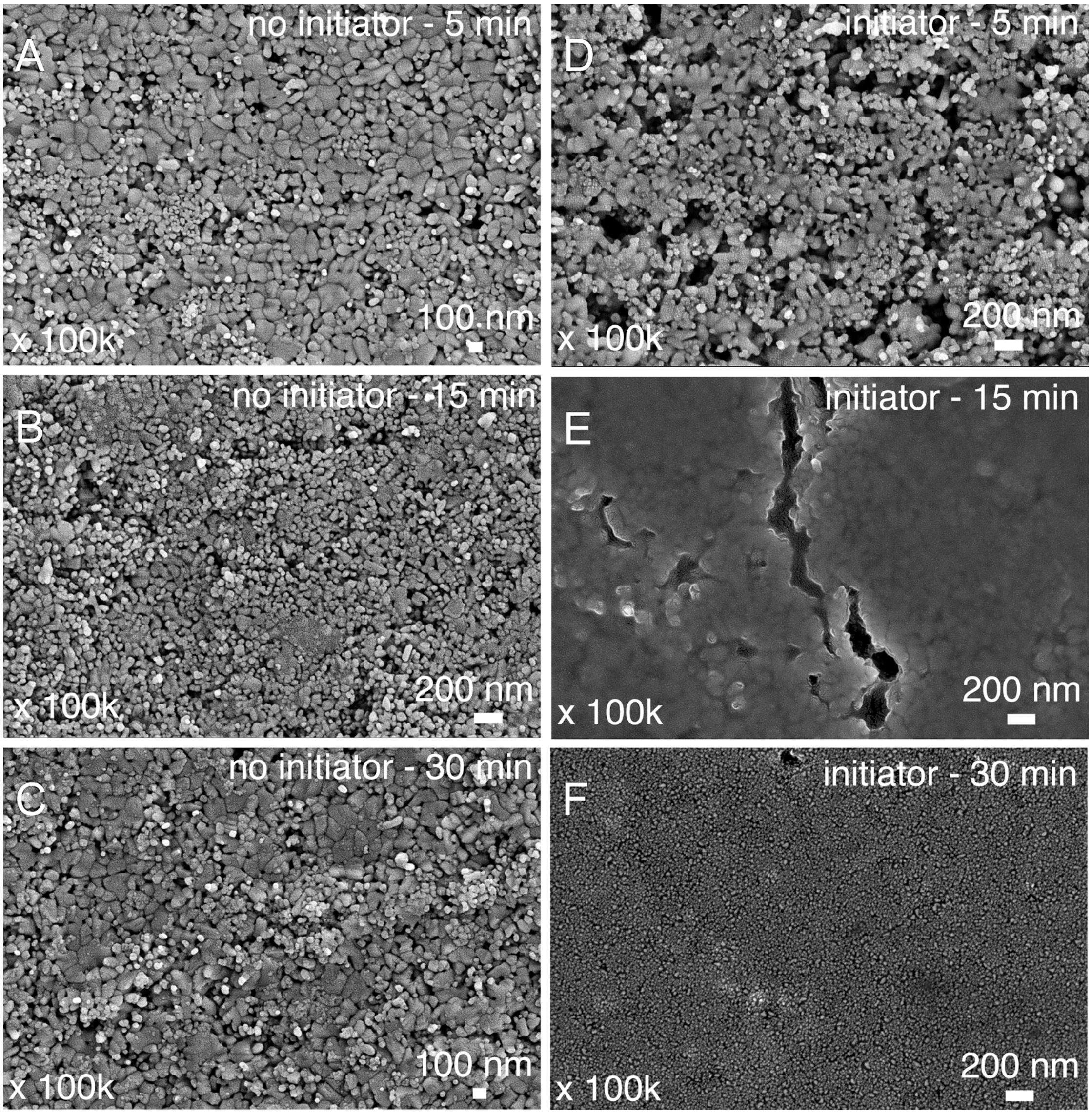

Figure 3-21: SEM images obtained for flat titania substrates with bound initiators exposed to different concentrations of macromonomer and time. The substrates exposed to 0M macromonomer were in A, B, and C for 5 min, 15 min and 30 min, respectively. Images D, E, and F were exposed to 0.27M macromonomer for 5 min, 15 min and 30 min respectively as well. Reproduced from Ref. 223 with permission from the Centre National de la Recherche Scientifique (CNRS) and The Royal Society of Chemistry.

It should be noted that while the SEM imagines appear to display a steady change in the surface morphology, the total film formation was not uniformly formed. Observing that non-uniform layers formed, the decision was to attempt a higher concentration of macromonomer, in the area of 0.67M, to be certain that the reaction could proceeded further (from the additional macromonomer reagents), and attempt to obtain a thick enough film that could fully cover the surface.

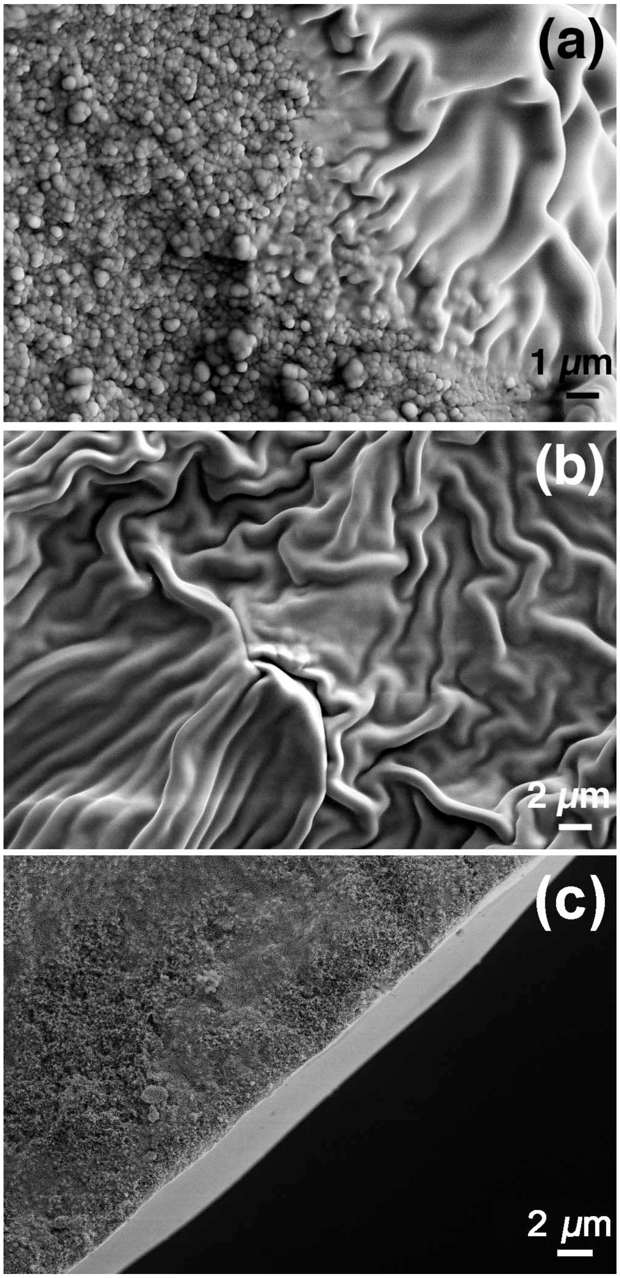

Figure 3-22: SEM images obtained with a flat titania substrate grafted and exposed to a 0.67 M solution of PEGMEMA for 1 hour: a) Flat titania surface/Polymer interface, b) polymer carpet topography and c) side view of Flat titania surface/polymer interface. Reproduced from Ref. 223 with permission from the Centre National de la Recherche Scientifique (CNRS) and The Royal Society of Chemistry.

The resulting change in concentration of macromonomer (or increase to 0.67M) can be found in Figure 3-22. These images clearly show that as we have nearly tripled our concentration, very nice and dense polymer films could be obtained on these surfaces. Of particular interest is Figure 3-22b and Figure 3-22c as they both illustrate that the dense film formed is a unique layer that differs from the flat titania surface. In this, the structure provides us with the knowledge and confirmation that the reaction works and can form a hybrid-coated system.

Looking back into literature, we can re-examine the work by Grajales *et al.*, which had been briefly presented earlier.[24] This work showed that it was possible to create thin layers of amorphous polymer containing Polyethylene Glycol (PEG) on model surfaces (such as gold coated anodized alumina), and that these films were very good at separating carbon-dioxide because of their limited thickness, which reduced the gas diffusion barrier.[24] However, switching from limited model surfaces to actual industrial supports remains a major challenge. Our present study with flat titania supports confirm that a PEG-based polymer can grow from a grafted surface, but achieving a uniform polymer film remained a challenge, despite multiple trials. However, control of thickness still remained an area that required more studies. Therefore, the combined knowledge obtained with grafted particles and substrate allowed us to define the protocol for the fabrication of our nanocomposite membrane, using commercial porous tubular supports, which we will explore in Chapter 5.

SEM showed that Flat Titania substrates could form polymeric films, which could become significantly thicker upon increasing the concentration of macromonomer.

3.8. Conclusions

This chapter described the fundamentals and controls that can be used in ATRP, and subsequently si-ATRP. From the literature presented, the best operational conditions to perform si-ATRP on our experimental setup were applied on the functionalized Evonik particles. We successfully confirmed that the core-shell structure was formed when we performed si-ATRP, and thus arrived at a degree of polymerization of roughly 1220 (determined from TGA with the assumption of no free macromonomer left) at a conversion of ~50%.

Our continued work on flat titania surfaces also yielded very nice films that not only confirmed the reaction proceeded, but also observations of a folded carpet-like structure upon film formation. However, there could exist challenges transferring this work onto curved ceramic tubes or the CTI porous tubes, such as ensuring a continuous uniform film formation.

Chapter 4

Surface-initiated Ring-Opening Metathesis Polymerization of Norbornene (NB) and Norbornene-PEG (NB-PEO) based Macromonomers

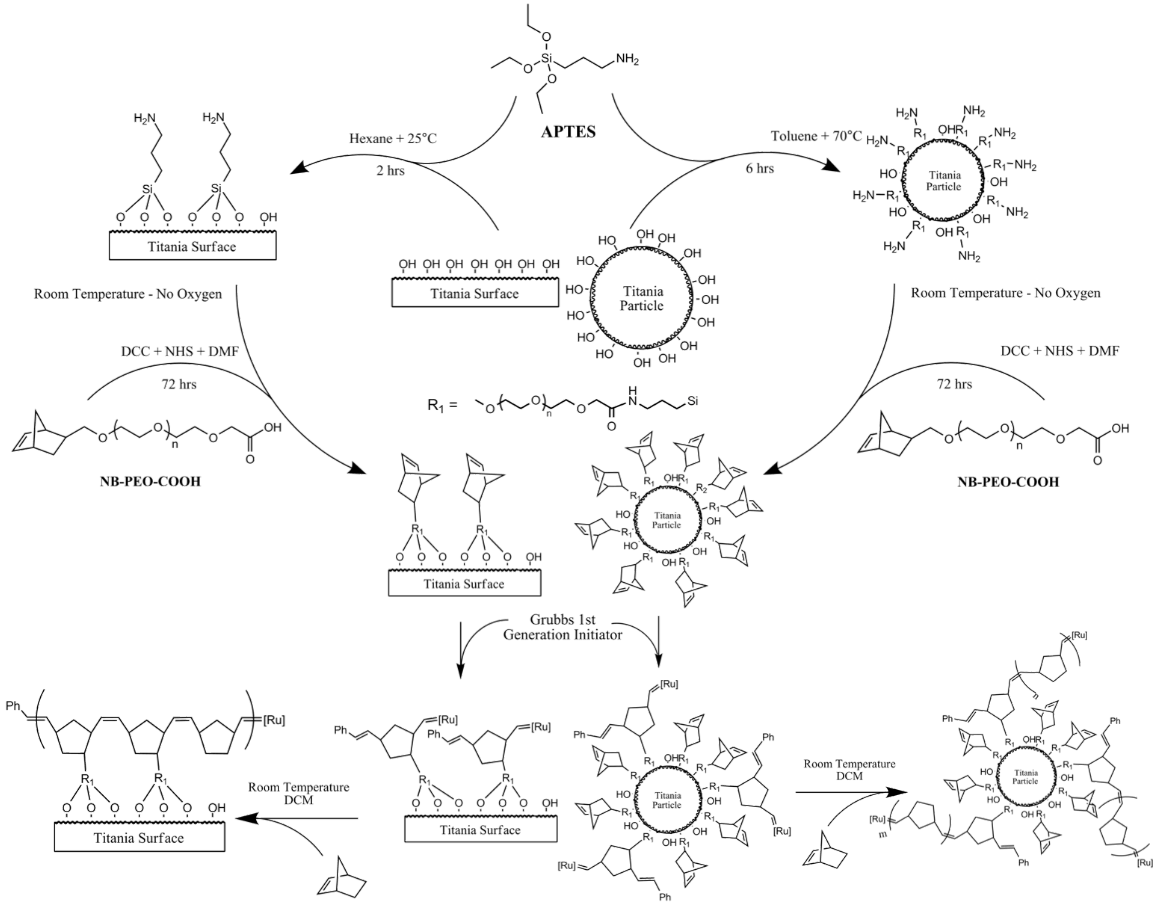

Ideal mechanism for si-ROMP used in this Chapter

4.1. Introduction

Previous chapters focused heavily on the fundamentals and background on different components of this project; varying from the different types and forms of membranes used in separation, to surface modification of inorganic oxides, and the application of one polymerization technique (i.e. si-ATRP). In this chapter, we will continue this polymeric study with a different form of polymerization known as Ring-Opening Metathesis Polymerization, or ROMP.

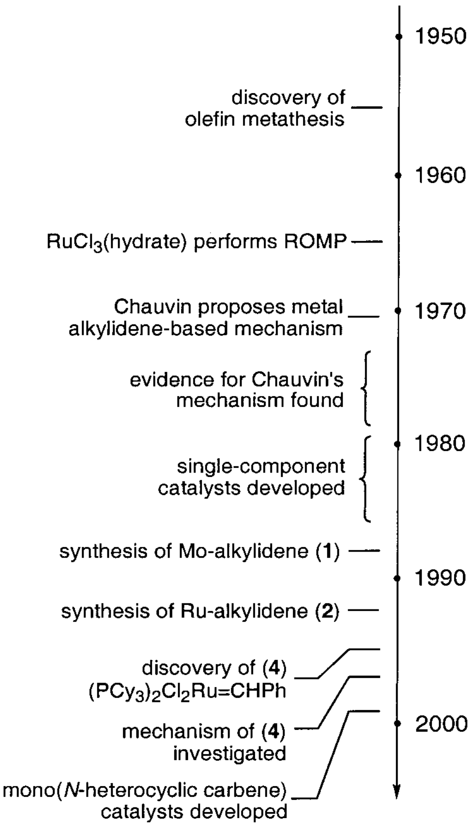

Figure 4-1: Timeline of events for metathesis of olefins and subsequent development of the Grubbs and Schrock Catalyst.[224] Reprinted with permission from Reference 224. Copyright 2001 American Chemical Society.

ROMP has been known as a relative success story in polymerization. With the discovery of olefin metathesis in the mid 1950's, the mechanism captivated researchers trying to explain this unknown reaction. Various researchers proposed different theorized mechanisms, such as the mechanism by Banks and Baileys,[225] which was experimentally supported by the work by Calderon *et al.*[226] However, it was Hérrison and Chauvin in 1971 that was able to propose the currently accepted mechanism of the metal-carbene being the active center,[227,228] which was later supported by Katz,[229] Grubbs[230,231] and Schrock[231,232] due to their improved stable metal carbene/alkylidene compounds. This knowledge eventually enabled many researchers to optimize their metal carbene/alkylidene systems to improve the metathesis reaction. For instance, this work directly led to the development of a variety catalyst, including the Schrock catalysts or the more famous Grubbs catalyst (3 generations that are commercially available). Most of the major developments can be seen from Figure 4-1.

This work eventually became so profound, that Chauvin, Grubbs and Schrock were awarded with the Nobel Prize in Chemistry in 2005.[228,231-233] Noting this milestone, and the continual work within this domain, there is considerable interest in applying this metathesis technique towards a plethora of areas for application.

As the direction of this chapter is for the study of surface-initiated ROMP (si-ROMP), the general fundamentals of ROMP will first be presented, followed by existing methods and examples of si-ROMP found in literature. The mechanism/experimental design for studying si-ROMP will then be presented on different titania surfaces (specifically the CTI porous titania surfaces, and the Evonik particles) followed by a conclusion.

4.2. Fundamentals

As the work within the domain of ROMP has been long established, we will briefly go through the mechanisms for this reaction. In many ways, the behaviour of ROMP can be controlled, leaving this technique to be counted as a "living" polymerization. The overall reaction of ROMP (both controlled and subsequent uncontrolled methods, which some initiators will cause)[234] can be seen from Figure 4-2.

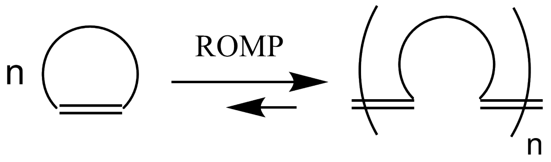

Figure 4-2: General ROMP reaction. Notice that the reaction keeps the double bond within the polymer backbone - a unique characteristic of this reaction.[235] In addition, the reaction is in equilibrium - favouring the polymer formation.

The reaction shows the general mechanism of ROMP, complete with the equilibrium between the strained olefin reagent, and the growing polymer chain. This equilibrium is determined by the strain of the olefin; that is, the higher the strain, the easier the polymer is formed. However, this oversimplified mechanism has multiple components such as initiation, propagation, and subsequent termination. The more detailed reaction can be found in Figure 4-3.

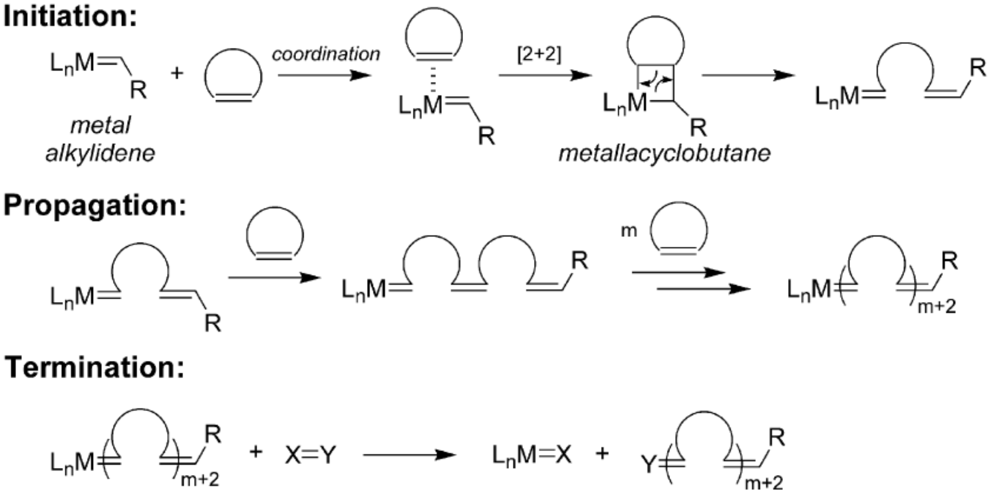

Figure 4-3: Ideal reaction mechanism of ROMP (not including backbiting or side-reactions).[235] Note that L_n is a ligand bonded to the metal atom.

In this reaction, the metal carbene/alkylidene coordinates with the double bond found in the strained olefin and eventually reconfigure the monomer to become the initiating unit in ROMP (some examples of these metal complexes can be found in Figure 4-4). The speed, or rate, at which this occurs can be represented as K_i (or the kinetic rate of initiation). Subsequently, the propagation step behaves in a similar manner in which the metal carbene/alkylidene group can form a similar interaction with another monomer unit to add each unit to the growing chain. This kinetic rate can also be represented as K_p. It should be also noted that while the value of K_i is determined by the type of initiator (i.e. G1, G2 etc..), K_p is determined partially by the monomer reactivity to the metal carbene/alkylidene group. Termination of the system is generally conducted *via* the introduction of a double bonded molecule that can cap the end terminus of the molecule and consequently "steal" the metal group from the polymer chain.

As previously mentioned, the kinetic rates are important parameters. In this sense, the rates help to determine if the living reaction is controlled or non-controlled, as illustrated by the parameters:

$K_i > K_p$ Controlled Polymerization
$K_i < K_p$ Non-Controlled Polymerziation

From these parameters, one can begin to determine what types of initiators can be used to produce a living polymer as opposed to a non-controlled system. Each unique initiator will determine the subsequent control of the system *via* the metal carbene/alkylidene structure, such as Grubbs Ruthenium initiators or Schrock Molybdenum initiators, as shown in Figure 4-4.

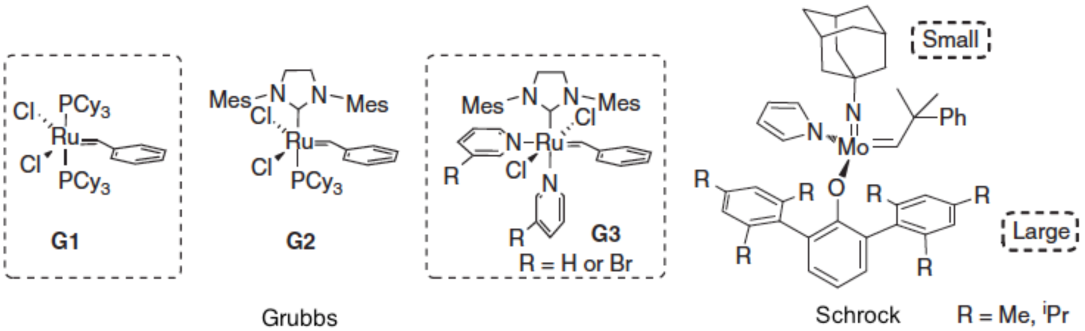

Figure 4-4: Different ROMP initiators available for use. The application of each initiator presented above yield different rates of control. The "G" series represent Grubbs initiator, and the Molybdenum alkydiene on the right is an example of a Schrock initiator.[234] NOTE: the "small" and "large" sign represents the relative bulkiness of the attached alkylidene groups in the region.

Understanding the different initiators here can help to determine their specific use and applications. For instance, if we look at the kinetic rates of G1 (or the Grubbs first generation initiator), we can see that it follows the standard parameters for a controlled polymerization (i.e. $K_i > K_p$).[236,237] However, G2 (or the Grubbs second generation initiator) does not appear to yield the same level of control ($K_i < K_p$), even though the structure (due to the N-heterocyclic ligand above) results in a more active and faster polymerization.[238] In what some researchers have dubbed Grubbs third generation initiator, the G3 initiators appear to proceed in a controlled manner, but also at a much faster rate.[239] In this case, the fast rate of initiation and rate of propagation has been shown to be an excellent method for the formation of block copolymers.[240-242] If we consider the Schrock initiator, it has been shown to control specific architecture of the growing polymer, specifically forming a syndiotatic structure in the polymeric chain.[243,244]

Comparing the different initiators, it should also be noted that while each presented initiator has their merits and drawbacks, the conditions for use should also be briefly touched upon. With Schrock based initiators and G3 initiators, their air and water tolerance is low.[234] However, G1 and G2 initiators are more air and water tolerant.[234,245] This point makes the application of G1 for more controlled systems favourable, even though they have been shown to have lower tolerance to monomers with stronger functional groups (or functionality).[246]

4.3. surface-initiated ROMP

As this section suggests, application of ROMP towards surface-initiated systems will be the main focus to be discussed next. While there exists many different methods of si-ROMP, a brief overview will be presented with several examples with respect to inorganic surfaces.

Perhaps the first example of si-ROMP can be found early on in 1999, from the work by Watson *et al*. In this work, the researchers modified gold nanoparticles with alkene-thiols along with a norbornenyl functionalized alkene-thiol and subsequently formed hybrid particles, including a double polymer shell with varying monomers derived with ferrocene with the help of Grubbs first generation initiator (G1).[145,247] Figure 4-5 shows the overall synthesis pathway used by Watson and his coworkers.

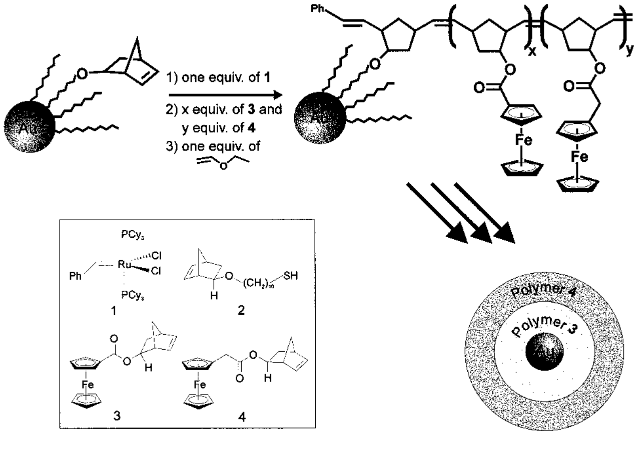

Figure 4-5: Schematic of the target reaction of functionalization of gold nanoparticles to form a double polymeric shell, as illustrated by Watson *et al.*[145] Reprinted with permission from Reference 145. Copyright 1999 American Chemical Society.

Similarly, the later work by Grubbs and his coworkers in 1999 (published by Weck *et al.*) provided a similar method of grafting *via* a alkene-thiol based norbornenyl terminated molecule, but showed that this was possible on a planar surface of gold.[248] What made this more important was that the work illustrated that it was possible to control where the norbornenyl-terminated molecule could be grafted. Since the gold surface was pre-coated with a dodecanethiol monolayer, the norbornenyl-terminated molecule was inserted from the domain boundaries between the dodecanethiol layer. Afterwards, the work by Bao and Grubbs (published by Rutenberg *et al.*) demonstrated that it was possible to perform si-ROMP without the dodecanethiol layer on the flat gold surface. Instead, the grafted norbornenyl group was activated with the Grubbs second generation initiator (G2), which was found to yield a faster and thicker film formation.[146]

In the collaborative groups of Nuzzo and Laibinis, a paper by Kim *et al.* showed that it was possible to functionalize and initiate si-ROMP on silicon wafers after grafting with a silane-modified norbornenyl group.[249] This is more particularly interesting, as the researchers here specifically mention that the previous method through functionalization of gold surfaces with the norbornenyl group after coating with a dodecanethiol monolayer yields extremely low levels of polymer film.[249] The previously mentioned paper by Rutenberg *et al.* also applied the coating technique of silane modified norbornenyl groups to functionalize a silicon surface and was eventually polymerized to form a dielectric layer.[146] This approach ultimately appeared to work (upwards of >90% of thin-film transistors worked), provided that the layer subjected to a short annealing time to close any porous structures.[146] In the case of silica particles, work had more recently been performed by Rolfe *et al.* to illustrate that si-ROMP could easily produce hybrid particles as well.[250] The authors specifically reference the protocol that Buchmeiser and his group developed in 2000. Buchmeiser *et al.* dived into two different methods of surface functionalization with polymers – either a “grafting to” method, in which a living polymer is attached to the surface functionalized group (i.e. a strained olefin in the case of ROMP), or a “grafting from” method, where the initiator is added to the surface, and the typical si-ROMP procedure takes over.[251-253] This work has subsequently enabled Buchmeiser and his group to develop monolithic supports for particle separation and catalysis.[252,254]

Considering the use of titania substrates, literature has yielded very few works published with any si-ROMP based routes. In the group of Dr. Feng Zhou, one work published by Ye *et al.* in 2010 did however show that it was possible with the use of a catechol based anchor that was bonded (*via* peptide bond) to a carboxylic functionalized norbornene molecule,[139] as shown in Figure 4-6. In a later publication by the same group (by Yan *et al.* in 2013), the group applied the same technique to form p-n heterojunctions and would help improve photoelectric performance due to better material integration.[161]

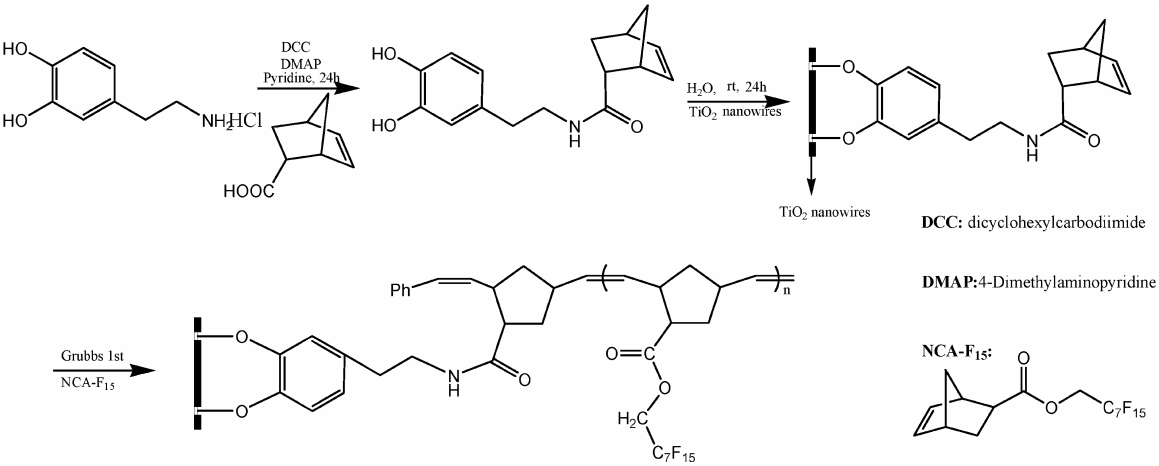

Figure 4-6: Method of anchoring group synthesis and subsequent application for si-ROMP on a titanium dioxide surface, as illustrated by Ye *et al.*[139] Reprinted with permission from Reference 139. Copyright 2010 American Chemical Society.

This work on titania supports or surfaces for their use in si-ROMP is shown to be an area that has not been developed as much as its silica or gold surface counterparts – specifically for the “grafting from” portion of the polymer growth, as opposed to the “grafting to” method, eloquently illustrated by the approach taken by Heroguez and her group.[125] In this work, the “grafting to” method involves the direct surface attachment of PNB-PEO core-shell nanoparticles functionalized with Gentamicin (GS). The final ideal structure of the system can be seen in Figure 4-7.

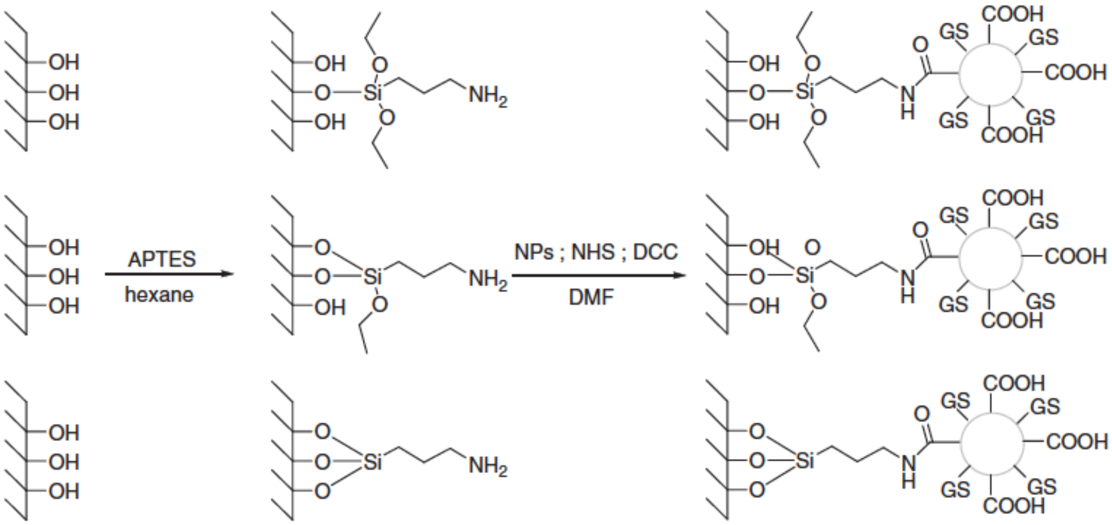

Figure 4-7: Surface attachment of nanoparticles (synthesized by ROMP) onto a titania surface previously functionalize with APTES. This grafting can be categorized as a "grafting to" method, in which the final application is the pH responsive release of gentamicin (GS).[125,255]

The direct application of this method of grafting was used to create a pH responsive system that could release anti-bacterial agents when the pH decreased (a sign of bacterial growth). The titanium biomaterial structure can placed as a bone implant to help reduce infections after invasive surgery.[125]

4.4. Design Pathway

From the briefly presented background on ROMP and si-ROMP, it is clear that there exists room for application of si-ROMP towards the intended objective of this project. As such, the decision was made to perform the si-ROMP study on first the CTI porous tubes, then on the Evonik particles (as illustrated in Figure 4-8).

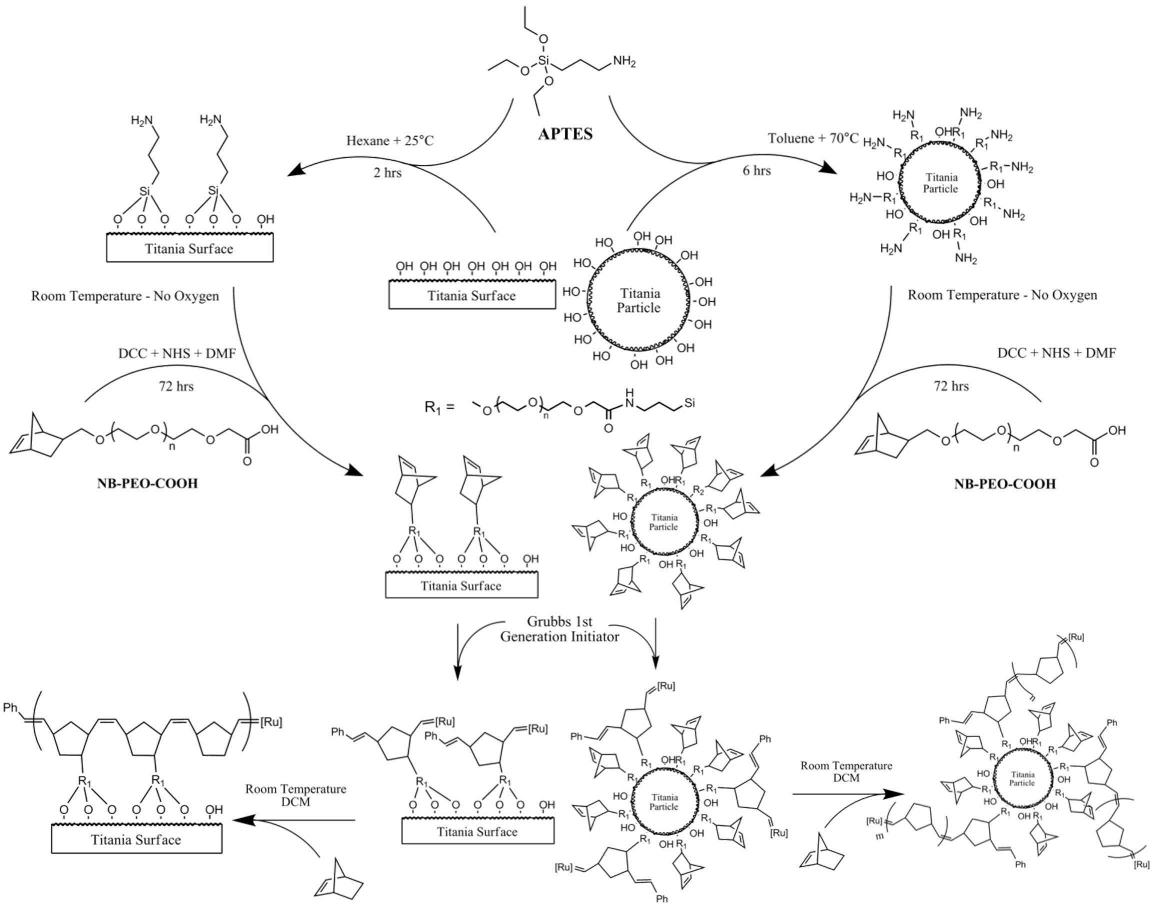

Figure 4-8: Design pathway to be explored in this Chapter. Left: Titania surfaces explored, which represents the study of CTI porous tube functionalized with APTES and bound with a norbornenyl terminated carboxylic acid molecule (also known and seen as NB-PEO-COOH). Subsequent activation with the Grubbs 1st generation initiator and exposure to norbornene (or NB) theoretically results in a film. Right: Evonik particles functionalized with APTES and bound with NB-PEO-COOH. Similar to the CTI porous tube pathway, the use of the Grubbs 1st generation initiator is deployed, alongside norbornene to form hybrid structures.

In both pathways, the functionalized surfaces with APTES are reacted with a synthesized norbornenyl derivative, also known as α-norbornenyl-ω-carboxylic acid poly(ethylene oxide) and shown as **NB-PEO-COOH** in Figure 4-8, through an amide bond (i.e. reacting the carboxylic acid group with an amine group). The norbornene group is then activated with the Grubbs first generation initiator (due to its tolerance to water and oxygen) and upon removal of any unbound ruthenium, si-ROMP can occur with exposure to norbornene (NB) in DCM.

Confirming these pathways, the discussion will first focus on the NB-PEO-COOH synthesis. Focus will then shift to the CTI porous tube modification with si-ROMP, and then with the Evonik particles modification towards si-ROMP.

4.5. Macromonomer Synthesis

The macromonomer that will be used in this study had to be first synthesized. As the project has been focused on highly PEG-ylated macromonomers, this was the key component to be made. In order to achieve this goal *via* ROMP, an existing procedure developed by Pichavant *et al.* in 2011 was adapted for this application.[124]

4.5.1. Materials and Procedure

4.5.1.1. Materials

Ethylene Oxide (EO) (>99.5%, Aldrich), NaH (60% in mineral oil, Aldrich), 5-norbornene-2-methanol (98%; mixture of both endo and exo; Aldrich), 2-bromoethyl acetate (97%, Aldrich), Sodium Sulphate (99%, Sigma Aldrich), and Norbornylene (99%, Aldrich) were ordered from Aldrich and used as received. Sodium cubes (99.9% trace metal in mineral oil, Sigma Aldrich), heptane (99%, Sigma Aldrich), dichloromethane (>99.8%, Sigma Aldrich), 1,4-dioxane (99.8%, Sigma Aldrich), HCl (Sigma Aldrich), diethylether (99.7%, Sigma Aldrich) were used without further processing. DMF (anhydrous 99.8%, Sigma-Aldrich), THF (J.T. Baker), Ethanol (96% purissimum grade pur; Xilab) were kept anhydrous using several scoops of benzophenone (99%, Sigma-Aldrich) and cyrodistilled before use. Methanoic acid was synthesized by mixing 5 drops of HCl (Sigma Aldrich) in 10 mL methanol (Xilab). Diphenyl methyl potassium (DPMK, 0.61 mol/L in THF) was synthesized and stored away from light. NaOH (98%, Fisher Scientific) was used to create the 0.1 M NaOH solution (4 g in 1 L DI Water). Celite (Prolab) was used for filtration to remove any unreacted DPMK. The water used in these experiments was 18 MΩ Ultra pure DI water (Millipore system).

4.5.1.2. Synthesis of NB-PEO-OH

The synthesis of NB-PEO-COOH proceeds in a similar fashion as which was described by Pichavant *et al.* (2011).[124] In this procedure, anionic polymerization was performed in order to synthesize the bulk of the macromonomer. To start, gaseous ethylene oxide (EO) is pumped into a fully sealed glass apparatus (1 L round bottom flask) that has been flamed 3 times with a stir bar and freshly cut sodium (0.5 cm x 0.5cm x 0.5cm pieces of about 10-20 pieces). In a D-ware container, ethanol is cool down to -30˚C (using liquid nitrogen) and used to cool the round bottom flask. The EO gas is introduced into the round bottom flask, and left to condense until the liquid EO just reaches above the stir bar.

WARNING: Ethylene Oxide (EO) is a flammable, compressed gas that can sterilize you! Always wear protective gear (face shield, gloves), ensure fumehood is in working order (shield is down) and that the EO canister is in a good distance inside the fumehood (i.e. not near the front of the fumehood).

After the EO canister is closed and disconnected from the round bottom flask (Note: leave the connection tube inside the fumehood for at least 20 minutes before removal), the mixture of EO with sodium was left to stir for 2 hours (temperature: -30˚C - -15˚C). The EO + sodium mixture was then cyrodistilled into another round bottom flask that had an extension that could measure volume in order to recover the pure EO (roughly 27 mL was collected; 0.541 mol).

In a separate round bottom flask, 300 mL of THF was cyrodistilled and 5-norbornene-2-methanol (1 mL; $8.323\text{x}10^{-3}$ mol) was injected under nitrogen flow (note that all conditions are under anhydrous, inert atmosphere). This mixture was left to stir for 20 minutes before DPMK (anionic initiator; 10.9 mL or $6.658\text{x}10^{-3}$ mol) was added. All the collected, purified EO was then added into this mixture and left to react over 72 hours.

Mixture was then deactivated with the addition of methanoic acid (5 mL) and left to stir for 20 minutes. Mixture was then precipitated in diethylether (dropwise) at room temperature, filtered and vacuumed for 2 hours. The sample was redispersed in DCM and filtrated over Celite (to remove DPMK). The collected eluent was then rotovaped to remove most of the DCM, then redissolved in THF to be re-preciptated in diethylether (0˚C). The collected perciptate was filtrated, collected, vacuumed for another 2 hours before redissolving in 1,4-dioxane (10 mL) and lyophilized overnight. The product (NB-PEO-OH; approx. 20 g) was then collected and stored in an argon glovebox until use.

4.5.1.3. Synthesis of NB-PEO-COOH

Sodium hydride (0.85 g; determined with the final molar ratio of 10:1 of NaH to NB-PEO-OH) was weighted in a disposable vial and dispersed in heptane (10 mL). The mixture was then filtered and washed with more heptane until a white powder is obtained. The powder is quickly transferred to a round bottom flask connected to a condenser. Cyrodistilled THF (15 mL) is then added to dissolve/disperse the NaH white powder. Continuous nitrogen flow is then added into the system while a solution of NB-PEO-OH (7.04 g) is mixed with cyrodistilled THF (40 mL) and added dropwise into the stirring NaH+THF. After the bubbling has subsided, the nitrogen flow was stopped and left to stir for another 90 minutes. 2-bromoethyl acetate (1 mL) was then syringed into the round bottom flask (via septum) and the mixture was heated (60˚C, refluxed) and left to react overnight (approx. 15 hours).

The mixture was then cooled down to room temperature, and pH was adjusted to roughly 7 using a 0.1 M NaOH solution. THF was then removed using the rotovap and then redispersed in DCM (20 mL). Sodium Sulphate (4-5 scoops) was added slowly to this mixture, stirred and then filtered. The collected eluent solution of DCM + macromonomer is then rotovaped again, precipitated in diethylether (0˚C) and filtrated. The collected powder (or macromonomer) is dispersed in 1,4-dioxane and lyophilized overnight.

The collected powder/macromonomer (5.25 g) is redissolved into 60 mL of 0.1 M NaOH and mixed with another 235 mL of 0.1 M NaOH. The mixture is then left to stir for 24 hours at 55˚C under reflux. 3 M HCl (10 mL) was then added to the mixture upon cooling to room temperature, and adjusted to pH = 7. Afterwards, water was removed using a rotovap. The new fully functionalized NB-PEO-COOH is redispersed in DCM (stirred for 2 hours) and sodium sulphate was added to remove any remaining water. The mixture is then filtered and the collected eluent is concentrated to 20 mL. Cold diethylether (0˚C) is then used to precipitate the mixture, and the collected powder is dried under vacuum for 1 hour. 1,4-dioxane (~40 mL) is then added to the round bottom flask, frozen and left to lyophilize overnight. The final collected powder (NB-PEO-COOH, 4.8 g) was then stored in the glovebox until used.

4.5.2. Characterization by ^{1}H NMR

As shown from previous chapters, the use of proton NMR, or ^{1}H NMR, has been useful. As a result, this was the ideal method of characterizing the growth and functionalization of the macromonomer. Note that the macromonomer is composed of 3 portions – the ROMP capable functionality provided by the norbornenyl group, the PEG chain for CO_2 selectivity, and the carboxylic acid group that can form the amide bond with the surface. The measurement after reacting 5-norbornene-2-methanol with ethylene oxide through anionic ring-opening polymerization can be seen in Figure 4-9. Although the reaction occurs with a variety of different steps, we can note that the subsequent groups highlighted from the figure show how each hydrogen component is linked to those found within the spectra (i.e. the faint blue rectangles found on the norbornenyl group double bonds correspond to the region found on the ^{1}H NMR spectra with the same colour).

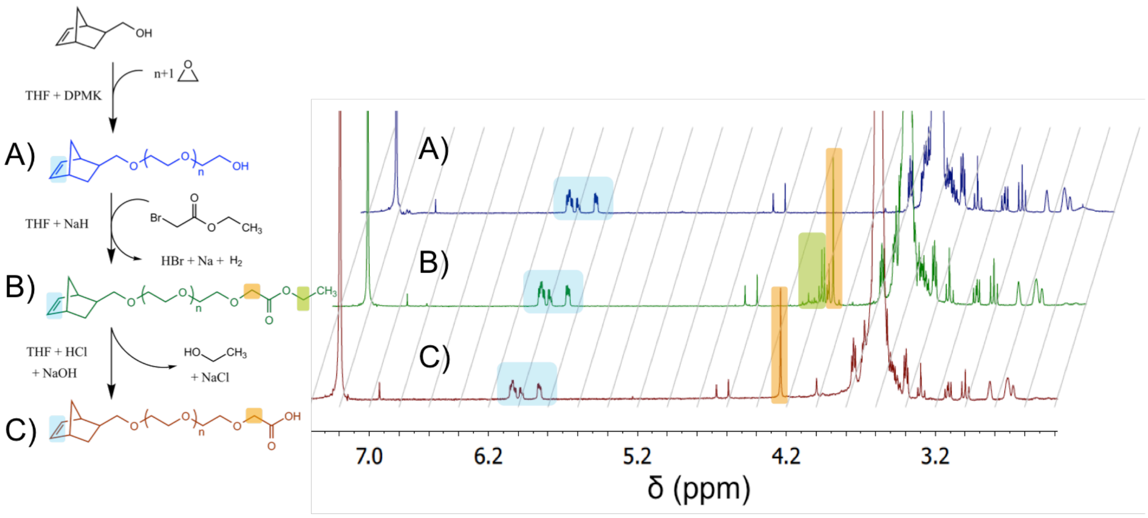

Figure 4-9: ^{1}H NMR spectra on the evolution of anionic polymerization of 2-norbornene-5-methanol to A) α-norbornenyl-poly(ethylene oxide) (or NB-PEO-OH) and subsequent 2-step functionalization to form B) α-norbornenyl-ω-ester poly(ethylene oxide) (or NB-PEO-$COCH_2CH_3$), and finally C) α-norbornenyl-ω-carboxylic acid poly(ethylene oxide) (or NB-PEO-COOH)

From the previously presented ^{1}H NMR spectra, we can conclude that the reaction has been achieved. In this case, the target molecular weight for the macromonomer was roughly 3500 g/mol. In order to determine this point, we can compare the different integration values for the peaks for each group (with the norbornenyl group set at a value of 2.0). The values can be found in Table 4-1 below.

Table 4-1: Integration values found for the synthesized macromonomer. Similar to Figure 4-9, the components are: A) NB-PEO-OH B) NB-PEO-$COCH_2CH_3$ and C) NB-PEO-COOH. The target values are the ideal values for ~75 repeating units.

Sample	Target	A	B	C
Norbornenyl Group: Double Bond - 5.8-6.1 ppm	2.0	2.0	2.0	2.0
PEG Group - ~3.6 ppm	300	298	301.7	323.3
Between Carboxylic Acid and Ester Group- 4.2 ppm	2.0*	-	-	1.48

* The values here are meant for the final product C). in order to calculate the final yield of functionalized macromonomer. Dividing the integrated value of 1.48 by the ideal/target value of 2.0 yielded the percent of functionalization of 74%.

As each group (norbornenyl group at 5.8-6.1 ppm, PEG groups around 3.57 ppm and the hydrogen atoms found between the final ethylene oxide group and the carboxylic acid group around 4.24 ppm) were good markers for following the functionalization of the macromonomer, these key peaks were integrated to determine the overall functionalization and the subsequent molecular mass. The functionalization of NB-PEO-

OH to NB-PEO-COOH yielded about 74%, or 74% of the final product had a carboxylic acid group for use. In the case of molecular mass, we can easily calculate each macromonomer by following some rules:

- Taking the PEG Group integration value, divide this value by 4 (representing 4 hydrogen atoms per repeating unit) and multiplying this value by 44 g/mol
- Adding the end group molecular weight (i.e. NB-PEO-OH ends in –OH, thus would be 17 g/mol, NB-PEO-$COCH_2CH_3$ ends in CH_2-CO-CH_2-CH_3 (71.07 g/mol) and NB-PEO-COOH ends in -COOH (59.03 g/mol)
- Adding the norbornenyl group up to the first oxygen unit, or 124 g/mol

These rules ultimately resulted in calculating the macromonomers to be in the range of 3500 g/mol to 4000 g/mol (specifically, NB-PEO-OH = 3422g/mol, NB-PEO-$COCH_2CH_3$ = 3517 g/mol, and NB-PEO-COOH = 3743 g/mol). In this case, the final product NB-PEO-COOH can be roughly taken as 3740 g/mol (and used for future calculations as such).

^{1}H NMR helped determine that the functionalized macromonomer NB-PEO-COOH, or α-norbornenyl-ω-carboxylic acid poly(ethylene oxide), had a molecular mass around 3740 g/mol.

4.6. General Procedure for Functionalization and Polymerization

4.6.1. Materials

Grubbs 1st Generation Initiator (Aldrich), Norbornylene (99%, Aldrich), and N-hydroxysuccinimide (NHS) (98%, Aldrich) were ordered from Aldrich and used as received. DMF (anhydrous 99.8%, Sigma-Aldrich) and dichloromethane (>99.8%, Sigma Aldrich) were used without further processing. 1,3-dicyclohexylcarbodiimide (DCC) (Alfa) was purchases and used as received from Alfa Aesar. The water used in these experiments was 18 MΩ Ultra pure DI water (Millipore system).

4.6.2. Functionalization of Titania Porous Substrates (CTI) with NB-PEO-COOH

Previously synthesized samples of CTI-g-APTES were reacted with 1,3-dicyclohexylcarbodiimide (DCC, 97 mg), N-hydroxysuccinimide (NHS, 241 mg), NB-PEO-COOH (111 mg) all dissolved in degassed DMF (2 mL) for 72 hours. The samples were then rinsed in ethanol several times before left to dry overnight in air. This final product is now called CTI-g-APTES-PEO-NB.

4.6.3. Functionalization of Titania Particles with NB-PEO-COOH

The previously synthesized particles of TiO_2-g-APTES (0.51 g) is reacted with NB-PEO-COOH (0.79 g) with the help of DCC (2.29 g) and NHS (1.43 g) in anhydrous DMF (20 mL). The reaction was left running at room temperature for 72 hours, then filtered and rinsed 6 times with ethanol. The collected powder (now TiO_2-g-APTES-PEO-NB) is vacuumed dried overnight, then stored in the argon glovebox.

4.6.4. Activation of CTI-g-APTES-PEO-NB

Grubbs 1st Generation Initiator (0.022 g) was added to a DCM (2 mL) and left to mix for 10 minutes. The synthesized CTI-g-APTES-PEO-NB was then submerged into the same vial and left to react for 4 hours to activate. After activation, the sample was quickly rinsed with DMF and Ethanol, and then used immediately. Note this sample will be referred to as CTI-g-APTES-PEO-NB*.

4.6.5. Activation of TiO_2-g-APTES-PEO-NB

TiO_2-g-APTES-PEO-NB (0.2 g) was dispersed in ethanol (8 mL) and left to stir for 10 minutes. In another vial, Grubbs 1st Generation Initiator (0.022 g) was added to a DCM (1 mL) and ethanol (1 mL) mixture. Using a syringe, the TiO_2-g-APTES-PEO-NB mixture was added dropwise into the vial with the Grubbs 1st Generation Initiator and left to stir for 3-4 hours.

Now that the particles are "activated" to become the initiator (i.e. TiO_2-g-APTES-PEO-NB*), an adapted centrifuge tube (Amicon Ultra 15 Milipore – 100 kDa) was used to centrifuge the particles (2000 rpm, 10 minutes), in order to remove the solvent. This step was repeated twice with ethanol to wash (re-centrifuged each subsequent time at the same setting).

4.6.6. Monomer Solution

To prepare the 0.3 M norbornene (NB) monomer solution, NB (1.22 g) was dissolved in DCM (40 mL) and syringed into a 500 mL flamed round bottom flask. A 3-cycle freeze-pump-thaw degasing method was used to remove the oxygen and left under vacuum until use.

4.6.7. Polymerization

After the activation of the titania particles (TiO2-g-APTES-NB*), 0.1 g of activated particles were dispersed in 5 mL ethanol to be used as a stock solution. Afterwards, 0.5 mL of this mixture was syringed into 5 mL of the 0.3 M norbornene solution to polymerize and left for 16 hours. Similarly, the activated CTI-g-APTES-PEO-NB* sample is submerged into 10 mL of the 0.3 M norbornene solution and left to react for 1 minute (NOTE: reaction was almost spontaneous).

4.7. Functionalization and Polymerization from CTI Porous Tubes

As the CTI porous tubes are the final target supports for use, the efforts to directly functionalize these surfaces were also attempted. From Chapter 2, the functionalization with APTES on the CTI porous tubes was shown to be low. However, to fully compare CTI porous tubes and the Evonik particles, functionalization of the APTES with the macromonomer, activation with the Grubbs 1st generation initiator and polymerization with norbornene was first studied on the CTI porous tubes to verify that it was still possible to attach a norbornenyl functionality to the surface. These substrates were then studied using XPS and SEM, and their results discussed.

4.7.1. Analysis and Characterization by XPS

The first characterization after the reaction for each step has been performed by XPS analysis. In this case, the elemental signals yielded the atomic percentages that can be found in Table 4-2 below.

Table 4-2: XPS data collected for the sample surfaces over the loading procedure from CTI porous tubes (or non-modified surface), to the polymerized sample (pNB). Note the highly peculiar absence of the ruthenium signal (was not locatable).

	CTI Porous Tubes	CTI-g-APTES	CTI-g-APTES-PEO-NB	Activation with Grubbs	Polymerization (with NB) - pNB
Al2p	8.56%	8.78%	-	5.43%	4.47%
Si2p	1.49%	3.25%	-	5.99%	5.61%
P2p	3.47%	3.14%	-	1.07%	-
Zr3d	-	-	-	-	-
Cl2p	-	-	-	0.62%	-
C1s	24.85%	25.61%	81.60%	52.67%	73.46%
K2p3	-	-	-	0.25%	0.49%
Ca2p	0.36%	0.37%	-	0.43%	-
N1s	0.71%	1.45%	9.78%	0.88%	0.62%
Ti2p	11.86%	10.99%	0.50%	3.62%	-
O1s	45.81%	44.02%	8.12%	28.60%	15.26%
Na1s	2.97%	2.39%	-	0.45%	0.08%

NOTE: sample acronyms: CTI = CTI Porous Tubes, APTES = (3-Aminopropyl)triethyoxysilane, NB = Norbornene, Grubbs = Grubbs 1st generation Initiator, pNB = Polynorbornene

First assessment of the collected data shows some interesting results. For instance, after formation of the amide bond to attach the NB-PEO moiety on the surface, the nitrogen content oddly increases by roughly a factor of 5. This strange phenomenon is more evident after the initiator portion is created through activation with the Grubbs 1st generation initiator. The results shown after this activation step highlights that certain regions reappear (i.e. reappearance of higher titania signals). However, the expected ruthenium content is not visible as no associated peaks could be detected. This leads us to believe that the polymerized sections after the final step (although observable) might not be simply explained.

4.7.2. Characterization by SEM

The next step was to confirm some of the speculations with the surface topography using SEM, and to ensure the surface yielded a polymer layer. The results for each step can be found in Figure 4-10.

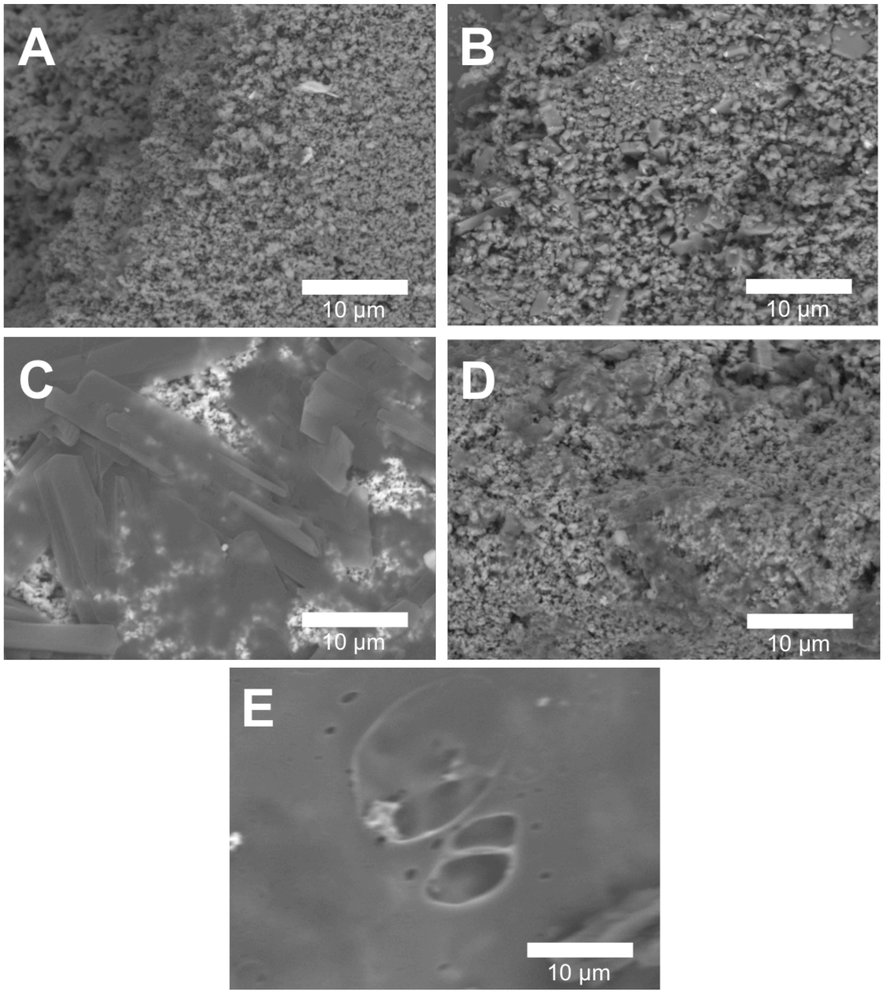

Figure 4-10: SEM topographic images for A – CTI Porous Tubes (no modification), B – CTI-g-APTES, C-CTI-g-APTES-PEO-NB, D – Grubbs Activated surface and E – Polymerized surface (with pNB).

These images quickly show the changes found after each step of the reaction. While the blank CTI porous tube surface enable us to compare and observe that changes do occur, the surface of sample Figure 4-10-C shows shards of crystal-like features on the surface.

4.7.3. Discussion

From the provided SEM images and XPS data collected, it is apparent that there are some promising results (including the formation of a polymeric film at the end of this process). However, with the higher nitrogen atomic percentages found in XPS alongside missing Grubbs ruthenium after addition of the Grubbs first generation initiator, there exists a need to investigate further.

The first problem with higher nitrogen yield found in the CTI-g-APTES-PEO-NB sample, or the sample after the amide bond formation, require a combination of SEM and XPS results to help explain this observation. From the SEM (i.e. Figure 4-10-C), the presence of crystal shards, along with the higher nitrogen yield in XPS help identify these crystal shards as urea-derivatives (which were difficult to completely remove). In a thorough review by El-Faham *et al.*, the reaction performed to form the amide bond has a side reaction of urea formation, as seen in Figure 4-11.

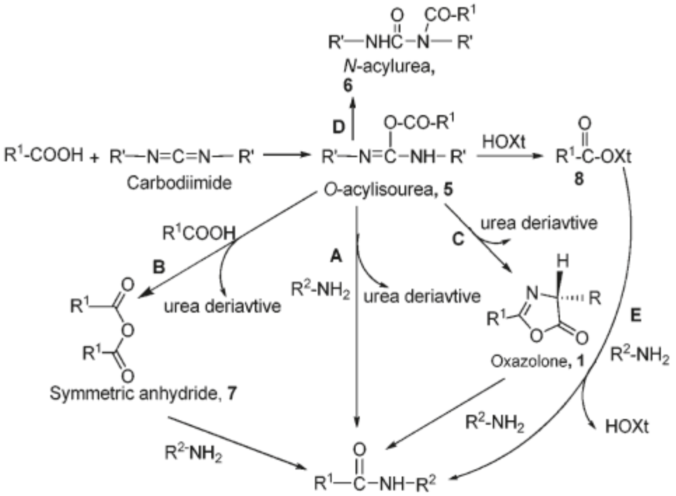

Figure 4-11: Reaction scheme for amide bond formation from a Carbodiimide-Mediated Reaction (Pathway A is the most common).[256] The appearance of a urea derivative explains the subsequent crystal shards found, and the presence of higher atomic percentages of nitrogen after the peptide bond is formed. Reprinted with permission from Reference 256. Copyright 2011 American Chemical Society.

The result of such urea-derivatives appears to just pose issues with the analysis of the surface. In this case, a stronger wash might help remove more of the urea-derivatives from the surface.

The second issue with the non-existence of ruthenium on the Grubbs activated sample poses another serious problem. However, hypothesizing that due to the pores from the CTI porous tubes, there exists the opportunity for the Grubbs first generation initiator to be mostly adsorbed into the porous structure (instead of activating the surface). In this method, the exposure to norbornene (NB) results in instant polymerization, but not directly linked to any surface. Looking into literature, this method of metathesis polymerization is not si-ROMP, but closely related to what is known as contact metathesis polymerization, or CMP, as presented by Caster and Walls.[253,257] Thus, the results obtained from the use of the CTI porous tubes were not effective si-ROMP systems, thus not used or applied to the ceramic tubes.

CTI porous tubes do not result in an effectively noticeable si-ROMP polymeric layer but instead, results in a contact metathesis polymerization (CMP) reaction to form the polymeric layer

4.8. Functionalization and Polymerization from Evonik particles

In the next work using Evonik particles, the study of binding the NB-PEO-COOH to the APTES functionalized Evonik particles and ensuing polymerization is first analyzed by XPS. Upon confirmation that similar issues shown from the CTI porous tubes did not arise, TGA was used to calculate the final grafting density of the macromonomer to determine the total number of initiator sites available. TGA is also used to determine the final degree of polymerization through the polymeric mass loss. Finally, SEM is used on the final product to confirm the integration of the particles with the film layer formed.

4.8.1. Characterization by XPS

The Evonik particles subjected to various stages of functionalization, ranging from APTES attachment, further reaction with NB-PEO-COOH, activation with the Grubbs first generation initiator, and polymerization were all characterized with XPS. These results can be found in Table 4-3.

Table 4-3: XPS results for Evonik particles from functionalization to activation and polymerization

Element	Evonik particles	Evonik particles-g-APTES	Evonik particles-g-APTES-PEO-NB	Grubbs Activated	pNB Layer
Al2p	2.27%	0.72%	0.61%	0.37%	-
Si2p	-	6.13%	4.89%	4.42%	5.35%
P2p	-	-	-	0.31%	-
Cl2p	-	-	-	0.24%	0.15%
Ru3d5	-	-	-	0.06%	-
C1s	21.39%	29.98%	40.16%	50.48%	82.34%
Ca2p	-	-	-	-	0.18%
N1s	1.04%	4.29%	6.46%	4.52%	0.19%
Ti2p	21.64%	14.51%	10.43%	8.94%	0.10%
O1s	53.40%	44.17%	37.45%	31.01%	11.54%
Na1s	-	-	-	-	0.18%

NOTE: sample acronyms: APTES = (3-Aminopropyl)triethyoxysilane, NB = Norbornene, Grubbs = Grubbs 1st generation Initiator, pNB = Polynorbornene

This first series of results with the Evonik particles clearly show that the problems that existed with the CTI porous tubes are not present here. The slightly higher nitrogen atomic percentage after the amide bond formation (for the sample "Evonik particles – APTES-PEO-NB") indicates that washing has removed most of the urea-derivative byproducts. Additionally, the presence of ruthenium after Grubbs activation with the Grubbs first generation initiator indicates the active initiator remains, even after several washes. Finally, the increase in carbon content after polymerization helps reinforce that a polymeric film had been formed.

4.8.2. Characterization by TGA

TGA has been shown previously in both Chapter 2 and Chapter 3 for use in determining the number of initiator sites alongside the degree of polymerization. Our work in this section will encompass both determining the total number of initiator sites possible, and the calculated DP obtained by each activated initiator site.

From Chapter 2, the observed grafting density of APTES was approximately 8 APTES/nm^2. While a fairly good value, this was not the final group that would yield our initiator; instead, the si-ROMP route requires a strained olefin (such as our norbornenyl group). Upon reacting the amine group from the APTES to the carboxylic acid group from NB-PEO-COOH macromonomer, the subsequent particles were assessed for their grafting yield. This resulting macromonomer degradation can be seen in Figure 4-12.

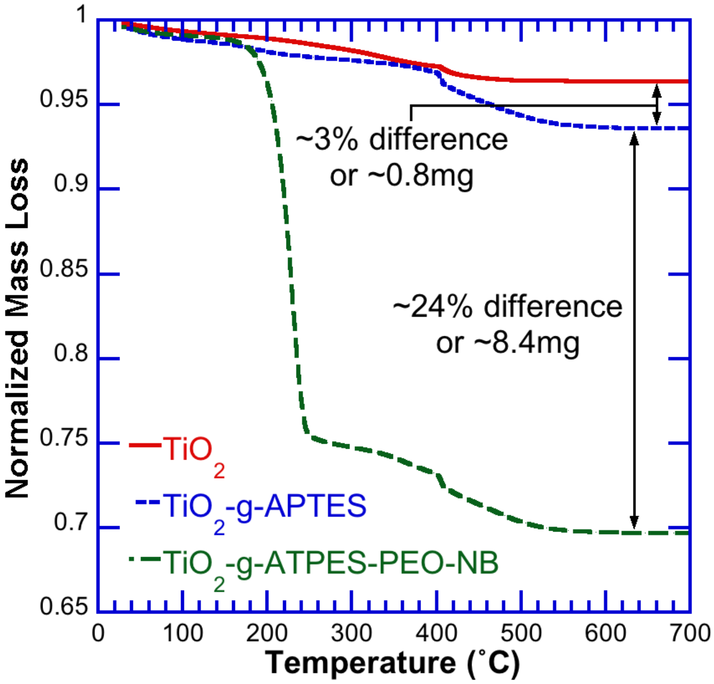

Figure 4-12: TGA graph for the degradation of Evonik particles (TiO_2), Evonik particles functionalized with APTES (TiO_2-g-APTES), and Evonik particles functionalized with both APTES and NB-PEO-COOH (TiO_2-g-APTES-PEO-NB)

Using these results along with several assumptions, specifically the same assumptions made in Chapter 2, with the addition of the mass loss including the molecular weight of the macromonomer (~3740 g/mol) and the resulting formation of the amide bond (loss of 18 g/mol):

1. The inorganic core of the hybrid particles will have a diameter of 100 nm
2. Using the previously calculated mass loss from the TiO_2-g-APTES molecule, we can determine the mass loss from the macromonomer (or

NB-PEO-COOH), thus we should calculate for a mass loss of 3723 g/mol (corrected for loss from one –OH group after binding reaction)

3. The particles are uniformly coated on the particle surface
4. The density of the Evonik particles is the same as regular titanium dioxide density (4.23g/cm^3)
5. Each Evonik particle is perfectly spherical

As a result, we can take the same values found from Table 2-14 in Chapter 2 in combination with these assumptions to update calculations on the number of norbornenyl groups attached to the surface. To accomplish this, we can perform the following calculations:

1) Determining the total number NB-PEO-COOH

$$Total\ Molecules_{NB-PEO-COOH} = \left[\frac{Mass\ Loss_{TiO_2-g-APTES-PEO-NB} - Mass\ Loss_{TiO_2-g-APTES}}{Molar\ Mass_{NB-PEO-CO*}}\right] x\ N_A$$

where:

- $Molecules_{NB-PEO-COOH}$ is in the units “molecules”
- $Mass\ Loss_{TiO_2-g-APTES-PEO-NB}$ is in the units “g”
- $Mass\ Loss_{TiO_2-g-APTES}$ is in the units “g”
- $Molar\ Mass_{NB-PEO-CO*}$ is in the units “g/mol” (or 3723 g/mol)
- N_A is Avogadro’s Number, which is 6.022x10^{23} molecules/mol

2) Determining the number of NB-PEO-COOH per Evonik Particle

$$Molecules\ Per\ Particle_{TiO_2} = \left[\frac{Total\ Molecules_{NB-PEO-COOH}}{Number\ of\ TiO_2\ Particles}\right]$$

where:

- $Total\ Molecules_{NB-PEO-COOH}$ is in units “molecules”
- $Number\ of\ TiO_2\ Particles$ is in units of “Particles”
- $Molecules\ Per\ Particle_{TiO_2}$ is in units of “molecules/particle”

3) To determine the NB-PEO-COOH grafting density

$$Grafting\ Density_{NB-PEO-COOH} = \frac{Total\ Molecules_{NB-PEO-COOH}}{(Surface\ Area_{\ each\ TiO_2}\ x\ Number\ of\ TiO_2\ Particles) x\ 10^{14}}$$

where:

- $Surface\ Area_{\ each\ TiO_2}$ is in units “cm^2” (is 3.14x10^{-10} cm^2)
- $Grafting\ Density_{NB-PEO-COOH}$ is in units of “molecules/nm^2”
- 10^{14} is used to convert cm^2 into nm^2

Using this method, the resulting calculated values are found in Table 4-4.

Table 4-4: Calculated values extracted from TGA to calculate the grafting density of the number of norbornenyl grafted initiator sites possible. Bolded regions represent the newly calculated values.

Step	Values	Units
Total Volume of TiO_2	$8.63\text{x}10^{-3}$	cm^3
Volume of each TiO_2	$5.24\text{x}10^{-16}$	cm^3/particle
Surface Area of each TiO_2	$3.14\text{x}10^{-10}$	cm^2
Number of TiO_2 Particles	$1.65\text{x}10^{13}$	particle
Total Molecules of NB-PEO*	**$1.41\text{x}10^{18}$**	**molecules**
Molecules of NB-PEO*/Particle	**$8.58\text{x}10^{4}$**	**molecules/particle**
Grafting Density of NB-PEO*	**2.73**	**molecules/nm^2**

*NB-PEO represents the number of α-norbornenyl-ω-carboxylic acid poly(ethylene oxide) attached to the surface, or NB-PEO-COOH that was attached to the surface.

Thus an estimated grafting density of the NB-PEO-COOH on the surface is about 2.73 molecules/nm^2. Taking this value, we can further calculate the DP of polynorbornene after activation of the grafted norbornenyl group. Using the same technique of TGA to determine the mass loss from the purely polymeric portion, we obtain Figure 4-13.

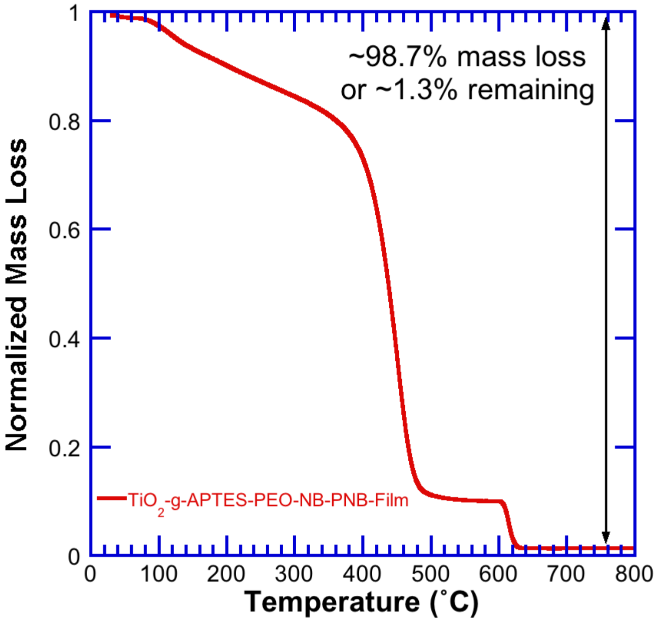

Figure 4-13: TGA graph for the subsequent degradation of the Evonik particles post polymerized with Norbornene (NB). The subsequent film formed was subjected to a different thermo-degradation program, with oxygen introduction at 600˚C instead of 400˚C for all other TGA graphs.

Again, to take the mass loss data and transform it into useful information, more assumptions had to be made. These assumptions included:

1). The remaining mass after the TGA cycle is solely due to the Evonik particles themselves

2). Due to the lower mass of the particles, we can assume that the grafted moiety (i.e. APTES bonded NB-PEO-COOH) contribution to the mass loss to be negligible, thus all the mass loss is due to the polymer layer only.

3). Each Evonik particle has a total volume of 5.24x10^{-16} cm^3/particle, surface area of 3.14x10^{-10} cm^2/particle, and a density of 4.23 g/cm^3

4). The density of Norbornenyl moieties on the surface is 2.73 initiators/nm^2, thus assuming all available norbornenyl sites become initiators (i.e. Grubbs first generation initiator activates all norbornenyl sites)

Thus, the following calculations can be performed:

1). Total Surface Area Calculation:

$$Total\ Surface\ Area = \left(\frac{3.14x10^{-10} \left(\frac{Mass\ Remaining_{TiO_2}}{\rho_{TiO_2}} \right)}{5.24x10^{-16}} \right) x10^{14}$$

- Where the total surface area is in units of nm^2

2). Total Moles of Initiators Calculation:

$$Total\ Moles\ of\ Initiators = \frac{Total\ Surface\ Area\ x\ 2.73}{6.022x10^{23}}$$

3). Moles of Monomers:

$$Moles\ of\ Monomers = \frac{Mass\ loss\ of\ Polymer}{94.15}$$

4). Degree of Polymerization:

$$Degree\ of\ Polymerization = \frac{Moles\ of\ Monomer}{Total\ Moles\ of\ Initiators}$$

This calculation would lead us to obtain the resulting values in Table 4-5.

Table 4-5: Calculated degree of polymerization for the resulting film of polynorbornene initiated by si-ROMP from Evonik particles.

Step	Values	Units
Original Mass of TiO_2-g-APTES-PEO-NB Film	3.58	mg
Mass Loss of Polynorbornene (PNB)	0.00353346	g
Mass Remaining of TiO_2	0.00004654	g
Total Surface Area	6.60x10^{14}	nm^2
Total Moles of Initiators	2.99x10^{-9}	mole
Moles of Monomer (NB)	3.75301x10^{-5}	mole
Degree of Polymerization	12534.77	

Thus, we have determined that the sample had a DP of roughly 12500 for polynorbornene from these functionalized Evonik particles.

TGA determined that the norbornenyl-moiety (NB-PEO-COOH) that was grafted onto the Evonik particles has a grafting density of 2.73 molecules/nm^2, and the DP was roughly 12500 with polynorbornene.

4.8.3. Characterization by SEM

The final point of this reaction was to visualize the surface of the formed polynorbornene film (as the final product was a film as opposed to a dispersion of latex particles) that was initiated by the functionalized Evonik particles. The resulting SEM images can be seen in Figure 4-14.

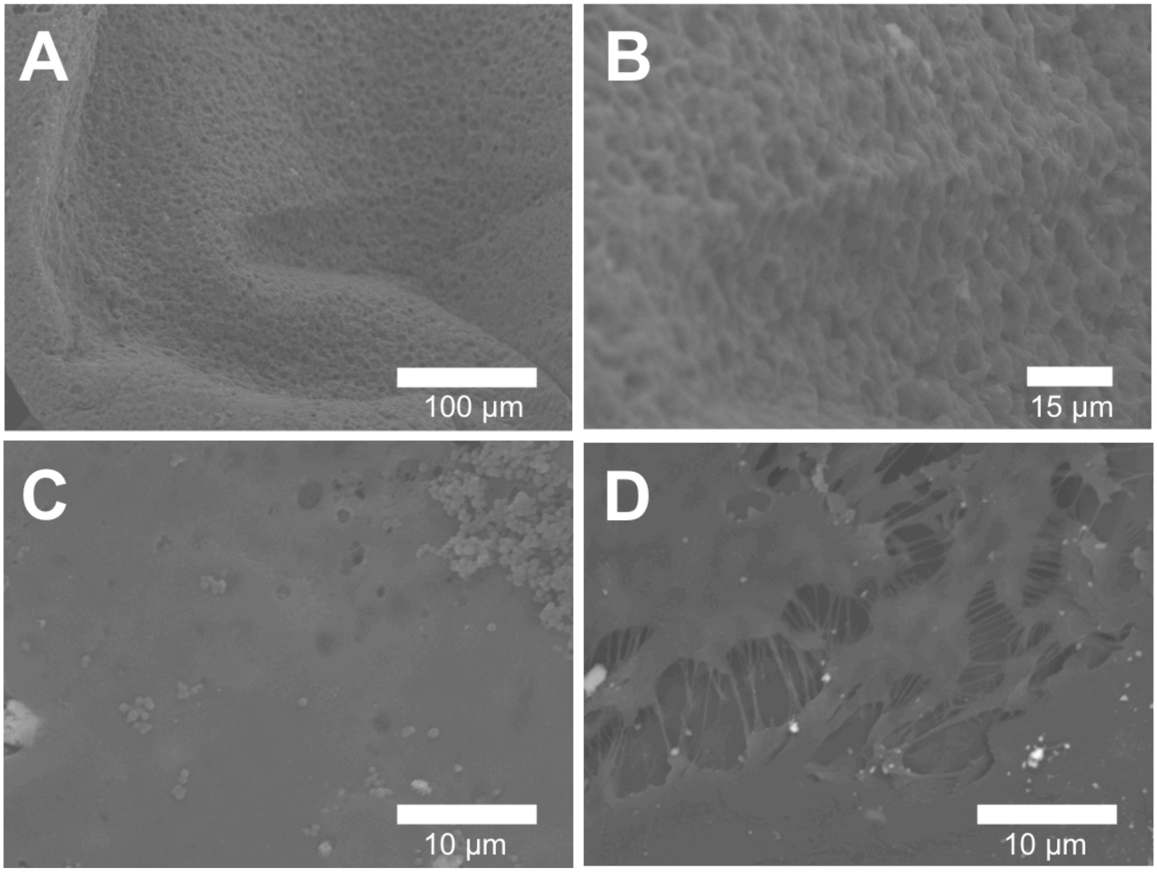

Figure 4-14: SEM images for the PNB (Polynorbornene) film. A) 500x magnification, B) 2000x magnification, C) 5000x magnification, D) 5000x magnification (other location). Notice the highly porous nature of the polymer film formed.

These images show a highly porous film surface, with some indication of inorganic particles on the surface. From literature, such as the work presented by the collaborative work by Grubbs and Bao, they had tried to used polynorbornene films as a dielectric layer as they have a high resistance, but can not be annealed to remove any porous channels.[146] While the porous nature of this film is not of importance during this study, it might be one option if polynorbornene films might be used for gas separation membranes during the testing phase.

4.9. Conclusion

In this chapter, the fundamentals and background on si-ROMP were introduced. This knowledge was then transferred into developing a mechanism towards titania-based surfaces (i.e. CTI porous tubes and Evonik particles). By adapting si-ROMP techniques and studying them on these titania supports, evaluation of the effectiveness applying si-ROMP to porous and particle systems were explored. Analysis techniques such as XPS, SEM and TGA (in the case of Evonik particles) could determine various properties of the structure, including verification if the reaction was truly si-ROMP.

Summarizing the main points of this chapter, it had been observed that the CTI porous tubes could initiate the polymerization of norbornene into polynorbornene, but not through the si-ROMP method. Instead, contact metathesis polymerization (CMP) was hypothesized to be the reason the reaction occurred (due to un-removed physisorbed initiator within the porous confines of the substrate). Moving onto Evonik particles, the grafting of the norbornenyl-moiety (or NB-PEO-COOH) resulted in a density of 2.73 molecules/nm^2 (which is not too far off from the C3-initiator grafting density). The subsequent DP was estimated through more assumptions/calculations with TGA results to yield approximately 12,000.

Chapter 5

Coating Ceramic Tubes

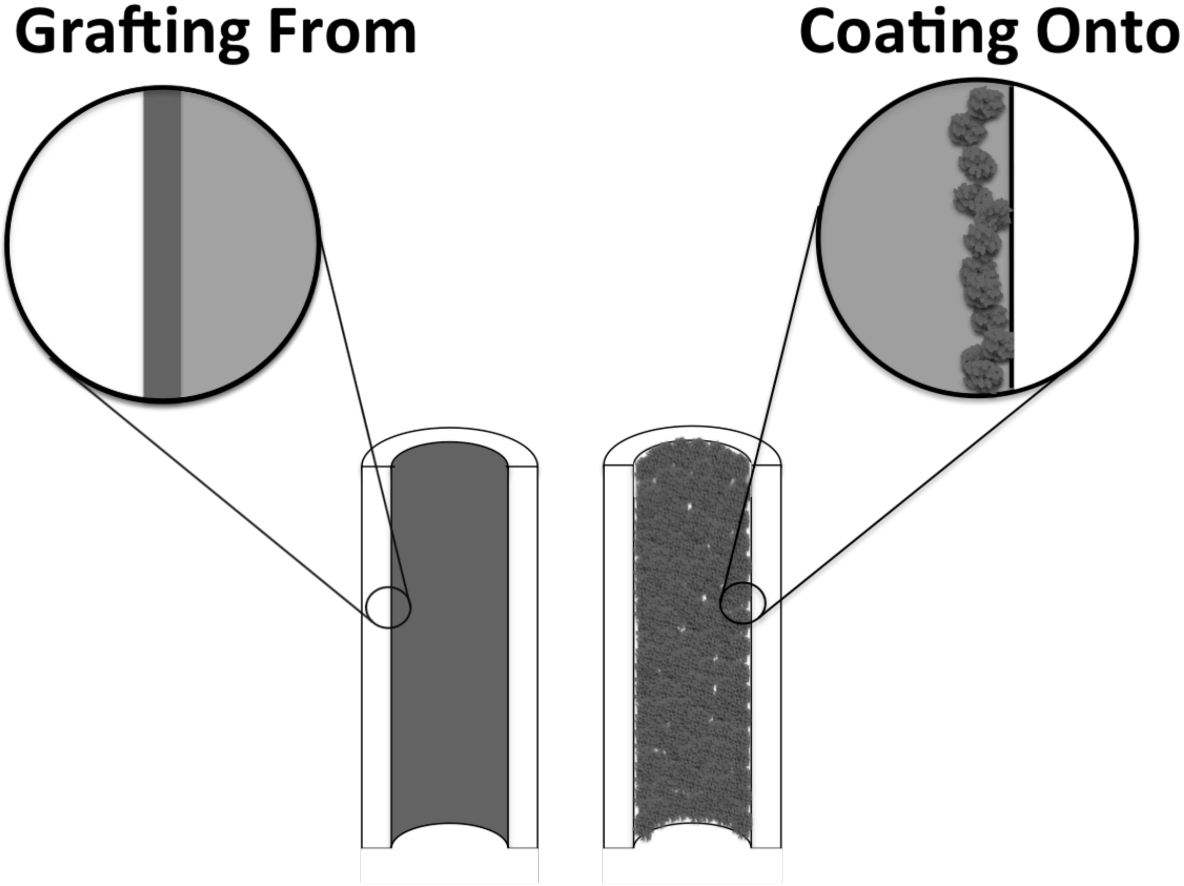

Pathways taken on the formation of hybrid membranes: the "Grafting From" directly the surface, and the "Coating Onto" the porous surface

5.1. Introduction

While all previous chapters were focused on the studies on building block/components in making a membrane, this chapter will serve to combine this work and discuss the experiments developed in forming our hybrid membranes. Being a difficult task, there were several methods of coating that were explored and assessed for film formation efficiency. This was then expanded to see if certain parameters would improve the film formation, such as subjecting the system to vacuum or through the motion of coating. Surface film characterization *via* SEM was then performed, to visualize the effectiveness of the coating, and a water droplet test could be used to quickly evaluate certain hydrophobic surface modifications. Conclusions were then made on the ideal film formation to be submitted for gas separation tests (and presented later in the final chapter, Chapter 6).

5.2. Pathways Assessed

The aspirations to create a membrane capable of CO_2 gas separation have been described in Chapter 1. In that chapter, we ended the section by introducing the ideal goal of growing a polymeric coating from an inorganic surface. From this point, there were two options for making a polymer layer on a ceramic surface, as illustrated in Figure 5-1.

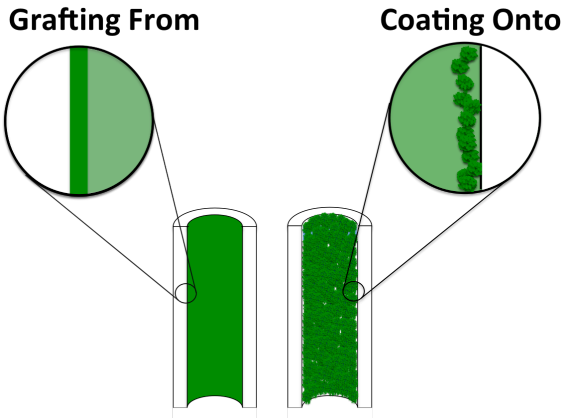

Figure 5-1: Pathway to be assessed. Left: "Grafting From" technique, where the polymer is grown from the surface direction. Right: "Coating Onto" method, which uses hybrid particles to be coated directly onto the surface.

The two pathways each have their own unique method of implementation. In the case of the “Coating Onto” method, the hybrid particles are first prepared and then directly coated onto the surface to plug/cover all porous regions. From this method, the ideal scenario presents a solution of hybrid particles in water, which is slip coated directly onto the surface of the interior CTI porous tubes. This action would leave a “cake” formation of hybrid particle films on the surface, while the solvent (i.e. water) would permeate through.

In the case of the “Grafting From” method, the ideal case is for the initiator site to be situated directly on the surface of the porous membrane tube, from which the polymer film can grow. However, Chapter 2 showed that direct attachment of grafting groups on porous materials was highly challenging. Taking this into account, a different method had to be developed. Considering that the pore size of the CTI tubes is roughly 200 nm (or larger than the Evonik particles), the decision was made to attempt to coat these pores with post functionalized Evonik particles with C3-Initiators (the TiO_2-g-C3-Initiator particles) or Norbornenyl based particles (TiO_2-g-APTES-PEO-NB). This modification would enable the polymeric layer to be grown from the surface, thus satisfying the “Grafting From” method from the surface of the tube interior.

5.2.1. “Coating Onto” - Hybrid Particle Coating

In the original plan regarding the “Coating Onto” portion of the project, the ideal case was presented as direct coating onto the surface. Upon solvent permeation through the porous inorganic membrane, the dried film would form the main membrane film. In achieving this setup, a protocol had to be implemented that could ensure the same setup would be achieved each test. The design made can be seen in Figure 5-2, which illustrates a simplified version of work found in Chapter 2 and Chapter 3 regarding the si-ATRP route combined with this chapter’s coating method.

From this work, an aqueous dispersion of hybrid particles was prepared. We used a 0.13 g/mL suspension of hybrid particles, made with 0.27 M PEGMEMA solution

(DP ~1200)), as described in Chapter 3. This main stock solution (hereby known as **S.S.**) is the coating solution used throughout this study.

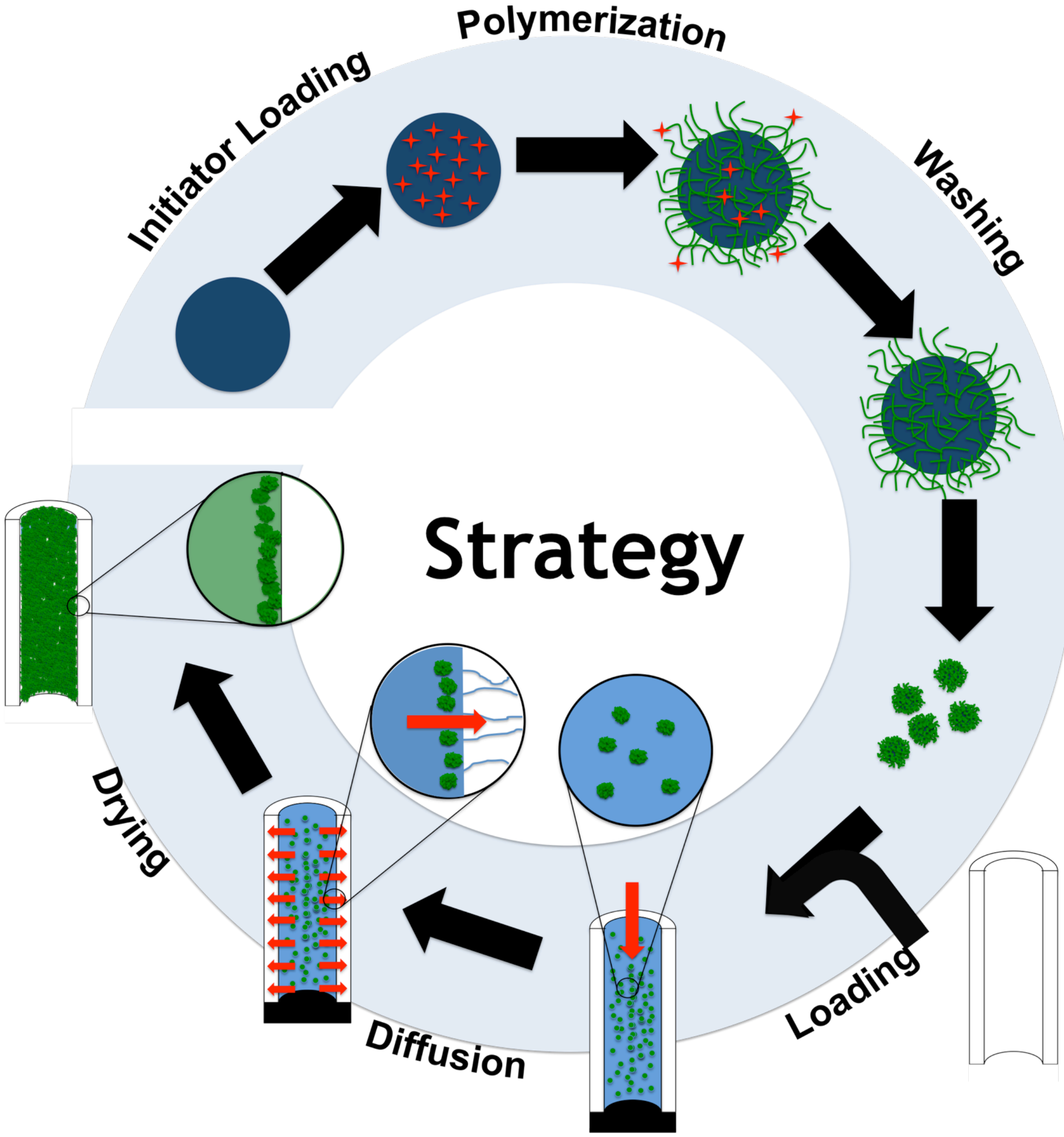

Figure 5-2: Strategy used for "Coating onto" pathway. Hybrid particles are coated directly onto the surface and left to dry to form polymeric coating.

Preparation of the ceramic tube consisted of cutting a 5 cm (OD: 10.4 mm, ID: 6 mm) length porous tube (CTI), rinsing with ethanol to clean, and then drying overnight in an 80˚C oven. One end was then sealed with parafilm, and 2-3 mL of **S.S.** was added into the tube. The solution was left to permeate (i.e. removal of all water) and was repeated as many times as required. This procedure can be seen in Figure 5-3.

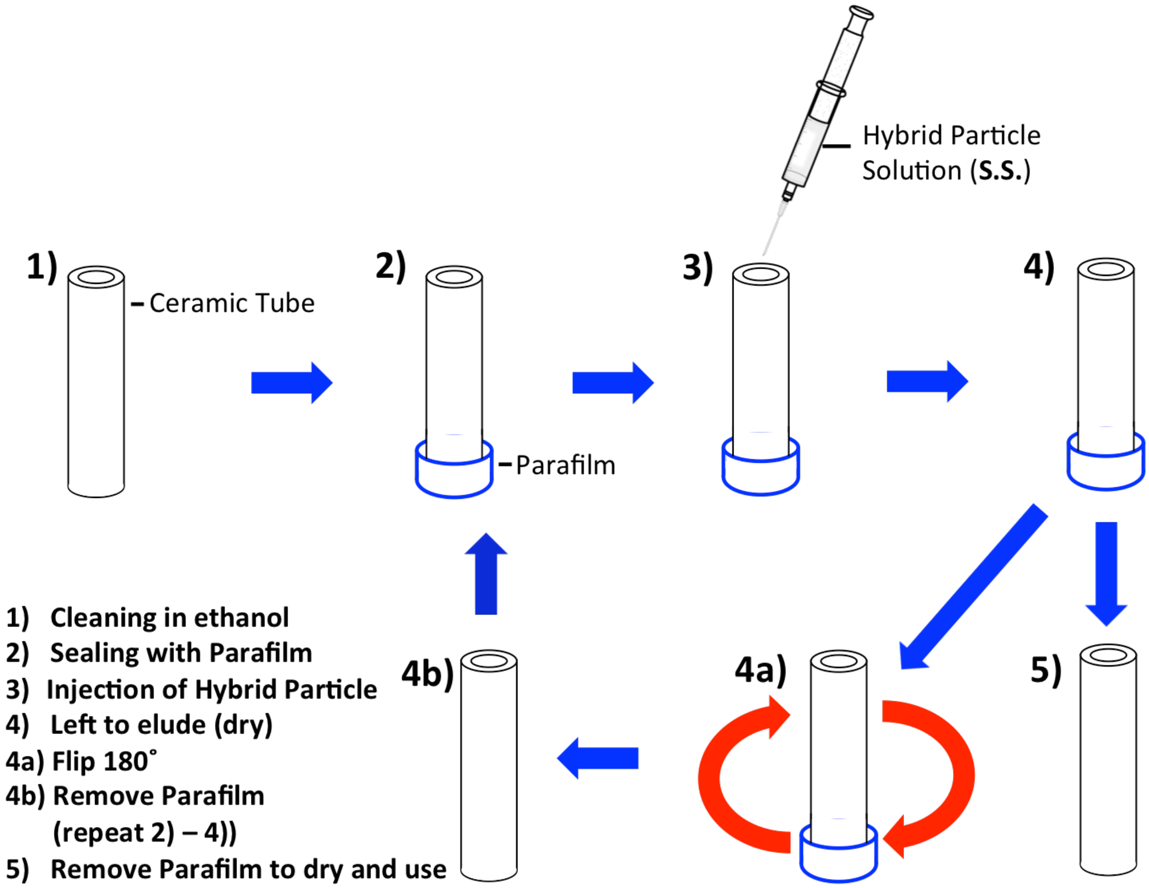

Figure 5-3: "Coating Onto" process with use of parafilm and ambient exterior conditions. Note that steps 4a) and 4b) are optional (if a second coating is required). Additional motions required can be applied if both ends are sealed with parafilm.

The initial use of parafilm was an easy method to validate the process, especially when it is used during the preparation of ceramic membrane samples for laboratory purposes. However, there can be unintended effects regarding its stability toward parameters like temperature or pressure changes, which we also aimed to explore. As vacuuming would also be another route to investigate, we developed another design, described in Figure 5-4. This divergence from parafilm to use of a Teflon/septum combination provided the seal required to successfully plug both ends of the tube to coat. This new system provided a better coating result compared to the parafilm, as will be discussed in the results later (i.e. section 5.3.1 “Coating Onto” - Hybrid Particle Coating).

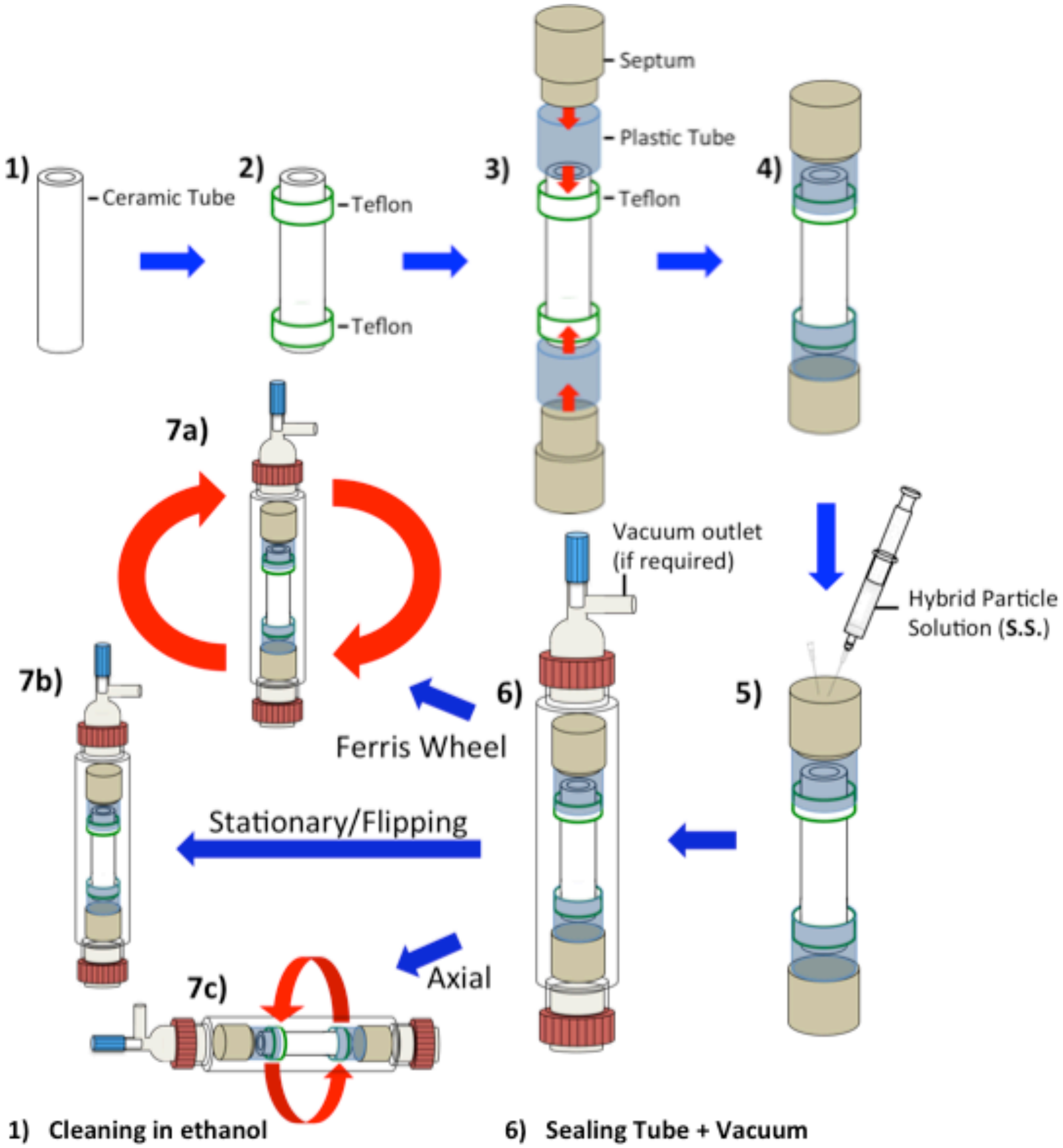

1) **Cleaning in ethanol**
2) **Sealing**
3) **End Capping**
4) **Prepare Tube**
5) **Injection of Coating Slurry**
6) **Sealing Tube + Vacuum**
7) **Coating Movement**
    - **7a) Ferris Wheel Motion**
    - **7b) Stationary**
    - **7c) Axial Spinning**

Figure 5-4: Schematic design of the "Coating Onto" process used (redesigned). Notice that the vacuum step is optional, and that the motions of “Ferris Wheel”, “Flipping” and “Axial” can be applied with the class tube as the container.

5.2.2. “Grafting From” – using Functionalized Particle – si-ATRP and si-ROMP – general procedure

With the “Grafting From” pathway, we used the initiator functionalized Evonik particles, specifically with the si-ATRP initiators (to be known as TiO_2-g-C3-Initiator) and si-ROMP initiators (to be known as TiO_2-g-APTES-PEO-NB*(or post-Grubbs activated particles, as was explained in Chapter 4)). The coating plan is described in Figure 5-5 while the used step-by-step pathway is illustrated in Figure 5-6.

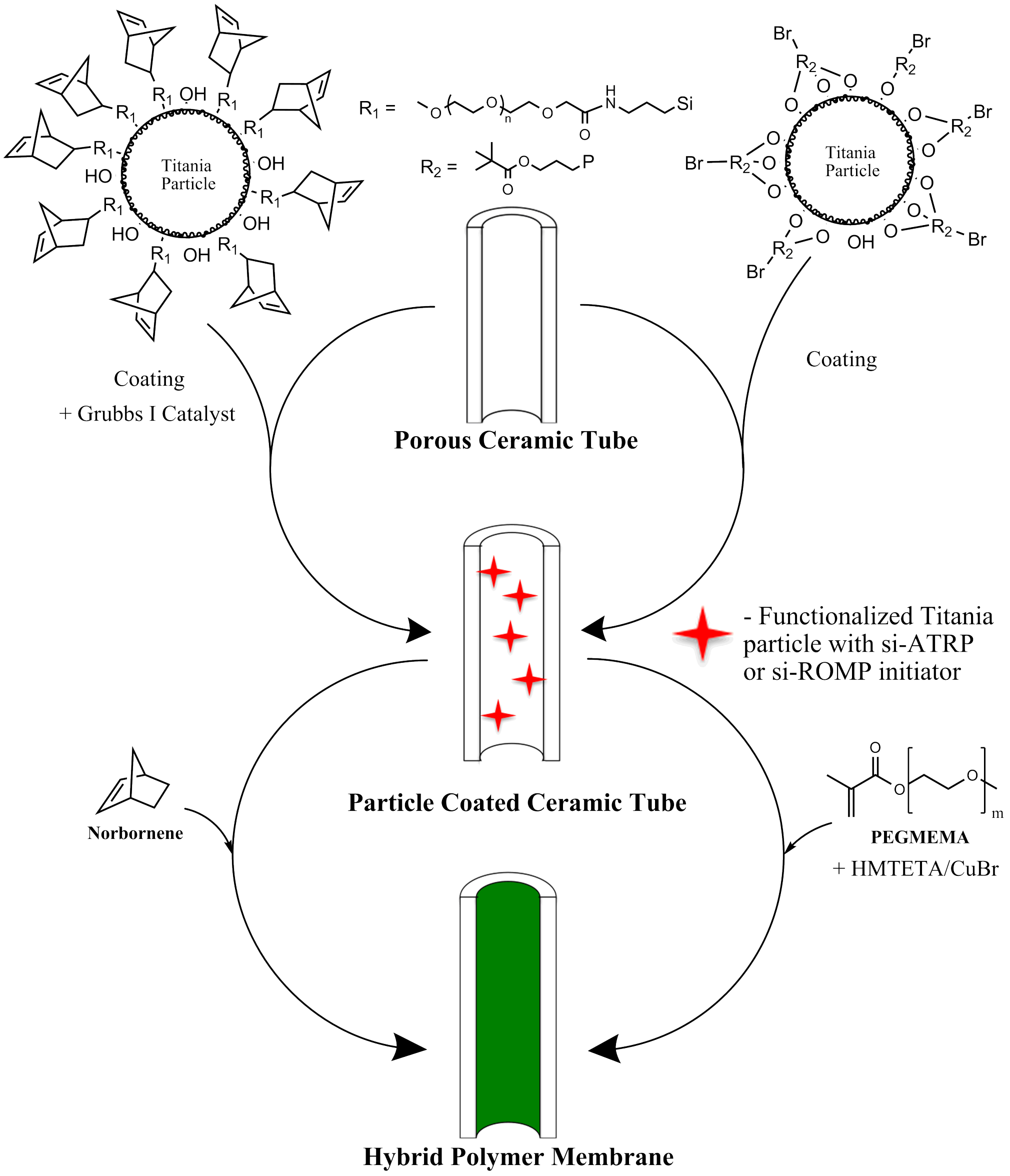

Figure 5-5: Pathway set out for "Grafting From" procedure. Left: si-ROMP pathway from coating onto CTI ceramic tube to polymerization using the TiO_2-g-APTES-PEO-NB. Right: si-ATRP route for coating onto CTI ceramic tube, to polymerization using the TiO_2-g-C3-Initiator.

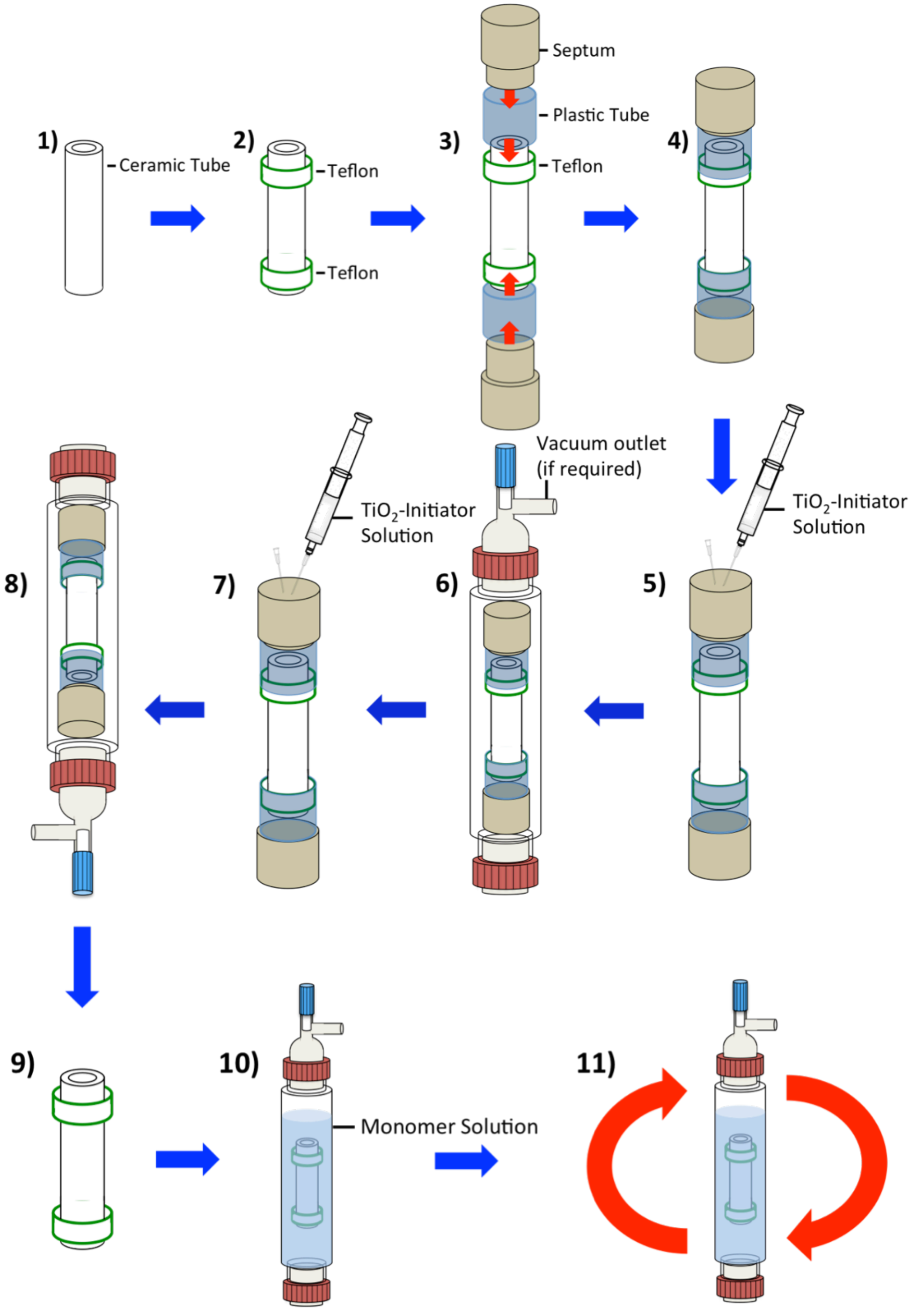

1) Cleaning in ethanol
2) Sealing with Teflon
3) End Capping
4) Prepare Tube
5) Injection of TiO_2-Initiator particles
6) Sealing/Vacuuming
7) Second Injection of TiO_2-Initiator
8) Flip coating + Vacuum
9) Short Rinse + Removal of End Caps
10) Added to Polymerization Solution
11) Ferris wheel motion during reaction (optional)

Figure 5-6: Schematic pathway for surface modification through the "Grafting From" process. Note that steps 6 – 8 can also be performed in the "Ferris Wheel" motion as well.

This method coated the CTI porous tube with the functionalized Evonik particles before polymerization with the (macro)monomer solution. Varying motions were also applied, either with the Vertical/Flipping or with the Ferris Wheel motion, in order to test their film formation abilities.

5.2.2.1. si-ATRP Preparation

The coating solution in the "Grafting From" procedure was prepared from TiO_2-g-C3-Initiator dispersed into water at a concentration of 0.015g/mL (or roughly $8.4\text{x}10^{-7}$ initiators/mL). We prepared 20 mL batches at a time, and used them as quickly as possible. As each ceramic tube is roughly 5 cm in length, both ends of the tube was sealed as illustrated in Figure 5-6, and roughly 3-4 mL of this mixture was injected. Vacuum was also used to help facilitate the permeation of water across the tube, and thus aid in creating a thin coating onto its surface. A second coating was performed accordingly. Finally, the CTI porous tube was gently rinsed with water upon removal of the end caps, and directly added into a reaction tube filled with prepared macromonomer + catalyst solution.

The polymerization mixture was prepared by taking a 9:1 volume ratio between the degassed macromonomer solution to the oxygen free catalyst (normally with a final volume of 20 mL, with a macromonomer concentration of 0.27 M – or as described in Chapter 3). This was achieved using a glass neck that was able to mix both volumes together without exposure to oxygen. The mixture was stirred for several minutes before use. The CTI porous supports coated with the TiO_2-g-C3-Initiator particles were directly added into the polymerization mixture and left to react for 24 hours.

5.2.2.2. si-ROMP Preparation

The preparation of particles was specifically adapted in the case of si-ROMP. Upon completion of both functionalization steps to yield a norbornenyl group on the Evonik particles (and mentioned in Chapter 2 and Chapter 4), a particle concentration of

0.02 g/mL was prepared (or roughly 1.4×10^{-6} norbornenyl groups/mL). The preparation involved the dispersion of the particles, or TiO_2-g-APTES-PEO-NB(unactivated), into ethanol (in this case, 0.2 g of the TiO_2-g-APTES-PEO-NB into 8 mL of ethanol). We prepared a separate vial in the glovebox of 0.02g of the Grubbs first generation initiator dispersed in 1 mL of dichloromethane and 1 mL ethanol mixture and left to stir. With a syringe, the 8 mL mixture of TiO_2-g-APTES-PEO-NB in ethanol was added (dropwise) into the 2 mL mixture of the Grubbs initiator. The sample was left to mix for 3 hours inside the glovebox. After this activation step, the 10 mL mixture was syringed into two falcon tubes with a 100,000 Da filter and centrifuged (at 2000 rpm for 10 minutes) to remove the solvent. The particles were then re-dispersed in ethanol and re-centrifuged at the same settings in order to wash the particles (where this washing step was repeated twice).

After the final wash, the activated particles of TiO_2-g-APTES-PEO-NB* were then re-dispersed for a final time into 10 mL of ethanol, and used/injected for coating immediately (note step 5 and step 7 in Figure 5-6). This injection, like the si-ATRP pathway, was then vacuumed in a sealed tube to ensure all the ethanol was removed, and re-injection for a second coating. The CTI tube was then rinsed and subjected to a norbornene monomer solution of 0.3M in dichloromethane, or a mixture of norbornene/NB-PEO-OH.

In order to prepare the monomer/macromonomer solution of NB/NB-PEO-OH, a mixture of purely NB-PEO-OH (2.1 g) dissolved in DCM (2 mL) was made. The sample was degassed using the 3-cycle freeze-pump-thaw method, and kept under vacuum. Upon use, the 0.3 M NB solution in DCM (8 mL) (previously mentioned in Chapter 4) was syringed into the same flask as the NB-PEO-OH solution to create the 80/20 ratio of NB/NB-PEO-OH mixture.

The now coated and activated CTI sample tubes were directly subjected to the monomer mixture of choice (i.e. 0.3M of NB or 0.3M mixture of NB/NB-PEO-OH). The shorter 5 cm tubes used about 5-6 mL of the monomer solution and left to react for 15 hours (or overnight).

5.2.3. Coating Motions Possible

As presented in the previous section, various motions ranging from Vertical/Flipping, Ferris Wheel and Axial Spinning were mentioned. This section serves to explain how each of these motions is achieved.

5.2.3.1. Vertical/Flipping

The setup for the Vertical/Flipping system only requires the ceramic tube to be suspended vertically and flipped occasionally by hand. Thus, any stationary stand (such as a clamp attached to a metal stand) can be used to hold and sustain the tube during coating. This simplistic setup is illustrated in Figure 5-7 with a glass tube system, but of course not limited to use of glassware (i.e. naked CTI ceramic tube with parafilm is also used with the Vertical/Flipping method).

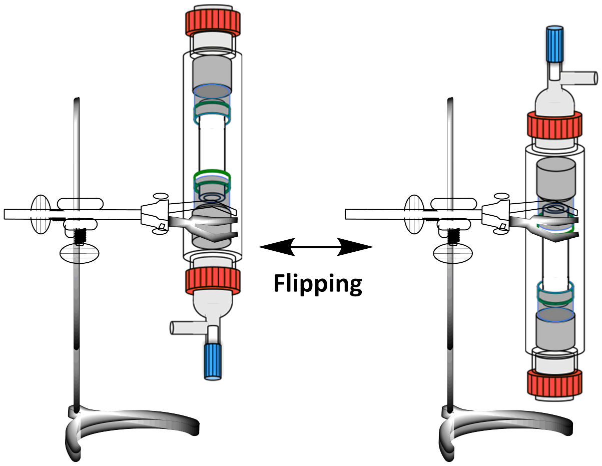

Figure 5-7: Vertical/Flipping system using a metal stand and clamp setup. The glass tube with the CTI ceramic tube are suspended in order to complete the coating process (with the help of gravity). Note that this setup does not necessarily require the glass tube, and that the procedure with a parafilm sealed CTI ceramic tube can also use this setup.

5.2.3.2. Ferris Wheel

In this specific case, the "ferris wheel" motion was exactly as it sounds – in a typical ferris wheel found in any theme park or carnival. Thus, any equipment that could rotate in such a manner was adapted towards suiting this coating need. The carousel tube rotator, as shown in Figure 5-8, fulfilled this requirement and was successively used for this motion.

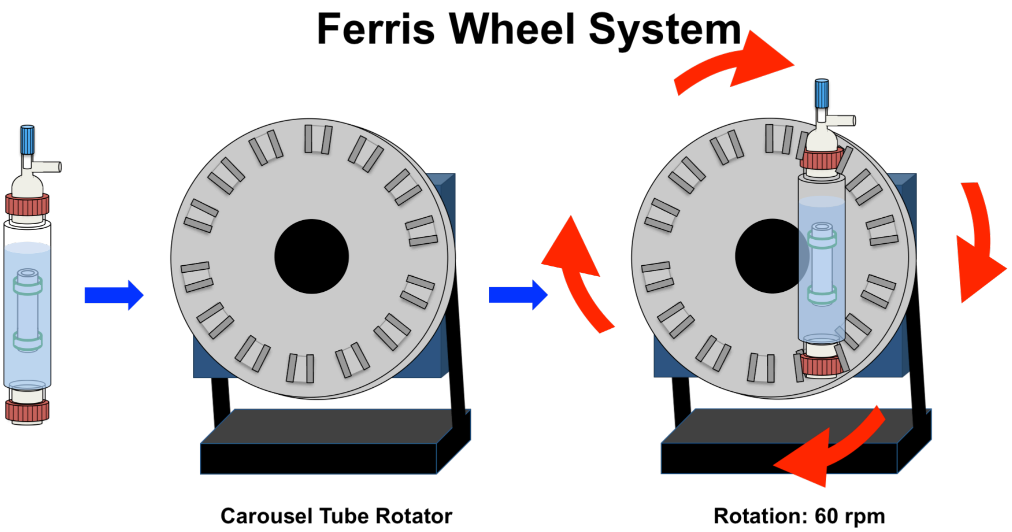

Figure 5-8: Ferris wheel setup using a carousel tube rotator (standard laboratory equipment).

5.2.3.3. Axial Spinning

The final motion discussed is an axial motion (or Axial Spinning). As the target coating material is normally the CTI ceramic tube, these cylindrical tubes can be spun axially to create a centripetal force outwards. With this outward force, the ideal result is a buildup of the hybrid material (either the TiO_2-g-C3-Initiator, TiO_2-g-APTES-PEO-NB* or the hybrid particles (**S.S.**)) on the surface of the interior tube, and permeating the solvent through the ceramic pores. This setup used a shear-mixer in order to achieve this motion. An adaptor made with a syringe tube poked through a septum created the connector necessary to link the shear-mixer system to the end of a glass tube. This system was then supported on clamps to ensure the axial motion did not tilt the glass tube. The setup (minus the clamp supports) is shown in Figure 5-9.

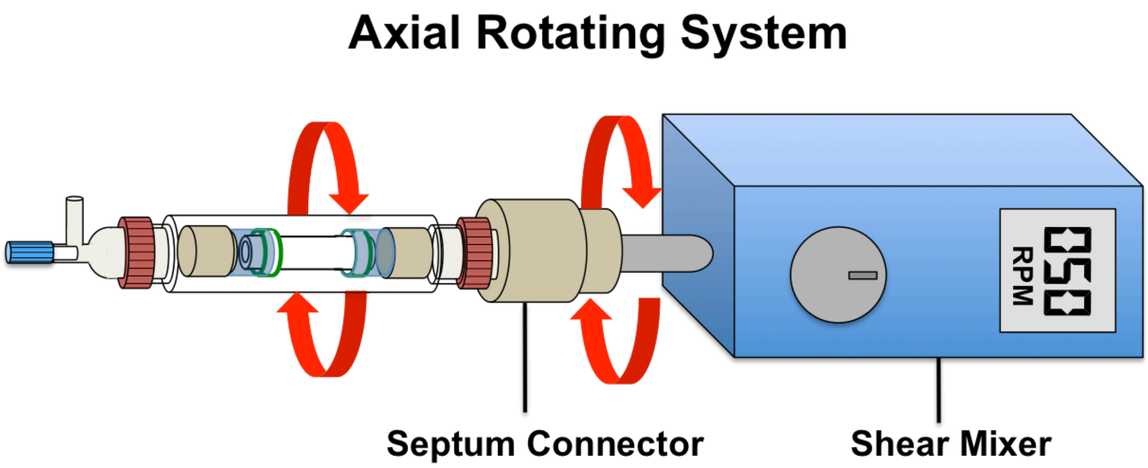

Figure 5-9: Axial rotation system created using a shear-mixer adapted with a connector fashioned from a septum and syringe tube. The speed can be easily control from the shear-mixer to induce the axial motion on the CTI ceramic tube.

5.2.4. Vacuuming

Vacuum can also be applied to the system as an option to help speed up solvent permeation. Vacuum primarily comes in the form of static or dynamic vacuuming. In static vacuum, one vacuums the glass tube once, and leaves the CTI ceramic tube under vacuum. In the dynamic vacuum case, the vacuum line is never cut, and thus left to continuously vacuum and force all liquid to be removed (under applied force).

5.3. Characterization by SEM of the different Pathways

When assessing the options available to evaluate the grown films on these CTI porous supports, there is immediate evidence that the structure is difficult to characterize. Specifically, the ceramic tubes that are used as our support material for the growing polymer or coated hybrid particles are situated on an extremely hard and curved material. The curvature of the interior (when attempting to analyze) rules out direct contact (or near contact) methods that need flat surfaces – leaving AFM, ellipsometry and profilometry techniques infeasible. Therefore, a distance non-contact based imaging technique like SEM was better at providing an image of a curved surface (albeit, difficult to image the entire tube without damaging/alterations from gold sputtering). Thus, this section will focus on the different coating techniques along with the experimental conditions altered and imaged. Note that the full series of SEM images can be found in Appendix B.

5.3.1. "Coating Onto" - Hybrid Particle Coating

As previously presented, the "Coating Onto" process presented two possible pathways: one with ambient conditions using parafilm, the other used Teflon and Septums to seal the ends of the CTI ceramic tubes. By varying the conditions (such as application of vacuum or a rotational motion during coating), the sample topography changed, as illustrated from the combination of Table 5-1 and Figure 5-10. Both of these methods used the same **S.S** solution, specifically the hybrid particles with a hydrodynamic diameter of ~350 nm (Chapter 3).

From these images, samples that used parafilm under ambient conditions (no vacuum) resulted in poor coverage. Additionally, the axial rotation left the particles to form what appear to be fibers. While interesting, this did not yield the desired film formation, leaving us to abandon this coating motion.

Table 5-1: "Coating Onto" experiments performed with varying properties (from coating method, to sealing end and substrate).

Sample ID	Type of CTI Tube	Coating		
		Vacuum	Setup	Method
TC-1	TiO_2	None	Parafilm Ends	Vertical – 2-pass (flip)
TC-2	TiO_2	None	Parafilm Ends	Vertical - 1 pass
TC-3	TiO_2	None	Parafilm Ends	Axial - 50 rpm
TC-4	TiO_2	None	Parafilm ends	Axial - 100 rpm
TC-5	TiO_2	None	Parafilm ends	Axial – 100+ rpm
TC-6	TiO_2	Static	Glassware + septum	Vertical – 1-pass
TC-7	TiO_2	**Dynamic**	Glassware + septum	Vertical – 2-pass (flip)
TC-8	TiO_2	Static	Glassware + septum	Vertical – 2-pass (flip)
TC-9	**ZrO_2 (10-15 nm pores)**	Static	Glassware + septum	Ferris Wheel (60 rpm)
TC-10	**ZrO_2 (10-15 nm pores)**	Static	Glassware + septum	Vertical – 2-pass (flip)

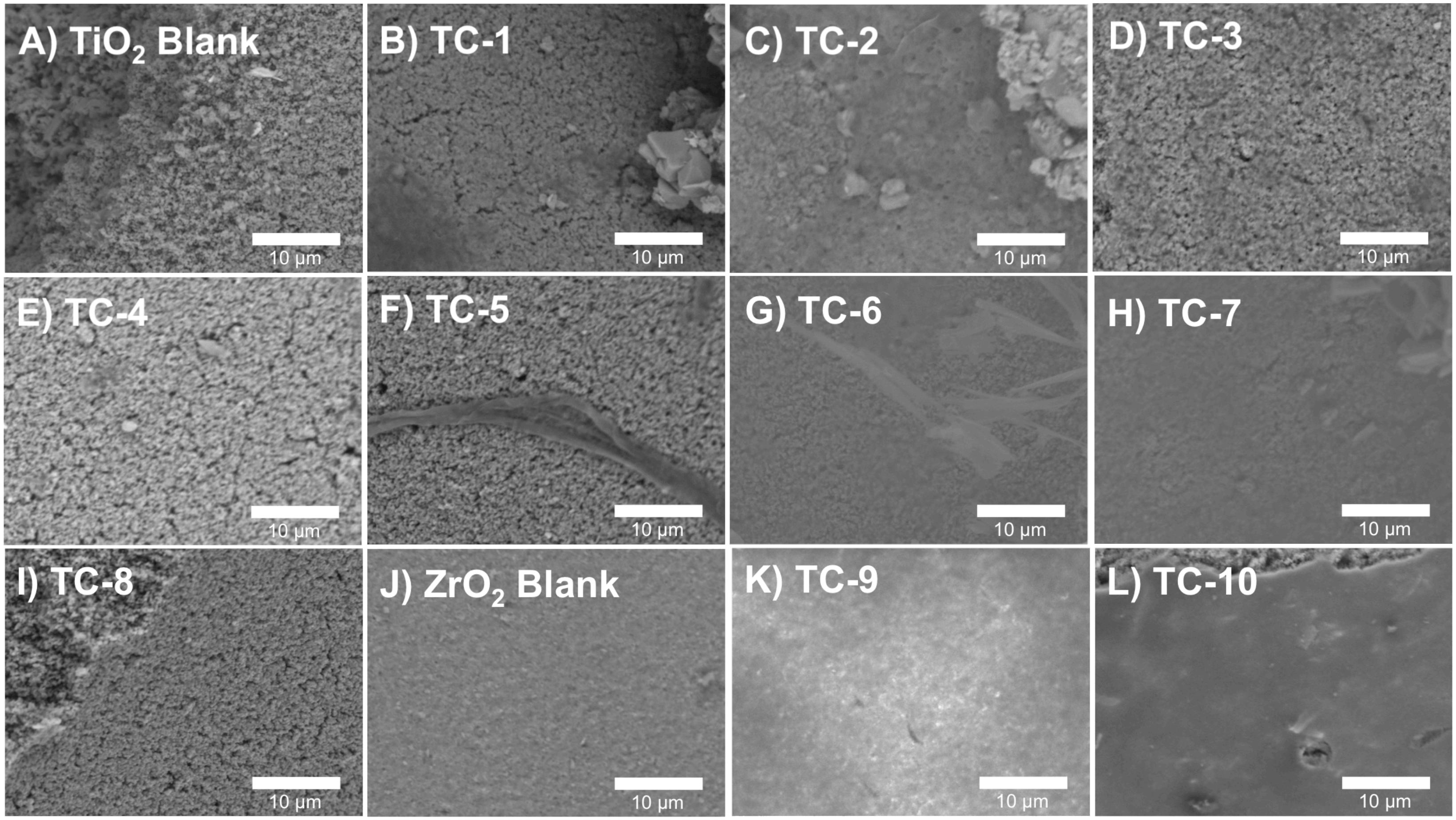

Figure 5-10: SEM images collected at 5000x magnification in the "Coating Onto" process with the hybrid particle solution (or S.S.). The images can be crossed referenced with Table 5-1. In this particular case, we have the TiO_2 sample with: A) nothing (unmodified), B) S.S. mixture with vertical/flipping with 2 pass, C) S.S. mixture with vertical/flipping with 1 pass, D) S.S. mixture with axial spinning (50 rpm), E) S.S. mixture with axial spinning (100 rpm), F) S.S. mixture with axial spinning (100+ rpm), G) S.S. mixture with static vacuum and vertical 1 pass, H) S.S. mixture with dynamic vacuum and vertical 2 pass, I) S.S. mixture with static vacuum and vertical 2 pass, J) Zirconium blank sample, K) Zirconium sample with static vacuum and ferris wheel, L) Zirconium sample with static vacuum and vertical 2 pass.

Surprisingly, these first results showed unexpected result with the TiO_2 based substrate with respect to the number of passes (i.e. TC-1 and TC-2 alongside TC-6 with TC-8). It does appear that the 1-pass samples are much better coated than the 2-pass samples. We hypothesize that the second pass could cause the hybrid particles to detach from their original surface during the flipping process (as the sample tubes remain in a wet state).

From these SEM observations, we conclude that the largest effect stems from the porosity of the samples. Compared to the titanium oxide based CTI ceramic tubes (200 nm average pore size), the zirconium oxide CTI ceramic tubes yielded a much smaller pore system, roughly 10-15 nm in diameter. These ZrO_2 tubes show a better layer because of the smaller pore system (ex: film formed in Figure 5-10L), as opposed to all the other substrates prepared with TiO_2 substrates. In this specific case, vacuuming (static or dynamic) did not result in an improved surface. While we do acknowledge that dynamic vacuum resulted in better coverage, as shown in Figure 5-10H (TC-7) vs. Figure 5-10B (TC-1), smaller cracks/pores still exist between the coated layers. Thus, it is mandatory to use substrates with significantly smaller pores when trying to use the "Coating Onto" method.

In the "Coating Onto" method, use of Vertical flipping (2-pass) with static vacuum on the zirconium oxide ceramic tubes (with 10-15 nm pores) yielded the best film formation on the tube surface.

5.3.2. "Grafting From" – using Functionalized Particle – si-ATRP

The "Grafting From" procedure in the case of si-ATRP (or use of the TiO_2-g-C3-Initiator) proved to be a challenging feat. The planned experimental design is shown in Table 5-2, and the results of each scenario can be found in Figure 5-11. This setup varied between the types of CTI ceramic support used (TiO_2 or ZrO_2), application of vacuum (static), the motion of the coating (Vertical/flipping, axial or Ferris wheel), and the polymerization with PEGMEMA with rotation, or varying concentrations.

Table 5-2: "Grafting From" experiments performed with varying coating properties (i.e. vacuum and method of coating for TiO_2-g-C3-Initiator particles) and polymerization technique (i.e. rotational method used and concentration of macromonomer PEGMEMA).

Sample ID	Type of CTI Tube	Coating		Polymerization	
		Vacuum	Method	Rotation	Concentration
si-ATRP-T1	TiO_2	Static	Vertical – 2-pass (flip)	Vertical	0.27M
si-ATRP-T2	TiO_2	Static	Vertical – 1-pass	Vertical	0.27M
si-ATRP-T3	TiO_2	**None**	Axial – 1-pass	Vertical	0.27M
si-ATRP-T4	TiO_2	Static	Axial – 1-pass	Ferris Wheel	0.27M
si-ATRP-T5	TiO_2	Static	Ferris Wheel (60 rpm) - 1 pass	Ferris Wheel	0.27M
si-ATRP-T6	**ZrO_2**	Static	Ferris Wheel (60 rpm) - 2 pass	Vertical	0.27M
si-ATRP-T7	TiO_2	Static	Vertical – 2-pass (flip)	Ferris Wheel	**0.09M**
si-ATRP-T8	TiO_2	Static	Vertical – 2-pass (flip)	Ferris Wheel	**0.45M**

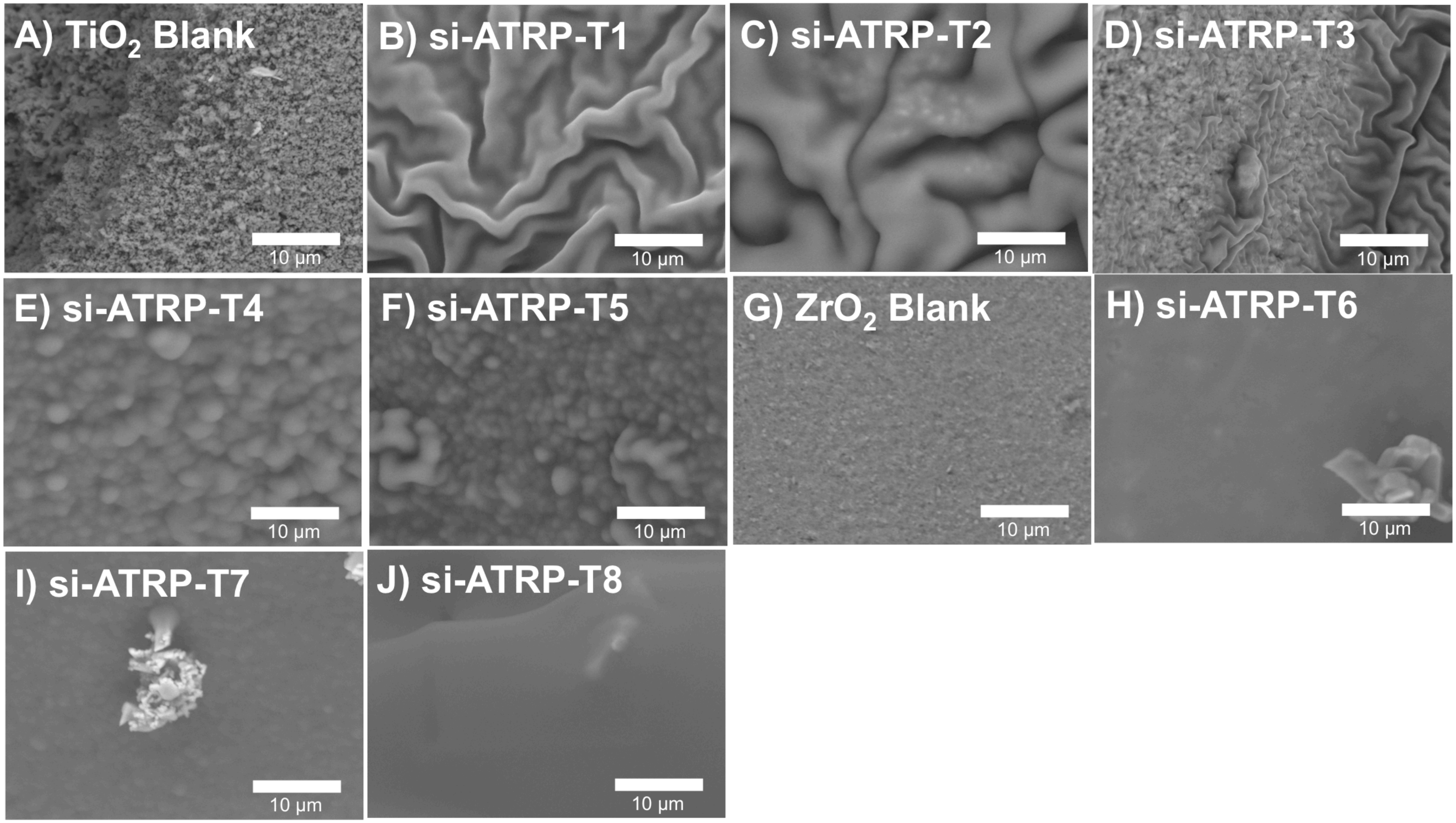

Figure 5-11: SEM images collected at 5000x magnification in the "Grafting From" process *via* si-ATRP. The images can be crossed referenced with Table 5-2 with varying coating procedures and polymerization procedures.

The results illustrate that several parameters are important when coating tubular membranes. For instance, when comparing si-ATRP-T2 and si-ATRP-T3, static vacuuming is more important during the coating step to help achieve a better polymeric film as opposed to a non-vacuumed sample. Figure 5-11C and Figure 5-11D showed how the vacuum process helps provide a more uniform film.

Taking sample si-ATRP-T4, we see that axial coating appeared to yield a better final film than sample si-ATRP-T5, which was prepared with the ferris wheel motion; there was a better film uniformity in si-ATRP-T4 compared with the blotchy, uneven surface found in si-ATRP-T5. However, the comparison between these two sample films with si-ATRP-T1 and si-ATRP-T2 illustrated that the vertical method yielded the best-formed films (Figure 5-11B and Figure 5-11C).

If we consider the substrate effect, the use of ZrO_2 compared to TiO_2 appeared to produce a relatively flat film (i.e. si-ATRP-T6), similar to si-ATRP-9. However, comparing these films to si-ATRP-T1 and si-ATRP-T2, the samples made with vertical/flipping (si-ATRP-T1 and si-ATRP-T2) appeared similar to the images obtained in Chapter 3, with the flat titania supports subjected to 0.68 M PEGMEMA solution (Figure 3-22).

By combining all the features observed, we have determined that the best format in which this “Grafting From” procedure with respect to si-ATRP should be as followed:

- Static vacuum applied to the coating of the TiO_2-g-C3-Initiator
- Vertical/Flipping process is better for the coating process (1-pass and 2-pass)
- Vertical polymerization appeared to yield the best final film from observing each film that was imaged
- Concentration should remain at 0.27 M
- Use of the TiO_2 sample appeared to yield a better result (but ZrO_2 can also be considered)

With the vertical coating, both 1-pass and 2-pass samples presented good polymer films. However, we observed that the 2-pass provided slightly better coating yields (through more TiO_2-g-C3-Initiator particle exposure), with the polymeric film weave being much more defined (*i.e*. smaller folds observed in Figure 5-11B)).

In the "Grafting From" method *via* si-ATRP, use of Vertical flipping (2-pass) with static vacuum on the titanium oxide ceramic tubes (with 200 nm pores) and polymerized in 0.27M PEGMEMA yielded the best film formation on the tube

5.3.3. "Grafting From" – using Functionalized Particle Coating – si-ROMP

This final setup in the "Grafting From" procedure looked at application of the TiO_2-g-APTES-PEO-NB samples for use in si-ROMP on the CTI ceramic tubes. While similar variables were explored, as in the previous section working in si-ATRP, the use of a mixture of norbornene (NB) and norbornene-PEG (NB-PEO-OH, or also shown as NB-PEO) was also introduced into the study (i.e. si-ROMP-T3/T5/T8). The experimental parameters and SEM observations are reported in Table 5-3 and Figure 5-12, respectively.

While the results illustrate that the film formation was less aesthetically appealing when compared to the si-ATRP "Grafting From" results, there were indications that film formation had been achieved (albeit, less uniform than the si-ATRP samples). This "rocky" nature is hypothesized to form due to the activation of the norbornenyl group with the Grubbs first generation initiator in solution, which could have caused aggregation and covalently linking various Evonik particles together.

Table 5-3: "Grafting From" experiments performed with varying coating properties (i.e. vacuum and method of coating for TiO_2-g-APTES-PEO-NB) and polymerization technique (i.e. rotational method used and concentration of monomer, Norbornene (NB) with/without Norbornene-PEG (NB-PEO)).

Sample ID	Type of CTI Tube	Coating		Polymerization			
		Vacuum	Rotation	Rotation	NB	NB-PEO	NB/NBPEO ratio
si-ROMP-T1	ZrO_2	Static	Ferris Wheel (60rpm) – 1-pass	Vertical	**0.43M**	-	-
si-ROMP-T2	ZrO_2	Static	Vertical – 2-pass	Vertical	**0.6M**	-	-
si-ROMP-T3	ZrO_2	Static	Vertical – 2-pass	Vertical	**0.6M**	0.3M	80/20
si-ROMP-T4	ZrO_2	Dynamic	Vertical – 1-pass	Vertical	0.3M	-	-
si-ROMP-T5	ZrO_2	Dynamic	Vertical – 1-pass	Vertical	0.3M	0.3M	80/20
si-ROMP-T6	**TiO_2**	Dynamic	Vertical – 1-pass	Ferris Wheel	0.3M	-	-
si-ROMP-T7	**TiO_2**	Dynamic	Vertical - 1-pass	Ferris Wheel	0.3M	0.3M	80/20
si-ROMP-T8	**TiO_2**	Dynamic	Vertical – 2-pass	Vertical	0.3M	-	-
si-ROMP-T9	ZrO_2	Dynamic	Vertical – 2-pass	Vertical	0.3M	-	-

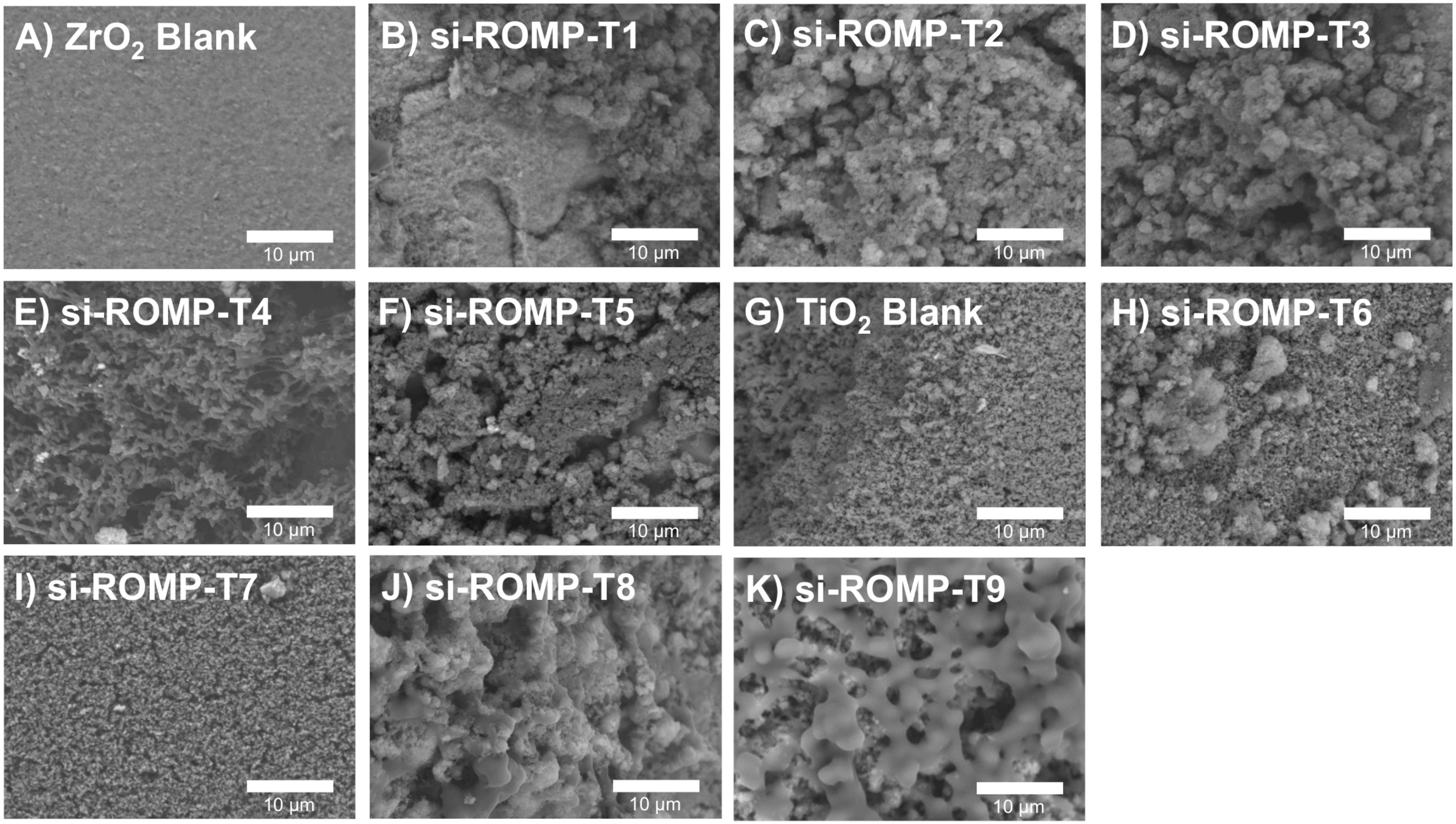

Figure 5-12: SEM images collected at 5000x magnification in the "Grafting From" process *via* si-ROMP. The images can be crossed referenced with Table 5-3 with varying coating procedures and polymerization procedures.

In the first case, the use of the ferris wheel rotation in si-ROMP-T1 compared to the vertical sample si-ROMP-T2 shows fairly similar topography. However, closer inspection does indicate that the density of coating appeared better with the vertical 2 pass than when using the ferris wheel motion. Expanding on the vertical method, comparison between 1-pass (si-ROMP-T4) vs. 2-pass (si-ROMP-T9) clearly shows a superior film formation with the 2 pass coating procedure. Thus the vertical/flipping – 2-pass process should be considered.

Use of vacuum (dynamic or static) can be determined by observing the differences between si-ROMP-T2 and si-ROMP-T9. While the monomer concentrations were different, it is evident that a better polymer film was formed on the surface of si-ROMP-T9 when using dynamic vacuum. Thus, we confirm that use of dynamic vacuum during the coating step (before polymerization) resulted in improved film quality.

In the case of using a mixture of 80/20 NB with NB-PEO-OH or purely NB, the samples using ZrO_2 substrate tube (i.e si-ROMP-T2/T3 and si-ROMP-T4/T5) show very similar film formation. However, the final film coating appeared slightly denser with the monomer/macromonomer mixture, as illustrated in Figure 5-12D and Figure 5-12F. Changing this substrate to TiO_2 while using a ferris wheel type motion for polymerization resulted in the opposite observation, as illustrated with the comparison between si-ROMP-T7 and si-ROMP-T8. The mixture of 80/20 NB with NB-PEO-OH did not modify the TiO_2 surface (Figure 5-12J), while there is only a slight modification of surface with the purely NB monomer solution (Figure 5-12I). However, TiO_2 tubes can be polymerized vertically (without any motion), as illustrated in Figure 5-12J, for sample si-ROMP-T8. This sample appears fairly well coated on the surface, with much fewer cracks when compared to si-ROMP-T6.

From all these results, the ideal film formation appeared very similar to that found in si-ROMP-T9. Thus, the final membrane should consider:

- Dynamic vacuum applied to the coating of the TiO_2-g-APTES-PEO-NB
- Vertical/Flipping – 2-pass process is better for the coating process

- Mixed monomer/macromonomer solution appeared slightly better (80/20 NB/NB-PEO-OH)
- Sample using ZrO_2 tubular supports appeared to yield better films than TiO_2 tubular supports

Careful attention should be placed in the studies with the mixture of 80/20 NB/NB-PEO-OH. The films formed on the surface were still porous, which means that additional coatings should be provided, or the coating process being optimized. This could be achieved by additional coatings of the TiO_2-g-APTES-PEO-NB solution, or by playing with higher concentrations of monomer/macromonomer. Nonetheless, tubes made with a similar process than that reported in Figure 5-12K can be used as the template for scaling up.

In the "Grafting From" method *via* si-ROMP, use of Vertical flipping (2-pass) with dynamic vacuum on the zirconium oxide ceramic tubes (with 10-15 nm pores) and polymerized in 0.3 M NB/NB-PEO (80/20 mixture) yielded an acceptable film formation on the tube surface. (And suggested that this be expanded to longer tubes for testing).

5.3.3.1. Qualitative Water droplet test

Noting that polynorbornene (pNB) is fairly hydrophobic in nature, the decision was made to attempt to visualize the surface modification with a water droplet test. In this case, a drop of water could help determine if the surface were hydrophilic or hydrophobic, all with how spherical or flat the droplet would sit on the surface. The results to this can be seen in Figure 5-13.

From these results, we see how polynorbornene surfaces retain well-defined droplets on their surface, while samples with higher PEO content (i.e. Figure 5-13D) spread the water droplet, as a result of a more hydrophilic surface. This point only highlights the notion of surface property modification resulting from the type of polymer layer. We noted that the blank zirconium oxide sample has a droplet rest on its surface while the titanium oxide sample no longer shows sign of a droplet formation. As zirconia has a much smaller porosity (15-20 nm) than titania (200 nm these small pores might indicate that the surface tension of water is too high for the water to diffuse through the pores.

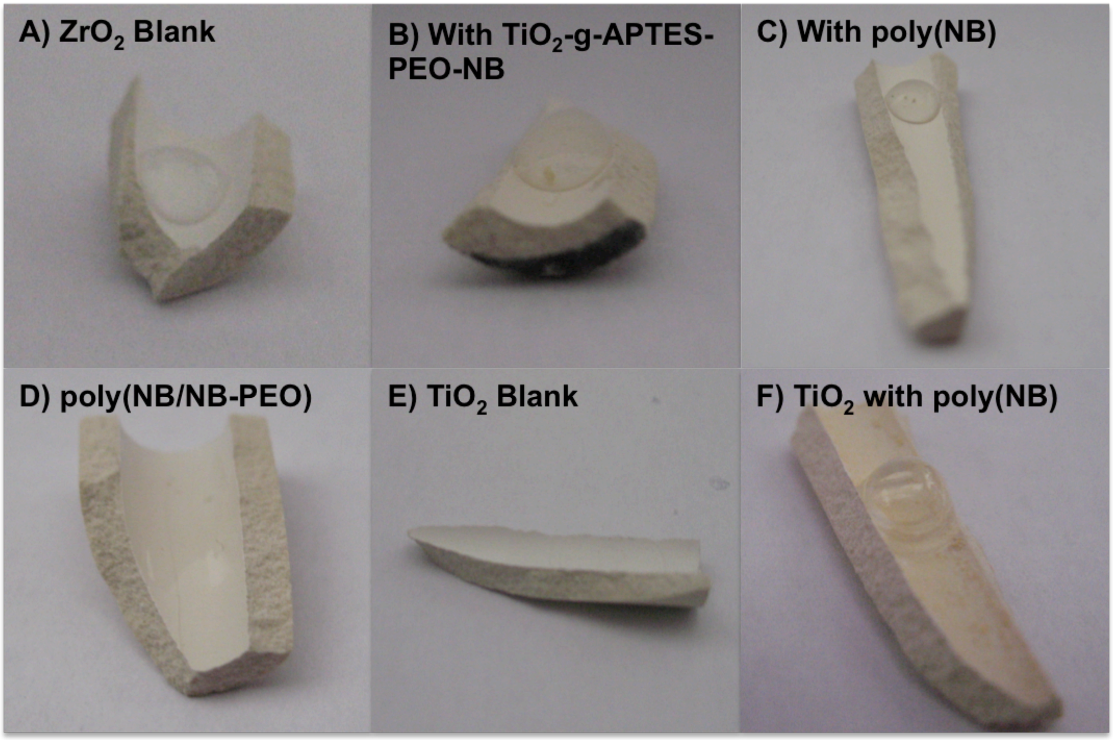

Figure 5-13: Hydrophobic droplet test performed on varying surfaces performed with samples taken from the "Grafting From" process *via* si-ROMP. Samples include A) zirconium oxide blank, B) zirconium oxide with coated TiO_2-g-APTES-PEO-NB, C) zirconium oxide with polymerized NB (pNB), D) zirconium oxide with polymerized NB/NB-PEO-OH, E) titanium oxide blank and F) titanium oxide with polynorbornene (pNB). Note how sample B), C) and F) all have very pronounced water droplets indicating hydrophobicity.

A water droplet test can be performed as a quick method to assess if the surface has changed in the case of si-ROMP with norbornene or norbornene-PEO (NB/NB-PEO-OH). In this case, samples with higher PEO content will favour water spreading out quickly, thus showing no droplet resting on the surface.

5.4. Conclusions

In conclusion, the study on the different techniques to modify these ceramic supports, either through the “Coating Onto” method or the “Grafting From” method, have been illustrated and performed. It was found that in the “Coating Onto” method with the hybrid particles (or **S.S.** mixture), the coating procedure with the optimal conditions were to apply static vacuum outside the ceramic tube (which was sealed with Teflon/septum setup). In addition, coating using a vertical/flipping method achieved a good coating on a sample with small pores (i.e. the 10-15 nm pores found with the zirconium oxide, ZrO_2, support).

In the "Grafting From" case, there were two options explore: either through si-ATRP or si-ROMP. With si-ATRP, the conditions found that vertical flipping (2 pass) with static vacuum on the regular titanium oxide ceramic tubes resulted in good film formation. However, the si-ROMP method found that the best conditions were achieved with dynamic vacuuming on zirconium oxide ceramic tubes (i.e. 10-15 nm pores) before polymerizing in a monomer/macromonomer mixture of NB/NB-PEO. Additionally, the si-ROMP route also had a method to verify the surface modification through a water droplet test. As polynorbornene is hydrophobic, the surface water droplets would behave differently over the course of the modification.

Taking all these lessons, one can further expand upon the tube synthesis, and start to synthesize longer tubes for testing, as we will see in the proceeding chapter 6.

Chapter 6

Gas Separation Results and Analysis

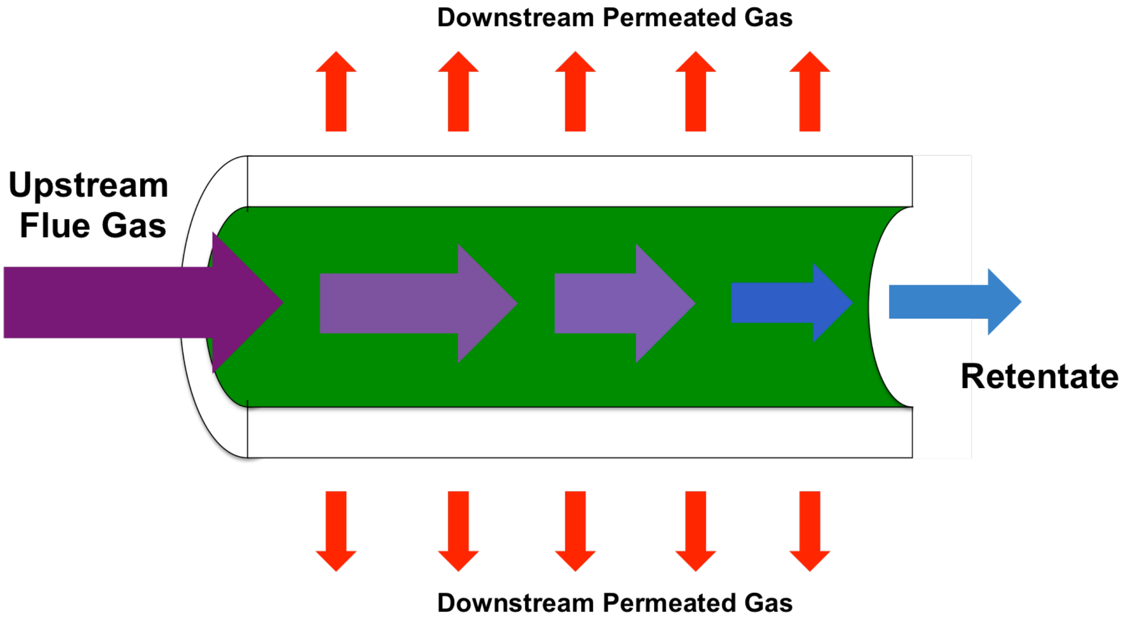

Ideal membrane function for synthesized gas separation ceramic tube

6.1. Introduction

This final chapter aims to describe the behaviour of nanocomposite membranes for their CO_2 selectivity compared to N_2. Membrane optimization and tests are always a challenging step, which require significantly long durations for testing. As previous chapters might have alluded, the material development took longer than initially expected. This was mostly due to unforeseen issues with the grafting initiators, which required a full analytical study when the original expectation was for an "off-the-shelf" product. Therefore, the present chapter is shorter than planned, and describes the preliminary tests conducted with the expertise of Dr. Sophie Cerneaux at the European Institute of Membranes (CNRS-UMR5635) in Montpellier.

The direction of this work will focus on the application of Chapter 5 towards the synthesis of our target ceramic hybrid membranes. From the drawn conclusions, such as membrane coating conditions and materials used, synthesis of longer membranes were made and tested for their permeance and single gas permeation selectivity ($\alpha_{i/j}$) were calculated. In this case, the first set of results obtained will be presented and briefly discussed. Recommendations will then be made upon future work to progress and improve these membranes.

6.2. Experimental Setup

This experiment was first designed with the results of Chapter 5 in mind. As it was found that the si-ROMP sample appeared a bit more porous in nature than its si-ATRP counter part (in the case of the "Grafting From" sample), the si-ATRP route was the first sample to be translated into a longer, 20 cm length tube (note that TiO_2 CTI porous tubes were used, which had an outer-diameter of 10.4 mm and an inner-diameter of 6 mm). In the case of the "Coating Onto" tube, the method of applying static vacuum with a double pass (with flipping) on the zirconium oxide ceramic tubes was made. However, the decision to compare with use of the titanium oxide ceramic tubes was also attempted. The samples made are summarized in Table 6-1.

Table 6-1: Ceramic tubes made to be tested for CO_2 and N_2 gas permeance and selectivity.

Membrane ID	Coating Method	Length of Tube Made	Length of Tube
TiO_2-Blank	-	20 cm	15 cm
ZrO_2-Blank	-	20 cm	15 cm
TC-A-TiO_2	static vacuum (2 pass)	20 cm	15 cm
TC-B-ZrO_2	static vacuum (2 pass)	20 cm	15 cm
si-ATRP-A	static vacuum (2 pass) + polymerization in 0.27M PEGMEMA	20 cm	15 cm

The samples were then packaged and sent to the European Institute of Membranes (CNRS-UMR5635) in Montpellier (France); a laboratory specializing in membrane manufacturing and processes, including gas separation.

6.2.1. Permeance Results

As was briefly mentioned in Chapter 1, the permeance is a value that is directly proportional to the permeability of a membrane. The main difference is that this value is normalized against the membrane thickness; that is, this value can ignore the effects of thickness to provide a parameter that can be used to determine gas selectivity. In this case, the permeances for various pressures were measured and plotted to provide the figures found in Figure 6-1 on the next page.

We first report the permeance values for the blank TiO_2 (Figure 6-1A) and ZrO_2 (Figure 6-1B) supports. The zirconia support has a smaller pore size (15 nm) than titania (200 nm), but this does not affect the gas flow, and both display similar values. Figure 6-1 C & D compare the permeance for TiO_2 and ZrO_2, respectively, with a polymer layer made from the “Coating Onto” method. We observe that values are divided by a factor 1,000 for TC-A-TiO_2, and 100 for TC-B-ZrO_2, which demonstrates that the coating was effective. For the TiO_2-based membrane prepared via the si-ATRP route (or "Grafting From" method), the reduction factor is only 10, but still significant.

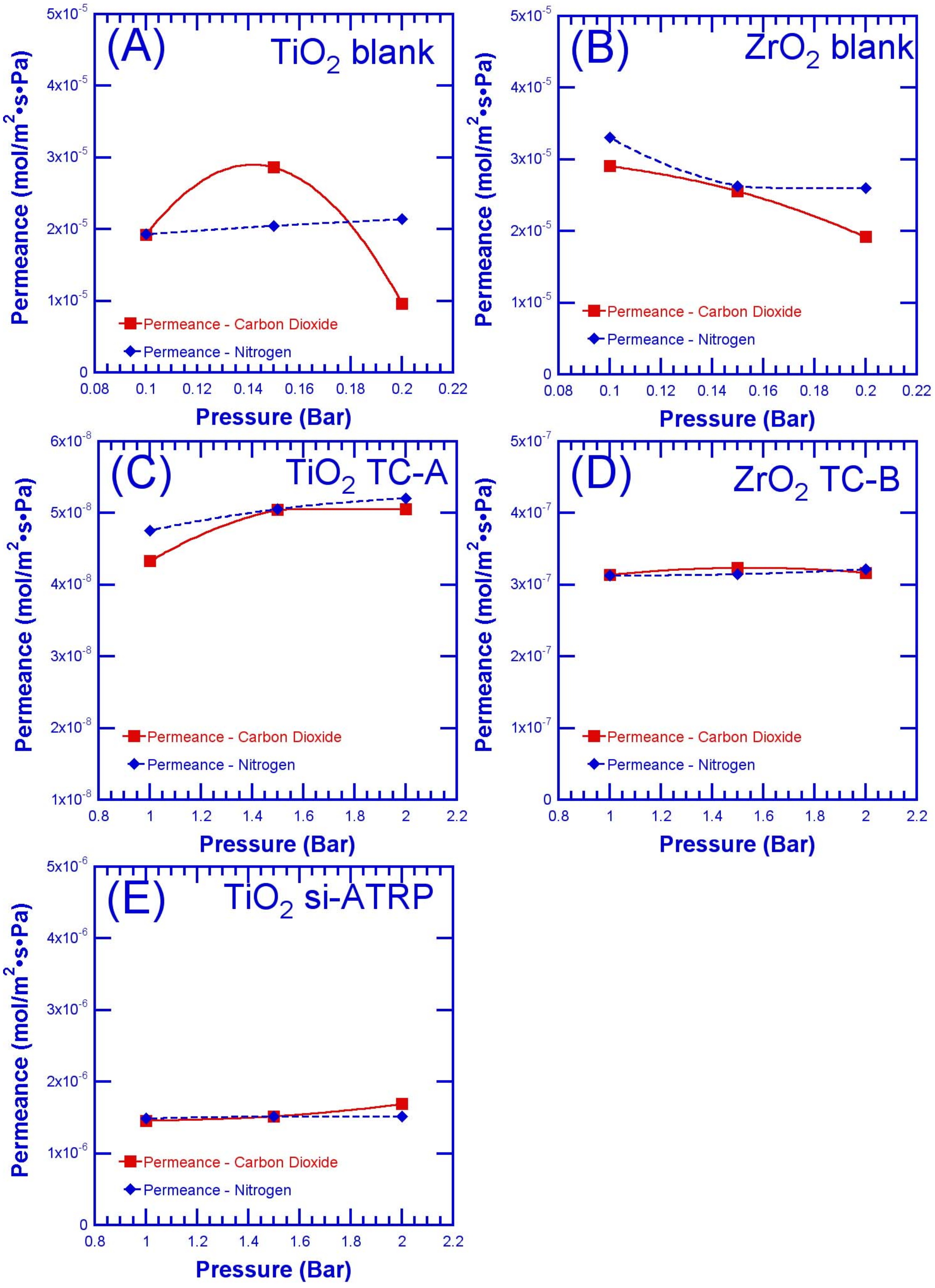

Figure 6-1: Gas permeances versus pressure for A) TiO_2-Blank, B) ZrO_2-Blank, C) TC-A-TiO_2, D) TC-B-ZrO_2, and E) si-ATRP-A

6.2.2. Selectivity Results

"Ideal" selectivity obtained by dividing the permeability (or permeance) values for two gas aims to provide information on the material affinity toward a target gas. Actual selectivity measurements should take into account a mixture of gas, and the stage-cut parameter, which defines the gas glow ratio between permeate and retentate flux. The results of the gas selectivity calculated from the permeance data, can be found in Table 6-2. We see that none of our membranes display a differential affinity toward CO_2.

We previously mentioned that the membranes for this first series of samples seem to display a rather good quality, as gas flow reduction is observed. However, selectivity can be destroyed even with very few pinhole defects. In addition, the nature and composite structure of the actual membrane has to be questioned, since selectivity is the result of differential molecular interactions between the gas and the polymer. If the polymer fraction is too low, these interactions are limited and cannot be effective.

Table 6-2: Selectivity values measured and provided by IEM. Note that the values were averaged over 3 data points.

Membrane ID	Selectivity ($\alpha_{CO2/N2}$)
TiO_2-Blank	0.95
ZrO_2-Blank	0.86
TC-A-TiO_2	1.03
TC-B-ZrO_2	1.01
si-ATRP-A	0.96

6.2.3. Discussion

As we mentioned initially, our project had to be adapted to face initial issues regarding the material synthesis. Our first tests reveal some promising results, but also some negative results.

On the positive side, the permeance tests have demonstrated that we could coat our composite films over a rather large surface on a commercial ceramic support. From our knowledge, this is the first time that such a result is obtained. The important reduction in gas flow proves that the nanocomposite membrane has a good coverage of the internal surface of the ceramic tube.

However, the negative aspect of this result is the lack of selectivity. Nonetheless, we must remember that these are preliminary results; achieving performing membranes for gas permeation is a challenge. As we have validated our process and demonstrated that it could be scaled-up, there are different lessons learned from this failure. Among them is the fact the membranes might not be perfectly uniform, with the potential for local defects that could destroy any gas selectivity. We must also study if the fraction of polymers in this nanocomposite membrane is high enough to provide the expected molecular selective affinity.

6.3. Recommendations for Future Work

These results indicate that issues still remain with regards to the hybrid membrane formation. As pinholes potentially remain a problem, and that the polymeric content might need to be increased, several recommendations exist, such as:

1). In the case of hybrid particles with the "Coating Onto" process, additional coats (3 or more) should be tested on the longer 15 cm ceramic tubes (specifically with the ZrO_2 membranes with 10-15 nm pores)

2). In the case of the surface-initiated ATRP route for the "Grafting From" process, additional coatings with the functionalized Evonik particles (i.e. TiO_2-g-C3-Initiator) should be attempted before polymerization (and studied on longer 15 cm tubes).

3). While no preliminary results existed for the surface-initiated ROMP route for the "Grafting From" process, the work should continue to synthesize the membrane with a mixture of NB-PEO-OH and NB (norbornene) to form the uniform polymeric layer. Note that norbornene is used for easier propagation of the reaction.

4). As scaling up has been shown to be tricky, increasing the number of coating layers may allow the increase of material built up on the surface however, additional parameters such as increasing mixture viscosity or addition of other organic polymer fillers can be studied to improve membrane formation.

5). Addition of heat for low temperature annealing can also be a route for improving membrane uniformity, as was previously highlighted from work referenced in Chapter 4.

While not the most exhaustive list, this does highlight the direction this project can continue if one were to explore other avenues to expand upon this presented study.

6.4. Conclusion

This chapter's main goal was to briefly present the preliminary results obtained with the application of our newly developed coating techniques towards gas separation. While the data indicated the failure of our preliminary tests, we believe that our general process has been validated overall. The preparation of membranes for gas permeation is always challenging work, especially if one wants to initiate a method based on commercial supports produced at the industrial scale. Our tests show that there exists room for improvement because the membrane material shows great promise, providing a different approach to membrane synthesis. The recommended direction for further improvement was thus presented, and a pathway for future development was acknowledged.

General Conclusions

Final Statement

The studies this thesis presented illustrated the work that went towards the formation of a membrane with the ultimate goal towards gas separation. Each chapter had put forth work that studied the components that would eventually be applied towards formation of a tubular membrane. We saw how the initial literature search on membrane materials provided the knowledge and direction for this project; specifically, that hybrid structures were the ideal membrane material. In this case, the use of inorganic titania was the inorganic component of choice. However, integration of the inorganic titania component was vital with the polymeric matrix, which had been difficult. Realization of this point, studies and work on surface modification techniques were performed. Working with both silane-based (APTES) and phosphonic acid-based (C3-Initiator) grafting units, the titania surfaces were functionalized to be used as the "seeds" to grow the polymeric layer to form the membrane.

In the case of the phosphonic acid-based pathway, surface-initiated atom-transfer radical polymerization (si-ATRP) was applied to form both hybrid particles and modified flat surfaces with a highly PEG-ylated polymer membrane. This study enabled us to characterize and determine the best conditions for hybrid structure formation. In the case of hybrid particle formation, the grafting density of the C3-initiator (2.5 initiators/nm^2) resulted in an estimated degree of polymerization of 1200 units of PEGMEMA with a size roughly 350 nm in diameter.

Similarly in the silane-based pathway with APTES, the amine group was reacted with a terminal carboxylic acid group linked to a norbornenyl polyethylene oxide macromonomer to form titania particles with exposed norbornenyl groups. The latter particles are then able, after exposure to the Grubbs first generation initiator, to promote surface-initiated ring-opening metathesis polymerization (si-ROMP) of norbornene and norbornene/norbornene-PEG structures. Studies that were performed help determine that the hybrid particles had a grafting density of 2.7 norbornenyl groups/nm^2 with a degree of polymerization of 12500 units of polynorbornene hybrid particles.

However, all of these studies provided the foundation work towards the synthesis of the membrane themselves. The formation of these hybrid membranes resulted in two pathways for membrane formation – the “Grafting From” method, and the “Coating Onto” method. Our application of the “Grafting From” procedure with coating pre-functionalized particles that would situate within pores (or coating them) proved it was possible to modify surfaces through this method; using the functionalized titania particles as the “seeds” to directly form the polymeric membrane on the surface of the ceramic tubes. Additionally (to our knowledge), this work encompassed the first method of application of the hybrid particles directly onto a tubular support, which resulted in our “Coating Onto” method.

These results eventually led to testing to find their gas separation properties, and while the preliminary results showed that the selectivity needed improvement, there was potential in this route. Recommendations were then made to improve this, such as increasing the number of coating passes on the ceramic tubes in both pathways (“Grafting From” and “Coating Onto”).

References

1. Bloom, D. E. 7 Billion and Counting. *Science* **333,** 562–569 (2011).
2. Kan, H., Chen, R. & Tong, S. Ambient air pollution, climate change, and population health in China. *Environment International* **42,** 10–19 (2012).
3. Lior, N. Sustainable energy development (May 2011) with some game-changers. *Energy* **40,** 3–18 (2012).
4. Le Treut, H., Cubasch, U. & Allen, M. 2007: Historical Overview of Climate Change Science. *Climate Change 2007: The Physical Science Basis. Contribution of Working Group I to the Fourth Assessment of the Intergovernmental Panel on Climate Change (IPCC),* 95-127 (2007).
5. Du, N., Park, H. B., Dal-Cin, M. M. & Guiver, M. D. Advances in high permeability polymeric membrane materials for CO_2 separations. *Energy Environ. Sci.* **5,** 7306–7322 (2012).
6. Favre, E. Carbon dioxide recovery from post-combustion processes: Can gas permeation membranes compete with absorption? *Journal of Membrane Science* **294,** 50–59 (2007).
7. Aaron, D. & Tsouris, C. Separation of CO_2 from Flue Gas: A Review. *Separation Science and Technology* **40,** 321–348 (2005).
8. Lide, D. R. *CRC Handbook of Chemistry and Physics, 85th Edition*. (CRC Press, 2004).
9. Bates, E. D., Mayton, R. D., Ntai, I. & Davis, J. H. CO_2 Capture by a Task-Specific Ionic Liquid. *J. Am. Chem. Soc.* **124,** 926–927 (2002).
10. Danckwerts, P. V. The reaction of CO_2 with ethanolamines. *Chemical Engineering Science* **34,** 443–446 (1979).
11. Boryta, D. A. & Maas, A. J. Factors influencing rate of carbon dioxide reaction with lithium hydroxide. *Ind. Eng. Chem. Process Des. Develop.* **10,** 489–494 (1971).
12. Satyapal, S., Filburn, T., Trela, J. & Strange, J. Performance and Properties of a Solid Amine Sorbent for Carbon Dioxide Removal in Space Life Support Applications. *Energy Fuels* **15,** 250–255 (2001).
13. Krishna, R. & van Baten, J. M. A comparison of the CO_2 capture characteristics of zeolites and metal-organic frameworks. *Separation and Purification Technology* **87,** 120–126 (2012).
14. Meisen, A. & Shuai, X. Research and development issues in CO_2 capture. *Energy Conversion and Management* **38,** S37–S42 (1997).
15. Riemer, P., Webster, I. C., Ormerod, W. G. & Audus, H. Results and full fuel cycle study plans from the IEA greenhouse gas research and development programme. *Fuel* **73,** 1151–1158 (1994).
16. Schussler, U. & Kummel, R. Carbon dioxide removal from fossil fuel power plants by refrigeration under pressure. *Energy Conversion Engineering*

Conference, 1989 IECEC-89, Proceedings of the 24th Intersociety, 1789–1794 (IEEE, 1989). doi:10.1109/IECEC.1989.74714

17. Jacobs, M. & Finney, B. *Carbon dioxide pressure-temperature phase diagram - Wikimedia Commons*. at <https://commons.wikimedia.org/wiki/File:Carbon_dioxide_pressure-temperature_phase_diagram.svg> [Accessed: July 2015]
18. Cot, L., Ayral, A., Durand, J., Guizard, C. & Hovnanian, N. Inorganic membranes and solid state sciences. *Solid State Sciences* **2,** 313–334 (2000).
19. May-Britt, H. Membranes in Chemical Processing A Review of Applications and Novel Developments. *Separation and Purification Methods* **27,** 51–168 (1998).
20. Pandey, P. & Chauhan, R. S. Membranes for gas separation. *Progress in Polymer Science* **26,** 853–893 (2001).
21. Yeo, Z. Y., Chew, T. L., Zhu, P. W., Mohamed, A. R. & Chai, S.-P. Conventional processes and membrane technology for carbon dioxide removal from natural gas: A review. *Journal of Natural Gas Chemistry* **21,** 282–298 (2012).
22. Reijerkerk, S. R., Wessling, M. & Nijmeijer, K. Pushing the limits of block copolymer membranes for CO_2 separation. *Journal of Membrane Science* **378,** 479–484 (2011).
23. May-Britt, H. NTNU: Innovation and Creativity - Membranes for environmental friendly energy - part I. *NTNU Course Notes*, 1–41 [Accessed May 2015].
24. Grajales, S. T., Dong, X., Zheng, Y., Baker, G. L. & Bruening, M. L. Effects of Monomer Composition on CO_2−Selective Polymer Brush Membranes. *Chem. Mater.* **22,** 4026–4033 (2010).
25. Koros, W. J. & Fleming, G. K. Membrane-based gas separation. *Journal of Membrane Science* **83,** 1–80 (1993).
26. Vaughn, J. T., Koros, W. J., Johnson, J. R. & Karvan, O. Effect of thermal annealing on a novel polyamide–imide polymer membrane for aggressive acid gas separations. *Journal of Membrane Science* **401-402,** 163–174 (2012).
27. Robeson, L. M. Correlation of separation factor versus permeability for polymeric membranes. *Journal of Membrane Science* **62,** 165–185 (1991).
28. Robeson, L. M. The upper bound revisited. *Journal of Membrane Science* **320,** 390–400 (2008).
29. Budd, P. *et al.* Gas separation membranes from polymers of intrinsic microporosity. *Journal of Membrane Science* **251,** 263–269 (2005).
30. Orme, C. J., Harrup, M. K., Luther, T. A. & Lash, R. P. Characterization of gas transport in selected rubbery amorphous polyphosphazene membranes. *Journal of Membrane Science* **186,** 249–256 (2001).
31. Koros, W. J. & Mahajan, R. Pushing the limits on possibilities for large scale gas separation: which strategies? *Journal of Membrane Science* **175,** 181–196 (2000).
32. Prouzet, E. NE499 - Mesoporous Materials, *University of Waterloo NE499*

Course notes, (2011).

33. Merkel, T. C. *et al.* Ultrapermeable, Reverse-Selective Nanocomposite Membranes. *Science* **296,** 519–522 (2002).
34. Freeman, B. & Pinnau, I. Separation of gases using solubility-selective polymers. *Trends in polymer science* **5,** 167-173 (1997).
35. Wind, J. D., Paul, D. R. & Koros, W. J. Natural gas permeation in polyimide membranes. *Journal of Membrane Science* **228,** 227–236 (2004).
36. Vu, D. Q., Koros, W. J. & Miller, S. J. Mixed matrix membranes using carbon molecular sieves: I. Preparation and experimental results. *Journal of Membrane Science* **211,** 311–334 (2003).
37. Clausi, D. T. & Koros, W. J. Formation of defect-free polyimide hollow fiber membranes for gas separations. *Journal of Membrane Science* **167,** 79-89 (2000).
38. Goeppert, A. *et al.* Carbon Dioxide Capture from the Air Using a Polyamine Based Regenerable Solid Adsorbent. *J. Am. Chem. Soc.* **133,** 20164–20167 (2011).
39. Kim, T.-J., Li, B. & Hagg, M.-B. Novel fixed-site-carrier polyvinylamine membrane for carbon dioxide capture. *Journal of Polymer Science Part B: Polymer Physics* **42,** 4326–4336 (2004).
40. Utracki, L. A. History of commercial polymer alloys and blends (from a perspective of the patent literature). *Polymer Engineering & Science* **35,** 2–17 (1995).
41. Car, A., Peinemann, K. V., Stropnik, C. & Yave, W. Pebax®/polyethylene glycol blend thin film composite membranes for CO_2 separation: Performance with mixed gases. *Separation and Purification Technology* **62,** 110–117 (2008).
42. Car, A., Stropnik, C., Yave, W. & Peinemann, K. V. PEG modified poly(amide-b-ethylene oxide) membranes for CO_2 separation. *Journal of Membrane Science* **307,** 88–95 (2008).
43. Peinemann, K. V. *et al.* Gas permeability and free volume in poly(amide-b-ethylene oxide)/polyethylene glycol blend membranes. *Journal of Membrane Science* **339,** 177–183 (2009).
44. Reijerkerk, S. R., Knoef, M. H., Nijmeijer, K. & Wessling, M. Poly(ethylene glycol) and poly(dimethyl siloxane): Combining their advantages into efficient CO_2 gas separation membranes. *Journal of Membrane Science* **352,** 126–135 (2010).
45. Kim, J. H. & Lee, Y. M. Gas permeation properties of poly (amide-6-b-ethylene oxide)–silica hybrid membranes. *Journal of Membrane Science* **193,** 209–225 (2001).
46. Kim, J. H., Ha, S. Y. & Lee, Y. M. Gas permeation of poly (amide-6-b-ethylene oxide) copolymer. *Journal of Membrane Science* **190,** 179-193 (2001).
47. Sanders, D. F. *et al.* Energy-efficient polymeric gas separation membranes for a sustainable future: A review. *Polymer* **54,** 4729–4761 (2013).
48. McGrail, P. T. Polyaromatics. *Polymer International* **41,** 103–121 (1996).

49. NIIR Board of Consultants & Engineers. *Speciality Plastics, Foams (Urethane, Flexible, Rigid) Pet & Preform Processing Technology Handbook*. (ASIA PACIFIC BUSINESS PRESS Inc., 2005).
50. Henis, J. & Tripodi, M. K. Multicomponent membranes for gas separations. *United States Patent Office 4,230,463* (1980).
51. Huang, Y., Wang, X. & Paul, D. Physical aging of thin glassy polymer films: Free volume interpretation. *Journal of Membrane Science* **277,** 219–229 (2006).
52. Sidney, L. & Sriniva, S. High flow porous membranes for separating water from saline solutions. *United States Patent Office 3,133,132* (1964).
53. Heinze, T. & Liebert, T. 4.2 Chemical characteristics of cellulose acetate. *Macromol. Symp.* **208,** 167–238 (2004).
54. Sidney, L. & Sourirajan, S. in *Saline Water Conversion - II; Advances in Chemistry - American Chemical Society: Washington DC*, 117–132 (1963).
55. Saka, S. & Matsumura, H. 2.3 Wood pulp manufacturing and quality characteristics. *Macromol. Symp.* **208,** 37–48 (2004).
56. Niwa, M. *et al.* Gas Separation of Asymmetric 6FDA Polyimide Membrane with Oriented Surface Skin Layer. *Macromolecules* **34,** 9039–9044 (2001).
57. Mclain, E. A. & Mahon, H. I. Permselective hollow fibers and method of making. *United States Patent Office 3,423,491* (1969).
58. Larbot, A., Fabre, J. P., Guizard, C. & Cot, L. Inorganic membranes obtained by sol-gel techniques. *Journal of Membrane Science* **39,** 203–212 (1988).
59. Biesheuvel, P. M. & Verweij, H. Design of ceramic membrane supports: permeability, tensile strength and stress. *Journal of Membrane Science* **156,** 141–152 (1999).
60. Larbot, A., Fabre, J. P., Guizard, C., Cot, L. & Gillot, J. New Inorganic Ultrafiltration Membranes: Titania and Zirconia Membranes. *J American Ceramic Society* **72,** 257–261 (1989).
61. Benito, J. M., Conesa, A., Rubio, F. & Rodríguez, M. A. Preparation and characterization of tubular ceramic membranes for treatment of oil emulsions. *Journal of the European Ceramic Society* **25,** 1895–1903 (2005).
62. van de Water, L. G. A. & Maschmeyer, T. Mesoporous Membranes—A Brief Overview of Recent Developments. *Topics in Catalysis* **29,** 67–77 (2004).
63. Guliants, V. V., Carreon, M. A. & Lin, Y. S. Ordered mesoporous and macroporous inorganic films and membranes. *Journal of Membrane Science* **235,** 53–72 (2004).
64. Noack, M., Kölsch, P., Schäfer, R., Toussaint, P. & Caro, J. Molecular Sieve Membranes for Industrial Application: Problems, Progress, Solutions. *Chemical Engineering Technology* **25,** 221–230 (2002).
65. Noble, R. D. & Agrawal, R. Separations Research Needs for the 21st Century. *Ind. Eng. Chem. Res.* **44,** 2887–2892 (2005).
66. Zhang, J.-L., Li, W., Meng, X.-K., Wang, L. & Zhu, L. Synthesis of mesoporous silica membranes oriented by self-assembles of surfactants. *Journal of Membrane Science* **222,** 219–224 (2003).

67. Kresge, C. T., Leonowicz, M. E., Roth, W. J., Vartuli, J. C. & Beck, J. S. Ordered mesoporous molecular sieves synthesized by a liquid-crystal template mechanism. *Nature* **359,** 710–712 (1992).
68. Beck, J. J., Roth, W. J., Leonowicz, M. E. & Kresge, E. T. A New Family of Mesoporous Molecular Sieves Prepared with Liquid Crystal Templates. *J. Am. Chem. Soc.* **114,** 10834–10843 (1992).
69. Nishiyama, N., Park, D. H., Koide, A. & Egashira, Y. A mesoporous silica (MCM-48) membrane: preparation and characterization. *Journal of Membrane Science* **182,** 235–244 (2001).
70. Prouzet, E. NE 499 - Mesoporous Materials - Lecture Set 7. *University of Waterloo NE499 course,* (2011).
71. Soler-Illia, G. J., Crepaldi, E. L., Grosso, D. & Sanchez, C. Block copolymer-templated mesoporous oxides. *Current Opinion in Colloid and Interface Science* **8,** 109-126 (2003).
72. Higgins, S., Kennard, R., Hill, N., DiCarlo, J. & DeSisto, W. J. Preparation and characterization of non-ionic block co-polymer templated mesoporous silica membranes. *Journal of Membrane Science* **279,** 669–674 (2006).
73. Liu, C., Wang, J. & Rong, Z. Mesoporous MCM-48 silica membrane synthesized on a large-pore α-Al2O3 ceramic tube. *Journal of Membrane Science* **287,** 6–8 (2007).
74. Grosso, D. *et al.* Periodically ordered nanoscale islands and mesoporous films composed of nanocrystalline multimetallic oxides. *Nat Mater* **3,** 787–792 (2004).
75. Chowdhury, S. R., Peters, A. M., Blank, D. H. A. & Elshof, J. E. T. Influence of porous substrate on mesopore structure and water permeability of surfactant templated mesoporous silica membranes. *Journal of Membrane Science* **279,** 276–281 (2006).
76. Boissière, C. *et al.* Ultrafiltration Membrane Made with Mesoporous MSU- X Silica. *Chem. Mater.* **15,** 460–463 (2003).
77. Boissiere, C., Martines, M., Larbot, A. & Prouzet, E. On the specific filtration mechanism of a mesoporous silica membrane, prepared with non-connecting parallel pores. *Journal of Membrane Science* **251,** 17–28 (2005).
78. Prouzet, E. & Boissière, C. A review on the synthesis, structure and applications in separation processes of mesoporous MSU-X silica obtained with the two-step process. *Comptes Rendus Chimie* **8,** 579–596 (2005).
79. McCusker, L. B., Liebau, F. & Engelhardt, G. Nomenclature of structural and compositional characteristics of ordered microporous and mesoporous materials with inorganic hosts:(IUPAC recommendations 2001). *Microporous and Mesoporous Materials* **58,** 3-13 (2003).
80. Liebau, F. Ordered microporous and mesoporous materials with inorganic hosts: definitions of terms, formula notation, and systematic classification. *Microporous and Mesoporous Materials* **58,** 15–72 (2003).
81. Olson, D. H., Baerlocher, C. & McCusker, L. B. *Atlas of Zeolite Framework Types*. **6** (Elsevier, 2007).

82. Mitsui Engineering & Shipbuilding Co. LTD. Pervaporization technology first commercially realized in Japan. <https://www.mes.co.jp/english/business/environ/environment3.html> [Accessed: July 2015]
83. Lai, Z. *et al.* Microstructural Optimization of a Zeolite Membrane for Organic Vapor Separation. *Science* **300,** 456–460 (2003).
84. Nishiyama, N., Matsufuji, T., Ueyama, K. & Matsukata, M. FER membrane synthesized by a vapor-phase transport method: its structure and separation characteristics. *Microporous materials* **12,** 293–303 (1997).
85. Bowen, T. C., Noble, R. D. & Falconer, J. L. Fundamentals and applications of pervaporation through zeolite membranes. *Journal of Membrane Science* **245,** 1–33 (2004).
86. McLeary, E. E., Jansen, J. C. & Kapteijn, F. Zeolite based films, membranes and membrane reactors: Progress and prospects. *Microporous and Mesoporous Materials* **90,** 198–220 (2006).
87. Zhang, X., Liu, H. & Yeung, K. L. Novel two-layered zeolite NaA-silicalite-1 membranes. *Journal of Physics and Chemistry of Solids* **66,** 1034–1038 (2005).
88. Piera, E., Giroir-Fendler, A. & Dalmon, J. A. Separation of alcohols and alcohols/O_2 mixtures using zeolite MFI membranes. *Journal of Membrane Science* **142,** 97–109 (1998).
89. Hedlund, J., Jareman, F., Bons, A.-J. & Anthonis, M. A masking technique for high quality MFI membranes. *Journal of Membrane Science* **222,** 163–179 (2003).
90. Noack, M. *et al.* Influence of the Si/Al-ratio on the permeation properties of MFI-membranes. *Microporous and Mesoporous Materials* **79,** 329–337 (2005).
91. Jareman, F., Hedlund, J. & Sterte, J. Effects of aluminum content on the separation properties of MFI membranes. *Separation and Purification Technology* **32,** 159–163 (2003).
92. Yan, Y., Davis, M. E. & Gavalas, G. R. Use of diffusion barriers in the preparation of supported zeolite ZSM-5 membranes. *Journal of Membrane Science* (1997).
93. Li, S., Tuan, V. A., Falconer, J. L. & Noble, R. D. Properties and separation performance of Ge-ZSM-5 membranes. *Microporous and Mesoporous Materials* **58,** 137-154 (2003).
94. Xu, X. *et al.* Synthesis of NaA zeolite membrane on a ceramic hollow fiber. *Journal of Membrane Science* **229,** 81–85 (2004).
95. Kondo, M., Komori, M., Kita, H. & Okamoto, K. Tubular-type pervaporation module with zeolite NaA membrane. *Journal of Membrane Science* **133,** 133–141 (1997).
96. Morigami, Y., Kondo, M., Abe, J. & Kita, H. The first large-scale pervaporation plant using tubular-type module with zeolite NaA membrane. *Separation and Purification Technology* **25,** 251–260 (2001).
97. Van Hoof, V., Dotremont, C. & Buekenhoudt, A. Performance of Mitsui NaA

type zeolite membranes for the dehydration of organic solvents in comparison with commercial polymeric pervaporation membranes. *Separation and Purification Technology* **48,** 304–309 (2006).

98. Belaissaoui, B. & Favre, E. Membrane Separation Processes for Post-Combustion Carbon Dioxide Capture: State of the Art and Critical Overview. *Oil Gas Sci. Technol. – Rev. IFP Energies nouvelles* **69,** 1005–1020 (2014).

99. Paul, D. R. & Kemp, D. R. The diffusion time lag in polymer membranes containing adsorptive fillers. *Journal of Polymer Science: Polymer Symposia* **41,** 79–93 (1973).

100. Kulprathipanja, S., Hoffman, E., Neuzil, R. W., Grove, D. & Li, N. N. Separation of fluids by means of mixed matrix membranes. *United States Patent Office 4,740,219* (1988).

101. Duval, J. M., Folkers, B., Mulder, M., Desgrandchamps, G. & Smolders, C. A. Adsorbent filled membranes for gas separation. Part 1. Improvement of the gas separation properties of polymeric membranes by incorporation of microporous adsorbents. *Journal of Membrane Science* **80,** 189-198 (1993).

102. Aroon, M. A., Ismail, A. F., Matsuura, T. & Montazer-Rahmati, M. M. Performance studies of mixed matrix membranes for gas separation: A review. *Separation and Purification Technology* **75,** 229–242 (2010).

103. Goh, P. S., Ismail, A. F., Sanip, S. M., Ng, B. C. & Aziz, M. Recent advances of inorganic fillers in mixed matrix membrane for gas separation. *Separation and Purification Technology* **81,** 243–264 (2011).

104. Husain, S. & Koros, W. J. Mixed matrix hollow fiber membranes made with modified HSSZ-13 zeolite in polyetherimide polymer matrix for gas separation. *Journal of Membrane Science* **288,** 195–207 (2007).

105. Ismail, A. F. & David, L. A review on the latest development of carbon membranes for gas separation. *Journal of Membrane Science* **193,** 1–18 (2001).

106. Mahajan, R. & Koros, W. J. Factors Controlling Successful Formation of Mixed-Matrix Gas Separation Materials. *Ind. Eng. Chem. Res.* **39,** 2692–2696 (2000).

107. Ng, L. Y., Mohammad, A. W., Leo, C. P. & Hilal, N. Polymeric membranes incorporated with metal/metal oxide nanoparticles: A comprehensive review. *Desalination* **308,** 15–33 (2013).

108. Shao, L., Samseth, J. & Hägg, M.-B. Crosslinking and stabilization of nanoparticle filled PMP nanocomposite membranes for gas separations. *Journal of Membrane Science* **326,** 285–292 (2009).

109. Merkel, T. C. *et al.* Effect of Nanoparticles on Gas Sorption and Transport in Poly(1-trimethylsilyl-1-propyne). *Macromolecules* **36,** 6844–6855 (2003).

110. Pacchioni, G. Physisorbed and chemisorbed CO_2 at surface and step sites of the MgO (100) surface. *Surface Science* **281,** 207–219 (1993).

111. Hosseini, S., Li, Y., Chung, T. & Liu, Y. Enhanced gas separation performance of nanocomposite membranes using MgO nanoparticles. *Journal of Membrane Science* **302,** 207–217 (2007).

112. Matteucci, S., Raharjo, R. D., Kusuma, V. A., Swinnea, S. & Freeman, B. D. Gas Permeability, Solubility, and Diffusion Coefficients in 1,2-Polybutadiene Containing Magnesium Oxide. *Macromolecules* **41,** 2144–2156 (2008).
113. Matteucci, S., Kusuma, V. A., Kelman, S. D. & Freeman, B. D. Gas transport properties of MgO filled poly(1-trimethylsilyl-1-propyne) nanocomposites. *Polymer* **49,** 1659–1675 (2008).
114. Pechar, T. W., Tsapatsis, M., Marand, E. & Davis, R. Preparation and characterization of a glassy fluorinated polyimide zeolite-mixed matrix membrane. *Desalination* **146,** 3–9 (2002).
115. Li, Y., Guan, H.-M., Chung, T.-S. & Kulprathipanja, S. Effects of novel silane modification of zeolite surface on polymer chain rigidification and partial pore blockage in polyethersulfone (PES)–zeolite A mixed matrix membranes. *Journal of Membrane Science* **275,** 17–28 (2006).
116. Nair, S. *et al.* Silylated Mesporous Silica Membranes on Polymeric Hollow Fiber Supports. *US Patent US2015/0114906.* (2015).
117. Trzpit, M. *et al.* The Effect of Local Defects on Water Adsorption in Silicalite-1 Zeolite: A Joint Experimental and Molecular Simulation Study. *Langmuir* **23,** 10131–10139 (2007).
118. Li, J.-R., Sculley, J. & Zhou, H.-C. Metal–Organic Frameworks for Separations. *Chem. Rev.* **112,** 869–932 (2012).
119. Howdeshell, M. & Huang, R. Comparison of Ceramic and Polymeric Membranes in Wastewater Treatment. *Singapore International Water Week 2011* (Poster, 2011).
120. Lin, H. & Freeman, B. D. Gas solubility, diffusivity and permeability in poly(ethylene oxide). *Journal of Membrane Science* **239,** 105–117 (2004).
121. Lin, H. & Freeman, B. D. Materials selection guidelines for membranes that remove CO_2 from gas mixtures. *Journal of Molecular Structure* **739,** 57-74 (2005).
122. Judeinstein, P. & Sanchez, C. Hybrid organic-inorganic materials: a land of multidisciplinarity. *J. Mater. Chem.* **6,** 511–15 (1996).
123. Kagan, C. R. Organic-Inorganic Hybrid Materials as Semiconducting Channels in Thin-Film Field-Effect Transistors. *Science* **286,** 945–947 (1999).
124. Pichavant, L., Bourget, C., Durrieu, M.-C. & Héroguez, V. Synthesis of pH-Sensitive Particles for Local Delivery of an Antibiotic via Dispersion ROMP. *Macromolecules* **44,** 7879–7887 (2011).
125. Pichavant, L. *et al.* pH-controlled delivery of gentamicin sulfate from orthopedic devices preventing nosocomial infections. *Journal of Controlled Release* **162,** 373–381 (2012).
126. Wight, A. P. & Davis, M. E. Design and Preparation of Organic−Inorganic Hybrid Catalysts. *Chem. Rev.* **102,** 3589–3614 (2002).
127. Matyjaszewski, K. *et al.* Polymers at Interfaces: Using Atom Transfer Radical Polymerization in the Controlled Growth of Homopolymers and Block Copolymers from Silicon Surfaces in the Absence of Untethered Sacrificial Initiator. *Macromolecules* **32,** 8716–8724 (1999).

128. Advincula, R. C. Surface Initiated Polymerization from Nanoparticle Surfaces. *Journal of Dispersion Science and Technology* **24,** 343–361 (2003).
129. Barbey, R. *et al.* Polymer Brushes via Surface-Initiated Controlled Radical Polymerization: Synthesis, Characterization, Properties, and Applications. *Chem. Rev.* **109,** 5437–5527 (2009).
130. Park, J. T., Koh, J. H., Koh, J. K. & Kim, J. H. Surface-initiated atom transfer radical polymerization from TiO_2 nanoparticles. *Applied Surface Science* **255,** 3739-3744 (2009).
131. Park, J. T., Koh, J. H., Seo, J. A., Cho, Y. S. & Kim, J. H. Synthesis and characterization of TiO_2/Ag/polymer ternary nanoparticles via surface-initiated atom transfer radical polymerization. *Applied Surface Science* **257,** 8301–8306 (2011).
132. Elias, L., Fenouillot, F., Majesté, J. C., Martin, G. & Cassagnau, P. Migration of nanosilica particles in polymer blends. *Journal of Polymer Science Part B: Polymer Physics* **46,** 1976–1983 (2008).
133. Hagrman, P. J., Hagrman, D. & Zubieta, J. Organic–Inorganic Hybrid Materials: From 'Simple' Coordination Polymers to Organodiamine-Templated Molybdenum Oxides. *Angew. Chem. Int. Ed.* **38,** 2638–2684 (1999).
134. Sanchez, C., Julián, B., Belleville, P. & Popall, M. Applications of hybrid organic–inorganic nanocomposites. *J. Mater. Chem.* **15,** 3559 (2005).
135. Hoogeveen, N. G., Stuart, M. A. C. & Fleer, G. J. Adsorption of charged block copolymers with two adsorbing blocks. *Faraday Discuss.* **98,** 161 (1994).
136. Hoogeveen, N. G., Stuart, M. A. C. & Fleer, G. J. Polyelectrolyte Adsorption on Oxides - I. Kinetics and Adsorbed Amounts. *Journal of Colloid And Interface Science* **182,** 133–145 (1996).
137. Hoogeveen, N. G., Stuart, M. A. C. & Fleer, G. J. Polyelectrolyte Adsorption on Oxides - II. Reversibility and Exchange. *Journal of Colloid And Interface Science* **182,** 146–157 (1996).
138. Fan, X., Lin, L., Dalsin, J. L. & Messersmith, P. B. Biomimetic Anchor for Surface-Initiated Polymerization from Metal Substrates. *J. Am. Chem. Soc.* **127,** 15843–15847 (2005).
139. Ye, Q., Wang, X., Li, S. & Zhou, F. Surface-Initiated Ring-Opening Metathesis Polymerization of Pentadecafluorooctyl-5-norbornene-2-carboxylate from Variable Substrates Modified with Sticky Biomimic Initiator. *Macromolecules* **43,** 5554–5560 (2010).
140. Papra, A., Gadegaard, N. & Larsen, N. B. Characterization of Ultrathin Poly(ethylene glycol) Monolayers on Silicon Substrates. *Langmuir* **17,** 1457–1460 (2001).
141. Djafer, L. N., Ayral, A., Boury, B. & Laine, R. M. Journal of Colloid and Interface Science. *Journal of Colloid And Interface Science* **393,** 335–339 (2013).
142. Laibinis, P. E. *et al.* Comparison of the structures and wetting properties of self-assembled monolayers of n-alkanethiols on the coinage metal surfaces,

copper, silver, and gold. *J. Am. Chem. Soc.* **113,** 7152–7167 (1991).

143. Rundqvist, J., Hoh, J. H. & Haviland, D. B. Poly(ethylene glycol) Self-Assembled Monolayer Island Growth. *Langmuir* **21,** 2981–2987 (2005).

144. Xue, Y., Li, X., Li, H. & Zhang, W. Quantifying thiol-gold interactions towards the efficient strength control. *Nature Communications* **5,** 1–9 (2014).

145. Watson, K. J., Zhu, J., Nguyen, S. T. & Mirkin, C. A. Hybrid Nanoparticles with Block Copolymer Shell Structures. *J. Am. Chem. Soc.* **121,** 462–463 (1999).

146. Rutenberg, I. M. *et al.* Synthesis of Polymer Dielectric Layers for Organic Thin Film Transistors via Surface-Initiated Ring-Opening Metathesis Polymerization. *J. Am. Chem. Soc.* **126,** 4062–4063 (2004).

147. Folkers, J. P., Laibinis, P. E. & Whitesides, G. M. Self-assembled monolayers of alkanethiols on gold: comparisons of monolayers containing mixtures of short-and long-chain constituents with CH_3 and CH_2OH terminal groups. *Langmuir* **8,** 1330–1341 (1992).

148. Bach, L. G., Islam, M. R., Seo, S. Y. & Lim, K. T. A novel route for the synthesis of poly(2-hydroxyethyl methacrylate) grafted TiO_2 nanoparticles via surface thiol-lactam initiated radical polymerization. *Journal of Applied Polymer Science* **127,** 261–269 (2012).

149. Kim, J. B., Huang, W., Miller, M. D., Baker, G. L. & Bruening, M. L. Kinetics of surface-initiated atom transfer radical polymerization. *Journal of Polymer Science Part A: Polymer Chemistry* **41,** 386–394 (2003).

150. Ma, H., Wells, M., Beebe, T. P. & Chilkoti, A. Surface-Initiated Atom Transfer Radical Polymerization of Oligo(ethylene glycol) Methyl Methacrylate from a Mixed Self-Assembled Monolayer on Gold. *Advanced Functional Materials* **16,** 640–648 (2006).

151. Shah, R. R. *et al.* Using Atom Transfer Radical Polymerization To Amplify Monolayers of Initiators Patterned by Microcontact Printing into Polymer Brushes for Pattern Transfer. *Macromolecules* **33,** 597–605 (2000).

152. White, J. C., Dutta, P. K., Shqau, K. & Verweij, H. Synthesis of Ultrathin Zeolite Y Membranes and their Application for Separation of Carbon Dioxide and Nitrogen Gases. *Langmuir* **26,** 10287–10293 (2010).

153. Lee, H., Scherer, N. F. & Messersmith, P. B. Single-molecule mechanics of mussel adhesion. *Proceedings of the National Academy of Sciences of the United States of America* **103,** 12999–13003 (2006).

154. Yang, H.-C., Luo, J., Lv, Y., Shen, P. & Xu, Z.-K. Surface engineering of polymer membranes via mussel-inspired chemistry. *Journal of Membrane Science* **483,** 42–59 (2015).

155. Ball, V., Del Frari, D., Toniazzo, V. & Ruch, D. Kinetics of polydopamine film deposition as a function of pH and dopamine concentration: Insights in the polydopamine deposition mechanism. *Journal of Colloid And Interface Science* **386,** 366–372 (2012).

156. Fan, X., Lin, L. & Messersmith, P. B. Cell Fouling Resistance of Polymer Brushes Grafted from Ti Substrates by Surface-Initiated Polymerization: Effect of Ethylene Glycol Side Chain Length.

Biomacromolecules **7,** 2443–2448 (2006).

157. Lee, H., Dellatore, S. M., Miller, W. M. & Messersmith, P. B. Mussel-inspired surface chemistry for multifunctional coatings. *Science* **318,** 426-430 (2007).
158. Sileika, T. S., Barrett, D. G., Zhang, R., Lau, K. H. A. & Messersmith, P. B. Colorless Multifunctional Coatings Inspired by Polyphenols Found in Tea, Chocolate, and Wine. *Angew. Chem. Int. Ed.* **52,** 10766–10770 (2013).
159. Yan, J. & Zhou, F. TiO_2 nanotubes: Structure optimization for solar cells. *J. Mater. Chem.* **21,** 9406–13 (2011).
160. Yan, J., Ye, Q. & Zhou, F. Polymer brushes assisted loading of high density CdS/CdSe quantum dots onto TiO_2 nanotubes and the resulting photoelectric performance. *RSC Adv.* **2,** 3978–8 (2012).
161. Yan, J., Ye, Q., Han, X. & Zhou, F. Step-by-step build-up of ordered p–n heterojunctions at nanoscale for efficient light harvesting. *RSC Adv.* **3,** 166–171 (2013).
162. Mutin, P. H., Guerrero, G. & Vioux, A. Hybrid materials from organophosphorus coupling molecules. *J. Mater. Chem.* **15,** 3761-3768 (2005).
163. Witucki, G. L. A silane primer: chemistry and applications of alkoxy silanes. *Journal of coatings technology* **65,** 57-60 (1993).
164. Marcinko, S. & Fadeev, A. Y. Hydrolytic Stability of Organic Monolayers Supported on TiO_2 and ZrO_2. *Langmuir* **20,** 2270–2273 (2004).
165. Mutin, P. H. *et al.* Selective Surface Modification of SiO_2−TiO_2 Supports with Phosphonic Acids. *Chem. Mater.* **16,** 5670–5675 (2004).
166. Davis, T. P. & Matyjaszewski, K. *Handbook of Radical Polymerization*. **1,** 1–935 (2002).
167. Kobayashi, M., Matsuno, R. & Otsuka, H. Precise surface structure control of inorganic solid and metal oxide nanoparticles through surface-initiated radical polymerization. *Science and Technology of Advanced Materials* **7,** 617-628 (2006).
168. Li, C. & Benicewicz, B. C. Synthesis of Well-Defined Polymer Brushes Grafted onto Silica Nanoparticles via Surface Reversible Addition−Fragmentation Chain Transfer Polymerization. *Macromolecules* **38,** 5929–5936 (2005).
169. Husseman, M. *et al.* Controlled Synthesis of Polymer Brushes by 'Living' Free Radical Polymerization Techniques. *Macromolecules* **32,** 1424–1431 (1999).
170. Matsuno, R., Yamamoto, K., Otsuka, H. & Takahara, A. Polystyrene- and Poly(3-vinylpyridine)-Grafted Magnetite Nanoparticles Prepared through Surface-Initiated Nitroxide-Mediated Radical Polymerization. *Macromolecules* **37,** 2203–2209 (2004).
171. Matsuno, R., Otsuka, H. & Takahara, A. Polystyrene-grafted titanium oxide nanoparticles prepared through surface-initiated nitroxide-mediated radical polymerization and their application to polymer hybrid thin films. *Soft Matter* **2,** 415-421 (2006).
172. Babu, K. & Dhamodharan, R. Grafting of Poly(methyl methacrylate) Brushes

from Magnetite Nanoparticles Using a Phosphonic Acid Based Initiator by Ambient Temperature Atom Transfer Radical Polymerization (ATATRP). *Nanoscale Res Lett* **3,** 109–117 (2008).

173. Devillers, S., Barthélémy, B., Delhalle, J. & Mekhalif, Z. Induction Heating vs Conventional Heating for the Hydrothermal Treatment of Nitinol and Its Subsequent 2-(Methacryloyloxy)ethyl 2-(trimethylammonio)ethyl Phosphate Coating by Surface-Initiated Atom Transfer Radical Polymerization. *ACS Appl. Mater. Interfaces* **3,** 4059–4066 (2011).

174. Bernardoni, F., Kouba, M. & Fadeev, A. Y. Effect of Curvature on the Packing and Ordering of Organosilane Monolayers Supported on Solids. *Chem. Mater.* **20,** 382–387 (2008).

175. Song, Y.-Y., Hildebrand, H. & Schmuki, P. Optimized monolayer grafting of 3-aminopropyltriethoxysilane onto amorphous, anatase and rutile TiO_2. *Surface Science* **604,** 346–353 (2010).

176. Guerrero, G., Vioux, A. & Mutin, P. H. Anchoring of Phosphonate and Phosphinate Coupling Molecules on Titania Particles. *Chem. Mater.* **13,** 4367–4373 (2001).

177. Raghuraman, G. K., Rühe, J. & Dhamodharan, R. Grafting of PMMA brushes on titania nanoparticulate surface via surface-initiated conventional radical and 'controlled' radical polymerization (ATRP). *J Nanopart Res* **10,** 415–427 (2007).

178. Minet, I., Delhalle, J., Hevesi, L. & Mekhalif, Z. Surface-initiated ATRP of PMMA, PS and diblock PS-b-PMMA copolymers from stainless steel modified by 11-(2-bromoisobutyrate)-undecyl-1-phosphonic acid. *Journal of Colloid And Interface Science* **332,** 317–326 (2009).

179. Barthélémy, B., Devillers, S., Minet, I., Delhalle, J. & Mekhalif, Z. Induction heating for surface triggering styrene polymerization on titanium modified with ATRP initiator. *Journal of Colloid And Interface Science* **354,** 873–879 (2011).

180. Ramadan, A. R., Yacoub, N., Amin, H. & Ragai, J. The effect of phosphate anions on surface and acidic properties of TiO_2 hydrolyzed from titanium ethoxide. *Colloids and Surfaces A: Physicochemical and Engineering Aspects* **352,** 118–125 (2009).

181. Webster, O. W., Hertler, W. R. & Sogah, D. Y. Group-transfer polymerization. 1. A new concept for addition polymerization with organosilicon initiators. *J. Am. Chem. Soc.* **105,** 5706–5708 (1983).

182. Wang, J.-S. & Matyjaszewski, K. Controlled/'Living' Radical Polymerization. Halogen Atom Transfer Radical Polymerization Promoted by a Cu(I)/Cu(II) Redox Process. *Macromolecules* **28,** 7901–7910 (1995).

183. Barner-Kowollik, C., Vana, P. & Davis, T. P. Chapter 4 - The Kinetics of Free-Radical Polymerization. *Handbook of Radical Polymerization* 187-261 (2002).

184. Coullerez, G., Carlmark, A., Malmström, E. & Jonsson, M. Understanding Copper-Based Atom-Transfer Radical Polymerization in Aqueous Media. *J.*

Phys. Chem. A **108,** 7129–7131 (2004).

185. Matyjaszewski, K. & Xia, J. Atom Transfer Radical Polymerization. *Chem. Rev.* **101,** 2921–2990 (2001).

186. Matyjaszewski, K., Wang, J.-L., Grimaud, T. & Shipp, D. A. Controlled/``Living'' Atom Transfer Radical Polymerization of Methyl Methacrylate Using Various Initiation Systems. *Macromolecules* **31,** 1527–1534 (1998).

187. Gnanou, Y. & Taton, D. Chapter 14 - Macromolecular Engineering by Controlled/Living Radical Polymerization. *Handbook of Radical Polymerization* 775-844 (2002).

188. News, C. E. Patrick McCarthy. *Chemical and Engineering News* **90,** 44 (2012).

189. Matyjaszewski, K. Atom Transfer Radical Polymerization (ATRP): Current Status and Future Perspectives. *Macromolecules* **45,** 4015–4039 (2012).

190. Matyjaszewski, K. Controlled Radical Polymerization: State-of-the-Art in 2014. *ACS Symposium Series* **1187,** 1–17 (2015).

191. Nicolaÿ, R., Kwak, Y. & Matyjaszewski, K. A Green Route to Well-Defined High-Molecular-Weight (Co)polymers Using ARGET ATRP with Alkyl Pseudohalides and Copper Catalysis. *Angewandte Chemie* **122,** 551–554 (2010).

192. Min, K., Jakubowski, W. & Matyjaszewski, K. AGET ATRP in the Presence of Air in Miniemulsion and in Bulk. *Macromol. Rapid Commun.* **27,** 594–598 (2006).

193. Pintauer, T. & Matyjaszewski, K. Atom transfer radical addition and polymerization reactions catalyzed by ppm amounts of copper complexes. *Chem. Soc. Rev.* **37,** 1087–11 (2008).

194. Kwak, Y. & Matyjaszewski, K. ARGET ATRP of methyl methacrylate in the presence of nitrogen-based ligands as reducing agents. *Polymer International* **58,** 242–247 (2009).

195. Matyjaszewski, K., Coca, S., Gaynor, S. G., Wei, M. & Woodworth, B. E. Zerovalent Metals in Controlled/'Living' Radical Polymerization. *Macromolecules* **30,** 7348–7350 (1997).

196. Konkolewicz, D. *et al.* SARA ATRP or SET-LRP. End of controversy? *Polym. Chem.* **5,** 4396-4417 (2014).

197. Percec, V. *et al.* Ultrafast Synthesis of Ultrahigh Molar Mass Polymers by Metal-Catalyzed Living Radical Polymerization of Acrylates, Methacrylates, and Vinyl Chloride Mediated by SET at 25 °C. *J. Am. Chem. Soc.* **128,** 14156–14165 (2006).

198. Vorobii, M., de los Santos Pereira, A., Pop-Georgievski, O., Kostina, N.Y., Rodriguez-Emmeneggar, C., Percec, V. Synthesis of non-fouling poly[N-(2-hydroxypropyl)methacrylamide] brushes by photoinduced SET-LRP. *Polym. Chem.* **6,** 4210–4220 (2015).

199. Magenau, A. J. D., Strandwitz, N. C., Gennaro, A. & Matyjaszewski, K. Electrochemically Mediated Atom Transfer Radical Polymerization. *Science* **332,** 81–84 (2011).

200. Treat, N. J. *et al.* Metal-Free Atom Transfer Radical Polymerization. *J. Am. Chem. Soc.* **136,** 16096–16101 (2014).

201. Miyake, G. M. & Theriot, J. C. Perylene as an Organic Photocatalyst for the Radical Polymerization of Functionalized Vinyl Monomers through Oxidative Quenching with Alkyl Bromides and Visible Light. *Macromolecules* **47,** 8255–8261 (2014).

202. Perkowski, A. J., You, W. & Nicewicz, D. A. Visible Light Photoinitiated Metal-Free Living Cationic Polymerization of 4-Methoxystyrene. *J. Am. Chem. Soc.* **137,** 7580–7583 (2015).

203. Xu, F., Geiger, J. H., Baker, G. L. & Bruening, M. L. Polymer Brush-Modified Magnetic Nanoparticles for His-Tagged Protein Purification. *Langmuir* **27,** 3106–3112 (2011).

204. Huang, X., Doneski, L. J. & Wirth, M. J. Surface-Confined Living Radical Polymerization for Coatings in Capillary Electrophoresis. *Anal. Chem.* **70,** 4023–4029 (1998).

205. Fischer, H. The Persistent Radical Effect: A Principle for Selective Radical Reactions and Living Radical Polymerizations. *Chem. Rev.* **101,** 3581–3610 (2001).

206. Ohno, K., Morinaga, T., Koh, K., Tsujii, Y. & Fukuda, T. Synthesis of Monodisperse Silica Particles Coated with Well-Defined, High-Density Polymer Brushes by Surface-Initiated Atom Transfer Radical Polymerization. *Macromolecules* **38,** 2137–2142 (2005).

207. Ejaz, M., Yamamoto, S., Ohno, K., Tsujii, Y. & Fukuda, T. Controlled Graft Polymerization of Methyl Methacrylate on Silicon Substrate by the Combined Use of the Langmuir−Blodgett and Atom Transfer Radical Polymerization Techniques. *Macromolecules* **31,** 5934–5936 (1998).

208. Matyjaszewski, K., Patten, T. E. & Xia, J. Controlled/'Living' Radical Polymerization. Kinetics of the Homogeneous Atom Transfer Radical Polymerization of Styrene. *J. Am. Chem. Soc.* **119,** 674–680 (1997).

209. Matyjaszewski, K., Shipp, D. A., Wang, J.-L., Grimaud, T. & Patten, T. E. Utilizing Halide Exchange To Improve Control of Atom Transfer Radical Polymerization. *Macromolecules* **31,** 6836–6840 (1998).

210. Jousset, S., Qiu, J., Matyjaszewski, K. & Granel, C. Atom Transfer Radical Polymerization of Methyl Methacrylate in Water-Borne System. *Macromolecules* **34,** 6641–6648 (2001).

211. Jewrajka, S. K., Chatterjee, U. & Mandal, B. M. Homogeneous Atom Transfer Radical Polymerization of Methyl Methacrylate at Ambient Temperature in Aqueous Ethanol. *Macromolecules* **37,** 4325–4328 (2004).

212. Huang, W., Kim, J. B., Bruening, M. L. & Baker, G. L. Functionalization of Surfaces by Water-Accelerated Atom-Transfer Radical Polymerization of Hydroxyethyl Methacrylate and Subsequent Derivatization. *Macromolecules* **35,** 1175–1179 (2002).

213. Nanda, A. K. & Matyjaszewski, K. Effect of [bpy]/[Cu(I)] Ratio, Solvent, Counterion, and Alkyl Bromides on the Activation Rate Constants in Atom

Transfer Radical Polymerization. *Macromolecules* **36,** 599–604 (2003).

214. Braunecker, W. A., Tsarevsky, N. V., Gennaro, A. & Matyjaszewski, K. Thermodynamic Components of the Atom Transfer Radical Polymerization Equilibrium: Quantifying Solvent Effects. *Macromolecules* **42,** 6348–6360 (2009).

215. Edmondson, S., Vo, C.-D., Armes, S. P. & Unali, G.-F. Surface Polymerization from Planar Surfaces by Atom Transfer Radical Polymerization Using Polyelectrolytic Macroinitiators. *Macromolecules* **40,** 5271–5278 (2007).

216. Tang, W. *et al.* Understanding Atom Transfer Radical Polymerization: Effect of Ligand and Initiator Structures on the Equilibrium Constants. *J. Am. Chem. Soc.* **130,** 10702–10713 (2008).

217. Tsarevsky, N. V., Braunecker, W. A. & Matyjaszewski, K. Electron transfer reactions relevant to atom transfer radical polymerization. *Journal of Organometallic Chemistry* **692,** 3212–3222 (2007).

218. Bozukova, D. *et al.* Imparting Antifouling Properties of Poly(2-hydroxyethyl methacrylate) Hydrogels by Grafting Poly(oligoethylene glycol methyl ether acrylate). *Langmuir* **24,** 6649–6658 (2008).

219. Liu, H. *et al.* Effect of catalyst on formation of poly(methyl methacrylate) brushes by surface initiated atom transfer radical polymerization. *J. Cent. South Univ.* **21,** 3049–3056 (2014).

220. Qian, H. & He, L. Surface-Initiated Activators Generated by Electron Transfer for Atom Transfer Radical Polymerization in Detection of DNA Point Mutation. *Anal. Chem.* **81,** 4536–4542 (2009).

221. Wang, X. S. & Armes, S. P. Facile Atom Transfer Radical Polymerization of Methoxy-Capped Oligo(ethylene glycol) Methacrylate in Aqueous Media at Ambient Temperature. *Macromolecules* **33,** 6640–6647 (2000).

222. Truelsen, J. H., Kops, J., Batsberg, W. & Armes, S. P. Synthesis of end-branched poly(ethylene glycol)s by aqueous atom transfer radical polymerization. *Polymer Bulletin* **49,** 235–242 (2002).

223. Cao, E., Prouzet, E. & Héroguez, V. Organic-inorganic hybrid materials designed by controlled radical polymerization and mediated using commercial dual functional organophosphorous coupling agents. *New Journal of Chemistry* **38,** 6081–6087 (2014).

224. Trnka, T. M. & Grubbs, R. H. The Development of L_2X_2Ru=CHR Olefin Metathesis Catalysts: An Organometallic Success Story. *Acc. Chem. Res.* **34,** 18–29 (2001).

225. Banks, R. L. & Bailey, G. C. Olefin disproportionation. A new catalytic process. *Industrial & Engineering Chemistry Product Research and Development* **3,** 170–173 (1964).

226. Calderon, N., Ofstead, E. A. & Ward, J. P. Olefin metathesis. I. Acyclic vinylenic hydrocarbons. *Journal of the American Chemical Society* **90,** 4133–4140 (1968).

227. Hérisson, J.-L. & Chauvin, Y. Catalyse de transformation des oléfines par les complexes du tungstène. II. Télomérisation des oléfines cycliques en

présence d'oléfines acycliques. *Die Makromolekulare Chemie* **141,** 161–176 (1971).

228. Chauvin, Y. Olefin Metathesis: The Early Days (Nobel Lecture). *Angew. Chem. Int. Ed.* **45,** 3740–3747 (2006).

229. Katz, T. J., Lee, S. J. & Acton, N. Stereospecific polymerizations of cycloalkenes induced by a metal-carbene. *Tetrahedron Letters* **47,** 4247-4250 (1976).

230. Grubbs, R. H., Burk, P. L. & Carr, D. D. Mechanism of the olefin metathesis reaction. *Journal of the American Chemical Society* **97,** 3265–3267 (1975).

231. Grubbs, R. H. Olefin-Metathesis Catalysts for the Preparation of Molecules and Materials (Nobel Lecture). *Angew. Chem. Int. Ed.* **45,** 3760–3765 (2006).

232. Schrock, R. R. Multiple Metal–Carbon Bonds for Catalytic Metathesis Reactions (Nobel Lecture). *Angew. Chem. Int. Ed.* **45,** 3748–3759 (2006).

233. Rouhi, M. A. Olefin metathesis gets Nobel nod. *Chemical and Engineering News* **83,** 8 (2005).

234. Slugovc, C. Chapter 1 - Synthesis of Homopolymers and Copolymers. *Handbook of Metathesis, Second Edition* **3,** 1-23 (2015).

235. Bielawski, C. W. & Grubbs, R. H. Living ring-opening metathesis polymerization. *Progress in Polymer Science* **32,** 1–29 (2007).

236. Nguyen, S., Grubbs, R. H. & Ziller, J. W. Syntheses and activities of new single-component, ruthenium-based olefin metathesis catalysts. *Journal of the American Chemical Society* **115,** 9858–9859 (1993).

237. Robson, D. A., Gibson, V. C., Davies, R. G. & North, M. A New and Highly Efficient Grubbs Initiator for Ring-Opening Metathesis Polymerization. *Macromolecules* **32,** 6371–6373 (1999).

238. Bielawski, C. W. & Grubbs, R. H. Highly Efficient Ring-Opening Metathesis Polymerization (ROMP) Using New Ruthenium Catalysts Containing N-Heterocyclic Carbene Ligands. *Angew. Chem. Int. Ed.* **39,** 2903–2906 (2000).

239. Love, J. A., Morgan, J. P., Trnka, T. M. & Grubbs, R. H. A Practical and Highly Active Ruthenium-Based Catalyst that Effects the Cross Metathesis of Acrylonitrile. *Angew. Chem. Int. Ed.* **41,** 4035–4037 (2002).

240. Burtscher, D. *et al.* Controlled living ring-opening metathesis polymerization with a ruthenium indenylidene initiator. *Journal of Polymer Science Part A: Polymer Chemistry* **46,** 4630–4635 (2008).

241. Choi, T. L. & Grubbs, R. H. Controlled Living Ring-Opening-Metathesis Polymerization by a Fast-Initiating Ruthenium Catalyst. *Angewandte Chemie* **115,** 1785-1788 (2003).

242. Riegler, S., Demel, S., Trimmel, G., Slugovc, C. & Stelzer, F. Ring opening metathesis polymerization initiated by $RuCl_2$(3-bromopyridine)$_2$(H_2IMes)(CHPh). Scope and limitation in block copolymer synthesis. *Journal of Molecular Catalysis A: Chemical* **257,** 53–58 (2006).

243. Flook, M. M., Jiang, A. J., Schrock, R. R. & Hoveyda, A. H. Z-Selective Olefin Metathesis Processes Catalyzed by a Molybdenum Hexaisopropylterphenoxide Monopyrrolide Complex. *J. Am. Chem. Soc.* **131,**

7962–7963 (2009).

244. Flook, M. M., Gerber, L. C. H., Debelouchina, G. T. & Schrock, R. R. Z-Selective and Syndioselective Ring-Opening Metathesis Polymerization (ROMP) Initiated by Monoaryloxidepyrrolide (MAP) Catalysts. *Macromolecules* **43,** 7515–7522 (2010).

245. Schrodi, Y. & Pederson, R. L. Evolution and applications of second-generation ruthenium olefin metathesis catalysts. *Aldrichimica Acta* **40,** 45-52 (2007).

246. Demel, S. *et al.* Ruthenium-initiated ROMP of nitrile monomers. *Inorganica Chimica Acta* **345,** 363–366 (2003).

247. Watson, K. J., Zhu, J. & Nguyen, S. Redox-active polymer-nanoparticle hybrid materials. *Pure and Applied Chemistry* **72,** 67-72(2000).

248. Weck, M., Jackiw, J. J., Rossi, R. R., Weiss, P. S. & Grubbs, R. H. Ring-Opening Metathesis Polymerization from Surfaces. *J. Am. Chem. Soc.* **121,** 4088–4089 (1999).

249. Kim, N. Y. *et al.* Surface-Initiated Ring-Opening Metathesis Polymerization on Si/SiO$_2$. *Macromolecules* **33,** 2793–2795 (2000).

250. Rolfe, A., Loh, J. K., Maity, P. K. & Hanson, P. R. High-Load, Hybrid Si-ROMP Reagents. *Org. Lett.* **13,** 4–7 (2011).

251. Buchmeiser, M. R., Sinner, F., Mupa, M. & Wurst, K. Ring-Opening Metathesis Polymerization for the Preparation of Surface-Grafted Polymer Supports. *Macromolecules* **33,** 32–39 (2000).

252. Buchmeiser, M. R. Metathesis Polymerization To and From Surfaces. *Advanced Polymer Science* **197,** 137–171 (2006).

253. Anderson, E. B. & Buchmeiser, M. R. Chapter 11 - Functional Supports and Materials. *Handbook of Metathesis, Second Edition* **3,** 253-281 (2015).

254. Buchmeiser, M. R. & Sinner, F. Method of producing monolithic support materials. *European Patent EP 1190244 B1* (2000).

255. Héroguez, V., Chemtob, A. & Quemener, D. Chapter 2 - ROMP in Dispersed Media. *Handbook of Metathesis, Second Edition* **3,** 25-44 (2015).

256. El-Faham, A. & Albericio, F. Peptide Coupling Reagents, More than a Letter Soup. *Chem. Rev.* **111,** 6557–6602 (2011).

257. Caster, K. C. & Walls, R. D. Adhesion of Fibers to Natural Rubber Elastomer using Ring-Opening Metathesis Polymerization (ROMP). *Advanced Synthesis & Catalysis* **344,** 764–770 (2002).

Appendix A

Characterization Techniques Used

A.1. Characterization Techniques

A.1.1. NMR

NMR (or Nuclear Magnetic Resonance) was used for the analysis of several products (solid titania surfaces and macromonomer or initiator evaluation).

A.1.1.1. ^{1}H NMR (Liquid)

The structure of the initiator molecules before reaction was checked with ^{1}H NMR (Bruker AVANCE, 400MHz) and compared to the reference spectra provided by Specific Polymers. In each case, about 10 mg of the compound was mixed with 450 µL of $CDCL_3$ (or deuterated chloroform) to be measured. When measuring the C3-Initiator or C1-Initiator, a relaxation time of 1 second with 16 scans was used. During the analysis of functionalizing the measuring the NB-PEO derived compounds (i.e. NB-PEO-COOH, NB-PEO-OH etc…), the relaxation time was doubled to 2 seconds with 32 scans.

A.1.1.2. ^{31}P NMR (Solid)

Solid-state 31P NMR spectra were also recorded (Bruker AVANCE), at 10000 Hz frequency (unless specified 1000 Hz was used), to confirm that the phosphonate groups are actually bound to the surface of the titania. Samples were prepared through taking portions of the C3-initiator grafted titania (Evonik particles of TiO_2-g-C3-Initiator, or those of the CTI porous supports) and performing their analysis in powdered form.

A.1.2. UV-Visible Spectroscopy

A SpetraMax® M2e Multimode Microplate Reader (Molecular Devices, LLC.) was used to perform the UV-spectra measurements. A quartz cuvette was used (1 cm cell width) and the spectra were taken at 1 nm wavelength intervals starting from 200 nm –

600 nm. All samples prepared were measured against an ethanol blank using the same cuvette.

A.1.3. DLS

The DLS was performed using a Vasco Particle Size Analyzer from Cordouan Technologies (France). The system was able to determine the subsequent size of the Evonik particles by extracting the hydrodynamic diameter calculated from the measured diffusion coefficient. Each timed measurement sample was taken from the reacting medium during the polymerization. A 0.2 mL volume of the reacting nanoparticle suspension with the growing polymer was taken at varying times and diluted/dispersed immediately into 15 mL of filtered ethanol. Each sample was then sonicated for 30 minutes and then measured with the DLS system, with 6 runs of 2-3 minutes each, to ensure the statistical accuracy and reproducibility of the data.

A.1.4. XPS

XPS (ThermoFisher Scientific K-ALPHA) was used for surface analysis with a monochromatized AlK_{α} source (hν = 1486.6 eV) and a 200 micron spot size. A pressure of 10^{-7} Pa was maintained in the chamber during analysis. The full spectra (0-1350 eV) were obtained with constant pass energy of 200eV and high-resolution spectra at a constant pass energy of 40 eV. Charge neutralization was required for all insulating powders pressed onto indium foil. High-resolution spectra were quantified using the Scofield library loaded in the AVANTAGE software provided by ThermoFisher Scientific.

A.1.5. TGA

TGA (TA Instruments, Q500) was used for the measurement of degradation of samples (as seen in Chapter 2, Chapter 3 and Chapter 4). The samples used a platinum tray that was subjected to the following program:

1). Use only Gas 1 (Nitrogen)
2). Condition to 50˚C to start recording data
3). Heating rate of 10˚C/min until 400˚C is reached
4). Upon reaching 400˚C, Gas 2 (Oxygen – 40% of flow) is introduced
5). Heating rate continues at 10˚C/min until 700˚C is reached
6). Sample stops recording data and cools down until room temperature.

A.1.6. SEM

The higher magnification scanning electron microscopy images were taken using a Leo FESEM 1530 operating at 5 kV. Two series of concentrations were used with this machine were 0 M (control) and 0.27 M (found in Chapter 3). In both cases, samples of the flat titania substrates were polymerized for 5 minutes, 15 minutes and 30 minutes. The subsequent samples were then prepared for imaging by vacuum drying overnight and gold coated before imaging.

For all other images, a Hitachi Tabletop Microscope TM-1000 was used to obtain the SEM images to determine the surface morphology before and after hybrid particle coating. As the samples were non-conductive, a layer of sputtered gold was necessary before imaging was possible.

A.1.7. Water Droplet Test

A water droplet test was setup in a manner shown in Figure A-1. A syringe full of water is used to drop water droplets directly on the cut titania support/surface. A camera was used to immediately capture the droplet interaction with the surface.

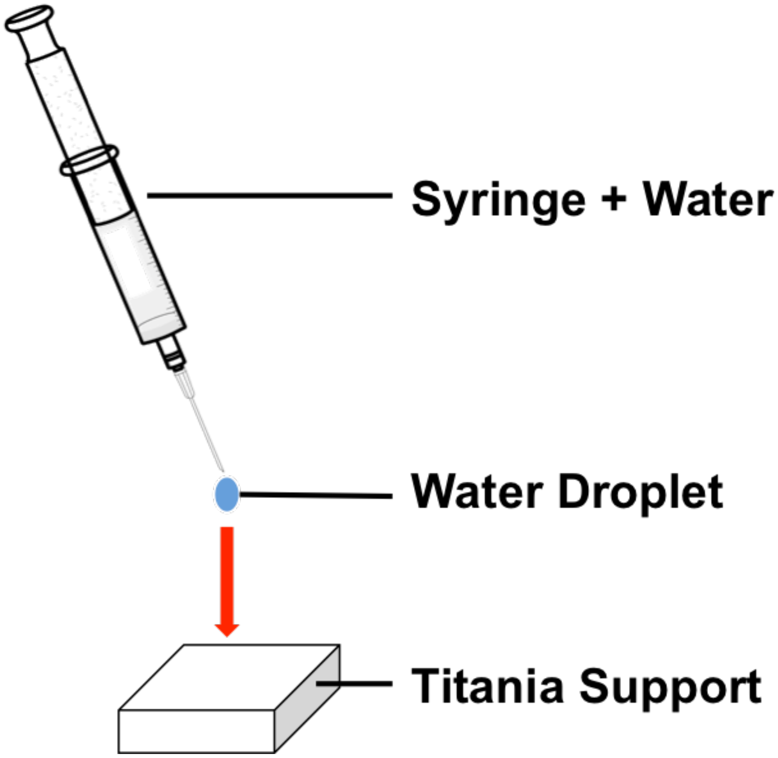

Figure A-1: Waterdroplet setup used for obtaining hydrophobic/hydrophilic test images in Chapter 5

A.2. Results for ^{1}H NMR spectra – Chapter 2

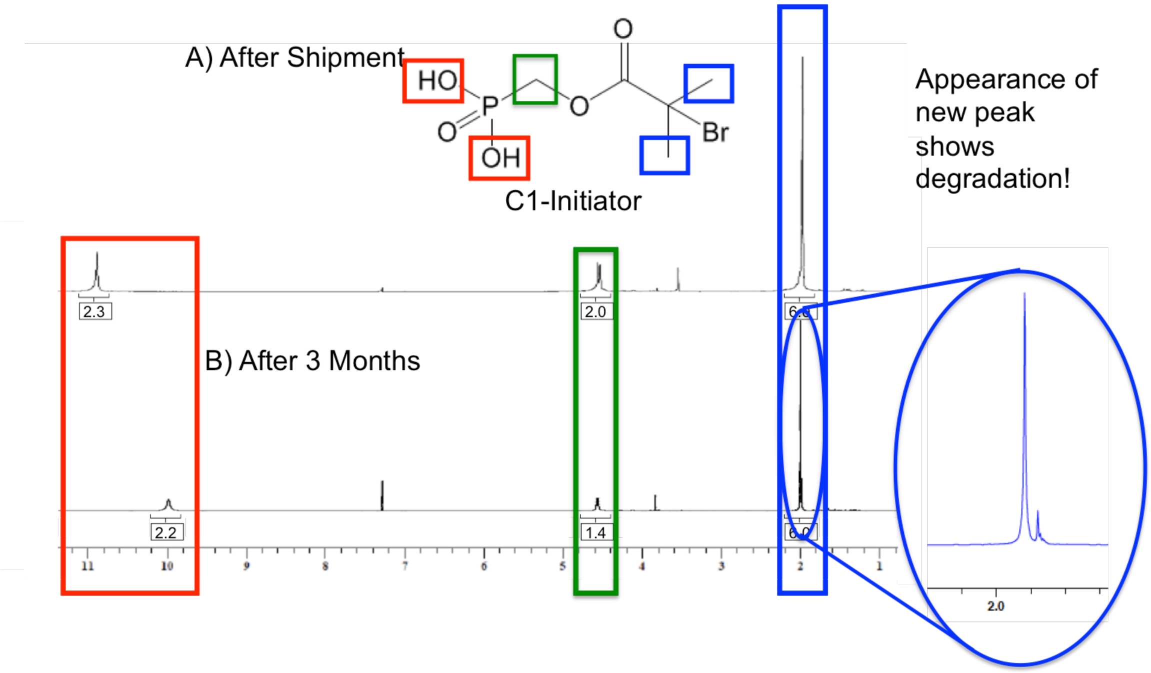
A) After Shipment

B) After 3 Months

Appearance of new peak shows degradation!

Figure A-2: ^{1}H NMR spectra for C1-Initiator in $CDCl_3$ for A) provided from supplier upon receiving product and B) 3 months after the C1-Initiator was received. We observe the formation of a new peak, indicating that there is degradation of the C1-Initiator.

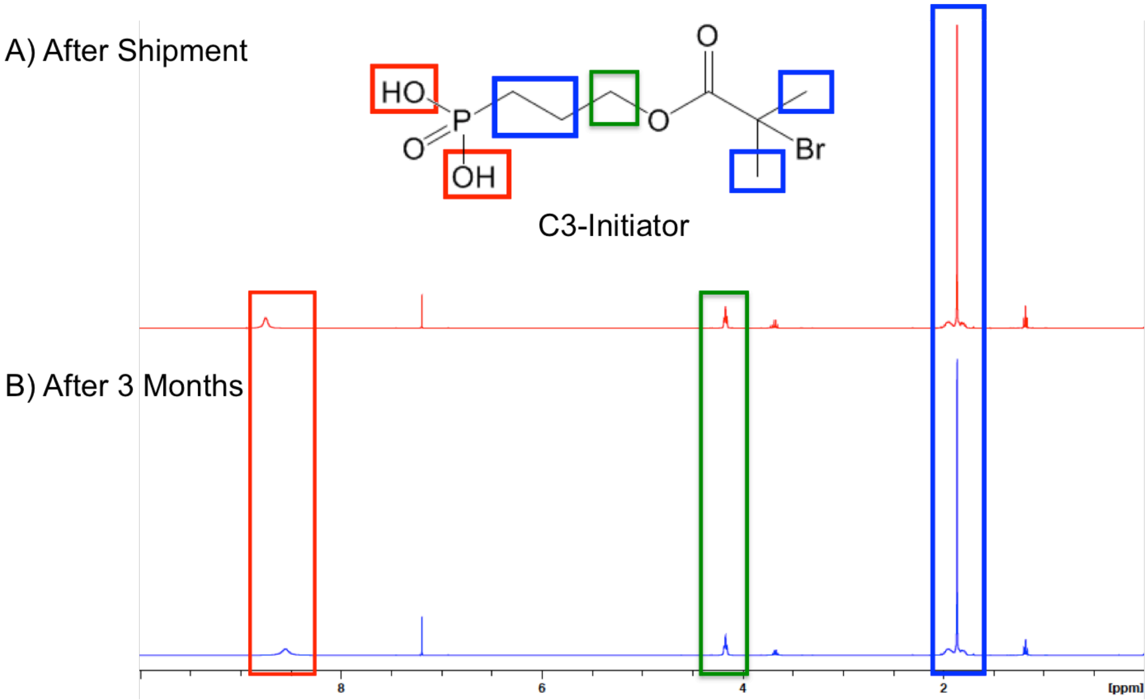
A) After Shipment

B) After 3 Months

Figure A-3: ^{1}H NMR spectra for C3-Initiator made A) after receiving product and B) after 3 months of storage at 4˚C. Notice that there does not appear to be any difference in the peaks over time (as compared to the C1-Initiator)

Appendix B

SEM images – Chapter 5

B.1. Introduction

The images captured for each case can be noted from the following images matched the following data tables (extracted from Chapter 5).

Table B-1: "Coating Onto" series of experiments using hybrid particles (synthesized by si-ATRP).

Sample ID	Type of CTI Tube	Coating		
		Vacuum	Setup	Method
TC-1	TiO_2	None	Parafilm Ends	Vertical - 2 pass (flip)
TC-2	TiO_2	None	Parafilm Ends	Vertical - 1 pass
TC-3	TiO_2	None	Parafilm Ends	Axial - 50 rpm
TC-4	TiO_2	None	Parafilm ends	Axial - 100 rpm
TC-5	TiO_2	None	Parafilm ends	Axial - 100 rpm
TC-6	TiO_2	Static	Glassware + septum	Vertical - 1 pass
TC-7	TiO_2	Dynamic	Glassware + septum	Vertical - 2 pass (flip)
TC-8	TiO_2	Static	Glassware + septum	Vertical - 2 pass (flip)
TC-9	ZrO_2	Static	Glassware + septum	Ferris Wheel (60 rpm)
TC-10	ZrO_2	Static	Glassware + septum	Vertical - 2 pass (flip)

Table B-2: "Grafting From" method of experiments performed with si-ATRP.

Sample ID	Type of CTI Tube	Coating Vacuum	Polymerization		
			Method	Rotation	Concentration
si-ATRP-TI-1	TiO_2	Static	Vertical - 2 pass (flip)	Vertical	0.27M
si-ATRP-TI-2	TiO_2	Static	Vertical - 1 pass	Vertical	0.27M
si-ATRP-TI-3	TiO_2	**None**	Axial - 1 pass	Vertical	0.27M
si-ATRP-TI-4	TiO_2	Static	Axial - 1 pass	Ferris Wheel	0.27M
si-ATRP-TI-5	TiO_2	Static	Ferris Wheel (60 rpm) - 1 pass	Ferris Wheel	0.27M
si-ATRP-TI-6	**ZrO_2**	Static	Ferris Wheel (60 rpm) - 2 pass	Vertical	0.27M
si-ATRP-TI-7	TiO_2	Static	Vertical - 2 pass (flip)	Ferris Wheel	**0.09M**
si-ATRP-TI-8	TiO_2	Static	Vertical - 2 pass (flip)	Ferris Wheel	**0.45M**

Table B-3: "Grafting From" method studied with si-ROMP process.

Sample ID	**Type of CTI Tube**	**Coating**		**Polymerization**			
		Vacuum	**Rotation**	**Rotation**	**NB**	**NB-PEO**	**NB/NB PEO**
si-ROMP-T1	ZrO_2	Static	Ferris Wheel (60rpm) - 1 pass	Vertical	**0.43M**	-	-
si-ROMP-T2	ZrO_2	Static	Vertical - 2 pass	Vertical	**0.6M**	-	-
si-ROMP-T3	ZrO_2	Static	Vertical - 2 pass	Vertical	**0.6M**	0.3M	80/20
si-ROMP-T4	ZrO_2	Dynamic	vertical/horizontal - 1 pass	Vertical	0.3M	-	-
si-ROMP-T5	ZrO_2	Dynamic	vertical/horizontal - 1 pass	Vertical	0.3M	0.3M	80/20
si-ROMP-T6	**TiO_2**	Dynamic	vertical/horizontal - 1 pass	Ferrish Wheel	0.3M	-	-
si-ROMP-T7	**TiO_2**	Dynamic	vertical/horizontal - 1 pass	Ferrish Wheel	0.3M	0.3M	80/20
si-ROMP-T8	**TiO_2**	Dynamic	Vertical - 2 pass	Vertical	0.3M	-	-
si-ROMP-T9	ZrO_2	Dynamic	Vertical - 2 pass	Vertical	0.3M	-	-

B.2. “Coating Onto” Method – Hybrid Particles

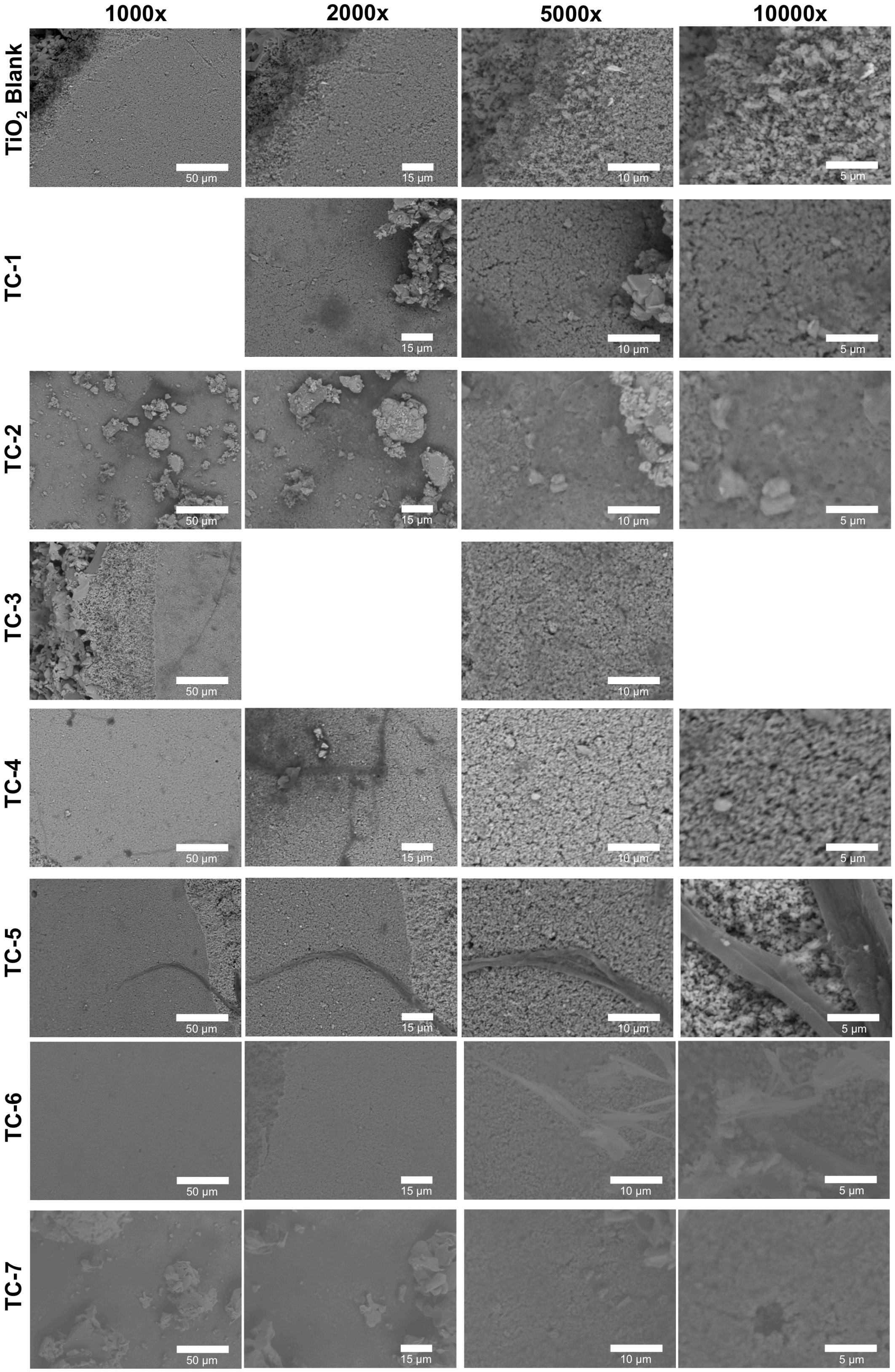

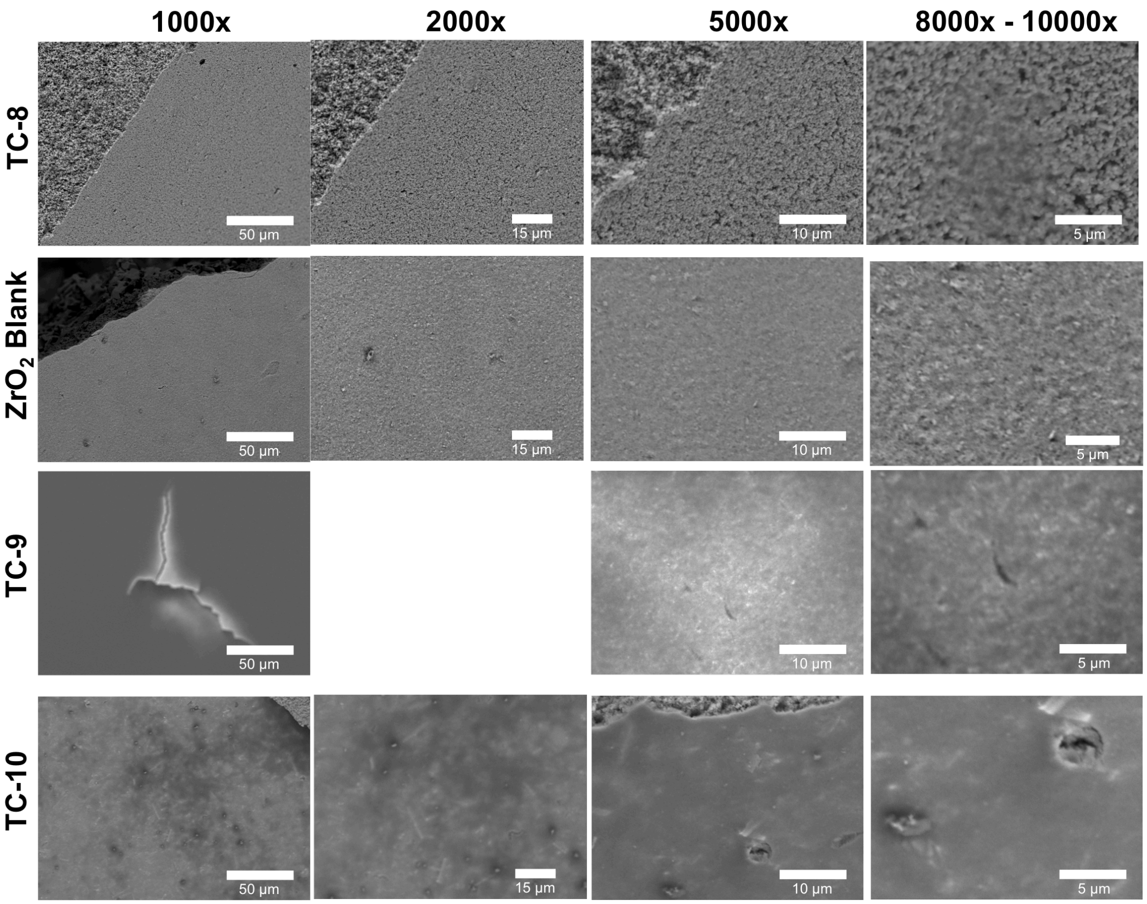
1000x
2000x
5000x
8000x - 10000x
TC-8
50 µm
15 µm
10 µm
5 µm
ZrO$_2$ Blank
50 µm
15 µm
10 µm
5 µm
TC-9
50 µm
10 µm
5 µm
TC-10
50 µm
15 µm
10 µm
5 µm

B.3. “Grafting From” – si-ATRP series

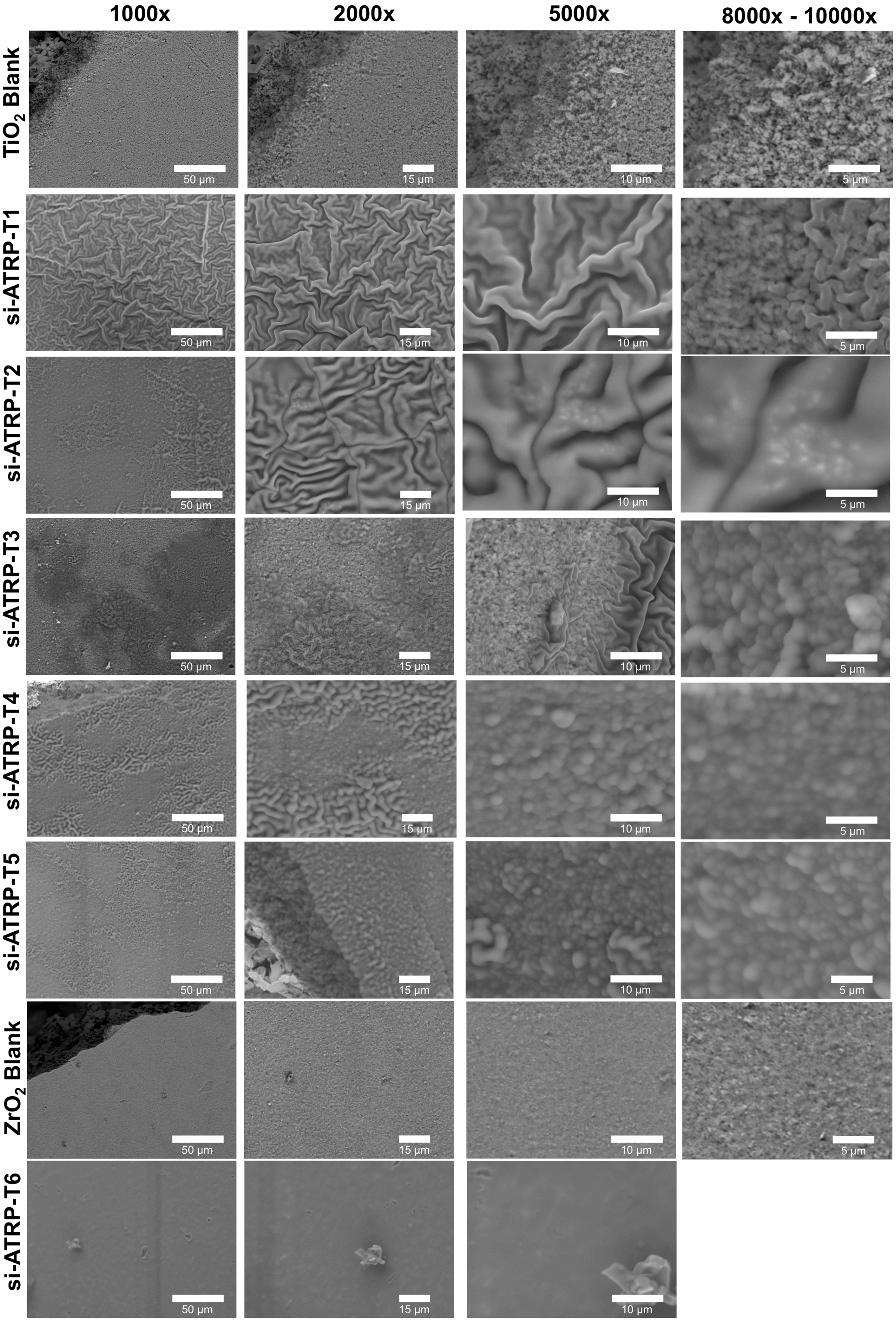

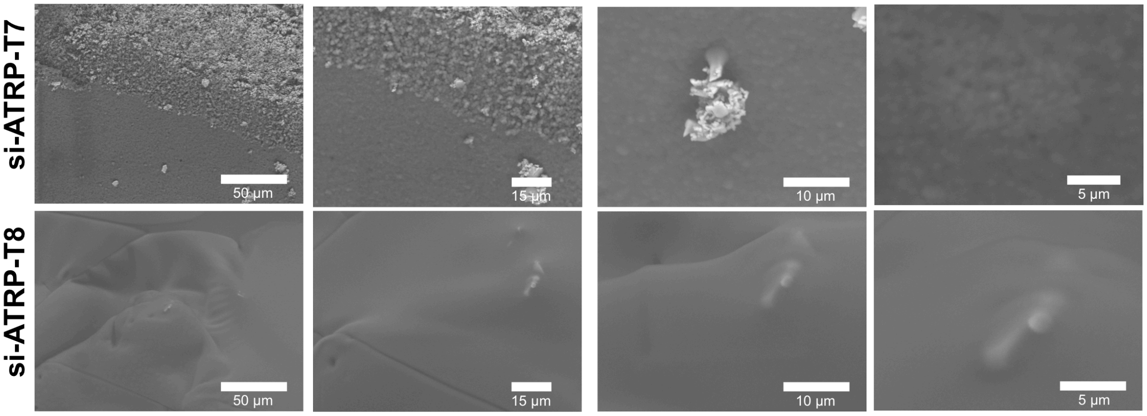
si-ATRP-T7
50 µm
15 µm
10 µm
5 µm
si-ATRP-T8
50 µm
15 µm
10 µm
5 µm

B.4. “Grafting From” – si-ROMP series

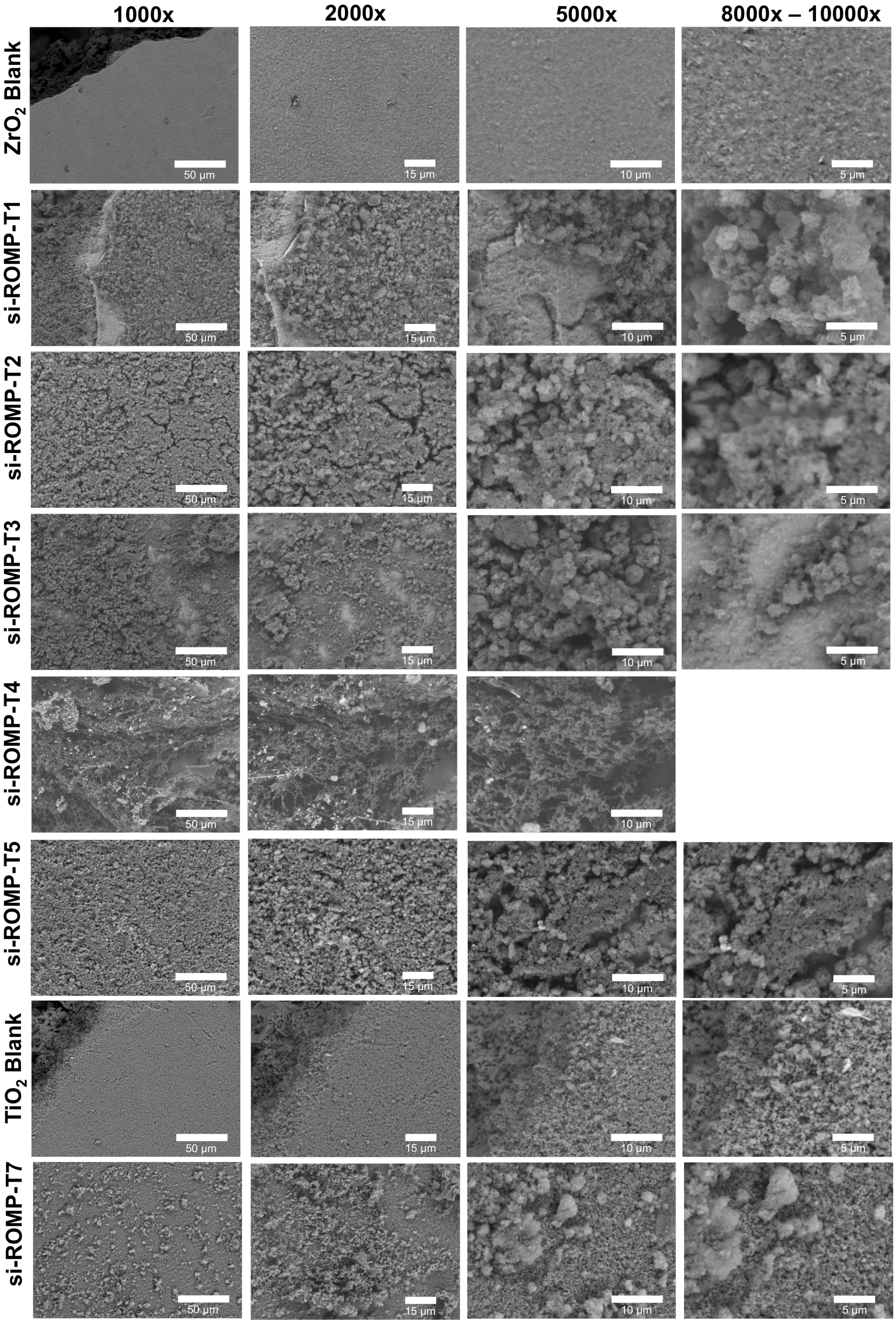

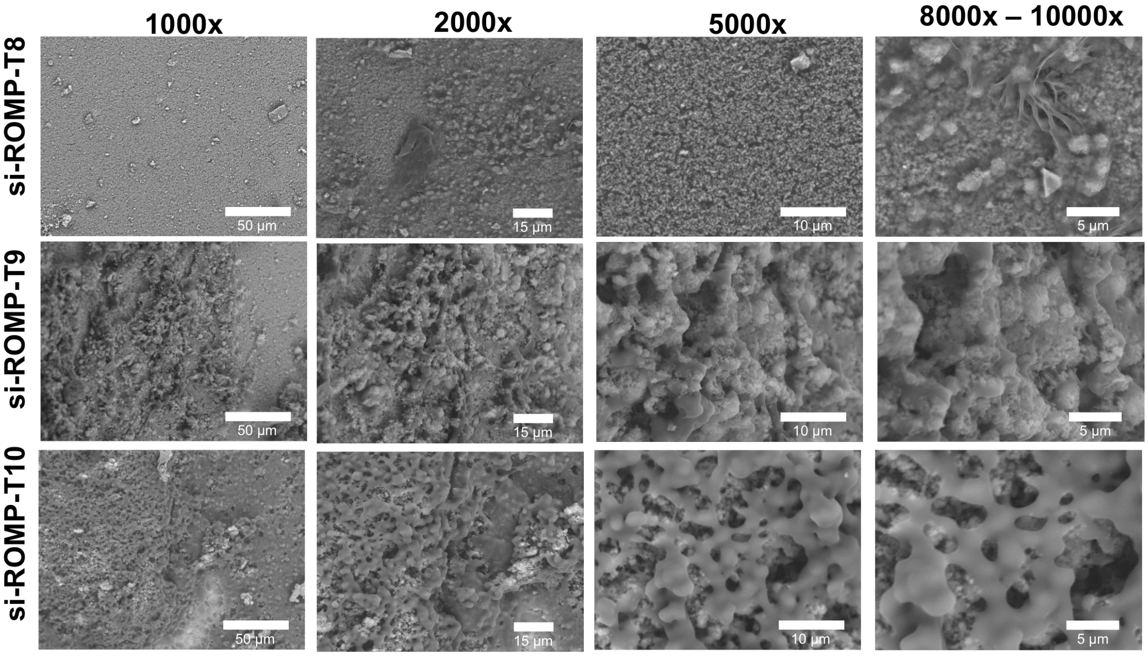
1000x
2000x
5000x
8000x – 10000x
si-ROMP-T8
si-ROMP-T9
si-ROMP-T10
50 µm
15 µm
10 µm
5 µm
50 µm
15 µm
10 µm
5 µm
50 µm
15 µm
10 µm
5 µm